

HENK KORTIER

ASSESSMENT OF HAND KINEMATICS AND INTERACTIONS

WITH THE ENVIRONMENT

HENK KORTIER

ASSESSMENT OF HAND KINEMATICS AND INTERACTIONS  
WITH THE ENVIRONMENT



**ASSESSMENT OF HAND KINEMATICS AND INTERACTIONS  
WITH THE ENVIRONMENT**

**USING ON-BODY SENSING**

**HENK KORTIER**

# UNIVERSITY OF TWENTE.

Faculty of Electrical Engineering, Mathematics and Computer Science  
Department of Biomedical Signals & Systems



Institute for Biomedical Technology and Technical Medicine  
P.O. Box 217, 7500 AE, Enschede, the Netherlands.



This research is supported by the Dutch Technology Foundation STW, which is part of the Netherlands Organization for Scientific Research (NWO) and partly funded by the Ministry of Economic Affairs, Agriculture and Innovation.



Financial support for printing of this dissertation was kindly provided by Xsens Technologies B.V.

Paranymphs: Anke Kortier & Dirk Weenk

Cover: Henk Kortier

Printing: Ipsonkamp B.V. Enschede

ISBN: 978-90-365-4475-7

DOI: [10.3990/1.9789036544757](https://doi.org/10.3990/1.9789036544757)

© H.G. Kortier, 2018 – All rights reserved

No part of this publication may be reproduced or transmitted in any form or by any means, electronic or mechanical, including photocopying, recording, or any information storage or retrieval system, without written permission from the author.

# ASSESSMENT OF HAND KINEMATICS AND INTERACTIONS WITH THE ENVIRONMENT

## DISSERTATION

to obtain  
the degree of doctor at the University of Twente,  
on the authority of the rector magnificus,  
prof. dr. T. T. M. Palstra,  
on account of the decision of the graduation committee,  
to be publicly defended  
on Friday the 9<sup>th</sup> of February 2018, at 14:45

by

Hendrik Gerhardus Kortier

born on the 13<sup>th</sup> of November, 1984  
in Hengelo (Ov), the Netherlands

This dissertation has been approved by:

Supervisor: Prof. Dr. Ir. P.H. Veltink

Co-supervisor: Dr. Ir. H.M. Schepers

## **Composition of the Graduation Committee:**

*Chairman and secretary:*

Prof. dr. P. M. G. Apers University of Twente

*Supervisor:*

Prof. dr. ir. P. H. Veltink University of Twente

*Co-supervisor:*

Dr. ir. H. M. Schepers Xsens Technologies B.V.

### *Members - internal:*

Dr. ir. R. J. Wiegerink University of Twente

Prof. dr. J. S. Rietman University of Twente,

Roessingh Research and Development

#### *Members - external:*

Prof. F. Gustafsson PhD Linköping University, Sweden

Prof. dr. ir. B. de Vries Technische Universiteit Eindhoven

Prof. dr. H. E. J. Veeger Vrije Universiteit Amsterdam

Technische Universiteit Delft



## SUMMARY

---

The hand is one of the most important instruments of our body. Its versatility enables the execution of a wide range of tasks that ask for a powerful, precise or gentle approach. Measuring hand and finger movements, and interaction forces, is therefore important for the assessment of tasks in daily life. However, measuring on-body kinematic and kinetic quantities is a delicate procedure due to the dexterity of the hand, and moreover, the little and complex shaped skin places for sensor attachment. This thesis proposes a new on-body assessment system that allows the measurement of movements and interaction forces of the hand, fingers and thumb.

The first objective, the development, evaluation and validation of an inertial and magnetic sensing system for the measurement of hand and finger kinematics is the topic of chapters 2 to 5. The second objective, assessment of the dynamic interaction between human hand and environment using combined force and movement sensing, is the topic of chapter 6.

Chapter 2 describes the hardware and algorithms for a sensing system which can be attached to the hand, fingers and the thumb. The hardware consists of multiple inertial and magnetic sensors to measure angular velocities, accelerations and the magnetic field. Each individual finger and the thumb is modelled as a kinematic chain where the bones correspond to the linkages and each joint is considered as an ideal ball-socket joint. Segmental lengths were determined by manual measurement, whereas the inertial sensors provided the input for a Kalman filter to estimate the 3D orientation of the corresponding segment. Hereafter, the orientation and tip position of each finger was estimated by applying forward kinematics. To our knowledge, it is the first system that uses inertial sensors for estimating finger kinematics. The estimation quality was expressed in terms of static and dynamic accuracy, dynamic range and repeatability. Differences with an active optical reference system were found to be a maximum of 13 mm for the finger tip distance difference during circular pointing movements. A standardized test protocol for instrumented gloves showed very good repeatability results compared to other datagloves, proven by the mean angle difference of < 2 degrees. Finally, a dynamic range was specified as a measure of how well the system is able to reconstruct joint angles when experiencing large angular velocities. The system showed accurate reconstruction up to 116 full index finger flex- extension movements per minute.

Chapter 3 reports an extensive comparison of our inertial sensing system against a passive opto-electronic marker system. It aims on typical hand-function tasks, including tapping, (fast) finger flexion, hand opening/closing, ab- adduction and circular pointing, which are used to quantify various motor symptoms for clinical diagnosis. Three subjects were included and instrumented with both systems. Differences in position, Range of Motion (RoM) and 3D

joint angles were noted of which the largest were found in fast and circular pointing tasks (between 3.3 deg and 8.4 deg). The differences between both measurement systems were attributed to three sources: optical marker movements, inertial sensor range and the anatomical calibration. First, despite adequate fastenings, relative marker displacements up to 8.4 mm were found during fast movements of rigid segments, indicating a limitation of the optoelectronic system. This relative displacement can result in segment orientation errors of 10 deg for typical adult finger dimensions. Secondly, a consistency investigation of the inertial sensor system revealed that the angular velocities estimated by the sensor fusion algorithm, taking the biomechanical model into account, were different compared to the angular velocities measured by the rate gyroscopes. Largest difference were found in fast tasks and pointing tasks which could be explained by either skin artifacts or sensor drift effects. Latter is possible when the filter cannot rely on the accelerometer inclination updates because the inertial accelerations, especially at the very distal ends, are too large or when rotations take place about a joint axis directed parallel to the global vertical. Thirdly, the anatomical calibration is of utmost importance for both the assessment of 3D joint angles as well as for a proper determination of the forward kinematics. Unfortunately, the anatomical calibration of both systems was not based on the same measurement set due to marker visibility issues during the inertial sensor hardware calibration procedure. Although the same helical axis definition had been used, the performance of both procedures could have large effects on the calibration quality. Chapter 3 concludes that the inertial measurement hardware can be used in a clinical setting but requires awareness of its limitations.

Chapter 4 describes a new method to ease the typical anatomical segment and sensor calibration procedures by estimating these parameters implicitly along with the estimation of the state variables. An optimization approach was presented by a set of stochastic equations for the description of inertial sensor readings, as well as, the kinematic relations applicable for the hand and fingers. Next, a general objective function was formulated and subsequently used to solve for different calibration parameters. These parameters include the sensor biases, the pose of sensor modules with respect to the segment to which it has been attached to, and the lengths of the proximal and medial segments. The method aims for simplifying the calibration procedure by estimating these parameters from simple voluntary hand movements. Traditional orientation estimators use the magnetometer for a drift free heading estimate, which is valid for a homogenous magnetic field, but could result in large deteriorated orientation estimates if the field is disturbed. Our approach estimates the relative poses solely using inertial sensors and is therefore invulnerable for hazardous magnetic environments. Different experiments were performed using similar hardware as described in chapters 2 and 3. The results demonstrate the potential of the approach taken as the estimation error of various parameter values were within 1 percent.

Chapter 5 presents a solution to estimate the full pose (3D position and 3D orientation) of the hand with respect to the sternum of the body using inertial sensors, magnetometers and a permanent magnet. Contrary to the previous chapter, magnetometers are used but not for estimating the heading from the earth magnetic field. We inferred the position of a permanent neodymium magnet by associating the magnetometer output to the static field induced by the magnet, which are in close vicinity to each other. The magnetic field strength, which is proportional to the dimensions of the magnet, is chosen such that magnetometers were able to pick up the field at distances up to 30 cm away from the permanent magnet. The human body is permeable for magnetic fields, which is very beneficial for measuring the kinematics of articulated structures, such as the arm, the hand and fingers. Furthermore, the use of a permanent magnet instead of an electromagnet provides the freedom of attaching it to small and poorly accessible spots as no external interfacing or powering is required. Experiments were performed by instrumenting the trunk with Inertial Measurement Units (**IMUs**) and magnetometers and attaching an **IMU** and a permanent magnet to the subject's hand. A complex task in which simultaneous movements of both trunk and hand was performed, resulted in an average Root Mean Square (**RMS**) position difference of  $19.4 \pm 2.2$  mm with respect to an optical reference system, whereas the relative trunk-hand and global trunk orientation error was  $2.3 \pm 0.9$  and  $8.6 \pm 8.7$  deg respectively.

Chapter 6 concerns the second research objective which is about the assessment of the physical interaction between the human hand and environmental objects. Dedicated sensors have been applied to measure 3D interaction forces for biomedical purposes. This hardware has been combined with the inertial hardware presented in the previous chapters and attached to the finger and thumb tips to measure interaction forces and finger motions simultaneously. The system is a first attempt to quantify the interactions of the hand with the environment without instrumenting the environment itself. A specific condition has been investigated in which the subject applied forces to different passive environmental objects and manipulated and moved these objects at the same time. The force and motion measurements enabled the estimation of the most dominant object characteristics. Experiments were conducted in which the weight of two mass like objects and the stiffness of a spring like object were estimated with an accuracy of  $19.7 \pm 10.6\%$  and  $29.3 \pm 18.9\%$  for a small (0.28 kg) and larger weight (0.44 kg) respectively, and  $14.8 \pm 9.6\%$  for the spring object.



## SAMENVATTING

---

De hand is een van de meest belangrijke instrumenten van ons lichaam. Zijn veelzijdigheid maakt het mogelijk om een brede selectie van taken uit te voeren die vragen om een krachtige, precieze of fijne aanpak. Het meten van hand en vinger bewegingen is daarom van belang voor de beoordeling van taken in het dagelijks leven. Vanwege de veelzijdigheid van de hand, en de beperkte mogelijkheden om meetinstrumentatie te bevestigen, is echter het meten van kinematische en kinetische grootheden niet gemakkelijk. Dit proefschrift presenteert een nieuw analysesysteem voor het meten van interactie krachten en bewegingen tussen de menselijke hand en zijn omgeving door gebruik te maken van sensoren die op de hand, vingers en duim geplaatst zijn.

Het eerste doel, de ontwikkeling, evaluatie en validatie van een inertieel en magnetisch meetsysteem voor de kinematica metingen van hand en vingers is het onderwerp van de hoofdstukken 2 tot en met 5. Het tweede doel, de beoordeling van de dynamische interactie tussen de menselijke hand en omgeving, door gebruik te maken van zowel kracht als bewegingsmetingen, is het onderwerp van hoofdtuk 6.

Hoofdstuk 2 beschrijft de hardware en algoritmen voor een meetsysteem dat op hand, vingers en duim geplaatst kan worden. De hardware bestaat uit meerdere inertiële en magnetische sensoren om de hoeksnellheden, versnellingen en het magnetisch veld te meten. Iedere vinger is gemodelleerd als een kinematische keten waarvan de kootjes corresponderen met de segmenten, en elk fysisch gewricht als een ideaal bol gewricht beschouwd wordt. De lengten van segmenten zijn handmatig bepaald, daar waar de inertiële sensoren het Kalman filter voeden om 3D oriëntaties te schatten van het desbetreffende segment. Vervolgens zijn de oriëntatie en positie van de vingertoppen geschat door het toepassen van de voorwaartse kinematica. Bij ons weten is dit het eerste systeem dat gebruik maakt van inertiële sensoren voor het afschatten van vinger kinematica. De kwaliteit van het afschatten is uitgedrukt in termen van statische en dynamische nauwkeurigheid, het dynamisch bereik en de herhaalbaarheid. Het maximum verschil in vingertop afstand ten opzichte van een actief optisch referentiesysteem werd vastgesteld op 13 mm tijdens circulaire vingerbewegingen. Een gestandaardiseerd testprotocol voor geïnstrumenteerde handschoenen resulteerde in een zeer goede herhaalbaarheid (gemiddeld verschil in hoek  $< 2$  graden) in vergelijking met andere datagloves. Als laatst is er een dynamische test gespecificeerd als zijnde een maat hoe goed het systeem in staat is om hoeken te reconstrueren onder invloed van grote hoekveranderingen. Het systeem bleek in staat om accurate reconstructies te genereren bij 116 volledige wijsvinger flex/extensie bewegingen per minuut.

Hoofdstuk 3 rapporteert een uitgebreidere vergelijking tussen het ontwikkelde inertiële meetsysteem en een passief opto-elektrisch meetsysteem. De

vergelijking is gericht op typische handfunctie taken, waaronder tikken, (snelle) vinger flexie, openen en dichtknijpen van de hand, ab- en adduceren en het maken van circulaire vingerbewegingen welk gebruikt worden voor de kwantificatie van verschillende motorsymptomen in de klinische diagnostiek. Drie proefpersonen werden geïncludeerd en uitgerust met beide hardware systemen. De verschillen in positie, bewegingsbereik (RoM) en 3D gewrichtshoeken werden geregistreerd waarvan de grootste verschillen werden gevonden in de snelle en de circulaire bewegingstaken (tussen de 3.3 graden en 8.4 graden). De verschillen in beide meetsystemen zijn toegewijd aan drie oorzaken: verplaatsing van de optische markers, het bereik van de inertiële sensoren en de anatomische kalibratie. Allereerst, ondanks het adequaat bevestigen van markers, werden relatieve marker verplaatsingen tot 8.4 mm bevonden tijdens de uitvoering snelle bewegingen. Dit zou een beperking van meten met een optisch systeem impliceren. Deze relatieve markerbeweging kan resulteren in een oriëntatie fout van 10 deg in het geval van een volwassen vingermaat. Ten tweede, uit een consistentie onderzoek van het inertiële sensor systeem kwam naar voren dat de hoeksnelheden geschat door het sensorfusie algoritme verschilden ten opzichte van de hoeksnelheden zoals gemeten met de gyrocoop sensoren. De grootste verschillen werden gevonden in de snelle- en wijstaken en kunnen verklaard worden door, dan wel de huid artefacten, dan wel een drift effect van het sensor systeem. Dit laatste is mogelijk doordat het filter niet kan vertrouwen op inclinatie updates van de accelerometer doordat de inertiële versnellingen, vooral gemeten op de meest distale punten, te groot zijn of wanneer de rotaties plaats vinden om de as die parallel staat met de globale verticaal. Ten derde, de anatomische kalibratie is van uiterst belang voor zowel de bepaling van 3D gewrichtshoeken alsmede een goede bepaling van de voorwaartse kinematica. Helaas was de anatomische kalibratie van beide meetsystemen niet gebaseerd op één zelfde dataset doordat het zicht van de optische markers onvoldoende was tijdens het uitvoeren van de inertiële sensor kalibratie. Ondanks dat dezelfde helische as definitie is gebruikt zou de uitvoering van beide procedures grote effecten kunnen hebben op de uiteindelijke kwaliteit van de kalibratie. Hoofdstuk 3 concludeert dat het inertiële sensorsysteem gebruikt zou kunnen in een klinische omgeving maar dat men wel rekening moet houden met de limitaties van het systeem.

Hoofdstuk 4 beschrijft een nieuwe methode om de typische anatomische kalibratie en sensor kalibratie procedures eenvoudiger te maken door deze parameters tegelijk met de toestandsvariabelen te schatten. Een optimalisatiefraamwerk is gepresenteerd door een set van stochastische vergelijkingen op te stellen voor zowel de beschrijvingen van sensor uitgangen, alsmede de kinematische relaties zoals men die in hand en vingers aantreft. Vervolgens is er een algemene kostfunctie geformuleerd die, na het oplossen, de verschillende kalibratieparameters oplevert. Deze parameter betreffen de sensor biases, de oriëntatie en positie van de sensoren ten opzichte van segmenten waar ze zich op bevinden, en de lengte van zowel het proximale en mediale vingersegment. De methode doelt op het vergemakkelijken van de kalibratie procedure door

de desbetreffende parameters te schatten uit data verkregen tijdens het uitvoeren van eenvoudige en willekeurige handbewegingen. Traditionele oriëntatieschatters gebruiken de magnetometer voor een drift vrije schatting van de koershoek, wat valide is voor homogene velden maar tot grote oriëntatiefouten kan leiden indien het veld verstoord is. In onze aanpak worden de oriëntaties enkel door gebruikmaking van de inertiële sensoren geschat en is dus ongevoelig voor magneetveld verstoringen. Verschillende experimenten zijn uitgevoerd met dezelfde hardware die gebruikt is in 2 en 3. De resultaten hebben de potentie van de aanpak aangetoond daar de verschillen met verschillende, onafhankelijk, bepaalde parameterwaarden binnen de 1 % bedroegen.

Hoofdstuk 5 presenteert een oplossing om de volledige 3D positie en oriëntatie van een menselijke hand ten opzichte het sternum te schatten door gebruik te maken van inertiële sensoren, magnetometers en een permanente magneet. In tegenstelling tot het vorige hoofdstuk worden magnetometers nu expliciet gebruikt, echter niet voor de schatting van de koershoek. We hebben de positie van een permanente neodymium magneet afgeschat door de magnetometer signalen te associeren met het statisch magnetisch veld wat door de permanente magneet geïnduceerd wordt op het moment dat de magneet en de magnetometer dicht bij elkaar in de buurt zijn. De magnetische veldsterkte, waarvan de grootte proportioneel is met de afmetingen van de magneet, is zo gekozen dat de magnetometers is staan waren om het velden tot een afstand van 30 cm tot de magneet op te pikken. Daar magnetische velden het menselijk lichaam gemakkelijke doordringen, maakt het een geschikt middel voor het metingen aan kinematische structuren als de arm, hand en vingers. Bovendien heeft een permanente magneet het voordeel ten opzichte van een electromagneet dat het geen elektrische voeding nodig heeft en het daardoor geschikt is om op moeilijk toegankelijke plekken geplaatst te worden. Experimenten zijn uitgevoerd waarbij de borstkas van een proefpersoon met verschillende Inertial Measurement Units ([IMUs](#)) en magnetometers is uitgerust en waarbij een enkele [IMU](#) plus een permanente magneet op de hand zijn bevestigd. Een complexe taak waarbij simultane bewegingen met het bovenlichaam en de hand uitgevoerd zijn resulterde in een gemiddeld Root Mean Square ([RMS](#)) positieverschil van  $19.4 \pm 2.2$  mm ten opzichte van een optisch referentiesysteem, waarbij de relatieve borstkas-hand en de globale borstkas oriëntatie fout respectievelijk  $2.3 \pm 0.9$  and  $8.6 \pm 8.7$  graden bedroegen.

Hoofdstuk 6 houdt zich bezig met de tweede onderzoeksdoelstelling welk over de bepaling van fysische interactie tussen een menselijke hand en objecten uit de omgeving gaat. Specifiek ontwikkelde krachtsensoren zijn toegepast om 3D interactie krachten te meten in biomedische toepassingen. Deze hardware is gecombineerd met de inertiële hardware, zoals die in de vorige hoofdstukken gepresenteerd is, en vastgezet op de toppen van de wijsvinger en duim om de interactiekrachten krachten en vingerbewegingen simultaan te kunnen meten. Dit systeem is een eerste poging om de interacties tussen de menselijke hand en zijn omgevingen te kwantificeren zonder dat de omgeving zelf met sensoriek uitgerust hoeft te worden. Een specifieke conditie is onder-

zocht waarin een proefpersoon krachten uitoefent op verschillende passieve omgevingslasten en daarbij, tegelijkertijd, het object verplaatst en manipuleert. De kracht- en bewegingsmetingen maakten het mogelijk om de meest dominante karakteristieke eigenschappen van het object te schatten. Experimenten zijn uitgevoerd waarin het gewicht van twee massaobjecten en de stijfheid van een veerobject zijn geschat met een nauwkeurigheid van  $19.7 \pm 10.6\%$  en  $29.3 \pm 18.9\%$  voor een klein (0.28 kg) en groot (0.44 kg) gewicht van de massa-objecten respectievelijk, en  $14.8 \pm 9.6\%$  voor de stijfheid van het veerobject.

## CONTENTS

---

SUMMARY	vii
SAMENVATTING	xi
LIST OF ACRONYMS	xvii
<b>1 INTRODUCTION</b>	<b>1</b>
1.1 Assessment of interactions between body and environment . . . . .	1
1.2 Historical perspective on assessing human hand interactions . . . . .	2
1.3 Kinematic Sensing and Analysis . . . . .	4
1.4 Force sensors . . . . .	11
1.5 Movement and Force sensing: The PowerSensor . . . . .	12
1.6 The PowerSensor project . . . . .	15
1.7 Research Objectives . . . . .	16
1.8 Thesis Outline . . . . .	17
<b>I ASSESSMENT OF HAND AND FINGER KINEMATICS USING INERTIAL AND MAGNETIC SENSORS</b>	
<b>2 INITIAL SYSTEM AND ALGORITHM DESIGN</b>	<b>21</b>
2.1 Introduction . . . . .	22
2.2 Methods . . . . .	23
2.3 Results . . . . .	36
2.4 Discussion and Conclusion . . . . .	38
2.5 Appendix . . . . .	43
<b>3 COMPARISON WITH AN OPTO-ELECTRONIC MARKER SYSTEM</b>	<b>45</b>
3.1 Introduction . . . . .	46
3.2 Methods . . . . .	47
3.3 Results . . . . .	52
3.4 Discussion and Conclusion . . . . .	57
<b>4 SIMULTANEOUS CALIBRATION AND POSE ESTIMATION</b>	<b>63</b>
4.1 Introduction . . . . .	64
4.2 Method . . . . .	68
4.3 Modeling . . . . .	70
4.4 Solving . . . . .	74
4.5 Experimental Methods and Results . . . . .	75
4.6 Discussion and Conclusion . . . . .	82
4.7 Appendix . . . . .	87

5	HAND POSE ESTIMATION BY USING A PERMANENT MAGNET	89
5.1	Introduction . . . . .	90
5.2	Methods . . . . .	92
5.3	Results . . . . .	101
5.4	Discussion and Conclusion . . . . .	104
5.5	Appendix . . . . .	108
<b>II ASSESSMENT OF HAND INTERACTIONS USING INERTIAL AND FORCE SENSORS</b>		
6	IDENTIFICATION OF OBJECT DYNAMICS	113
6.1	Introduction . . . . .	114
6.2	Method . . . . .	116
6.3	Results . . . . .	125
6.4	Discussion and Conclusion . . . . .	127
6.5	Appendix . . . . .	131
7	GENERAL DISCUSSION	133
7.1	Discussion and Outlook . . . . .	133
7.2	Conclusion . . . . .	141
<b>BIBLIOGRAPHY</b>		143
<b>JOURNAL PUBLICATIONS</b>		163
<b>CONFERENCE PUBLICATIONS</b>		165
<b>DANKWOORD</b>		167

## LIST OF ACRONYMS

---

ADC	Analog to Digital Converter
ADL	Activities of Daily Living
AMR	Anisotropic Magneto Resistance
BSS	Biomedical Signals and Systems
CMC	Carpometacarpal
CoM	Center of Mass
DIP	Distal interphalangeal
DoF	Degrees of Freedom
dRMS	Root Mean Square difference
dRoM	Range of Motion difference
EKF	Extended Kalman Filter
EM	Expectation Maximisation
EMG	Electromyography
GLRT	Generalized Likelihood Ratio Test
GPS	Global Positioning System
iid	independent identically distributed
ISB	International Society of Biomechanics
IMMS	Inertial and Magnetic Measurement System
IMMU	Inertial and Magnetic Measurement Unit
IMU	Inertial Measurement Unit
IP	Interphalangeal
MAP	Maximum A Posteriori
MCP	Metacarpophalangeal
MEMS	Micro Electrical Mechanical System
MEKF	Multiplicative Extended Kalman Filter
ML	Maximum Likelihood
MMSE	Minimum Mean Squared Error
MoCap	Motion Capture
OE	Optoelectronic
PCB	Printed Circuit Board
PD	Parkinson's disease
PDF	Probability density function
PIP	Proximal interphalangeal
RMS	Root Mean Square
RoM	Range of Motion
RLS	Recursive Least Squares
SD	Standard Deviation
SNR	Signal to Noise Ratio
STA	Soft tissue artifacts
TST	Transducer Science and Technology

WLS	Weighted Least Squares
UWB	Ultra Wide Band

## INTRODUCTION

---

### 1.1 ASSESSMENT OF INTERACTIONS BETWEEN BODY AND ENVIRONMENT

Physical interactions between the human body and its environment are essential in many fields. Monitoring of these interactions can lead to quantitative assessments and, subsequently, optimization of specific movements and tasks:

- In physical labor, interactions with the environment need to be performed within safe body loading limits [79, 88, 89].
- In rehabilitation, people need to relearn functional motor tasks [33, 102, 202] and interact with mobility support devices like wheelchairs or hand-cycling units [72, 215].
- In sports, motor tasks are trained to the ultimate, maximizing force and/or endurance and optimizing coordination [67, 73, 82]. In many sports, the athlete exercises in conjunction with objects like balls, rackets, bats - etcetera and ultimately wants to optimize the forces and motion applied to this sports equipment.
- In robotics, the versatility, dexterity and collaboration quality of a robot with other dynamical systems are increasingly important for the specifications of the robot. Haptic cyberphysical systems are able to execute tasks in direct conjunction with the human body, resulting in a vast set of training programs used, for example, by patients to relearn various upper and lower extremity motor tasks [98, 111, 123, 198]. These systems are characterized by the physical interaction between human body and environment, where it is the dynamic interaction that has been improved or optimized.

For this purpose, it is essential to assess this interaction quantitatively in terms of force and movement at the interface, power transfer and timing, work performed, and effective dynamics of the engaged bodies during the performance of functional tasks, preferably in the actual daily life setting. Such a quantitative assessment, possibly combined with electrophysiological measurements of muscle activation and biomechanical analysis, results in a better functional understanding of the neuromuscular system under healthy and diseased conditions during realistic dynamic interactions encountered in daily life. It should be noted that measuring at the interface of the human body and environment is actually a closed loop measurement where cause and consequence of forces and movements may be ambiguous.

---

This chapter is partly based on P.H. Veltink, H.G. Kortier, and H.M. Schepers, "Sensing Power Transfer Between the Human Body and the Environment" *Biomedical Engineering, IEEE Transactions on*, vol. 56, no. 6, pp. 1711-1718, 2009. [194]

The following sections outline the historical perspectives on interactions via the human hand, kinematic and kinetic sensing on the human body, and eventually the assessment of simultaneous force and movement sensing applied on the human hand.

## 1.2 HISTORICAL PERSPECTIVE ON ASSESSING HUMAN HAND INTERACTIONS

The human hand has always intrigued mankind because of its ability to perform a wide range of dexterous tasks. Only a few mammal species have the ability to use their frontal or, in case of a human, upper limbs with such precision. These limbs are weaker than the lower ones but allow much more flexibility in range of both distance and joint angles. A humorous, yet insightful way to visualise the contours of the human body related to brain capacity is called a homunculus, see Fig. 1.1. Body parts depicted relatively large correspond to a relatively large region of the, either sensory or motor, cortex. As one can see, hand and fingers require more cortical space whilst body parts that involve less dexterous movement, like the trunk, require less cortical space. Fingers are provided with some of the densest areas of nerve endings on the body. Tactile feedback from the hand, combined with the great positioning capability, make the hand intimately associated with the 'sense of touch'.

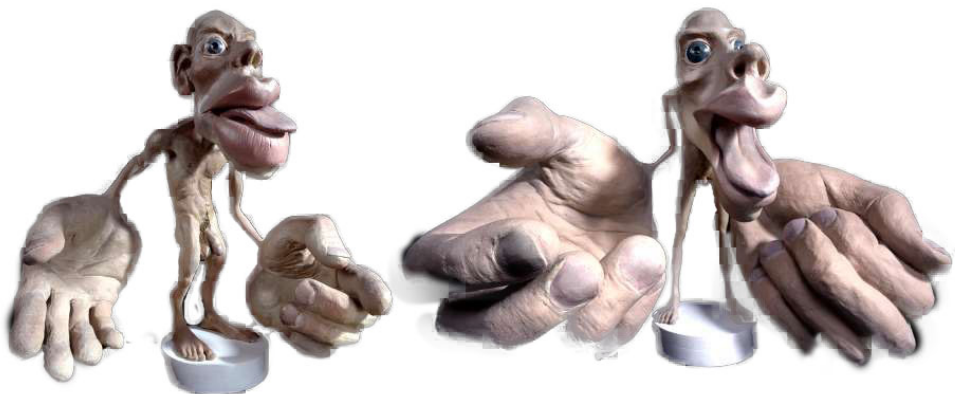
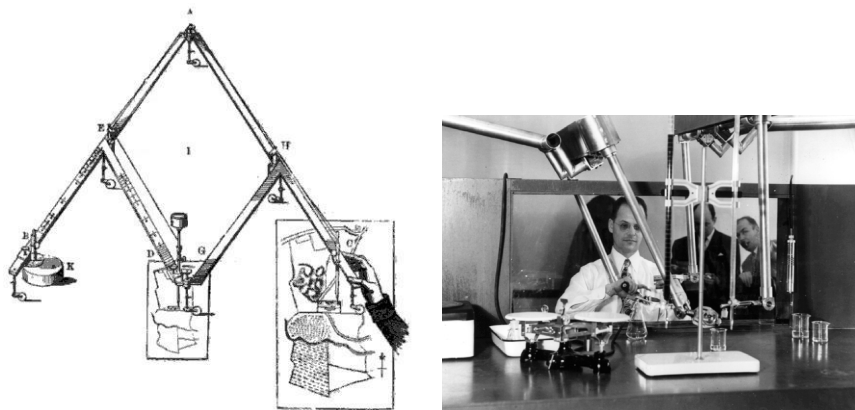


Figure 1.1: Homunculus. Reflection of the brain capacity for various limbs. Sensory input is depicted left and the area dedicated to motor control right. Adapted from [120].



(a) A pentograph, an archaic surveying tool. From "Nesbit's Practical Land Surveying", London, (1870). (b) Ray Goertz with his master-slave manipulator (1947) [59].

Figure 1.2: Historical examples of hand interaction devices.

Grasping an object requires information about the object to be grasped, such as shape, weight and intended use. Eventually this information determines how the hand and fingers are positioned and how forces by the fingers are exerted [39]. For almost one century researchers investigate different grasps and try to classify them into various postures. One popular method is based on the description in terms of forces that are applied to the opposed faces of the object to be grasped [81]. Three different postures were classified, opposing pads (pick up a pencil), opposing palm (hammer use), opposing side (turning a key in a lock). In literature two grasp approaches are distinguished, precision and power grasp. It depends on the user's task and object's shape which grasp strategy is chosen.

The importance of using hands in daily life led to widespread research in many fields, like tele-operations, diagnostics and treatment for impaired persons, or just as an input for computer devices. Capturing hand movements, either mechanically or electronically, started back in the renaissance by the invention of the pentograph [180] see Fig. 1.2a. After WWII, Ray Goertz from Argonne National Laboratory developed the first 'master-slave manipulator' and was able to perform lab operations remotely, see Fig. 1.2b. Using mechanical linkages, this master-slave manipulator offered some kind of force feedback to perform, rough, interactions with glass objects without destroying them.

Technological advances resulted in the development of robots that mediate within the rehabilitation process for patients following stroke. Different haptic robots, either end-effector (MIT-manus [74], HapticMASTER [193]) or exoskeleton based (ARMIN [130]) were used in different clinical studies and demonstrated neurorehabilitation as a significant emerging field in clinical medicine [115, 121].

Development of hand tracking devices, aside from the famous computer mouse, started at the MIT about four decades ago [180]. MIT researchers used the commercialised hardware from Polhemus to directly translate hand motion into a computer based input. The principle is based upon transmitting a pulsed magnetic field which is picked up by a sensing coil that can be placed anywhere on the body, for instance the hand. The difference between transmitted and received signal encodes the position and orientation information. This study initiated the development of tracking devices with different sensing modalities under different conditions. A summary will be outlined in the following section.

### 1.3 KINEMATIC SENSING AND ANALYSIS

Analysis of human body motions can be performed with a variety of sensing modalities. The most common sensing modalities, with respect to the amount of journal publications, are optical, magnetic, acoustic, radio and inertial. Depending on the application, a suitable sensor is selected that meets the particular demands of the user. Obviously, each sensing method has its advantage and disadvantages with respect to: sensing range, stability, accuracy, ease of use, sensitivity to external disturbances, etcetera.

Biomechanical analysis requires the combination of sensors with a biomechanical model of the human body to map sensor readings to kinematics of human body linkages. The kinematic accuracy, number of body parts to be tracked, robustness with respect to environmental changes, ease of use and realtime usage are some indicators that led to the development of many human body tracking systems. Some major contributions with respect to hand and arm tracking will be outlined in the following paragraphs.

#### 1.3.1 *Traditional hand finger tracking systems*

Traditionally, a mechanical serial linkage strapped to hand and fingers was used for direct joint angle measurements. An exoskeleton which uses two links per joint allows deformations of the finger without the need to align with the biomechanical joint axis and hindering the natural movements. A rotational encoder or potentiometer attached to the mechanical hinge joints is directly related to the actual joint angle [42]. Soon, non-contact tracking became available to avoid the procedure to align the system and finger joints that was necessary and, obviously, a cumbersome procedure to perform.

From the 1970's, glove based systems were introduced in different designs and based on various sensing techniques. Two categories can be distinguished: a sensor placed across the joint with its output directly related to the actual joint angle, and transmitter-receiver systems with sensors placed on the rigid segments.

Optical fibers and stretchable materials can be classified to the first group, see Fig. 1.3. The sensors are attached along the phalanges and cross one or



(a) Resistive strain sensing: Cyberglove II [41]



(b) Optical fiber sensing: 5DT DataGlove [1]

Figure 1.3: Instrumented glove examples.

more joints. The amount of refracted light, or measured resistance is dependent on bending of the material and therefore directly related to the joint angle [14, 131]. State-of-the-art sensing modalities within this field can be found in biological sensors, e.g. strain sensors based on carbon nanotubes' [222] and microfluidic strain sensing [31].

Electromagnetic acoustic and optical transceiver systems belong to the second category. The hand or forearm is equipped with an active transmitter and used in combination with passive trackers attached to the more distal segments, like finger tips [42]. The transmission medium could be either laserlight, ultrasonic or electromagnetic waves. Especially electromagnetic fields are easily generated in perpendicular directions which enables the reconstruction of the relative 3D position and 3D orientation [49].

In both categories, sensing systems are physically attached to the hand itself. Alternatively, the environment can be instrumented to capture body motions. Among a wide variety of sensing modalities, the marker-based Motion Capture (**MoCap**) systems are the most popular ones.

Cameras pick up light from passive marker reflections or direct light from active markers that are attached to body segments [138, 199, 200]. Clusters of rigid markers combined with a biomechanical model allow for accurate reconstructions of body poses. Especially for locomotion, these systems have a superior reputation and may be seen as the golden standard.

Marker based camera systems for hand tracking purposes never got popular due to the line of sight violations and limited space for marker attachment, especially during the performance of functional tasks. However, marker free camera solutions became increasingly popular since the emerge of computer vision systems [48]. Those systems use the contours of the hand in combination with colour or contrast encodings. Alternative systems project a point cloud of infrared light onto a body part which is captured by a sensitive camera situated in the same housing as the light source. The processing power of com-

puters and quality of cameras allow for accurate and fast reconstruction of the hand's pose. Various systems have been designed of which the LEAP device is probably, due to its small form factor, the most popular one nowadays [63, 106]. However, the biggest disadvantage of these systems is the need for external cameras which increases the chance of occluding images and therefore limits the trackable movements substantially.

In contrast to the above mentioned systems, which are limited to a specific measurement space and therefore not suitable for proper analysis of motion in daily life tasks, inertial sensors are not restricted to such environmental factors.

### 1.3.2 Rotation Kinematics and Inertial Sensors

Inertial sensors contain an accelerometer and a gyroscope which enable 3D measurements of object kinematics in an inertial reference frame. Traditionally, they have been used for aerospace applications, but gained popularity in movement analysis since Micro Electrical Mechanical System ([MEMS](#)) technology enabled the fabrication of inertial sensors on a much smaller footprint compared to the tactical grade inertial sensors, see Fig.[1.4](#). The accuracy of [MEMS](#) inertial sensors was initially poor, but has significantly been improved over the last years. Moreover, [MEMS](#) based inertial sensors are bulk fabricated, embodied in tiny chip packages (millimeter scale), are low-cost and have low power consumption compared to tactical grade sensors.

Before briefly explaining the different sensors and typical models being used, it is necessary to explain the different coordinate frames: First, the inertial coordinate frame,  $\Psi_i$ , is static with the origin positioned at the center of the earth and its orientation is determined by the constellation of stars. Inertial sensors measure accelerations and angular velocities with respect to this frame. Second, a global navigation frame  $\Psi_n$  (in chapter [2](#) denoted as  $\Psi_G$  and in chapter [4](#) denoted as  $\Psi_L$ ), is a local frame at an arbitrary static position and orientation on earth. This frame is generally used for navigation purposes and therefore stationary to earth. Third, the sensor body frame  $\Psi_b$  is defined statically with respect to the sensor's casing with the origin positioned at the center of the accelerometer. Inertial sensor readings are always expressed in this coordinate frame.

Rotating a 3D vector from one coordinate frame to another coordinate frame can be performed using the operators of different orientation parameterizations. Throughout this thesis we used both the rotation matrix and quaternion parameterization.

A rotation matrix (e.g.  $R^{n^b}$ ) is a member of the special orthogonal group  $SO(3)$ . Rotating a 3D vector  $v^b$  expressed in frame  $\Psi_b$  to frame  $\Psi_n$  is a linear operation and performed by a matrix multiplication:

$$v^n = R^{n^b} v^b \quad (1.1)$$

Alternatively, one can use a unit quaternion which relates as follows to the rotation matrix [100]:

$$R(q^{nb}) = q^{nb} q^{nb,T} + \left( q_0^{nb} \right)^2 I_3 + 2q_0^{nb} [q^{nb}]_\times + [q^{nb}]_\times^2 \quad (1.2)$$

where  $q^{nb}$  is a unit quaternion describing the rotation from frame  $\Psi_b$  to  $\Psi_n$ ,  $q_0^{nb}$  is the scalar part and  $q^{nb}$  the vector part of the quaternion respectively,  $T$  is the vector transpose operator, and  $\square_\times$  the skew symmetric matrix operator.

Transforming a vector using the unit quaternion representation is performed by:

$$v^n = q^{nb} \odot v^b \odot \bar{q}^{nb} \quad (1.3)$$

where  $v^n$  and  $v^b$  are the quaternion equivalents of  $v^n$  and  $v^b$ ,  $\odot$  is the quaternion product operator, and  $\bar{q}$  is known as the quaternion conjugate. The quaternion equivalent of a vector is defined as

$$v = [0, v], \quad (1.4)$$

whereas the quaternion conjugate is defined as

$$\bar{q} = [q_0, -q]. \quad (1.5)$$

The quaternion product operator  $q^a \odot q^b$  is defined (see also Hol [77]) as:

$$\begin{aligned} q^a \odot q^b &= \left[ q_0^a q_0^b - q^{a,T} q^b, q_0^a q^b + q_0^b q^a + q^a \times q^b \right] \\ &= \begin{bmatrix} q_0^a & -q^{a,T} \\ q^a & q_0^a I_3 + [q^a]_\times \end{bmatrix} \begin{bmatrix} q_0^b \\ q^b \end{bmatrix} = \begin{bmatrix} q_0^b & -q^{b,T} \\ q^b & q_0^b I_3 - [q^b]_\times \end{bmatrix} \begin{bmatrix} q_0^a \\ q^a \end{bmatrix} \end{aligned} \quad (1.6)$$

Lastly, we frequently make use of the quaternion logarithm and exponential which are defined as:

$$\log q = \frac{q}{\|q\|_2} \arccos q_0 \quad (1.7)$$

$$\exp v = \left[ \cos \|v\|_2, \frac{v}{\|v\|_2} \sin \|v\|_2 \right]. \quad (1.8)$$

The rotation dynamics of a rigid body is provided by the derivative of a rotation (a derivation can be found in Hol [77]) and is given by:

$$\dot{q}^{bn} = \frac{1}{2} \omega_{bn}^b q^{bn} = \frac{1}{2} \omega_{nb}^n q^{nb} \quad (1.9)$$

where, for example,  $\omega_{bn}^b$  is the angular velocity of the body to which it has been attached to, with respect to the global frame.

A gyroscope measures the sensor's angular velocity using the Coriolis effect, i.e. the rate of change of the sensor's orientation. A typical linear model for the gyroscope is given by:

$$\mathbf{y}_g^b = \boldsymbol{\omega}_{bn}^b + \mathbf{b}_g^b + \mathbf{e}_g \quad (1.10)$$

where  $\mathbf{b}_g^b$  is a bias term and  $\mathbf{e}_g$  is an independent identically distributed (*iid*) white Gaussian noise source.

An accelerometer measures the external specific force acting on the sensor. The specific force consists of both the sensor's acceleration  $\mathbf{a}^n$  and the earth's gravity  $\mathbf{g}^n$ . An accelerometer can be modeled as:

$$\mathbf{y}_a^b = R^{bn}(\mathbf{a}^n - \mathbf{g}^n) + \mathbf{b}_a^b + \mathbf{e}_a \quad (1.11)$$

where  $R^{bn}$  is the rotation matrix describing the orientation difference between the global and the sensor frame,  $\mathbf{b}_a^b$  is a bias term,  $\mathbf{e}_a$  is an *iid* Gaussian noise source.

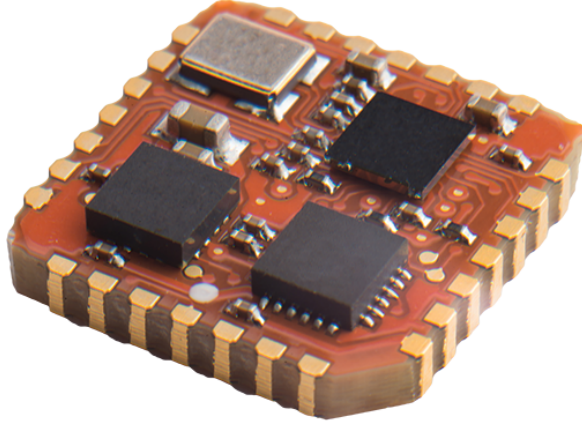


Figure 1.4: Xsens MTi-1 (1.2x1.2 cm) IMU. Visible are the chips containing the accelerometer and gyroscope, a magnetometer and micro-controller for data processing and sensor fusion. Adapted from [221].

### 1.3.3 Magnetometers

Magnetometers measure the local magnetic field, which is composed of both the earth magnetic field as well as any induced field by a magnetic source in the environment. Such a magnetic source is either a passive material, for instance a ferromagnetic alloy, or actively induced by moving currents in some conductive material. Traditionally, as in a mechanical compass, the magnetic field was measured with a magnetised object which could rotate freely. The dominant magnetic force resulted in an unique position of the object, see Fig. 1.5a.



(a) Si (Pointing to) Nan (The south). One of the earliest compasses developed during the Han dynasty (2000 years ago), adapted from [172].

(b) Dip needle for measuring the vertical aspect of the Earth's magnetic field, by W. Wilson, London, (1900), adapted from [36].

Figure 1.5: Historical examples of compass devices

If two magnetometers are constellated orthogonally and both are positioned tangential to the earth's surface, the sensor can be used as a compass. However, to do so, it is necessary that the earth magnetic field is measured exclusively. Disturbances from other magnetic source could cause a deviation in the estimated heading of the magnetic poles.

Nowadays, 3D Hall and AMR magnetometers are widely available since they can be fabricated on tiny footprints by integrating the hall plates or magnetoresistive material in silicon [27]. They have three orthogonal sensitive axes, which make them suitable to measure the field in all directions. That enables us to measure the direction of the magnetic north, which is the horizontal component at that location, as well as the magnetic inclination (or dip) angle, which is the vertical component at that location, see 1.5b.

The output of a 3D magnetometer can be modeled as:

$$\mathbf{y}_m^b = R^{bn} \mathbf{m}^n + \mathbf{b}_m^b + \mathbf{e}_m \quad (1.12)$$

where  $R^{bn}$  is the rotation matrix describing the orientation from navigation to sensor frame,  $\mathbf{m}^n$  the total magnetic field,  $\mathbf{b}_m^b$  a bias, and  $\mathbf{e}_m$  an iid Gaussian noise source.

The total magnetic field  $\mathbf{m}^n$  is composed of the earth magnetic field and any superimposed field. Latter is often unwanted and therefore filtered out using sensor fusion filtering strategies. This will be outlined in the next sections.

However, if the strength of the additional source is known it might be possible to extract position and orientation information of this source. For example, the magnetic field generated by an active magnetic transducer system can be described accurately. This information, possibly with additional inertial information, can be used for the estimation of position and orientation differences between source and receiver [147, 154, 166].

### 1.3.4 Sensor Fusion

Sensor fusion is the foundation for extracting new, or obtaining more reliable, information by fusing different sensor outputs and combining them with knowledge about dynamics or physical relations. Optimal fusion is possible by expressing these different information sources as probabilistic models. Next, the aim is to deduce relevant information, or states  $x$ , from these modelled measurements  $y$ , which is referred to as probabilistic inference.

Within this field, one can distinguish between two common posterior Probability density functions (PDFs), namely a smoothing  $p(x_{1:N}|y_{1:N})$  and a filtering  $p(x_t|y_{1:t})$  distribution. The smoothing PDF provides the desired states,  $x$ , given all measurements,  $y_{1:N}$ , whereas the filtering PDF provides the current state,  $x_t$ , given the measurements up to the current sample  $y_{1:t}$ . The filtering approach is often more interesting as one does not have to wait until all measurements are finished before an estimate can be calculated.

Using Bayes' formula one can write the posterior smoothing distribution as:

$$p(x_{1:N}|y_{1:N}) = \frac{p(y_{1:N}, x_{1:N})}{p(y_{1:N})} = \frac{p(y_{1:N}|x_{1:N})p(x_{1:N})}{p(y_{1:N})} \quad (1.13)$$

where  $p(y_{1:N}|x_{1:N})$ ,  $p(x_{1:N})$  and  $p(y_{1:N})$  are known as the likelihood, prior and measurement distribution respectively.

Maximizing the smoothing distribution gives us the so called point estimate of the state,  $\hat{x}_{1:N}$ , and is referred to as the Maximum A Posteriori (MAP) estimate:

$$\begin{aligned} \hat{x}_{1:N} &= \arg \max_{x_{1:N}} p(x_{1:N}|y_{1:N}) \\ &= \arg \max_{x_{1:N}} p(y_{1:N}|x_{1:N})p(x_{1:N}) \end{aligned} \quad (1.14)$$

In a similar fashion, and applying the Markov property for the conditional densities, one could expand the filtering distribution  $p(x_t|y_{1:t})$  [64]. An analytic closed form solution of the filtering problem exists, under the condition that the PDFs are Gaussian distributed, and is well known as the widely used Kalman filter [64, 84].

### 1.3.5 Sensor fusion for inertial and magnetic sensors

A typical sensor fusion example is the combination of triaxial accelerometer, gyroscope and magnetometer output signals for drift-free estimation of 3D orientations. Such a device is commonly referred to as an **IMMU**, see Fig. 1.4.

As the estimation problems are nonlinear and different parameterizations of the orientation need to be considered, much scientific literature exist in this field [38, 62].

A wide range of products do contain an **IMMU** these days, for example smartphones, controllers for gaming devices, television remotes and virtual headset devices. Moreover, a diverse and ever growing number of applications have embraced inertial sensors and **IMMUs**, including robotics, biomechanics and sports [6, 68, 77]. As a consequence, extensive literature exists on the use of inertial sensors for position and orientation estimation [69, 117, 225]

Chaining multiple **IMMUs** resulted in the development of systems that enable the estimation of anatomical joint angles [112]. Eventually those developments resulted in full body **MoCap** systems which appear to be a full-fledged alternative to traditional optical markers systems, see Fig. 1.6.



(a) Xsens MVN [221]



(b) MotionNode [127]

Figure 1.6: Example inertial sensor **MoCap** systems.

## 1.4 FORCE SENSORS

Tiny force sensors, smaller than one centimeter squared, are widely available and applied in various areas like robotics, rehabilitation, automotive and other industries.

Typically, those sensors have a small measurement range ( $< 10 \text{ N}$ ) and offer a high sensitivity ( $< 1 \cdot 10^{-3} \text{ N}$ ). However, force sensors operating in the desired range of contact forces (up to  $100 \text{ N}$ ) are either too big considering placement on finger tips, or do not offer the sensitivity desired for haptic applications [19].

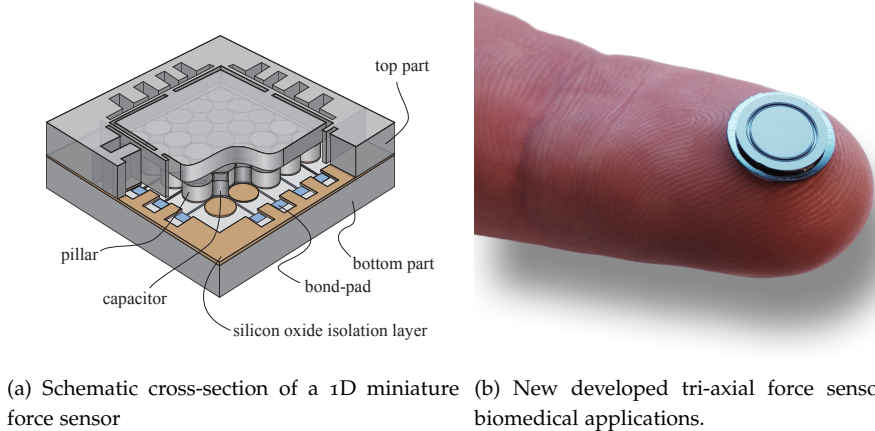


Figure 1.7: [MEMS](#) based multi-axial force sensor for biomedical applications being developed by Brookhuis et.al. [22].

A force sensor requires a spring and a sensing element. Traditionally, two approaches, resistive and capacitive, are used for measuring the deformation of the spring element. Resistive based force sensors use a strain gauge that is directly attached to the spring element. Material deformations due to any applied load results in a strain which the gauge subsequently transforms to an electrical signal. Alternatively, the deflection or distance, between two suspended structures can be measured by capacitive means when each structure is equipped with an electrode. Especially, when a capacitive sensor is fabricated in silicon much freedom to the design process is offered while still accounting for a high measurement range and large sensitivity. Hence, capacitive sensing is favourable over resistive sensing when a small form factor is required and sensitivity in multiple directions is desired.

Brookhuis et.al. developed a new [MEMS](#) based force sensor for biomedical purposes, see Fig. 1.7. The sensor is small and offers a large sensitivity, yet it is able to measure the relatively large contact forces between the human hand and its environment [18].

## 1.5 MOVEMENT AND FORCE SENSING: THE POWERSENSOR

Traditionally, the analysis of human body movements and interaction forces of both feet and hands is performed in instrumented environments. Examples can be found in studies of human performance in sports [73, 82] and physical rehabilitation training [34, 72, 99, 111, 215]. Lumbar loading during lifting has been analyzed using force plates and an optical 3D movement analysis system in combination with biomechanical models [35, 89, 177]. More recently, a combination of Electromyography ([EMG](#)), inertial sensor measurements of

body movements and biomechanical modeling, was proposed for estimating lumbar loading, without actually measuring the mechanical interaction with the load or the ground [87].

Little scientific literature exists on the assessment of the dynamic interactions between the human body and its environment during a specific activity. Research about the power transfer between the human body and its environment has only been performed during restrained movements in a restricted environment, for example, based on a measured crank moment and pedal frequency during cycling [215] or using instrumented ergometers [82].

Power transfer and assessment of dynamic interactions between the human body and the environment, during free movements at arbitrary locations, have to our knowledge, never been assessed by measuring forces and movements at the interface of both. However, assessment of this information is certainly relevant since energy flows between interacting bodies contains information about the dynamical characteristics of both bodies, the synergies between both bodies, and quality of interaction, see Fig. 1.8 [17].

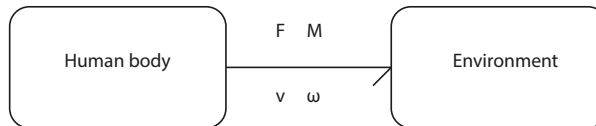


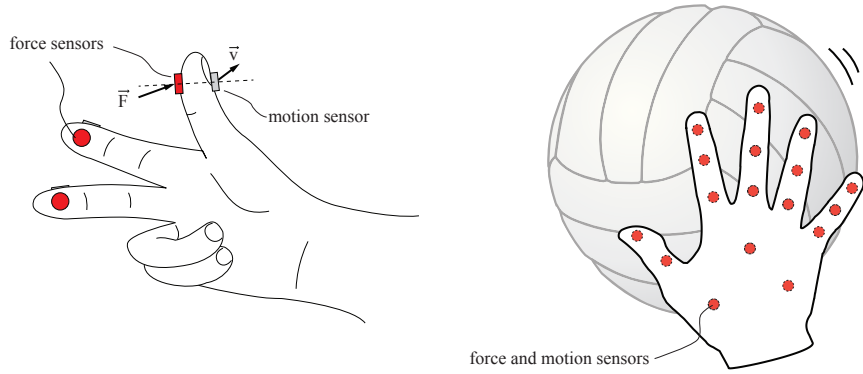
Figure 1.8: A bondgraph description of the dynamic interactions expressed in terms of kinematic and kinetic quantities measured at the interface. Power transfer is described by the product of flow variables force ( $F$ ) and velocity ( $v$ ) and moment ( $M$ ) and angular velocity ( $\omega$ ). The relation between the force and movement entities determine the mechanical impedance.

Particularly, power at any time ( $P_t$ ) transferred between human body and environment, is defined as the product of translational force  $F$  and velocity  $v$  vectors, and the product of moment  $M$  and angular velocity  $\omega$  vectors measured at the interface of contact. This description is mathematically given by the following equation:

$$P_t = F_t^T v_t + M_t^T \omega_t \quad (1.15)$$

Secondly, the coupled dynamics of interacting systems are given by the impedance or admittance and therefore directly relate to force and movement quantities. Hence, signals from a combined force and movement sensor at the contact interface might provide rich information about the dynamic interaction.

The idea of combined force and movement sensing is referred to as 'Power Sensing'. Despite the name, it means the simultaneous measurement of forces and movements of two bodies and information deduced from these quantities which is generally referred to as dynamic interaction. An illustrative drawing of such a 'PowerSensor' attached to the human hand and a glove with a distributed set of 'PowerSensors' embodied in a 'PowerGlove' is depicted in Fig. 1.9.



(a) PowerSensor: combined force and motion sensing. (b) PowerGlove: PowerSensors distributed along the hand and fingers.

Figure 1.9: Conceptual drawings of the PowerSensor (left) and PowerGlove (right), adapted from [22].

Full estimates of force and movement signals would require 3D measurements of translational forces and velocities and rotational torques and angular velocities. In clinical research, the perpendicular component of the interaction forces between body and environment is commonly measured using matrices of pressure sensitive resistors [52]. However, this approach does not provide shear force measurements which are of utmost importance during the manipulation of objects with the hands. So far, no 3D stress sensors are available that could be used at the interface between the human body and the environment, despite studies, that have used either piezoelectric or optical transduction methods [116, 151].

Three dimensional velocity can be adequately estimated from inertial and magnetic sensors placed on the human body. In recent years, many studies have developed methods to derive orientation, velocity, and change of position from such sensors [113, 156, 167].

Recently, combined inertial and force sensing is proposed in the analysis of the ground reaction forces during the stance and swing phase of gait [165, 195, 196]. It should be noted, however, that power transfer has no viable meaning under this condition, since the velocities are approximately zero during stance phase and thus no power is transferred during ambulation.

## 1.6 THE POWERSENSOR PROJECT

The 'PowerSensor' project is initiated at the University of Twente and granted by the 'Stichting Technische Wetenschappen' (STW). It is the objective of the PowerSensor project to develop modalities for quantitative assessment of dynamic interactions in daily life of the human body or robot and its environment. The University of Twente facilitated the project in two research groups, Transducer Science and Technology ([TST](#)) and Biomedical Signals and Systems ([BSS](#)). In addition, various business, research and medical parties were involved.

The realisation of a miniaturised, multi Degrees of Freedom ([DoF](#)), force sensor that could be applied on the hand and fingers was assigned to the [TST](#) group [22]. The [BSS](#) group was responsible for the development of various algorithms that incorporate those force sensors in combination with inertial sensors. Specifically, the development of optimal algorithms to calculate power, work, 3D kinematics (3D acceleration, velocity and position as a function of time), and 3D forces from the signals derived from the PowerSensor and to characterise the dynamics of the interacting bodies [197]. In addition, the [BSS](#) group conducted research in potential applications like rehabilitation and ergonomics [135].

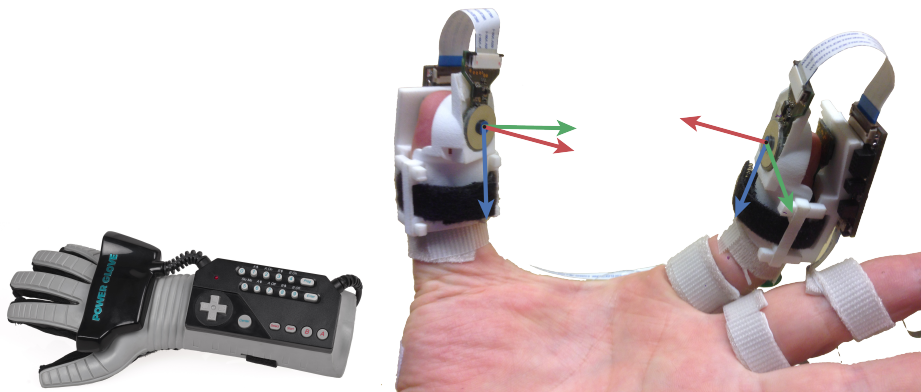


Figure 1.10: The hardware developed in the PowerSensor project contain force sensors on finger and thumb tips and inertial sensors that have been attached to the dorsal side of the index finger, thumb and hand.

Eventually, the development of the PowerSensor, should result in a new but completely different version of Nintendo's 'PowerGlove', see Fig. 1.10b, as the Nintendo version was only able to detect a change of finger joint angles with a resolution of a single bit and had nothing to do with measuring mechanical power. The new system should be able to measure forces and movements in different directions such that the information required for the assessment of 3D dynamic interactions is obtained.

### 1.7 RESEARCH OBJECTIVES

This thesis has two objectives which have been formulated within the PowerSensor project.

1. Develop, evaluate and validate a sensing system that is able to reconstruct the pose, that is position and orientation, of the hand, and the joint angles of fingers and thumb using a non-obtrusive, on-body sensing system.
2. Assess the dynamic interaction between human hand and environment using combined force and movement sensing.

## 1.8 THESIS OUTLINE

Based on the two research objectives, the following chapters are included in this thesis of which each of them will be outlined briefly.

2. **Initial system and algorithm design (published in [97]), related to research objective 1.** This chapter introduces the concepts of measuring hand kinematics using inertial sensors attached to fingers and thumb. Initial non-functional measurements and validations using an optical system are performed.
3. **Comparison with an opto-electronic marker system (published in [192]), related to research objective 1.** The kinematic hardware being developed has been applied to different subjects and tested under various conditions against an optical system.
4. **Simultaneous calibration and pose estimation (submitted), related to research objective 1.** The initial version of the kinematic filters have various drawbacks that have been addressed in this chapter. A general optimization framework has been designed that allowed the estimation of calibration parameters and joint angles simultaneously. In addition, it is able to use movement information to correct for heading drifts.
5. **Hand pose estimation by using a permanent magnet (published in [95]), related to research objective 1.** In various applications it is necessary to have translational position and velocity information of the hand with respect to other body parts. This chapter uses a constellation of magnetometers fused with inertial sensors and a permanent magnet attached to the hand to obtain a drift free position estimate of the hand.
6. **Identification of object dynamics (published in [96]), related to research objective 2.** Ultimately tiny 3 DoF, fingertip size, force sensors were used and applied to the finger and thumb tips. Custom made cuffs were designed to align them with the inertial sensors. This is the first prototype of the powerglove. It demonstrates the possibilities of millimeter size 3 DoF force sensors being attached to a human's hand and serve a sensing layer between the finger tips and an object that can be manipulated. Movement and force information is used to assess the interaction by estimating the object's dynamics.
7. **General discussion.** This final chapter concludes and discusses the results obtained during this project and mentions some future research directions.

1

## Part I

### ASSESSMENT OF HAND AND FINGER KINEMATICS USING INERTIAL AND MAGNETIC SENSORS



## INITIAL SYSTEM AND ALGORITHM DESIGN

### ABSTRACT

Assessment of hand kinematics is important when evaluating hand functioning. Major drawbacks of current sensing glove systems are lack of rotational observability in particular directions, labour intensive calibration methods which are sensitive to wear, and lack of an absolute hand orientation estimate.

We propose an ambulatory system using inertial sensors that can be placed on the hand, fingers and thumb. It allows a full 3D reconstruction of all finger and thumb joints as well as the absolute orientation of the hand. The system was experimentally evaluated for the static accuracy, dynamic range and repeatability.

The RMS position norm difference of the fingertip compared to an optical system was  $5 \pm 0.5$  mm (mean  $\pm$  standard deviation) for flexion-extension and  $12.4 \pm 3.0$  mm for combined flexion-extension abduction-adduction movements of the index finger. The difference between index and thumb tips during a pinching movement was  $6.5 \pm 2.1$  mm. The dynamic range of the sensing system and filter was adequate to reconstruct full 80 degrees movements of the index finger performed at 116 times per minute, which was limited by the range of the gyroscope. Finally, the reliability study showed a mean range difference over five subjects of  $1.1 \pm 0.4$  deg for a flat hand test and  $1.8 \pm 0.6$  deg for a plastic mold clenching test, which is smaller than other reported data gloves.

Compared to existing data gloves, this research showed that inertial and magnetic sensors are of interest for ambulatory analysis of the human hand and finger kinematics in terms of static accuracy, dynamic range and repeatability. It allows for estimation of multi-degree of freedom joint movements using low-cost sensors.

---

Published as:

H. G. Kortier, V. I. Sluiter, D. Roetenberg, and P. H. Veltink, "Assessment of hand kinematics using inertial and magnetic sensors" *J NeuroEngineering Rehabil*, vol. 11, no. 1, p. 70, Apr. 2014. [97]

## 2.1 INTRODUCTION

Analysis of hand kinematics is important in several application areas, such as rehabilitation, sports, ergonomics and animation industry. In particular, ambulatory tracking of the whole hand configuration is valuable for kinematic assessment under daily life conditions. This chapter describes a new kinematic tracking system for the human hand which is based on inertial and magnetic sensors and offers various benefits compared to existing systems.

Current hand capturing systems can be divided into two categories, namely camera-based systems and datagloves.

Camera-based systems either use the contours of the hand or are guided by markers attached to the finger segments. The major drawback of camera based-systems is that the measurements are restricted to the volume in which the cameras are placed. In addition, occlusion of the hand-segments or markers result in a non-observable situation, inducing a poor estimate of the hand pose [48, 179].

Datagloves form a large group of sensing devices that are worn on the hand. They differ in the way kinematic information is obtained. Two popular sensing methods are resistive-bend sensors and optical fiber sensors, with the latter one giving the highest accuracy (< 1 deg), [42].

Disadvantages of both methods are related to sensor placement. Both measure the relative orientation of articulated segments by mounting the sensor across the joint of interest. This requires an accurate alignment of sensors with the particular joint. Often, re-calibration during utilisation is necessary to mitigate estimation errors due to sensor displacements.

A third sensing method used in datagloves is based on local magnetic actuation. Those sensors provide a high resolution without crossing finger joints. However, the cost of such a system rapidly increases as the degrees-of-freedom required increases. In addition, a magnetic actuator is required and manipulating ferromagnetic objects could interfere with the actuation signals [43, 49]. An exception are passive magnetic systems, which are low cost and easy to wear [5, 158]. However, they only allow to estimate a reduced set of kinematic finger variables.

A general disadvantage of datagloves is the lack of user customisation for individual subjects' hands and obstruction of tactile sensing from the palmar surface of the hand. Often this inherently goes with mounting space required for embedding the sensors in clothing.

Inertial and Magnetic Measurement System ([IMMS](#)), containing inertial and magnetic sensors, have proven to be accurate in estimating body segment orientations without the need for external actuators or cameras [152]. The availability of [MEMS](#) technology resulted in tiny and low-cost [IMMS](#) devices that can be implemented in textile clothing easily without impairing the freedom of movement and tactile sensation.

A glove system using accelerometers was presented by Hernandez-Rebollar et.al. [70]. The system uses six dual axis accelerometers placed on the back of

the hand and fingers. It was able to detect different static postures of the hand, which is useful for sign recognition. An extended version using triaxial accelerometers was presented, which was able to recognise more complex postures and simple gestures as well [86]. However heading observation was not examined and only a limited number of joints could be measured independently. Often, existing glove systems have been extended with a single IMMS placed on the back of the hand providing 3D orientation of the hand.

A glove instrumented with multiple IMMS's has never been proposed to our knowledge. We propose a novel data glove that uses inertial combined with magnetic sensors placed on various hand and finger segments which is able to accurately assess full 3D hand and finger kinematics. Multiple Extended Kalman Filters (EKFs) are designed to estimate the optimal orientation trajectories of hand and fingers. Change in hand position can be measured during short movement intervals.

In addition to presenting the instrumented glove, including sensor fusion methods, we evaluate the static accuracy, dynamic range and reproducibility of the system.

## 2.2 METHODS

The kinematics of each finger and thumb are treated individually and calculated using forward kinematics outlined in the next section. Subsequently, four sections exploit an EKF for the calculations of optimal relative finger, and absolute hand kinematics. Finally the experimental methods will be elucidated.

### 2.2.1 Determination of phalangeal joint angles and finger tip position

The articulated finger configuration can be modeled as a kinematic chain, originating from the hand coordinate frame  $\Psi_H$ , see Fig. 2.1. For the left hand this frame is defined by the y-axis pointing to the Metacarpophalangeal (MCP) joint of the middle finger (distal), the x-axis pointing outwards with respect to the back of the palm (dorsal) and the z-axis is defined according the right-handed coordinate frame (radial). The proximal, medial and distal phalanges are modeled as rigid bodies of which the local coordinate frame is defined such that the z-axis is aligned with the functional flexion-extension axis (radial) of the joint and x-axis pointed dorsally. This definition is in accordance with the International Society of Biomechanics (ISB) [217] recommendations with positive angles for flexion (z-axis), abduction (x-axis) and pronation (y-axis).

The position of the finger tip  $\mathbf{p}_E^H$ , expressed in the hand coordinate frame, see Fig. 2.1, can be derived using forward kinematics:

$$\begin{bmatrix} \mathbf{p}_E^H \\ 1 \end{bmatrix} = H^{HP} H^{PM} H^{MD} \begin{bmatrix} \mathbf{p}_E^D \\ 1 \end{bmatrix} = H^{HD} \begin{bmatrix} \mathbf{p}_E^D \\ 1 \end{bmatrix} \quad (2.1)$$

Where, the transformation between two consecutive bodies is expressed by  $H^{HP}$ ,  $H^{PM}$  and  $H^{MD}$ . The superscript denotes the two coordinate frames of which the transformation is described: Hand (H), Proximal (P), Medial (M) and Distal (D). The total transformation  $H^{HD}$  is given by the product of each consecutive contribution:

$$H^{HD} = \begin{bmatrix} R(q^{HD}) & p_D^H \\ 0_3^T & 1 \end{bmatrix} \quad (2.2)$$

where  $R(q^{HD})$  is the orientation of the distal phalanx with respect to the hand, and  $p_D^H$  is the position of the distal frame expressed in the hand frame. The rotation matrix is defined by a unit quaternion, described in the general introduction 1.2, because they require a minimal set of parameters and have some appealing mathematical properties [100].

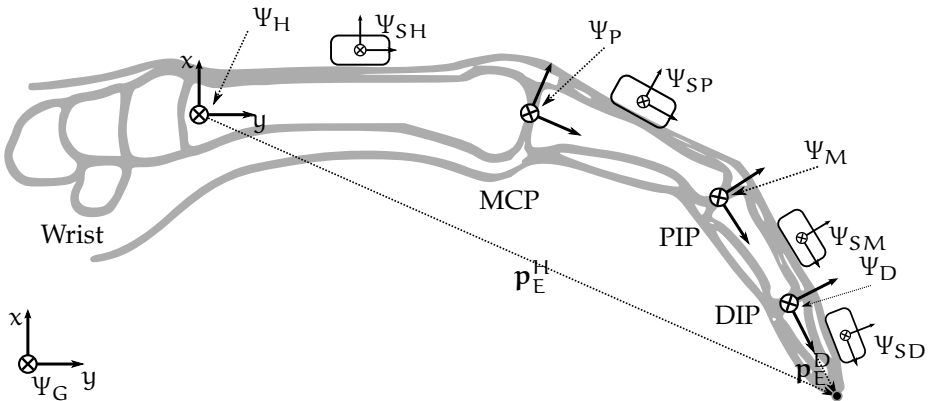


Figure 2.1: Sagittal view of the left index finger. Given are the coordinate frame definitions for hand ( $\Psi_H$ ), proximal ( $\Psi_P$ ), medial ( $\Psi_M$ ), distal ( $\Psi_D$ ) segment, and corresponding joints: Meta Carpal Phalangeal (MCP), Proximal Inter Phalangeal (PIP) and Distal Inter Phalangeal (DIP). To all segments a triaxial gyroscope-accelerometer combination was attached. In addition the hand and distal segment include a magnetometer as well. The coordinate frame of various sensors is indicated with an S placed in front of the letter that indicates the segment. The position of the finger tip  $p_E$  expressed in the hand frame  $\Psi_H$  can be calculated using the joint positions  $p_{ij}$  and relative orientations  $R^{ij}$ , were  $i,j$  are two connected segments. Figure modified from Wu et al. [217].

The relative orientation between two bodies can be obtained by solving the following differential equation [100]:

$$\dot{q}^{ij} = q^{ij} \odot \frac{1}{2} \omega_{ij}^j \quad (2.3)$$

where  $q^{ij}$  is the unit quaternion describing the orientation of frame  $\Psi_j$  with respect to frame  $\Psi_i$ ,  $\odot$  is the quaternion multiplication operator [100], and  $\omega_{ij}^j$  is the relative angular velocity of body  $j$  with respect to  $\Psi_i$  expressed in frame  $\Psi_j$ .

The relative angular velocity  $\omega_{ij}^j$  is obtained by subtracting the absolute angular velocities of two articulated bodies. The angular velocity of a single body is measured using an 3D rate gyroscope, whose output  $y_\Omega$  can be modeled as:

$$y_\Omega^b = \omega_{Gb}^b + b_\Omega^b + e_\Omega \quad (2.4)$$

where  $\omega_{Gb}^b$  is the angular velocity of the body with respect to a global frame expressed in the body frame,  $b_\Omega^b$  a slowly varying sensor bias and  $e_\Omega$  iid white Gaussian noise. Subsequently, the relative angular velocity between two linked bodies ( $i$  and  $j$ ) can be modeled as:

$$\omega_{ij}^j = (y_\Omega^j - b_\Omega^j - e_\Omega^j) - R^{ji} (y_\Omega^i - b_\Omega^i - e_\Omega^i) \quad (2.5)$$

### 2.2.2 Filter design: relative finger orientation

An EKF structure is designed for optimal estimation of phalangeal orientations. The filter operates on the error of the actual state. This method has an excellent reputation in navigation purposes for airplanes and satellites [38] and, more recently, for MEMS based IMMS tracking as well [113, 154, 161, 225]. It is advantageous to ordinary extended Kalman filtering because differences in estimated and true orientation is assumed to be much smaller than the actual orientation difference, which eventually result in a smaller linearization error. In addition, it is an appropriate method to circumvent the constraint in orientation descriptions. We will use the multiplicative error quaternion method [38], where the filter operates on the error quaternion which can be expressed as a non-constrained vector. Parameterization of the true quaternion  $q^{ij}$  by the nominal quaternion  $\bar{q}^{ij}$  and error quaternion  $\delta q$  is given by:

$$q^{ij} = \bar{q}^{ij} \odot \delta q \quad (2.6)$$

Subsequently the error quaternion can be approximated using helical angles  $\delta\theta^{ij}$ :

$$\delta q \approx \begin{bmatrix} 1 & \frac{1}{2}\delta\theta^{ij} \end{bmatrix}^T \quad (2.7)$$

where  $\theta^{ij}$  is the unit vector indicating a rotation axis and  $\delta$  is the magnitude of the rotation around that axis. For each finger and thumb a single EKF is deployed of which the structure is illustrated in Fig. 2.2.

The filter uses a general state space model for dynamics  $x_{k+1}$  and measurements  $y_k$ :

$$x_{k+1} = f(x_k) + v \quad (2.8)$$

$$y_k = h(x_k) + e \quad (2.9)$$

Where  $f(x_k)$  and  $h(x_k)$ , denote the transition and measurement function respectively. Process and measurement noise contributions are given by  $v$  and  $e$ . The state  $x$  is defined as:

$$x = \begin{bmatrix} p_E^H & q^{HP} & q^{PM} & q^{MD} & b_{\Omega,l}^b \end{bmatrix}^T \quad (2.10)$$

where  $p_E^H$  is the finger tip position,  $q^{ij}$  are the relative orientations between phalangeal segments. Because MEMS based rate gyroscopes have a low bias stability which would result in erroneous estimates of the orientation when the gyro output is integrated over long periods, gyro bias ( $b_{\Omega,l}^b, l=1..4$ ) has to be estimated over time, and therefore included in the state vector.

The filter operates on the error state which is defined as:

$$\delta x = \begin{bmatrix} \delta \theta^{HP} & \delta \theta^{PM} & \delta \theta^{MD} & \delta b_{\Omega,l}^b \end{bmatrix}^T \quad (2.11)$$

which include the error angles of various relative orientations and the error bias estimates of gyroscopes.

After state initialisation, the filter is fed with information from various sensors and performs, every iteration, multiple measurement updates, a state update and time update. We distinguish measurement updates from accelerometer and magnetometer, both denoted by  $y_{vector}$  and biomechanical information, denoted by  $y_{biomech}$ .

During each measurement update step, the Kalman gain is calculated and the error state with its covariance is updated according to [64]:

$$K_k = P_k^- H_k^T \left[ H_k P_k^- H_k^T + R_k \right]^{-1} \quad (2.12)$$

$$P_k^+ = [I - K_k H_k] P_k^- \quad (2.13)$$

$$\delta \hat{x}_k^+ = \delta \hat{x}_k^- + K \left[ \delta y - h(\delta x_k^-) \right] \quad (2.14)$$

Where, the minus and plus sign denote the a-priori and a-posteriori estimate respectively,  $H$  denote the linearized (or sensitivity) matrix of the measurement equation  $h(\delta x)$ ,  $I$  is an identity matrix,  $R$  is the measurement covariance corresponding to the measurement uncertainty and  $\delta y$  the difference in estimated and measured sensory input.

During the state update, nominal states are updated accordingly to:

$$\begin{aligned} q_k^{ij} &= \bar{q}_k^{ij} \odot \exp\left(\frac{1}{2} \delta \theta^{ij}\right) \\ b_k &= \bar{b}_k + \delta b \end{aligned} \quad (2.15)$$

where  $\exp$  denotes the quaternion exponential, given in the general introduction 1.8. In addition, the tip position  $p_E^H$  is updated according to equation 2.1.

Finally, during the time update, error states are set to zero and the corresponding covariance  $P$ , is propagated according the discretized process model  $F$  (described in the next section) and process noise  $Q$ .

$$P_{k+1} = F_d P_k F_d^T + Q_d \quad (2.16)$$

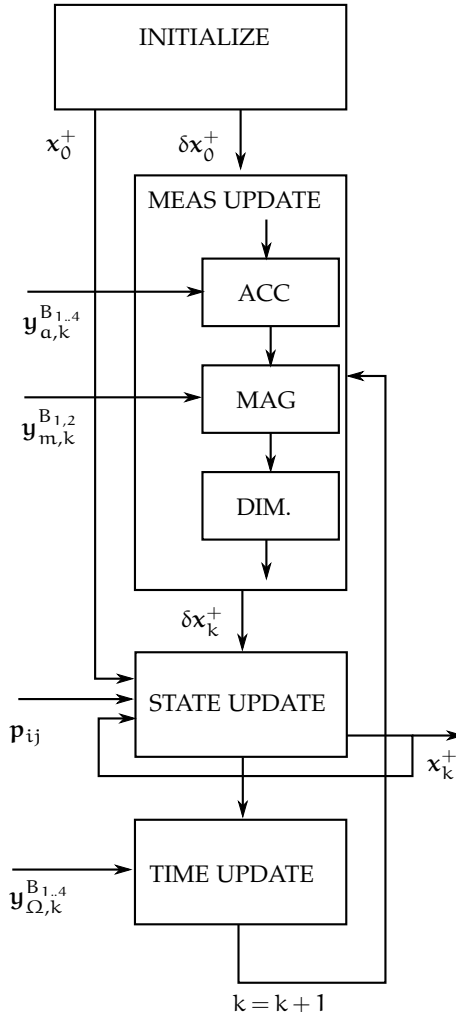


Figure 2.2: Filter topology for each finger. After initialization of both the state  $x$  and error state  $\delta x$ , a measurement update of error states according the measured acceleration and magnetometer signals ( $y_a$ ,  $y_m$ ) and biomechanical dimensionality information (DIM) can be performed. Thereafter states are updated, which are the relative orientations, finger tip positions and gyro bias estimates. Subsequently gyroscope information  $y_\Omega$  is used as an input to perform an update of the process (time update). Finally signals are propagated ( $k = k + 1$ ), and the described procedure is repeated.

#### *Relative orientation filter: Process model*

The estimated angular velocity (see also equation 2.5) is given by :

$$\hat{\omega}_{ij}^j = \left( y_{\Omega}^j - \hat{b}_{\Omega}^j \right) - \hat{R}^{ji} \left( y_{\Omega}^i - \hat{b}_{\Omega}^i \right) \quad (2.17)$$

The true orientation is derived using a rotation matrix approximation of equation 2.6 where the nominal orientation is given by the actual estimate:

$$R^{ij} \approx \hat{R}^{ij} \left[ I + [\delta\theta^{ij}]_{\times} \right] \quad (2.18)$$

where  $[\cdot]_{\times}$  denotes a skew-symmetric matrix. Finally, one can deduce the following equations to describe the error propagation process  $F_d$  (a detailed derivation of the equation is given in the Appendix 2.5):

$$\dot{\delta\theta}^{ij} = -[\hat{\omega}_{ij}^j]_{\times} \delta\theta^{ij} + \delta\omega_{ij}^j \quad (2.19)$$

$$\dot{\delta b}_\Omega = e_b \quad (2.20)$$

using equation 2.5, 2.17 and 2.18 yields the difference angular velocity:

$$\begin{aligned} \delta\omega_{ij}^j &= \omega_{ij}^j - \hat{\omega}_{ij}^j \\ &= \hat{R}^{ji} \left[ y_\Omega^i - b_\Omega^i \right]_{\times} \delta\theta^{ji} \\ &\quad + \hat{R}^{ji} \delta b_\Omega^i - \delta b_\Omega^j - e_\Omega^j + R^{ji} e_\Omega^i \end{aligned} \quad (2.21)$$

and difference in gyro bias with:

$$\delta b = b - \hat{b} \quad (2.22)$$

### 2.2.3 Relative orientation filter: Measurement equations

#### Acceleration and Magnetic field update

Each phalanx contains a 3D accelerometer that provides information of both inclination and experienced inertial acceleration. The output of a 3D accelerometer can be modeled by:

$$\mathbf{y}_a^b = R^{bG}(\mathbf{a}^G - \mathbf{g}^G) + \mathbf{b}_a^b + \mathbf{e}_a \quad (2.23)$$

where  $\mathbf{a}^G$  and  $\mathbf{g}^G$  are the inertial and gravitational acceleration respectively, both expressed in global coordinate frame,  $R^{bG}$  is the orientation from global to body coordinates,  $\mathbf{b}_a^b$  is a slowly varying sensor bias and  $\mathbf{e}_a$  is iid Gaussian noise. The difference in accelerations experienced by two consecutive rigid bodies provides information about the relative orientation. In a pseudo static situation ( $\mathbf{a}^G \approx 0$ ) the difference in inclination can be obtained. During movements the contribution of inertial accelerations is not negligible with respect to the gravitational acceleration. However, if the rotational acceleration part is significantly smaller than the translational part, it is assumed that both bodies undergo the same acceleration. In this particular situation the 3D accelerometer pair might provide both inclination and heading information.

On the hand and finger tips a 3D magnetometer is deployed. The output  $\mathbf{y}_m^b$  can be modeled (in absence of ferromagnetic materials) as

$$\mathbf{y}_m^b = R^{bG}\mathbf{m}^G + \mathbf{e}_m \quad (2.24)$$

where  $\mathbf{m}^G$  is the local static magnetic field, and  $\mathbf{e}_m$  is iid white Gaussian noise. The magnetometer gives information about the heading difference between various bodies.

A general equation for both accelerometer and magnetometer vector outputs  $\mathbf{y}_{\text{vector}}$  is used as a measurement update in our filter. Consider two vectors,  $\mathbf{r}^i$  and  $\mathbf{r}^j$ , which are either an accelerometer or magnetometer output, measured in frame  $\Psi_i$  and  $\Psi_j$  respectively. Now the estimate of  $\mathbf{r}^j$  given in frame  $i$  is determined by the estimated orientation  $\hat{\mathbf{R}}^{ij}$ :

$$\hat{\mathbf{r}}^i = \hat{\mathbf{R}}^{ij}\mathbf{r}^j \quad (2.25)$$

The difference between the true and estimated vector should be related to the error angle  $\delta\theta$  and obtained by equation 2.18 and 2.25:

$$\begin{aligned} \delta\mathbf{y}_{\text{vector}} &= \mathbf{r}^i - \hat{\mathbf{r}}^i \\ &= \hat{\mathbf{R}}^{ij} \left( I_3 + [\delta\theta^{ij}]_{\times} \right) \mathbf{r}^j - \hat{\mathbf{R}}^{ij} \mathbf{r}^j + \mathbf{e}_r \\ &= -\hat{\mathbf{R}}^{ij} [\mathbf{r}^j]_{\times} \delta\theta^{ij} + \mathbf{e}_r \end{aligned} \quad (2.26)$$

Where  $\mathbf{e}_r$  is iid white Gaussian noise of the particular vector measurement.

As being mentioned before, two assumptions according the accelerometer and magnetometer measurements are made:

1. Only inertial accelerations due to translational movements are to be expected
2. The local static magnetic field is homogeneous throughout the whole hand

Obviously these conditions are easily violated during daily life tasks and would therefore deteriorate the kinematic estimates. It is therefore necessary that the validity of relevant signals is tested before being handled by the Kalman filter. A decision algorithm is used that either accepts or rejects accelerometer or magnetometer measurements using the following conditions:

- The absolute difference in magnitude of both the magnetometer and accelerometer output pairs is approximately equal:

$$\left| \left\| \mathbf{y}_{\{a,m\}}^i \right\|_2 - \left\| \mathbf{y}_{\{a,m\}}^j \right\|_2 \right| < \epsilon_a \quad (2.27)$$

- Accelerometer information is only accepted if the angular acceleration is negligible compared to the linear acceleration. This can be tested by the absolute angular velocities of both consecutive bodies which should be significantly small:

$$\left\| \mathbf{y}_\Omega^{\{i,j\}} \right\|_2 < \epsilon_b \quad (2.28)$$

Where  $\epsilon_{a,b}$  are chosen according the desired movement complexity. In addition, the measurement covariance of  $e_r$  can be modified each Kalman iteration such that it scales with the error of above equations.

#### *Joint dimensionality constraint*

In addition to sensory input measurements, biomechanical model constraints imposed by the morphology of the hand are enforced by considering the joint constraint as an artificial measurement. The limited degrees of freedom of phalangeal joints highly constrain the relative orientation between segments. In general pronation-supination is not permitted within all phalangeal joints. In addition, only the MCP joint allows abduction-adduction. The pronation-supination angle ( $\gamma_{MCP}$ ) can be described as the angle between the z-axis of the hand and x-axis of the proximal finger frame minus 90 degrees, which can be modeled as [113]:

$$\gamma_{MCP} = \mathbf{u}_{H_z}^P \cdot \mathbf{u}_{P_x}^H + e_\gamma \quad (2.29)$$

where  $\cdot$  is the inner product operator,  $e_\gamma$  is iid white Gaussian measurement noise, and  $\mathbf{u}$  denotes a unit vector which is projected onto a second body frame:

$$\begin{aligned} \mathbf{u}_{H_z}^P &= \hat{\mathbf{R}}^{PH} \left( \mathbf{I}_3 - \left[ \delta \boldsymbol{\theta}^{HP} \right]_x \right) \mathbf{u}_z, \quad \mathbf{u}_z = \begin{bmatrix} 0 & 0 & 1 \end{bmatrix}^T \\ \mathbf{u}_{P_x}^H &= \hat{\mathbf{R}}^{HP} \left( \mathbf{I}_3 + \left[ \delta \boldsymbol{\theta}^{HP} \right]_x \right) \mathbf{u}_x, \quad \mathbf{u}_x = \begin{bmatrix} 1 & 0 & 0 \end{bmatrix}^T \end{aligned} \quad (2.30)$$

Neglecting the error product terms, and assuming that  $\hat{\gamma}_{MCP} = 0$ , yields the estimated error pronation-supination angle ( $\delta\gamma$ ) as a function of estimated error angles ( $\delta\theta$ ):

$$\begin{aligned}\delta y_{biomech} &= \gamma_{MCP} - \hat{\gamma}_{MCP} \\ &= (\mathbf{u}_{H_z}^P \cdot \mathbf{u}_{P_x}^H) - (\hat{\mathbf{u}}_{H_z}^P \cdot \hat{\mathbf{u}}_{P_x}^H) + e_\gamma \\ &\approx -[\hat{\mathbf{R}}^{PH} \mathbf{u}_z]^T \hat{\mathbf{R}}^{HP} [\delta\theta]_x \mathbf{u}_x + [\hat{\mathbf{R}}^{PH} [\delta\theta]_x \mathbf{u}_z]^T \hat{\mathbf{R}}^{HP} \mathbf{u}_x + e_\gamma \\ &\approx \mathbf{u}_z^T \hat{\mathbf{R}}^{HP} \hat{\mathbf{R}}^{HP} [\mathbf{u}_x]_x \delta\theta - [\mathbf{u}_z]_x \delta\theta]^T \hat{\mathbf{R}}^{HP} \hat{\mathbf{R}}^{HP} \mathbf{u}_x + e_\gamma \\ &\approx \mathbf{u}_z^T \hat{\mathbf{R}}^{HP} \hat{\mathbf{R}}^{HP} [\mathbf{u}_x]_x \delta\theta - \mathbf{u}_x^T \hat{\mathbf{R}}^{PH} \hat{\mathbf{R}}^{PH} [\mathbf{u}_z]_x \delta\theta + e_\gamma \\ &\approx (\mathbf{u}_{H_z}^P \hat{\mathbf{R}}^{HP} [\mathbf{u}_x]_x - \mathbf{u}_{P_x}^H \hat{\mathbf{R}}^{PH} [\mathbf{u}_z]_x) \delta\theta + e_\gamma\end{aligned}\quad (2.31)$$

The finger's Proximal interphalangeal (PIP), Distal interphalangeal (DIP) and thumb's Interphalangeal (IP) joint constraints can be modeled in a similar fashion, only now the abduction-adduction angle  $\beta$  is constrained as well:

$$\begin{aligned}\beta_{PIP} &= \mathbf{u}_{P_y}^M \cdot \mathbf{u}_{M_z}^P + e_\beta ; \quad \gamma_{PIP} = \mathbf{e}_{P_z}^M \cdot \mathbf{u}_{M_z}^P + e_\gamma \\ \beta_{DIP} &= \mathbf{e}_{M_y}^D \cdot \mathbf{u}_{D_x}^M + e_\beta ; \quad \gamma_{DIP} = \mathbf{e}_{M_z}^D \cdot \mathbf{u}_{D_x}^M + e_\gamma\end{aligned}\quad (2.32)$$

#### 2.2.4 Filter design: Absolute hand filter

The absolute hand orientation is calculated in a similar fashion as the relative orientations except that the orientation of the hand is calculated with respect to the global navigation frame  $\Psi_G$ , see Fig. 2.1. An additional Kalman filter derived from Roetenberg *et al.* [152] is exploited to estimate the optimal absolute hand kinematics. The filter state  $[\mathbf{p} \quad \mathbf{v} \quad \delta\theta]$  equations are given by:

$$\begin{aligned}\dot{\mathbf{p}}^G &= \mathbf{v}^G \\ \dot{\mathbf{v}}^G &= \mathbf{R}^{GH} \mathbf{a}^H + \mathbf{g}^G \\ \dot{\delta\theta}^{GH} &= -[\hat{\boldsymbol{\omega}}_{GH}^H]_x \delta\theta^{GH} - \delta\mathbf{b}_\Omega\end{aligned}\quad (2.33)$$

where  $\mathbf{a}^H$  is given by equation 2.23 after rotation from sensor frame  $\Psi_{SH}$  to hand frame  $\Psi_H$ . The position  $\mathbf{p}^G$  and velocity  $\mathbf{v}^G$  are obtained by strapdown integration [15], and  $\boldsymbol{\omega}_{GH}^H$  is the angular velocity of the hand with respect to the global frame expressed in the hand coordinate frame.

Orientation drift is prevented by applying a measurement update using the accelerometer and magnetometer pair positioned on the hand, where the sensor outputs are projected onto the gravitational acceleration and earth magnetic field respectively.

Without additional position information, integration drift immediately occurs. Therefore, the position estimate is only acceptable for a couple of seconds. In order to reduce drifting errors, an additional zero velocity detector

is implemented to detect no-movement situations in which the integrators are set to zero [176].

### 2.2.5 Experimental methods

The instrumentation hardware of the experimental setup is depicted in Fig. 2.3. The system contains multiple strings of flexible-rigid Printed Circuit Board (PCB) which are mounted on the dorsal side of the hand, fingers and thumb using double sided adhesive tape (experiment 1,2,3) or mounted on an polyamide/elastane fabricated glove (Falke) (experiment 4,5). Each string deploys three triaxial gyroscope and accelerometer pairs (ST LSM330DLC), one for each finger or thumb segment. In addition, a triaxial magnetometer (Honeywell HMC5983) is placed on the finger's tip and on the back of the hand. Sensor data is sampled (@200 Hz for the gyroscope and @100 Hz for the accelerometer and magnetometer) by a microcontroller (Atmel XMEGA), collected by a master microcontroller (Atmel XMEGA) and subsequently transmitted via USB to the computer. Online sensor acquisition and filter execution is performed using MATLAB®. Parameters of process and sensor noise distributions is given in Table 2.1.

Table 2.1: Standard deviation values of accelerometer, magnetometer, angular rate, gyro bias stability and biomechanical constraints noise. Given values are determined empirically using allan variances or obtained from datasheets.

	$e_a$ (m/s <sup>2</sup> )	$e_m$ (mG)	$e_\Omega$ (rad/s)	$e_b$ (rad/s)	$e_\gamma$ (deg)	$e_\beta$ (deg)
$\sigma$	$4 \cdot 10^{-2}$	$10^{-3}$	$5 \cdot 10^{-4}$	$10^{-4}$	$10^{-5}$	$10^{-5}$

The medical ethics committee acknowledged that medical ethical approval was not required for all experiments described in the next subsections, because the intent of this study is assessment of the proposed system and not the subject's task performance.

The following subsections describe, first the sensor to segment calibration, and, a study with an optical reference system with one subject (experiments 1,2), subsequently, a second study with one subject without optical reference (experiments 3,4), and finally in a third study the repeatability of the system which was performed by 5 subjects. It should be noted that in all experiment the subject was seated at a table.

#### *Sensor-to-segment calibration*

Assessment of hand and finger kinematics, and thus all described experiments, requires a mapping from sensor coordinate frames to the corresponding segment frames. In this typical calibration problem we seek for the transformation

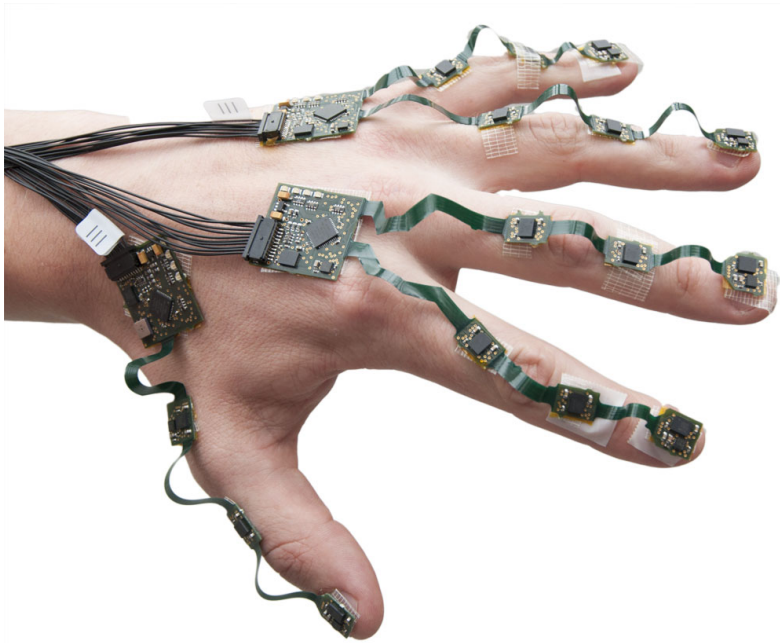


Figure 2.3: Glove hardware consisting of multiple [PCB](#) strings which are attached to each finger segment. Every segment contains a triaxial gyroscope accelerometer pair which are connected using a flexible [PCB](#) structure. In addition, the finger tips and the back of the hand contain a triaxial magnetometer.

matrix from sensor frame to segment body frame. First a coordinate frame should be defined within the particular segment of the hand, which is given in the first methods section. Next, after attachment of the sensor [PCB](#) to the finger segment, one should determine the orientation between both frames, for example between  $\Psi_{SH}$  and  $\Psi_H$ , see Fig. 2.1.

In order to construct this relative orientation, subjects were asked to perform the following procedure:

1. Place the hand on a flat surface with the back of the palm pointing up. This defines the abduction-adduction axis ( $x$ ), given by the accelerometer output:  $e_x^{Seg} = \frac{y_a}{\|y_a\|_2}$
2. Raise the hand and flex the [MCP](#), [PIP](#) and [DIP](#) joint of all fingers. During movement avoid abduction and adduction of the [MCP](#) joint. This defines the flexion-extension axis given by the gyroscope output:  $e_z^{Seg} = \frac{y_\Omega}{\|y_\Omega\|_2}$ .

The sensor to segment orientation is given by:

$$R^{SegSen} = \begin{bmatrix} e_x^{Seg} & (e_z^{Seg} \times e_x^{Seg}) & e_z^{Seg} \end{bmatrix} \quad (2.34)$$

The phalangeal segment lengths  $p_{ij}$  were approximated by first palpation of various joints and subsequently measuring the positions using a ruler. Alterna-

tively or as a first guess, segmental lengths can be estimated using a regression model of the hand and a measure of hand width and length [24], [16].

#### *Finger tip position comparison relative to an optical system*

In the first experiment the accuracy in terms of finger tip position of one subject was analysed. Two tests were performed, in which the subject started and finished with his hand flat on a table top and repeated each movement sequence 10 times with an interval of 1 minute.

In the first test, the subject was asked to repeatedly flex the index finger up to maximum flexion angle of **MCP**, **PIP** and **DIP** joint respectively, while having the arm horizontally stretched such that the back of the hand's palm is directed upwards. The cyclical movement has to be performed five times with a duration of approximately one second.

In a second test, the subject made circular-like movements with an outstretched index finger while the hand maintained a static posture such that the ab-adduction angle of the **MCP** joint was maximised each repetition. Similar to the first test, the cyclical movement was performed five times with a duration of approximately one second.

The estimated finger tip position was compared to the measurement output of an optical tracking system VZ-4000 (PTI VisualEyes). Both hand and index finger were instrumented with active optical markers placed on top of the inertial sensors, see Fig. 2.4. An additional marker was placed on the index finger's tip. The position of the tip is expressed in a common hand coordinate frame defined by the hand markers and aligned with the hand frame of the inertial sensor placed on the hand.

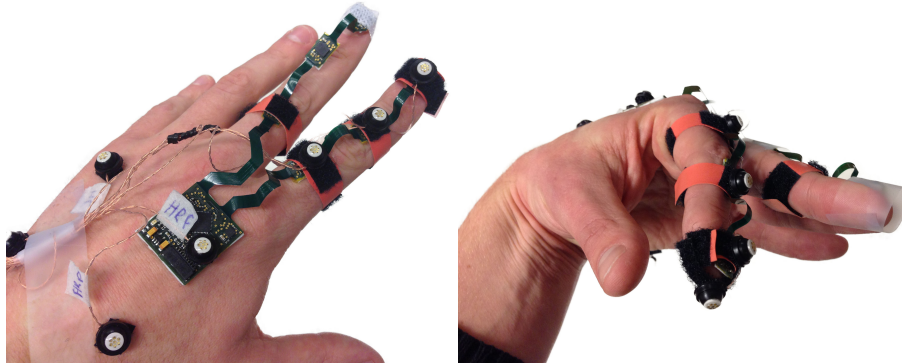


Figure 2.4: Hand and index finger instrumented with both inertial sensors and active optical markers. Four markers on the back of the hand define the hand coordinate frame.

### *Index finger and thumb pinching motion*

During the second experiment, the subject was asked to perform cyclical pinching movements of the thumb and index finger in which the tips of index finger and thumb touched each other at the end of the pinching movement. A spot was drawn on both tips and the subject was asked to coincide the spots during pinching as accurate as possible. The movement was performed 10 times in which each trial contains 10 cyclical pinching motions. The subject kept contact during the touching phase for about one second in which the hand could be oriented in any direction. During the touch phase, the position of both index finger and thumb tip was estimated.

### *Dynamic range*

In order to illustrate the ability to keep track of rapid finger movements a test was performed in which 30 repeated flexion-extension movements with all fingers joints were made. The subject was asked to start with the hand flat on a tabletop, raise the forearm and perform full hand opening and closing movements according to a metronome tempo of 116 BPM. This is the highest rate that can be achieved before clipping of the gyroscope signal (2000 deg/s) occurs. The PIP angle of the index finger was evaluated during the repeated flexion-extension movement. The subject was asked to keep the thumb joints extended such that the range of the PIP joint is constrained by the subject's minimum and maximum PIP flexion angle.

### *Repeatability*

The reliability of the system was assessed by determining the repeatability of the finger joint orientations in a defined hand posture. A standardized data-glove evaluation protocol, proposed by Williams et al [211] and frequently applied to evaluate datagloves [43, 210] was partly adopted. The protocol includes a gripped and flat hand position test respectively. For both tests Williams distinguished between with and without donning and doffing between the measurements. The donning- doffing tests were excluded in our study as the current hardware is not integrated in textile and the non donning-doffing tests mimic the proposed applications sufficiently over a short and long measurement duration.

Five healthy male volunteers, aged 21-53 years, with no known hand disorders participated in this experiment. All tests were performed with the subject's left hand, and depending on the size of the hand, either a small or large instrumentation set was fastened. The difference between a small or large instrumentation set lies only in the length of the flexible PCB structure.

In the first test subjects placed their hand flat on a table top within a designated area. This area is indicated by the contours of the subject's hand and used as a guideline to securely maintain hand position during the flat phase. Then the subjects were asked to raise their hand, flex all finger and thumb

joints, maintain this posture for 6 seconds and finally return back to the flat phase position for 6 seconds. This flexion / flat cycle was repeated 10 times.

The second test comprised a hand posture where a plaster mold was clenched. Prior to the start of the experiment the subjects moulded a heated thermoplastic material (ProtoPlast®) which returned to a solid state upon cooling.

During the experiment the participant clenched the mold for 6 seconds and subsequently released for 6 seconds. This clench/ release cycle was repeated 10 times. Subjects were allowed to maintain the hand in any orientation during the clench phase.

For both tests the subjects were asked to repeat the measurement 10 times, where a pause of 1 minute was included between each measurement.

The repeatability of both tests is indicated by the range and Standard Deviation (*SD*) of all joint angles over all trials and subjects during the flat phase (test 1) and during the clench phase (test 2).

## 2.3 RESULTS

### 2.3.1 Finger tip position comparison

As mentioned in the methods section, two movement conditions were performed and compared to an optical tracking system. Prior to the start of the experiments a required calibration trial was conducted to firstly align the hand coordinate frames of optical and inertial sensors, secondly to obtain the position of the *MCP* joint expressed in the hand coordinate frame and finally to obtain the position of the tip LED expressed in the distal coordinate frame.

On the left, Fig. 2.5 shows the position of the finger tip with respect to the back of the hand for a representative trial of the first experiment where the index finger was flexed and extended repeatedly. The error in tip position is defined as the absolute distance difference between estimated tip position by our inertial sensor system and optically measured tip position. It can be seen that the largest error contribution is caused by an error in the z-direction during maximum flexion (up to 10 mm).

On the right, Fig. 2.5 shows a representative trial for the second movement type where circle shaped movements were performed with the index finger. A large error is mainly visible in the minima of the z-direction which corresponds to the maximum abduction angle of the *MCP* joint.

Table 2.2 shows the RMS differences between both measurement systems of both movement types. Mean and *SD* values over 10 trials are given. The finger tip position correspondence was within  $5.0 \pm 0.5$  mm for the index finger during flexion movements and  $12.4 \pm 3.0$  mm during circle shaped movements. For both movement types the largest contribution of the total error was due to the difference in the z-direction. This is presumably caused by a misalignment of both sensor coordinate frames and the accumulation of errors caused by joint model imperfections and an incorrect estimation of segment lengths.

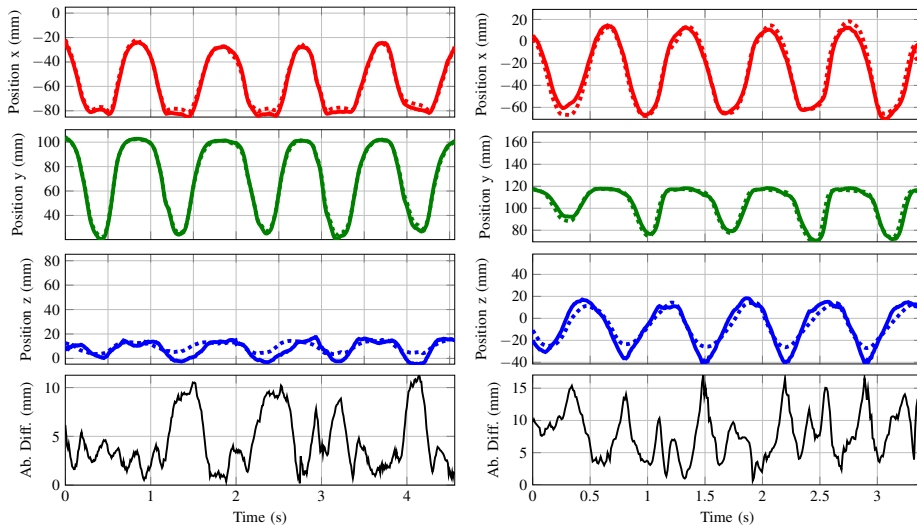


Figure 2.5: Reconstruction of the index finger position ( $x, y, z$ ) during a flexion-extension (left) and circle drawing movement (right) measured by the optical system (solid) and estimated by the inertial sensors (dashed). The lower plots show the absolute index finger tip position difference.

### 2.3.2 Index finger and thumb pinching motion.

In the third, so called pinching test, the distance difference was calculated during each contact phase of the thumb and index finger tips. In order to minimise reconstruction errors due to the rather coarse ball-socket model used for the thumb's Carpometacarpal (CMC) joint, the subject is instructed to avoid rotations of this joint as much as possible. However, this constraint did not hinder the ease of movement. The average RMS distance difference over all pinched movements is  $6.5 \pm 2.1$  mm which is  $3.7 \pm 1.2\%$  of the maximum tip distance difference, obtained during the maximum extension phases.

The average distance displacement of index finger and thumb was  $65.6 \pm 2.2$  mm and  $15.7 \pm 2.5$  mm, respectively.

### 2.3.3 Dynamic range

A representative trial of the rapid flexion motion of the index finger is depicted in Fig. 2.6. Shown are the estimated PIP angle along with the corresponding angular velocities of the index finger.

As can be seen, the total transition time was approximately 0.5 s for a full extension-flexion-extension cycle corresponding to the 116 BPM rate of the metronome. The difference in helical angles between minimum and maximum

Table 2.2: RMS differences in estimated (inertial) and measured (optical) index finger tip position during a flexion/extension movement and during a more complex circle-like movement. Both movement types were repeated 10 times.

	Flexion Extension		Circles	
	mean	std. dev.	mean	std. dev.
$p_{d,x}$ (mm)	2.2	0.4	5.7	2.2
$p_{d,y}$ (mm)	2.0	0.5	4.9	1.3
$p_{d,z}$ (mm)	3.3	0.6	9.7	2.1
$\ p_d\ $ (mm)	5.0	0.5	12.4	3.0

flexion was about 80 degrees, being determined in an independent static trial. Please note that the range of approximately 80 degrees is reconstructed each cycle with the derivative of the angular velocity approaching zero before the movement changes directions in several of the cycles, while the angular velocity stays within the range of the gyroscope (+/- 2000 deg/s). The bandwidth of the filter is apparently large enough to track these fast movements through the whole range.

### 2.3.4 Repeatability

Fig. 2.7 shows two representative reconstructions of one subject during the repeatability tests. On the left figure the flat hand phase is depicted, whereas on the right the flexion phase is depicted. Table 2.3 shows the average range, which is the mean difference between maximum and minimum angle of each trial, and SD of all joint angles during the flat hand phase (test 1) and during the clenching phase (test 2) for each subject. In addition, mean range and SD values over all subjects are listed ( $1.1 \pm 0.4$  deg) and ( $1.8 \pm 0.6$  deg) as well as the mean values obtained from other studies with different data gloves.

## 2.4 DISCUSSION AND CONCLUSION

Small scaled inertial and magnetic sensors combined with a biomechanical model of the hand, embodied in an EKF framework, result in a promising tool to assess 3D kinematics of the human hand in a quantitative manner.

In addition to existing glove systems which are often restricted to measuring a maximum of 2 DoF per joint, full 3D angles can be measured. This allows, for example, assessment of pronation-supination of various MCP joints.

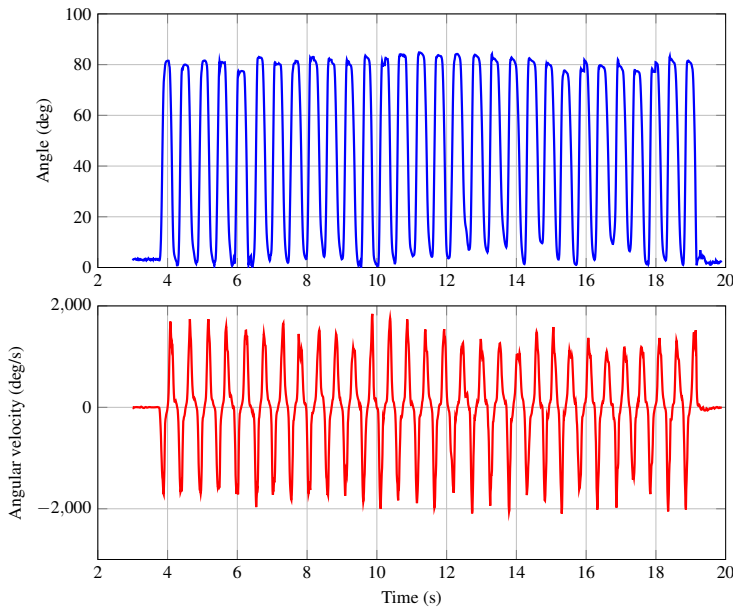


Figure 2.6: Helical angles (upper) and corresponding angular velocity (lower) of the index' PIP joint during 30 repeated flexion-extension movements of one subject.

To our knowledge existing glove systems have only been validated in static situations using repeatability tests described by Williams et al [211]. Assessment of actual tip positions and dynamic range have never been examined but are of great importance when the glove is to be used for daily-life manipulation tasks and therefore have been evaluated as well.

We have observed that the estimation accuracy strongly depends on the sensor to segment calibration procedure. In contrast to our approach, most of the existing data gloves measure across the joints and therefore give an output which is a direct function of the joint's angle. Calibrating such gloves might be easier but also tend to be more error-prone after long utilisation periods, as the sensor's axis should be aligned perfectly with the anthropomorphic joint axis.

The current system requires palpation measurements to determine phalangeal segment lengths and position of MCP joints centres with respect to a common hand reference frame. Accurate determination of functional joint position (MCP) and the axis of rotation (PIP, DIP) would improve the accuracy and decrease time and effort needed for sensor to segment calibration. The current filter can be extended such that those parameters are included and estimated online. In addition, the dominant functional segment axes are found by performing dedicated movements. However, if a certain neuro-muscular patient group may not be able to perform such movements, customized sensor to segment calibration procedures may be required.

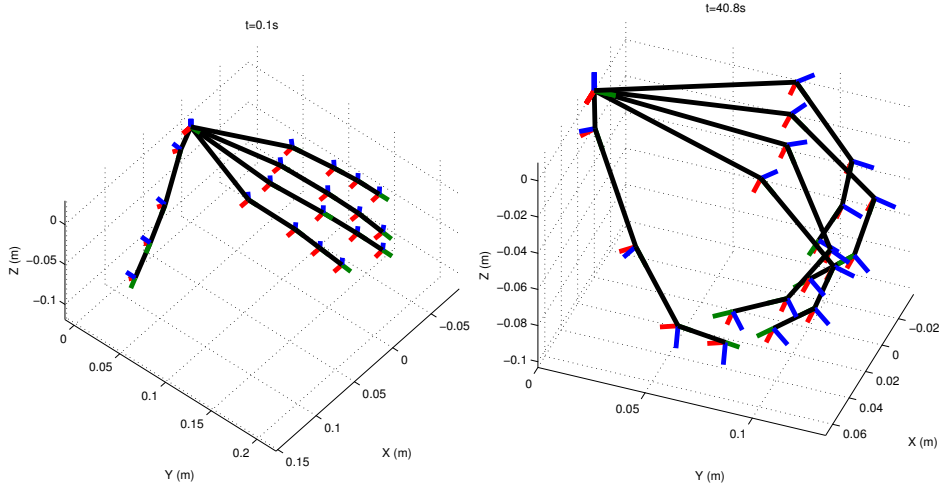


Figure 2.7: Representative hand posture reconstruction for both flat (left) and flexed fingers (right).

Likewise, the optical reference system requires a proper sensor to segment calibration. Independent segment orientation measurements require at least three rigidly connected markers attached to each finger segment. With a specified position accuracy of 0.5 mm RMS, markers should be separated sufficiently ( $> 6$  cm) to obtain an orientation accuracy less than 1 degree. Hence, this is almost impossible to accomplish for each finger segment due to either mounting space, occlusion difficulties or limitation of movement freedom. Therefore, we chose to compare finger tip positions calculated by both systems. However, this approach has a limitation because the error introduced in either the estimated orientation or measured segment length accumulates to an error in the estimated finger tip position, which makes localisation of the exact error source much more challenging. As the largest uncertainty is caused by determination of segment origins we expect that the primary contribution to the position difference is due to misalignments of both measurement systems.

All joints are considered to be perfect ball-socket hinges with 3 DoF. Joint dimensionality is soft-constrained by adding uncertainty to non-natural rotation axes which allows some joint laxity and imperfections. It should be noted that the soft-constrained updates assume that the rotational axes of multi DoF joint are intersecting and orthogonally directed. However, these assumptions are not valid and result in erroneous reconstructions [16]. This is for example visible in Fig. 2.5, where the reconstruction of the index finger position is much worse when the ab-adduction angle is maximal. This could be caused by disregarded pro-supination rotations, non-orthonormal rotation axes, or a translation of the joint's origin. Likewise for the thumb's CMC, a perfect ball

Table 2.3: Results of repeatability analysis. Mean range (difference between maximum and minimum angle during one trial) and SD is given for all joint angles of each subject during the hand flat phase and during clenching of a custom plaster mold. In addition, mean values of this study and mean values from others studies are given.

Subject	Flat Hand		Plaster mold	
	range (deg)	std. dev. (deg)	range (deg)	std. dev. (deg)
1	1.4	0.5	1.9	0.6
2	0.7	0.2	1.9	0.6
3	1.2	0.4	1.8	0.6
4	0.9	0.3	1.8	0.6
5	1.3	0.4	1.7	0.5
Mean Value	1.1	0.4	1.8	0.6
Dataglove Wise et al. [211]	4.5	1.6	6.5	2.6
Humanglove (Dipietro et al. [43])	3.8	1.2	7.5	2.4
Shadow monitor (Simone et al. [175])	1.5	0.5	5.2	1.6
WU glove (Gentner et al. [58])	2.6	0.9	6.1	1.9

socket joint is considered, which is obviously not the case. Mitigating those errors demands improved, and more complex, biomechanical joint models [16, 26]. Adaption of such models is the next step to improve the overall performance.

The described method uses six Kalman filters, one for each finger and one for the hand. This decoupled approach neglects some existing synergies within the hand, which means that not all available and relevant information is used in the model. However, it keeps the filter manageable in terms of computational resources, tuning and prevents unwanted coupling between states due to modeling errors. Alternatively, one could choose for a centralized structure, with one large state vector. This approach allows inclusion of synergies and therefore improve the kinematic estimates. However, the state will have approximately 100 elements and might require alternative, more sophisticated, filtering methods.

The current filter assumes a perfect homogeneous magnetic field throughout the hand. When interacting with ferro-magnetic object this assumption is easily violated. It is therefore necessary to extend the filter such that local magnetic field disturbances are tracked during operation and don not affect

the estimated kinematics. Nevertheless the magnetic field is only required for observability in long static posture periods.

For this study sensors were both mounted directly on the subject's skin as well as on a glove fabricated by an elastic textile. Movement artifacts caused by skin and textile deformations have not been investigated thoroughly. We expect that those artifacts are negligible with respect to errors caused by imperfection of the biomechanical joint model. Moreover, since the applied PCBs are light-weighted and have a flexible structure, visual inspection and feedback from the subjects confirmed that the sensors can be worn unobtrusively without hampering hand and finger movements. Nevertheless, a donning- doffing study should be performed whenever a suitable textile has been selected wherein the sensors can be integrated.

Our repeatability study showed similar (flat hand test) to slightly better (mold test) results compared to existing studies of different dataglove systems. It should be mentioned that those studies only evaluated the sensor variability over time. Simone et al [175], evaluated the "Shadow Monitor" which has a simpler approach and showed a comparable reliability. However, only a reduced set of joint angles could be measured. This is in contrast to our approach where all joint angles were estimated and evaluated using custom filters.

Although the repeatability studies are promising, additional testing of the absolute accuracy using an independent reference system is necessary. These studies should include multiple subjects in which all joint angles should be evaluated, especially during arm movements in which the hand is oriented in different poses.

It is shown in various studies that the accuracy of orientation estimates using inertial sensors is higher than joint orientation estimation shown in this study [154, 161, 225]. Hence, the tracking accuracy of hand kinematics is most probably not limited by inertial sensor accuracy nor the Kalman filter approach.

## CONCLUSION

The first results of our sensing system are favourable compared to existing datagloves. It is able to adequately reconstruct finger tip movements (< 13 mm), high dynamic range (116 full range finger movements per minute) and adequate repeatability (< 2 degrees). This makes the inertial sensor approach promising, especially, when bearing in mind that consumer-grade inertial sensors are getting smaller and less expensive, whereas the quality vastly improves. This study showed the possibilities and challenges to be faced when inertial sensing technology is applied for kinematic analysis of the human hand and fingers.

## 2.5 APPENDIX

### 2.5.1 Derivation error angle dynamics

Derivative of the parameterized orientation:

$$\dot{\hat{q}} = \dot{\hat{q}} \odot \delta q + \dot{\hat{q}} \odot \dot{\delta q} \quad (2.35)$$

gives:

$$\frac{1}{2} q \odot \omega = \frac{1}{2} \dot{\hat{q}} \odot \hat{\omega} \odot \delta q + \dot{\hat{q}} \odot \dot{\delta q} \quad (2.36)$$

rearranging:

$$\dot{\hat{q}} \odot \dot{\delta q} = \frac{1}{2} q \odot \omega - \frac{1}{2} \dot{\hat{q}} \odot \hat{\omega} \odot \delta q \quad (2.37)$$

$$\begin{aligned} 2\dot{\delta q} &= \begin{bmatrix} 0 & \delta\theta \end{bmatrix}^T = (\delta q \odot \omega - \hat{\omega} \odot \delta q) \\ &= \Omega(\omega)\delta q - \Gamma(\hat{\omega})\delta q \\ &= \begin{bmatrix} 0 & -(\omega - \hat{\omega})^T \\ (\omega - \hat{\omega}) & -[\omega + \hat{\omega}]_x \end{bmatrix} \begin{bmatrix} 1 \\ \frac{1}{2}\delta\theta \end{bmatrix} \end{aligned} \quad (2.38)$$

Where  $\Omega(\omega)$  and  $\Gamma(\hat{\omega})$  are the left and right quaternion product operators [100]. Subsequently, by taking the second row and neglecting second order terms gives:

$$\dot{\delta\theta} = -[\hat{\omega}]_x \delta\theta + \delta\omega \quad (2.39)$$

with:

$$\delta\omega = \omega - \hat{\omega} \quad (2.40)$$

Now we can calculate the dynamics originating from angular velocity differences measure:

$$\begin{aligned} \delta\omega_{ij}^j &= \omega_{ij}^j - \hat{\omega}_{ij}^j \\ &= \left[ \left( \mathbf{y}_\Omega^j - \mathbf{b}_\Omega^j - \mathbf{e}_\Omega^j \right) - R^{ji} \left( \mathbf{y}_\Omega^i - \mathbf{b}_\Omega^i - \mathbf{e}_\Omega^i \right) \right] \\ &\quad - \left[ \left( \mathbf{y}_\Omega^j - \hat{\mathbf{b}}_\Omega^j \right) - \hat{R}^{ji} \left( \mathbf{y}_\Omega^i - \hat{\mathbf{b}}_\Omega^i \right) \right] \\ &= -\delta\mathbf{b}_\Omega^j - \mathbf{e}_\Omega^j + R^{ji} \mathbf{e}_\Omega^i - \hat{R}^{ji} \left[ I_3 + [\delta\theta^{ji}]_x \right] \left( \mathbf{y}_\Omega^i - \mathbf{b}_\Omega^i \right) \\ &\quad + \hat{R}^{ji} \left( \mathbf{y}_\Omega^i - \hat{\mathbf{b}}_\Omega^i \right) \\ &= -\delta\mathbf{b}_\Omega^j - \mathbf{e}_\Omega^j + R^{ji} \mathbf{e}_\Omega^i - \hat{R}^{ji} \left[ \delta\theta^{ji} \right]_x \left[ \mathbf{y}_\Omega^i - \mathbf{b}_\Omega^i \right] + \hat{R}^{ji} \delta\mathbf{b}_\Omega^i \\ &= \hat{R}^{ji} \left[ \mathbf{y}_\Omega^i - \mathbf{b}_\Omega^i \right]_x \delta\theta^{ji} + \hat{R}^{ji} \delta\mathbf{b}_\Omega^i - \delta\mathbf{b}_\Omega^j - \mathbf{e}_\Omega^j + R^{ji} \mathbf{e}_\Omega^i \end{aligned} \quad (2.41)$$

Non stationary gyro bias can be modeled by a random walk process:

$$\dot{\mathbf{b}}_{\Omega} = \mathbf{e}_b \quad (2.42)$$

The error bias process is given by:

$$\begin{aligned}\delta \dot{\mathbf{b}}_{\Omega} &= \dot{\mathbf{b}}_{\Omega} - \hat{\dot{\mathbf{b}}}_{\Omega} \\ &= \mathbf{e}_b\end{aligned} \quad (2.43)$$

## COMPARISON WITH AN OPTO-ELECTRONIC MARKER SYSTEM

---

### ABSTRACT

Objective analysis of hand and finger kinematics is important to increase understanding of hand function and to quantify motor symptoms for clinical diagnosis. The aim of this chapter is to compare a new 3D measurement system containing multiple miniature inertial sensors (PowerGlove) with an Optoelectronic (OE) marker system during specific finger tasks in three healthy subjects. Various finger movement tasks were performed: flexion, fast flexion, tapping, hand open/closing, ab/adduction and circular pointing. 3D joint angles of the index finger joints and position of the thumb and index were compared between systems. Median RMS differences of the main joint angles of interest ranged between 3.3 and 8.4 deg. Largest differences were found in fast and circular pointing tasks, mainly in range of motion. Smallest differences for all 3D joint angles were observed in the flexion tasks. For fast finger tapping, the thumb/index amplitude showed a median difference of 15.8 mm. Differences could be explained by skin movement artefacts caused by relative marker movements of the marker system, particularly during fast tasks, large movement accelerations and angular velocities which exceeded the range of the inertial sensors, and by differences in segment calibrations between systems. The PowerGlove is a system that can be of value to measure 3D hand and finger kinematics and positions in an ambulatory setting. The reported differences need to be taken into account when using the system to study hand functioning and quantifying hand motor symptoms in clinical practice.

---

Published as:

J. C. van den Noort, H. G. Kortier, N. V. Beek, D. H. E. J. Veeger, and P. H. Veltink, "Measuring 3D Hand and Finger Kinematics-A Comparison between Inertial Sensing and an Opto-Electronic Marker System" PLoS ONE, vol. 11, no. 11, p. 1-16, 2016. [[192](#)]

### 3.1 INTRODUCTION

The human hand is important in many daily life activities and fine motor tasks. Performance of these tasks can become compromised with age and disease.

With aging, the biomechanical function and neurophysiological characteristics of the extrinsic hand muscles, which are responsible for individual finger coordination, may change and result in less finger-independency and a change in muscle interactions (passive coupling between muscle structures and neural control) [32, 104, 105]. To further increase our understanding of these phenomena, studying the finger-interdependency during various finger movement tasks in healthy young and aged subjects is important [7].

In clinical practice, assessment of hand motor symptoms and performance of hand motor tasks are of relevance in neurodegenerative diseases, such as Parkinson's disease (PD) to assess the neurological state of a patient [50], rheumatoid arthritis of the hand [232], arthritis of the carpometacarpal joint (in the thumb) [140] or evaluation of surgery after e.g. tendon transfer [181]. For this purpose clinicians often use clinical rating scores. However, assessment is highly dependent on experience which makes it hard to interpret the outcomes [142, 149]. An objective and reliable quantification of the hand motor symptoms could improve the clinical scoring to support clinical decision making and objective evaluation of treatment.

Several systems have been developed to measure hand and finger kinematics, such as camera-based marker systems and instrumented gloves (e.g. piezo-resistive bend sensors or optical fiber sensors) [42]. The disadvantages of most of these systems are limited accuracy, need for complex calibration, line of sight problems (OE markers), crosstalk due to misalignment of sensors, poor robustness, or limited usability during functional tasks or in clinical practice [97, 129, 174].

Recently, a measurement system to assess 3D hand and finger kinematics based on multiple miniature inertial and magnetic sensors has been proposed: the PowerGlove [97]. It enables a 3D reconstruction of all finger joints and orientation of the hand by using an extended Kalman filter algorithm that fuses all sensory inputs and a biomechanical hand model. The PowerGlove might enable an accurate measurement of finger dynamics and objective quantification of hand motor symptoms, which are of interest in elderly and patient populations.

To apply the PowerGlove for quantitative functional evaluation of hand and finger coordination, a validation for specific movement tasks is required. Prior evaluations of accuracy have been limited to the index and thumb fingertip-positions during flexion, circular and pinch motions (RMS difference with OE markers: 5.0-12.4 mm), and to repeatability tests for total joint angles in flat and flexed hand position (range difference: 0.7-1.9 deg), in which also a comparison in outcome measures with other data gloves has been made [97]. However, evaluation of the performance of the PowerGlove in a wider range of movements, especially focused on the 3D joint angles of the fingers, is necessary.

The aim of this study is therefore to evaluate the PowerGlove for the accurate measurement of various finger motor tasks in terms of flexion of the **MCP**, **PIP** and **DIP** joints of the index finger and position of the tip of the thumb and index finger. Additionally, index finger ab/adduction movements and circular pointing movements are included to evaluate measurement out of the sagittal plane, i.e. ad/adduction and rotation angles. 3D joint angles and fingertip positions measured with the PowerGlove are compared to kinematic data measured simultaneously with an **OE** marker system, a system that is often used for quantification of movement.

## 3.2 METHODS

### 3.2.1 Subjects

Three healthy subjects participated (age  $29.3 \pm 3.1$  years, BMI  $25.4 \pm 7.4 \text{ kg/m}^2$ ). The experiment was performed at the movement laboratory of the department of Human Movement Science of the VU University Amsterdam, Netherlands. The ethical board of the faculty approved the study protocol. The medical ethical committee of the Medisch Spectrum Twente (Enschede, NL) confirmed that no further ethical approval concerning the Medical Research Involving Human Subjects Act (WMO) was required, due to the nature of the study (technical). Written informed consent was obtained from all participant included in the study.

### 3.2.2 PowerGlove

Eleven inertial sensor units, each containing a 3D gyroscope and a 3D accelerometer (ST LSM330DLC) [97], were attached to the dorsal side of the left hand (2 sensors), on the metacarpal, proximal and distal phalanges of the thumb (3 sensors) and the proximal, middle and distal phalanges of the index (3 sensors) and middle fingers (3 sensors) using small Velcro straps (Fig. 3.1).

An anatomical calibration procedure was performed to determine the sensor-to-segment coordinate systems of the PowerGlove. This calibration procedure included several steps. First, the hand was placed on a flat horizontal surface (i.e. a table) for a few seconds, in such a way that the gravity vector was perpendicular to the palm of the hand, the fingers in neutral position with the phalanges aligned to each other, and the thumb in abduction (without overstretching [60]). Secondly, the thumb was placed on the table for a few seconds with the dorsal side of the thumb and the nail positioned horizontally, in such a way that the gravity direction was perpendicular to the long axis of the thumb. Then, the thumb was flexed three times in the **IP**, followed by three flexions of the finger **MCP** joints (fingers stretched, hand still), and three flexions of all finger joints (**MCP**, **PIP** and **DIP**; hand still). In between each movement the hand was placed on the table. The z-axes of the hand and finger segments were de-

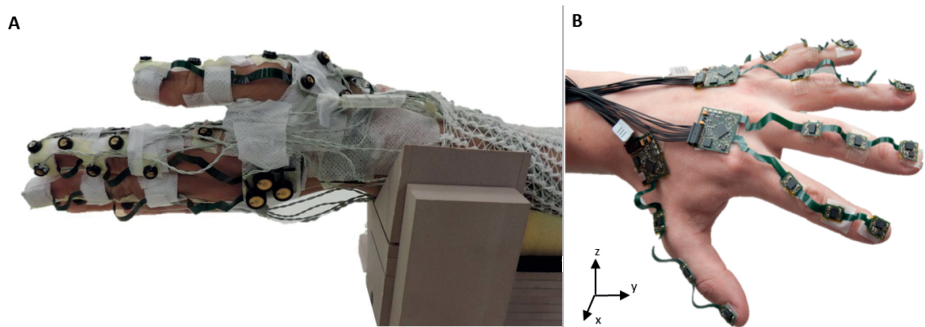


Figure 3.1: Set-up of the validation experiment: 23 OE markers (Optotrak) (A) and 11 inertial sensor units of the PowerGlove [97] (B) were placed on the hand and finger segments of the thumb, index and middle finger. Sensor units on the ring and small fingers were not applied in this study. The arm was placed on a custom-made arm-rest with a palmar position of the hand of 45 deg. The directions of the segment axes are described as: 1) z points dorsally, obtained from static posture on horizontal flat surface, 2) x points radially obtained from flexion movement, 3)  $y = z \times x$ , points distally.

terminated from the static postures of hand and thumb, pointing dorsally. The x-axes were determined from the flexion/extension movements and pointed radially. The y-axis followed from the cross-product of z and x and pointed distally (Fig. 3.1). Finally, the hands were placed together and moved in an eight-shaped movement for five seconds. Angular velocity measured on various hand segments were assumed equal during this movement but measured in different coordinate frames. Relative orientation was deduced, to express the signals of both units on the hand (thumb and index/middle) in a common reference frame [97].

To obtain joint orientations and segment positions from the actual movement trials, data of the PowerGlove were processed in an algorithm (custom-made, MATLAB-based) applying the anatomical segment calibration described above and information from gyroscopes, accelerometers and magnetometers from the movement trials. Primary inputs were angular velocities obtained from the gyroscopes, which were integrated to relative orientations and continuously corrected using biomechanical information (joint constraints in which the joints have limited degrees of freedom), common accelerations and angular velocities, and inclination information obtained from the accelerometers. To determine the positions and orientation of various joints and fingertips forward kinematics were applied using the length of the finger segments of the subjects as additional input. These segment lengths were measured using measurement tape (long fingers: mid of the MCP joint to the PIP joint, PIP to DIP joint, DIP joint to the tip of the finger; thumb: mid of the CMC to the MCP joint, MCP to IP joint, IP joint to tip of the finger) [97].

### 3.2.3 Optoelectronic system

Twenty-three active markers of an **OE** system (Optotrak 3020, Northern Digital Instruments, Canada) were attached to the lower arm (data not used in this study), hand and metacarpal of the thumb (clusters of three markers), and to the proximal, medial and distal phalanges of the index and middle fingers and proximal and distal phalanges of the thumb (Fig. 3.1). For the index and middle finger, markers were placed on the dorsal-radial side of the joints (**MCP**, **PIP**, **DIP** and tip of the finger) aligned in longitudinal finger direction. For the index finger one additional marker was placed on top of the inertial sensor unit resulting in three markers per segment. For the thumb, besides the cluster on the metacarpal, markers were placed on the **MCP** and **IP** joint and on the fingertip.

Small finger segment size and limited space due to the placement of the inertial unit caused the use of three separate markers per segment instead of one rigid cluster with three markers on the phalanges.

To estimate segment coordinate systems for the hand and fingers a few calibration steps were taken comparable to the calibration procedure of the PowerGlove: static hand posture with forearm (mid-pronation) and hand on the table, and a flexion/extension movement in all finger joints. From the static posture, the vertical z-axis was determined for all segments, pointing dorsally. From the flexion movement, the instantaneous helical axis [37, 60] was calculated for each joint (x-axis, pointing radially) (Fig. 3.1). In this way, the anatomical coordinate systems of the **OE** marker system were closest to the anatomical coordinate systems of the PowerGlove, however not measured simultaneously.

### 3.2.4 Protocol

Subjects were asked to perform the finger movements as listed in Table 3.1. During the flexion tasks, the arm was placed on a custom-made arm-rest with a palmar position of the hand of 45 deg for a correct inclination angle necessary for the hand accelerometer unit (Fig. 3.1). Data were recorded with a sample frequency of 100 Hz.

Table 3.1: Finger movement tasks

<b>Flexion tasks (<math>0.5 \pm 0.1</math> Hz; max 0.9 Hz)</b>	
1	MCP flexion of the index finger
2	PIP/DIP flexion of the index finger
3	MCP/PIP/DIP flexion of the index finger
4	MCP flexion of the middle finger
5	PIP/DIP flexion of the middle finger
6	MCP/PIP/DIP flexion of the middle finger
7	MCP flexion of the index and middle finger
8	PIP/DIP flexion of the index finger
9	MCP/PIP/DIP flexion of the index finger
<b>Fast tasks (<math>1.3 \pm 0.9</math> Hz; max 4.2 Hz)</b>	
10	MCP/PIP/DIP fast flexion of the index finger
11	finger tapping with index and thumb without wrist flexion
12	finger tapping with index and thumb with wrist flexion movements
13	hand open/close movements
<b>Ab/adduction task (<math>0.5 \pm 0.0</math> Hz; max 0.5 Hz)</b>	
14	MCP ab/adduction of the index finger
<b>Circular pointing task (<math>1.6 \pm 0.2</math> Hz; max 1.8 Hz)</b>	
15	circular pointing of the index finger (movement in MCP joint)

Similar tasks (1-10) are of importance in the study of finger interdependency in the aging population [7, 104, 226]. Tasks 11-13 are examples of clinical tests in diseases such as PD [50]. Finger ab/adduction and circular pointing (tasks 14 and 15) were included since accurate measurement of ab/adduction and rotation is also important for application of the PowerGlove (i.e. measurement of 3D joint angles).

Most tasks (1-9 and 14) were performed at a movement frequency of 0.5Hz using a metronome. Fast flexion, tapping and hand open/close tasks were performed as fast as possible. Movement velocity of pointing was not instructed. Each task was performed 3 times (i.e. 3 trials), with 10 repetitions within a trial for tasks 1-9, 14 and 15. Tapping and hand open/close tasks were performed for a duration of 30 seconds.

### 3.2.5 Data analysis

To compare the PowerGlove with the **OE** system, 3D angles of the **MCP**, **PIP** and **DIP** joints of the index finger measured with both systems during all tasks as listed in Table 3.1 were analysed. In addition, the position of the tip of the thumb with respect to the tip of the index finger (i.e. an amplitude) was analysed for the finger tapping tasks (tasks 11 and 12). Data of the middle finger could not be analysed due to limited visibility of the markers, but the small movements of the index finger during middle finger flexion were included in the analyses. Rotation matrices describing the relative joint orientations were decomposed in 3D joint angles following the Grood & Suntay sequence (flexion/extension; ab/adduction; exo/endorotation).

Posthoc cross correlation of joint angles and fingertip positions was used to synchronize data of the PowerGlove with data of the **OE** markers. For each joint angle of each task, the Root Mean Square difference (**dRMS**), offset (mean difference), **RMS** minus offset (**dRMS-offset**) and range of motion difference (Range of Motion difference (**dRoM**)) were calculated between the two systems over the **MCP**, **PIP** and **DIP** joint angles. The same outcome parameters were calculated for the amplitude between the thumb and index finger tips.

To explain possible differences between the both systems, additional analyses were performed by evaluation of internal consistency of movement reconstruction. First, relative marker movement of the three **OE** markers with respect to each other on a single finger segment were calculated (distance in mm). These three markers were assumed to represent a rigid body, although not rigidly connected by a cluster due to the limited space on and small size of each finger segment. However, skin movement artefacts or noisy spatial measures due to use of multiple cameras or marker occlusion may have caused slight movements of the markers with respect to each other [159, 178]. This could have affected the coordination system of the rigid body, especially when the markers were placed on small segments. In this study, the markers were placed with a maximal distance of 45 mm (proximal phalanx), 24mm (medial phalanx), and 20mm (distal phalanx). To analyse the effect of marker movement on the segment coordinate systems of those phalanges, a method based on singular value decomposition (SVD, described in [178]) was applied. The relative movement of the markers on the segment was calculated with respect to its starting position (i.e. hand flat), assuming no movement of markers with respect to each other during a movement task (i.e. assuming a rigid body). The new rotation matrix derived from the newly determined marker movements was then compared to the actual rotation matrix derived from the actual marker movements by calculating the angles between the individual axes that were determined by the markers (smallest angle between the vectors), as described in [203] and [60]. The mean marker movements and their effect on segment orientation were calculated for all trials and all index finger tasks, averaged over the three finger segments in all planes.

Second, to quantify errors in the processing algorithm of the PowerGlove [97], angular velocity measured directly by the gyroscope (expressed in segment axes) was compared to angular velocity derived from the relative segment orientation after sensor fusion filters were applied. The  $dRMS$  of the norm of 3D angular velocity was calculated with respect to maximal angular velocity measured for all trials and all tasks, averaged over the three finger segments.

### 3.3 RESULTS

Examples from data of the PowerGlove and the **OE** marker system during the various tasks are shown in Fig. 3.2.

The median  $dRMS$  of the main angles of interest of the index finger ranged between 3.3 and 8.4 deg over all subjects and tasks (Table 3.2 and Fig. 3.3; some movement trials had to be excluded from analysis due to marker occlusion).

Largest differences in the main angles of interest were found in the fast tasks and in the circular pointing task. Smallest differences in the main angles of interest were found during the **MCP** ab/adduction angles of the ab/adduction task (3.3 deg, which is 13% with respect to the total **RoM** of 24.7 deg), however this task showed high differences in exo/endorotation angles (10.6 deg). The **PIP** flexion angle during the fast task showed the smallest difference with respect to the total **RoM**, i.e. 9% (7.7 deg  $dRMS$  and 80.2 deg **RoM** as measured with **OE** marker system (OT)). On average, the smallest differences in 3D joint angles were found in the flexion tasks (1.3-7.3 deg), particularly in subject 2 (Fig. 3.3).

Differences in RMS of the joint angles were mainly caused by a **dRoM**, particularly in the fast tasks. An offset (i.e. a mean difference) >5 deg was observed for the **DIP** flexion angle of the flexion tasks and for the **MCP** ab/adduction angle of the circular pointing task (with a small **RoM** of 26 deg this results in a difference of 21% max **RoM**).

The thumb tip position showed a  $dRMS$  of 15.8 mm, also mainly caused by a difference in **RoM** (Table 3.2, **dRoM** 10.4 mm)

Mean marker movement between the **OE** markers on a segment was largest for the circular pointing task (1.1-8.4 mm) and the fast tasks (1.5-5.3 mm) (Fig. 3.4). This also resulted in the largest effect on segment orientation and joint angles (Fig. 3.3) for these two tasks, particularly for the fast tasks (about 10 deg) in subject 1.

Angular velocity measured directly by the gyroscopes of the PowerGlove showed a median  $dRMS$  below 7% max compared to the angular velocity derived from the segment orientations for all tasks (Fig. 3.5). Largest median difference was found in the pointing task (median 6.8% max), whereas the fast task also showed some individual differences >10% max.

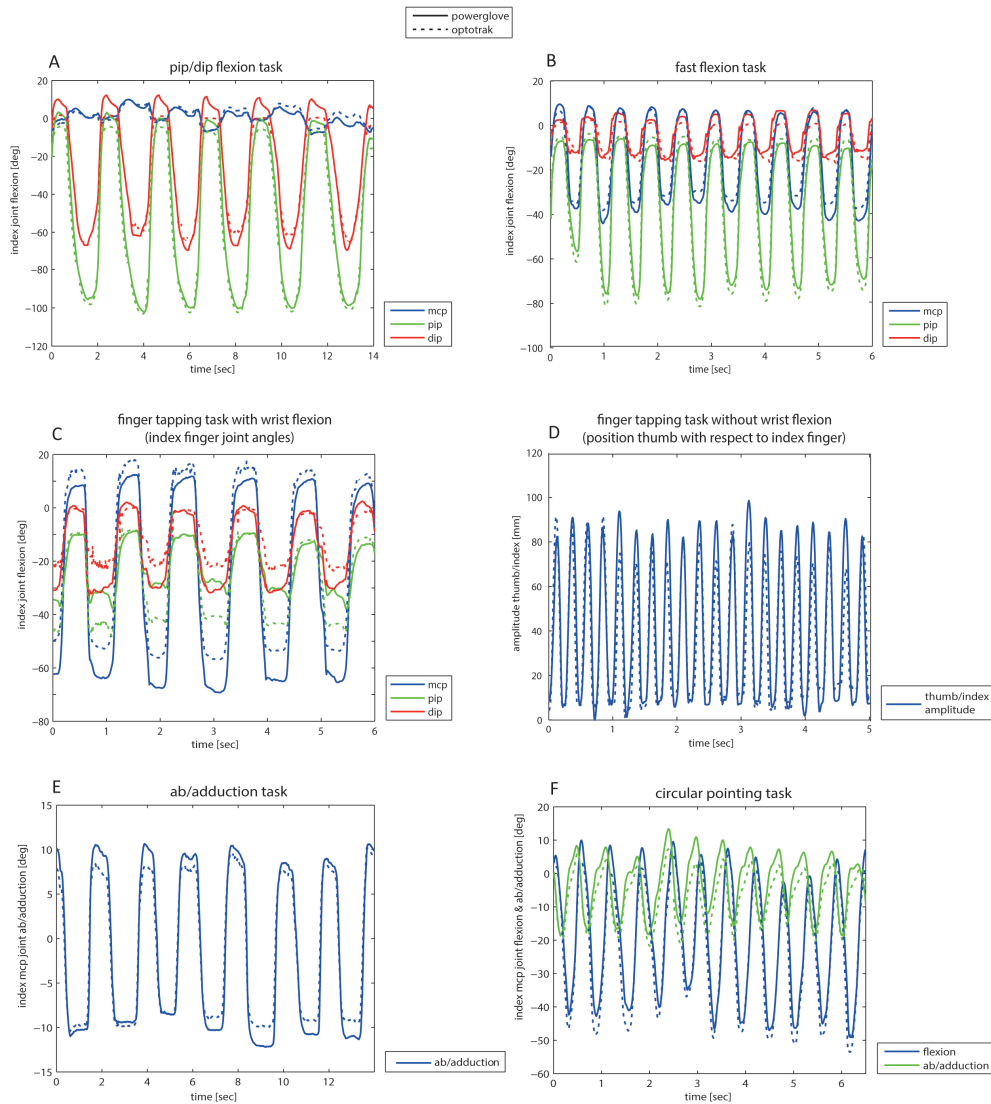


Figure 3.2: Examples of finger kinematics and positions during various finger tasks, measured simultaneously with the PowerGlove (solid lines) and OE markers (Optotak system, dashed lines): (A) index PIP/DIP flexion task with the largest joint flexion in the PIP joint; (B) fast task: index MCP/PIP/DIP flexion task with the largest joint flexion in the PIP joint; (C) thumb/index tapping task with wrist flexion, showing the index finger joint angles with the largest joint flexion in the MCP joint; (D) thumb/index tapping task without wrist flexion, showing the amplitude between the tip of the thumb and index finger; (E) index MCP ab/adduction task, showing the MCP joint ab/adduction angle; and (F) index circular pointing task showing both MCP joint flexion and ab/adduction angles.

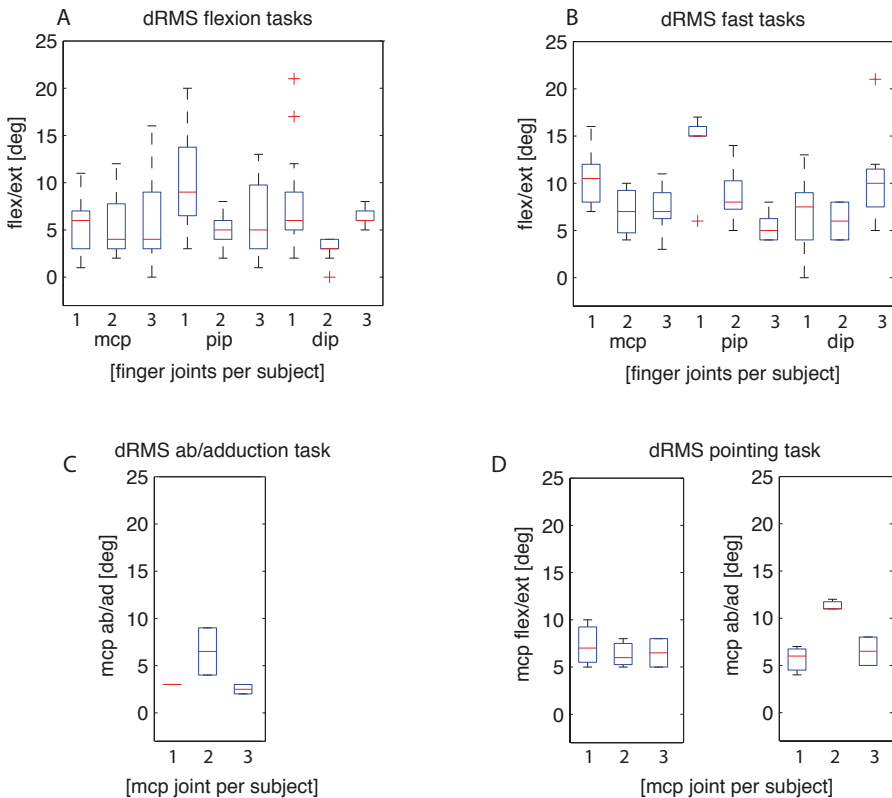


Figure 3.3: Boxplots of dRMS for index finger kinematics (MCP/PIP/DIP joint angles) between the PowerGlove and the OE marker system of all 3 subjects separately per task (1,2,3). Flexion task boxplot includes 15-23 trials per subjects (A), fast task boxplot includes 5-9 trials per subject (B), ab/adduction task boxplot includes 1-2 trials per subject (C) and circular pointing task boxplot includes 2-3 trials per subject (D).

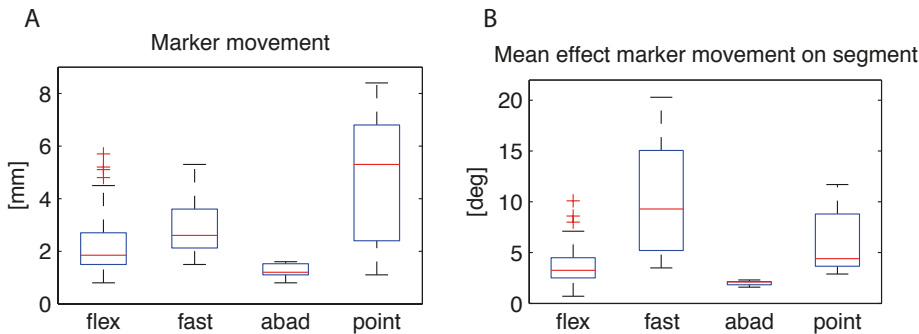


Figure 3.4: Boxplots of dRMS for index finger kinematics (MCP/PIP/DIP joint angles) between the PowerGlove and the OE marker system of all 3 subjects separately per task (1,2,3). Flexion task boxplot includes 15-23 trials per subjects (A), fast task boxplot includes 5-9 trials per subject (B), ab/adduction task boxplot includes 1-2 trials per subject (C) and circular pointing task boxplot includes 2-3 trials per subject (D).

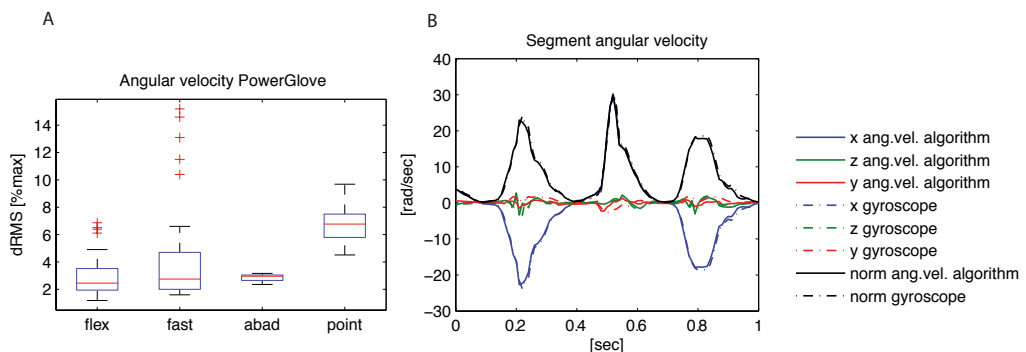


Figure 3.5: dRMS (A) of the norm of angular velocity as measured directly with the gyroscopes of the PowerGlove versus angular velocity determined from the segment orientation derived from the PowerGlove algorithm after processing of the data (expressed as percentage of maximal angular velocity) for the different movement tasks (flex = flexion tasks; fast = fast flexion tasks; abad = ab/adduction task; point = circular pointing task). (B): example of the different signals during a fast flexion task showing good correspondence.

Table 3-2: Outcomes (median and standard deviation) of the comparison of the PowerGlove versus the [OE](#) marker system for the index finger during various finger kinematic tasks and for the thumb tip position with respect to the index fingertip position.

		flexion tasks		fast tasks		ab/adduction tasks		circular pointing task		thumb/index tapping task	
		(54 trials)		(20 trials)		(5 trials)		(8 trials)		(7 trials)	
		MCP	PIP	DIP	MCP	PIP	DIP	MCP	PIP	MCP	Amplitude [mm]
main angles of interest											
$d_{RMSE}$	5.0 (3.3)	7.3 (4.3)	5.6 (3.7)	8.4 (3.2)	7.1 (4.7)	7.7 (4.2)	3.3 (2.8)	6.6 (1.9)	7.5 (2.9)	15.8 (9.2)	
$d_{RMSE}$ -offset	3.2 (3.1)	4.5 (3.2)	2.6 (2.0)	5.1 (2.6)	7.2 (3.4)	6.1 (1.5)	2.6 (0.8)	6.0 (1.8)	5.3 (2.0)	15.6 (4.5)	
offset	-1.1 (6.2)	-3.1 (4.1)	-5.1 (4.9)	0.9 (6.7)	-0.2 (7.6)	-2.0 (7.7)	2.2 (4.2)	1.0 (3.3)	-5.4 (5.6)	-2.8 (12.2)	
$d_{RoM}$	6.6 (5.6)	-4.6 (6.4)	6.6 (5.7)	8.0 (6.9)	-8.7 (6.2)	11.6 (7.3)	2.7 (1.4)	7.6 (7.4)	6.1 (3.0)	10.4 (27.7)	
RoM OT	46.0 (21.4)	62.5 (39.7)	26.0 (21.0)	71.8 (15.2)	80.2 (20.4)	43.6 (19.3)	24.7 (2.8)	61.1 (12.4)	27.6 (3.3)	108.8 (43.5)	
other angles											
	ab/adduction		ab/adduction		flex/extenstion		ab/adduction		flex/extenstion		
$d_{RMSE}$	3.8 (1.5)	1.7 (0.9)	2.7 (1.6)	4.0 (2.5)	3.1 (1.0)	3.3 (2.3)	3.7 (2.6)				
	exo/endorotation		exo/endorotation		exo/endorotation		exo/endorotation		exo/endorotation		
$d_{RMSE}$	2.9 (2.2)	1.6 (1.1)	1.3 (1.1)	4.3 (2.4)	3.2 (1.7)	2.1 (2.9)	10.6 (2.6)		4.8 (2.7)		

Values are expressed as median (standard deviation) in degrees of the joint angles (MCP, PIP and DIP finger joints) and in mm of the thumb/index position

MCP: metacarpophalangeal joint; PIP: proximal interphalangeal joint; DIP: distal interphalangeal joint

$d_{RMSE}$  = difference in root mean square

$d_{RMSE}$ -offset = difference in root mean square minus offset

offset = mean difference over the curve

$d_{RoM}$  = difference in range of motion

RoM OT = range of motion as measured with [OE](#) marker system

### 3.4 DISCUSSION AND CONCLUSION

This chapter compares inertial sensing (the PowerGlove) as an instrument for measurement of various finger movement tasks to an **OE** system. Tasks like these are relevant for the assessment of finger-interdependency in elderly and for assessment of hand motor symptoms in clinical practice. On average **dRMS** between the PowerGlove and an **OE** marker system used as reference system (Optotrak) ranged between 3 and 8 deg. Larger differences observed in fast tasks such as tapping and in circular pointing tasks were mainly expressed in differences in measured range of motion. Therefore, finger kinematics measured by inertial sensing is most comparable to an **OE** system during performance of slow flexion tasks.

To explain the differences, the internal consistency of movement reconstruction of both the **OE** marker system and the PowerGlove have been evaluated. First, an important factor that explains differences between the systems is high relative marker movement (up to 8.4 mm) of markers of the **OE** system on one segment that is assumed to be rigid, causing inaccurate segment orientation measured by the system which is used as a reference [60, 159]. This indicates that the **OE** system has its own limitations. Particularly in fast tasks, skin movement artefacts caused marker movements largely influencing the segment orientation (about 10 deg), which resulted in inaccurately measured joint angles by the **OE** system. Therefore, differences between the PowerGlove and the **OE** system cannot be explained by inaccuracy of the PowerGlove alone. Optimal validation of a movement analysis system would only be possible by measuring the movements of the bones itself, e.g. using fluoroscopy [80]. However, the **OE** system is currently used in many movement laboratories worldwide and a comparison against such a system provides good insight in the performance of the PowerGlove.

Second, by evaluating the internal consistency of movement reconstruction of the PowerGlove algorithm [97], using a comparison of the angular velocity directly measured with the gyroscope and angular velocity obtained from the segment orientation after processing, the highest inconsistency was found for the pointing tasks and fast tasks. Therefore, the PowerGlove also seems to be less accurate for these tasks, although differences were relatively small. Similar to the **OE** marker system, skin movement artefacts might have been present and affecting the orientation of the inertial sensor units. Besides, fast movement may lead to clipping of measured signals of the gyroscopes (i.e. reaching its maximum of 2000 deg/s), which will result in differences in **RoM** and offsets. This is mainly seen in **DIP** flexion angles. Furthermore, in fast movement tasks with large relative angular velocity differences (rapid flexion/extension or tapping), the algorithm does not benefit from any filter correction steps, i.e. estimated orientation does almost completely rely on integration of the gyroscope signals. Integration is started from an estimated initial which can be deteriorated as the static orientation might be partly unknown. Moreover, inclination information from the hand accelerometer, used to update the ori-

entation, could not always be used since the hand was not continuously in a correct inclination angle (i.e. at least 45 deg as supposed using the arm-hand rest (Fig. 3.1)). In circular pointing and ab/adduction, use of joint constraints (biomechanical model imposed by hand morphology [97] including limited degrees of freedom) still allowed measurement of ab/adduction in the MCP joint. Depending on the hand's acceleration, angular velocity and inclination angles of different finger segments, parts of the ab/adduction and flexion/extension angles could be updated.

Third, joint angle estimation is dependent on the anatomical segment calibration. Although the same approach was used for both systems, i.e. use of the helical axis method, a static reference posture and comparable segment axes definitions, data for the anatomical calibrations of the two systems were not simultaneously recorded (due to problems with marker visibility during the PowerGlove calibration). Therefore, differences could have occurred at joint axes orientation. Measurement of finger kinematics by different calibration methods and different systems have been studied in several other papers. However, although inertial sensors have been used in different applications, like clinical gait analysis [133] or upper extremity movements [40, 203], comparisons of performance of inertial sensors with respect to OE markers for measurement of finger kinematics have not been studied previously. A few studies used OE marker systems to evaluate anatomical calibrations for finger kinematics. Coupier et al. [37] showed a deviation up to 4 deg in joint angles between examiners when using the helical axis method, with a higher reproducibility for the MCP and PIP joints than for the DIP joint. Another study showed that different definitions of anatomical coordinate systems (helical axis/functional movement, reference posture and bony landmark based) resulted in total deviations between different segment axes between 14 and 22 deg [60], comparable to the effect we found of relative marker movement in the fast task (Fig. 3.4). The choice of anatomical coordinate system highly affected the ab/adduction and rotation angles of the joints during flexion tasks (mean differences 4-11 deg) [60]. Although we have been using the same definitions of anatomical coordinate systems for both systems, part of the differences in joint angles between systems could be explained by the performance of the segment calibration. For example, the difference in ab/adduction angles during circular pointing tasks in subject 2 (Fig. 3.3) could not be explained by relative marker movement alone, but might have been caused by the segment calibration. A third study used a minimal set of markers (only on hand and distal phalanges of thumb and index) in combination with a mathematical model, to compare MCP, PIP and DIP angles with data obtained from a complete set of markers on all the individual segments [129]. The mean differences they found in joint angles between the two methods (8-17 deg) exceeded the differences we found between the PowerGlove and the OE system.

In addition to joint angles of the index finger, the position of the tip of the thumb with respect to the tip of the index finger was evaluated, expressed as an amplitude, showing a dRMS of 15.8 mm. Previously, a dRMS of 5 mm and

12.4 mm for index finger tip position was reported in respectively flexion and circular pointing tasks [97]. The somewhat larger difference observed for the thumb/index amplitude in our study might be caused by involvement of two fingers with their own position errors summing up. Any differences between the two systems in thumb positions and index positions can be related to the measurement accuracy of the finger segment lengths using measurement tape, needed for the forward kinematics in the data processing of the PowerGlove, biomechanical modelling of the thumb using inertial sensors based on orientation of the CMC joint in combination with the anatomical segment calibration, the fast movement of the thumb and index during tapping reaching the maximum of the range of the gyroscopes, or accuracy of OE marker position measurement and skin movement artefacts. Due to the many degrees of freedom and the skin tissue movement in and around the CMC and MCP joints of the thumb, this finger remains the most difficult to measure using systems that are based on orientation only, like inertial sensor. Whether the reported difference is considered to be large or not depends on the application and measure of interest.

### 3.4.1 Application

The PowerGlove is a system that can be of value for measurement of various finger movement tasks in a variety of conditions and population. In finger movement tasks relevant for the study of finger-interdependency in elderly, small movements that occur in the non-instructed finger(s) are of great interest in addition to large movements in instructed finger(s) [104]. Small and slow flexion movements can be measured accurately by the PowerGlove (Fig. 3.3). Larger differences found (in fast tasks in all subjects and in flexion task in subject 1) can be explained by the relative marker movement during the finger movements, having the largest effect on the segment orientation (Fig. 3.4).

By not having to use a complete lab-based camera set-up with all its limitations like occlusion of markers, the PowerGlove is a flexible 3D measurement system that may facilitate the measurement of finger-interdependency in elderly or the measurement of hand motor symptoms in clinical practice very well. In particular in PD patients, the evaluation of tasks like finger tapping are part of the neurological exam in which for example the thumb/index amplitude and the MCP joint angles are important [50], whereas finger interdependency can be studied using finger flexion tasks with a focus on all three finger joints [7]. Objective measurements can be easily performed at home, in the hospital or even in the operating room.

For interpretation of the PowerGlove data in assessment of hand motor function the results as reported in this chapter need to be taken into account. Furthermore, one needs to be aware of the optimal condition of application of the PowerGlove, such as a correct inclination angle of the hand for orientation estimated from the acceleration, or change in movement to optimally use the gyroscopes [97].

### 3.4.2 Limitations of the study

The current study concerned a technical assessment of the performance of the PowerGlove in comparison to the conventional [OE](#) marker system. Therefore, in our opinion the three subjects included were sufficient to draw conclusions, since inter-subject differences are of less importance. Even, the evaluation could have been performed in only one subject such as has been done in other finger kinematic studies comparing systems or methods [37, 60, 97]. In addition, the variety of tasks show a wide range of applications of the PowerGlove. However, the multiple subjects show that performance of anatomical calibration, an individual procedure, might affect the accuracy of the results.

In this study we were not able to analyse the movement of the middle finger due to marker occlusion problems. During the measurement, three cameras were used to track the markers, however due to the hand position and the index finger being in the way, the middle finger could not be tracked very well. Using more cameras or a different marker set-up with e.g. small tripods with markers on the finger segments might have overcome the occlusion problem, although the latter could have impeded the finger movements. It could be expected though that measurement of the middle finger movement with the PowerGlove is comparable to the index finger, since a similar set-up and calibration of inertial sensor units is applied.

In literature, the CyberGlove (piezo-resistive technology) [42, 85], WU-glove [58] and NeuroAssess Glove [136] (resistive bend sensors) are considered as accurate instrumented glove systems currently available, although calibration and fitting do influence the accuracy [42]. A direct comparison between those systems and the PowerGlove for the specific movement tasks included in this study could not been made, since these systems were currently not available for the authors and results on measurement of 3D angles per each individual joint were hard to find in literature. Previously, repeatability outcomes for total joint angles (i.e. sum of individual joint angles) in flat and flexed hand position have been reported [97], showing a similar or better repeatability for the PowerGlove.

## CONCLUSION

Median differences in finger joint angles between the inertial sensor units (PowerGlove) and an [OE](#) marker system ranged between 3 and 8 deg. Smallest differences were observed in the flexion tasks. Larger differences observed in fast tasks such as tapping and circular pointing tasks were mainly differences in measured range of motion, due to skin movement artefacts caused by relative marker movements of the [OE](#) marker system, high velocity of the movement which exceeded the range of the inertial sensors or differences in segment calibrations between systems. For fast finger tapping, the thumb/index amplitude showed a median difference of 15.8 mm.

The PowerGlove is a system that can be of value for measurement of various finger movement tasks in a variety of conditions and population in an ambulatory setting. For interpretation of the PowerGlove data in assessment of hand motor function the results as reported in this chapter need to be taken into account.

4

## SIMULTANEOUS CALIBRATION AND POSE ESTIMATION

### ABSTRACT

Inertial sensors have shown to be a proven technology for human motion capture. Their size, cost and accuracy led to the development of many algorithms for the estimation of orientation and position of body parts. However, most of the approaches still suffer from typical problems inherent to inertial sensors. Among them is the heading estimation which requires additional sensory modalities like magnetometers, and the calibration of both intrinsic sensor parameters as well as the sensor to segment parameters. We propose a new method to solve both problems using a comprehensive stochastic optimization framework. The method assumes a kinematic chain like the human hand and fingers and makes use of the constraints available. Writing the sensor and kinematic models with corresponding uncertainties also allows for the inclusion of errors due to skin artifacts and joint imperfections. We repeatedly tested the method on an artificial finger setup. The average differences between estimated sensor to segment positions and a reference measurements were found to be  $0.8 \pm 2.0\%$ ,  $-0.4 \pm 7.0\%$ ,  $0.0 \pm 4.3\%$ ,  $-1.4 \pm 3.4\%$  for hand, index, medial and distal segment respectively. Good visual agreements were found for the sensor to segment orientations. Other estimated parameter values include sensor biases and proximal and medial segment lengths. In addition, the pose, which is relative segment orientations and positions, was estimated over time. Finally, we tested the method on the humans index and middle finger during arbitrary hand and finger movements. Good correspondence was visible for the estimated segments lengths compared to manual measurements, and the relative orientation of the sensors to underlying skeletal structure. The proposed method has therefore high potential for the automatization of calibration tasks related to inertial motion capturing and as an offline motion capturing system using only 3D gyroscope and accelerometers.

Submitted (2017) as: "Assessing hand kinematics using inertial sensors: Simultaneous calibration and pose estimation"

#### 4.1 INTRODUCTION

Capturing human body motions is of wide interest in application areas, such as rehabilitation, sports and the entertainment industry. Traditionally, body motions are measured using environmental sensors which are often based on optical principles [125].

With increasing popularity inertial sensors are used to capture body motions. These, small sized and light weighted sensors, especially when fabricated in **MEMS**, can be attached to the skin or integrated in textile clothing enabling on-body measurements. A major advantage is that such measurement systems operate in a self-contained manner. There is no need for environmental sensors, which avoids line-of-sight problems and enables measurements at any place outside instrumented environments.

Inertial sensors measure the 3D angular velocity (gyroscope) and 3D acceleration (accelerometer) expressed in the sensors' coordinate frames. Integration of angular velocity yields the change in orientation. The accelerometer measures the sum of gravitational, which is commonly used to estimate part of the orientation, and inertial accelerations. The former is known in the global reference frame and can be used as an absolute reference for the inclination. Often those sensors are combined with a 3D magnetic sensor for an estimate of the sensors' heading with respect to the earth magnetic field. Each sensor has its own imperfections but the individual sensors are complementary to each other. By processing these inertial and magnetic signals using a proper fusion algorithm, one can obtain a full 3 DoF drift free orientation estimate. Such sensors are widely known as an inertial and magnetic measurement unit (**IMU** or **IMMU**) and resulted in many scientific publications in which a large variety of estimation algorithms are described [51, 152, 161, 225].

By placing various **IMUs** on articulated body parts and transforming the sensor orientations to body segment orientations using a proper calibration method yields the relative orientation or angles between body limbs [113].

Not only for estimating human body postures but also in robotics, **IMUs** have been widely adopted. Kinematic linkages within mechatronic systems are known a-priori and allow for improved estimation of the end-effector's pose and sensor to segment calibration [9, 10, 137, 189].

Popular, yet relatively easy, full body sensor to segment calibration procedures include the N-pose and T-pose [156]. Those procedures use the static accelerometer and magnetometer readings as a reference and combine the signals with a predefined biomechanical model. These methods are prone to errors since the possibly distorted static measurements of the accelerometer and magnetometer are directly used to determine the calibration.

However, it is possible to find the position and direction of joint rotation axes by performing predefined rotations around functional rotation axes. Unfortunately, this is often a long and difficult procedure that requires the involvement of a movement specialist.

If sensor to segment orientations and lengths are known for articulated segments one could apply forward kinematics to obtain the pose of the total kinematic body structure at any time [143, 156]. Such systems are also known as MoCap system but do intrinsically not offer an absolute position with respect to an inertial frame as a camera based MoCap system would do. In addition, errors in the orientation estimates of individual sensors directly affect the segment orientation yielding inconsistent performance.

The accuracy of commercial motion capture and MoCap systems is tested in various studies in which the estimated pose trajectory is compared to an optical reference system [227]. Several factors limit the accuracy of commonly used MoCap systems which will be described below.

First, during indoor usage the earth magnetic field is disturbed by the vicinity of metallic structures. Often the field deflections can be detected in time and mitigated on short time intervals by some filtering means [108, 152]. However, long term disturbances cause heading drifting effects that eventually result in erroneous limb orientation estimates.

Second, estimates of joint rotations and end-effector positions require an accurate model of both segments and joints. Segmental lengths can be estimated by regressing on repeated measures of a similar subject group or measured directly by palpating bony landmarks. The former method is often inaccurate whereas the second approach is very time consuming. Single DoF anatomical joints can be modeled accurately but for multi DoF joints this is much more cumbersome due to the anatomical imperfections of human joints. The most, mathematically sound, convenient way to model these joints is a ball / socket joint. Methods have been developed to extract this information from raw accelerometer and gyroscope signals [163, 170, 171]. However, joints within the human body can often not be described by simple, mathematically sound, joints like hinges or ball-socket joints. This especially holds, for example, for the shoulder joint and CMC thumb joint of which the rotational freedoms are a function of a certain displacement of the rotation axes.

Third, placing sensors on soft tissue layers causes difficulties in reconstructing the underlying skeletal pose, because it deforms whenever the skeletal pose is changing. In various studies, the influence of position and orientation errors, or in general, sensor to segment calibration errors is addressed with respect to the estimated pose [124, 231].

Instead of modeling joint kinematics as a function of the measured data, one could choose for a much weaker assumption in which the measured data is a function of all unknown parameters and state variables of the applied kinematic model. This allows state and parameter estimation of more complex, non-linear, models in which the error sources cannot be assumed to be additive noise.

Todorov proposed such a probabilistic framework for estimation of human body kinematics using goniosensors and optical markers [185]. A generative model based on the residuals measured by orientation and position sensors attached to an articulated body chain was presented. This general approach has

the appealing property of including biomechanical constraints and allows for simultaneously estimating states variables such as joint angles and estimating model parameters such as joint locations and sensor positions. An EKF is used as an optimal filtering method to estimate the time varying parameters. Gabiccini et.al. modified this approach to handle non-linearities and Gaussian noise sources more accurately [57]. Subsequently, Wu et.al. improved this approach by alternating between estimating states and parameters and using an numerical optimisation algorithm [219]. Now, updating the state prediction is not only restricted to a single point in time but spans an arbitrary time window. This approach is less prone to divergence of the iterative estimation method, either occurring due to a bad initial estimate or the inclusion of erroneous measurements over a long time.

Kok et.al. developed a new optimization framework which is similar as the inference framework from Wu et.al. but now applied to an inertial sensor system, which has appealing properties regarding the avoidance of diverging problems and badly chosen initials [90].

The computational complexity of solving such problems grows both with measurement length and with the number of sensors and body segments considered. In a follow up article, Kok et.al. presented a scalable and distributed solution to this problem by exploiting the structure that is inherent in the problem [93]. This strategy would eventually allow for the development of online estimators. Similarly, Taetz et. al. [182] focused on estimating the parameters, simultaneously with the states using a sliding window Weighted Least Squares (WLS) optimization. Besides inertial sensor information, they included various information sources, like segment lengths, body shapes and joint ranges, as part of the cost function that is to be optimized.

In our previous study we developed a new hand and finger tracking system using inertial and magnetic sensors. The estimation algorithm assumes coupled segments by ball-socket joints. Using an a-priori sensor to segment calibration it was possible to apply forward kinematics to derive the position of finger tips with respect to the hand [97]. In a follow up study, the system and accommodating methods were applied to a larger subject pool and evaluated against an optical reference system [192]. Positional differences up to several millimeters were measured. However, the errors encountered could not be appointed solely to the inertial sensing system but also the optical reference method.

Various studies have shown the potential of including kinematic constraints to improve pose estimations using IMUs. Such aiding information makes the magnetometer superfluous for heading information [44, 153, 223], can be used to mitigate sensory drift [208] and does not require alignment and calibration procedures beforehand [128].

The objective of this chapter is to derive an optimization framework for the estimation of finger joint variables, the underlying biomechanical model parameters and the parameters of inertial sensors being attached to the skin of a finger.

Finger tracking systems based on inertial sensor measurements have gained popularity over the last years due to the small footprint of these sensors. Another trend can be found in tracking methods based on computer vision. This field is primarily focused on sensing devices that are not strapped to the human hand or arm but placed somewhere close to the subject's working environment. The quality of depth cameras, increasing processing power and accessibility of machine learning principles resulted in an enormous burst of publication in this field [173, 184].

This chapter follows the ideas and propositions as mentioned in Todorov [185], Kok [90] and Taetz [182]. Therefore, it pursues the descriptions that can be found in those articles. However, our method differs from those, in the sense that all biomechanical unknowns, which are the sensor to segments poses and segmental lengths, are included as estimation parameters and assumed to be unknown a-priori. In addition, the biases of gyroscopes and accelerometers have been added as unknown parameters.

Inclusion of various parameters in a single framework avoids the need for different explicit calibration procedures, and hence, improves the general system utilization and reduces the risk of incorrect calibrations.

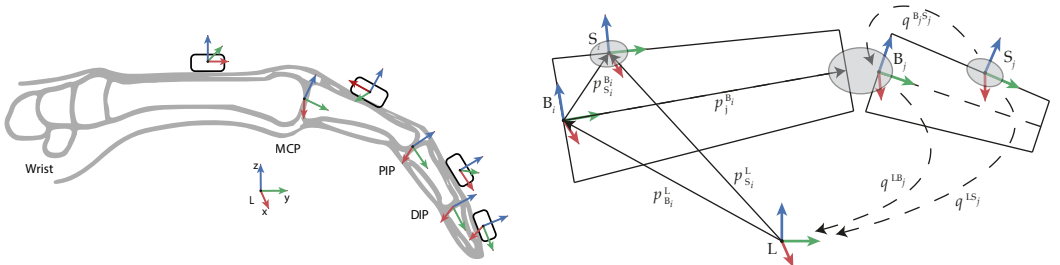
Another difference is the way segment connections enter the cost function. We do not include constraints in the cost formulation which gives the ability to use, more matured, unconstrained WLS solvers. Finally, the method is tested on the human hand and finger and therefore assumes no zero velocity points which can be applied to the feet during stance for example.

The proposed hardware and methods should eventually result in an plug-and-play glove that can be used for the assessment of hand and finger kinematics which does not require manual, often tedious and inaccurate, calibrations procedures before conducting the pose estimation measurements. Furthermore, by exploiting joint accelerations and angular velocities of segments, relative heading information can be extracted. Therefore, magnetometers can be excluded from the system, which is desirable as hands often handle magnetic objects.

Several aspects have to be considered to reach the goal of this chapter:

- Express a biomechanical model of the human finger that contains 4 segments which are, soft, connected via one 2 DoF joint (MCP) and two single DoF (PIP/DIP) joints.
- Derive a measurement model of various 3D accelerometers and gyroscopes which are placed on different finger segments.
- Derive an offline parameter and state estimator by fusing the biomechanical (process) model with inertial sensor measurements.

This chapter is structured as follows. First, in the method section, the optimization framework is introduced. Next, various models will be outlined which eventually results a general cost function that is to be optimized for all variables. Subsequently, in the experimental method and results sections two experimental setups are introduced and used to evaluate the proposed method. The setup is a 3D printed artificial finger of which the segmental



(a) Four rigid bodies illustrating the phalanges (metacarpal, proximal, medial and distal) of one finger. The origin and coordinate frame of each rigid segment is indicated by  $B_{\{i,j\}}$ . The IMU was attached of which its position is indicated by  $p_{S_{\{i,j\}}}$  and orientation by  $q_{S_{\{i,j\}}}^{B_{\{i,j\}}}$ . The global reference frame is indicated by  $L$ . Various positions ( $p$ ) and orientations ( $q$ ) are indicated. The uncertainty of the joint connection, as well as to sensor to segment calibrations, are indicated with grey areas.

Figure 4.1: Schematic illustrations of the biomechanical finger model in which all relevant variables are indicated.

lengths and sensor to segment positions are known. In a second setting the sensors are applied to a human index and middle finger. The chapter ends with the conclusion and some remarks for discussion.

## 4.2 METHOD

Figure 4.1 illustrates the inertial sensor hardware attached to a human finger. The left figure shows the positions of the sensors and the origins of the segment coordinate frames. Segment coordinate frames are defined such as they are displayed, the y-axis pointing along the segment's bone in the direction of the tip, and z-axis upwards and perpendicular to the y-axis. The sensors can be placed at an arbitrary position. Because the footprint of the PCB is relatively flat it is assumed that the sensor's z-axis, which is directed orthogonally to the PCB footprint, is directed perpendicular with respect to the underlying and longitudinally directed segment's y-axis. In the right figure, two rigid bodies,  $\{B_i, B_j\} \in \mathbb{B}$ , are displayed which corresponds to the articulation of two finger segments. It is assumed that the entire kinematic chain, as depicted on the left, consists of multiple articulations and can be translated and rotated with respect to a global reference frame ( $L$ ).

Each rigid body contains an IMU sensor (3D gyroscope and 3D accelerometer),  $S_i \in S$ , which is positioned at  $p_{S_i}^{B_i}$  and orientated at  $q_{S_i}^{B_i}$  with respect to body it has been attached to. The position and orientation of the sensor with respect to this body can be expressed as the sensor to segment calibration. The segments are supposed to be connected via a joint ( $J_k \in J$ ). However, contrary

to Kok [90] and Miezaal [182], joints connections are not incorporated as hard constraints in the framework. Instead, joint connections will be implemented as measurement functions with a relative low covariance. This allows for joint imperfections as well as using an unconstrained optimization algorithm.

The uncertainties in positions and orientations due to joint laxity, soft tissue artifacts, sensor to segment calibration errors and biomechanical model errors are indicated as grey ellipses. The origin of each segment frame is positioned in the most proximal joint of that particular segment. Yet, the hand segment origin coincides with the most proximal (metacarpal) joint. The position of a succeeding segment expressed in the actual segment is given by  $\mathbf{p}_j^{B_i}$ . Now, the length of the particular segment is defined as the Euclidean norm of that particular position vector  $\|\mathbf{p}_j^{B_i}\|$ .

Finally, the pose  $(\mathbf{p}_{B_{\{i,j\}}}^L, \mathbf{q}^{LB_{\{i,j\}}})$  of each segment with respect to a general, inertial frame L is illustrated.

Orientations are expressed as either unit quaternions or as a rotation matrix [78]. Segment lengths are expressed as scalar values. The remaining states and parameters are expressed as 3D vector values.

The following set of parameters ( $\theta$ ) are included in the optimization framework and are to be estimated:

4

1) *Gyroscope and Accelerometer biases:*

$$\left\{ b_g^{S_i}, b_a^{S_i} \right\} \quad \forall S_i \in \mathbb{S} \quad (4.1)$$

2) *Sensor to body segment pose (calibration):*

$$\left\{ \mathbf{p}_{S_i}^{B_i}, \mathbf{q}^{B_i S_i} \right\} \quad \forall S_i \in \mathbb{S} \quad (4.2)$$

3) Segment lengths of the proximal and medial phalanx:

$$l^{B_i} = \|\mathbf{p}_j^{B_i}\|_2 \quad \forall B_i \in \{B_{\text{prox}}, B_{\text{medial}}\} \quad (4.3)$$

In addition to the parameters, the following states ( $x_t$ ) are included:

4) *Sensor's position, velocity, acceleration, orientation, and angular velocity:*

$$\left\{ \mathbf{p}_{S_i,t}^L, v_{S_i,t}^L, a_{S_i,t}^L, q_t^{LS_i}, \omega_{S_i,t}^{S_i,L} \right\} \quad \forall S_i \in \mathbb{S}, \forall t \in \mathbb{T} \quad (4.4)$$

5) *Segment's pose:*

$$\left\{ \mathbf{p}_{B_i,t}^L, \mathbf{q}_t^{LB_i} \right\} \quad \forall B_i \in \mathbb{B}, \forall t \in \mathbb{T} \quad (4.5)$$

The following sections will explain the optimization framework and all cost functions that are involved within the framework. This can be divided in state initializations, parameter priors, dynamic models and measurement models.

### 4.2.1 Optimization framework

The problem of estimating the variable  $z$  consisting of the state vector  $x_{t \in T}$  and parameter vector  $\theta$  can be formulated as a Maximum A Posteriori (MAP) problem. We denote all the measurements, either real or virtual, by  $y_{t \in T}$ . Now, the joint PDF is given by the product of the measurement's conditional density and the prior density. Considering the densities as being Normally distributed ( $\mathcal{N}$ ) one can write:

$$p(y, z) = p(y|z)p(z) = \mathcal{N}_y(0, V)\mathcal{N}_z(\hat{z}^-, P^-) \quad (4.6)$$

The MAP results in the estimate of  $z$  that maximizes this function. Knowing that the logarithm is monotonically decreasing we can write the optimal estimate  $\hat{z}$  as:

$$\begin{aligned} \hat{z} &= \arg \max_z p(y, z) \\ &= \arg \min_z -\log p(y, z) \\ &= \arg \min_z \underbrace{-\log p(\theta)}_{\text{parameter prior}} - \sum_{t=1}^N \underbrace{\log p(y_t|x_t, \theta)}_{\text{measurement models}} \\ &\quad \underbrace{-\log p(x_1|y_1)}_{\text{dynamic initialization}} - \sum_{t=2}^N \underbrace{\log p(x_t|x_{t-1}, \theta)}_{\text{dynamic model}} \end{aligned} \quad (4.7)$$

The solution of the MAP problem (4.7) coincides with the unconstrained Minimum Mean Squared Error (MMSE) [64] or WLS estimator. An elaborate explanation for the stochastic formulations and least squares solution is given in Appendix 4.7.1.

## 4.3 MODELING

This section discussing the various terms that enter the total cost function (4.7). It should be noted that the covariances associated to each term do not enter the cost function and need to be set a-priori. Details on the values that have been used will be given in the experimental setup section.

### 4.3.1 Parameter prior:

All parameters are assumed to be unknown and therefore initialized with zero mean and unit covariance  $e_{\text{prior}}^{S_i} \sim \mathcal{N}(0, \Sigma_{\text{prior}}^S)$ . The sensor to segment orientation priors are initialized with unit quaternions.

### 4.3.2 Measurement models:

Various measurement models enter the cost function. Each will be described in the following section.

#### 4.3.2.1 Gyroscopes

The output of a gyroscope can be modeled as an angular velocity measured in sensor frame  $S_i$  with respect to an inertial frame L that is contaminated with a constant bias  $b_g^{S_i}$  and Gaussian noise  $e_{g,t}^{S_i}$ :

$$y_{g,t}^{S_i} = \omega_{S_i,t}^{S_i,L} + b_g^{S_i} + e_{g,t}^{S_i}, \quad e_{g,t}^{S_i} \sim \mathcal{N}(0, \Sigma^g) \quad (4.8)$$

#### 4.3.2.2 Accelerometers

The output of an accelerometer can be modeled as the sum of its experienced linear  $a_{S_i,t}^L$  and gravitational acceleration  $g^L$  expressed in the sensor's coordinate frame  $S_i$ . In addition, a local bias  $b_a^{S_i}$  and Gaussian noise  $e_{a,t}^{S_i}$  term are included:

$$y_{a,t}^{S_i} = R_t^{S_i,L} \left( a_{S_i,t}^L + g^L \right) + b_a^{S_i} + e_{a,t}^{S_i}, \quad e_{a,t}^{S_i} \sim \mathcal{N}(0, \Sigma^a) \quad (4.9)$$

It should be noted that the accelerometer bias of the hand sensor has not been included as it is unobservable due to the lack of an absolute position or velocity reference. Therefore, accelerometer bias estimates should not be considered as absolute sensor estimate but rather as a relative estimate with respect to the accelerometer placed on the hand.

#### 4.3.2.3 Sensor to segment calibration

The pose of each sensor with respect to the body on which it has been attached is assumed to be constant over time. These parameters are known as the sensor to segment calibration poses.

$$q_t^{LS_i} = q_t^{LB_i} \odot q^{B_i S_i} \odot \exp\left(\frac{1}{2} e_t^{q^{B_i S_i}}\right), \quad e_t^{q^{B_i S_i}} \sim \mathcal{N}(0, \Sigma^{q^{BS}}) \quad (4.10a)$$

$$p_{S_i,t}^L = p_{B_i,t}^L + R_t^{LB_i} \left( p_{S_i}^{B_i} + e_t^{p_{S_i}^{B_i}} \right), \quad e_t^{p_{S_i}^{B_i}} \sim \mathcal{N}(0, \Sigma^{p_B^S}) \quad (4.10b)$$

where  $e_t^{q^{B_i S_i}}$  and  $e_t^{p_{S_i}^{B_i}}$  denote an error angle and error position caused by any skin artifact in time corresponding to the pose calibration (4.2).

#### 4.3.2.4 Segment articulation

To ensure that segments are connected, a common position should be shared between articulated segments. This position defines the joint between both segments and can be modeled by:

$$p_{B_j,t}^L = p_{B_i,t}^L + R_t^{LB_i} \left( p_j^{B_i} + e_t^{J_k^P} \right), \quad e_t^{J_k^P} \sim \mathcal{N}(0, \Sigma^{J^P}) \quad (4.11)$$

where  $e_t^{J_k^P}$  denotes an error in the position difference between the two joints (whose magnitude determines the segment's length, 4.3), and effectively models the laxity of joints.

#### 4.3.2.5 Joint velocity

The difference in acceleration between two particular points on a rigid body is determined by the lever arm, angular velocity and angular acceleration of the particular body. Due to the articulated structure of the hand it is possible to exploit the accelerations at the interconnecting joints which gives information of segment lengths and the relative heading between segments [208]. The measured joint acceleration should be equal for both rigid bodies independently of the coordinate frame. In order to obtain angular accelerations one needs to differentiate the angular velocities by numerical means. Alternatively, this relation can be written in integrated form which gives the joint velocity constraint:

$$\begin{aligned} 0 &= v_{S_i,t}^L + R_t^{LS_i} \left( \omega_{S_i,t}^{S_i,L} \times \left( R^{S_i B_i} \left( p_j^{B_i} - p_{S_i}^{B_i} \right) \right) \right) \\ &\quad - \left( v_{S_j,t}^L + R_t^{LS_j} \left( \omega_{S_j,t}^{S_j,L} \times \left( -R^{S_j B_j} p_{S_j}^{B_j} \right) \right) \right) + e_t^{J_k^V} \end{aligned} \quad (4.12)$$

where:  $e_t^{J_k^V} \sim \mathcal{N}(0, \Sigma^{J^P})$  denotes the difference of the joint velocity error.

#### 4.3.2.6 Joint dimensionality

The PIP and DIP joints can be modeled with a single DoF, and therefore considered as hinge joints.

The following model constrains rotations around axes other than the hinge's rotation axis:

$$0 = h^{B_i} - R_t^{B_j L} R_t^{LB_i} h^{B_i} + e_t^{J^D}, \quad e_t^{J^D} \sim \mathcal{N}(0, \Sigma^{J^d}) \quad (4.13)$$

where  $h^{B_i}$  is a unit vector describing the direction of the rotational axis of that particular joint, and  $e_t^{J^D}$  describes an error angle.

#### 4.3.2.7 Segment surface model

Finger segments can be modeled as conic frustums [25]. Knowledge of the frustum's radii and the assumption that the IMU sensor is placed somewhere on

the frustum's surface gives the ability to constrain the IMU position [182]. Contrary to Taetz, we do not assume any knowledge of finger dimensions, hence no radii or segment length is known. We only take into account that the sensor is placed such that its z-axis directs radially with respect to an unit vector  $y_{S_i}$  that directs along the surface of the body segment in the distal direction. This can be modeled by ensuring that the inner product of the sensor's z-axis, given by the third row of the sensor to segment orientation matrix  $z_{B_i S_i} = R_{[3,:]}^{B_i S_i}$ , and the vector  $y_{S_i}$  is zero.

$$0 = z_{B_i S_i}^T y_{S_i} + e^{S_i^q}, \quad e^{S_i^q} \sim \mathcal{N}(0, \Sigma^{S_i^q}) \quad (4.14)$$

where  $e^{S_i^q}$  denotes an error angle.

#### 4.3.2.8 Zero acceleration

We assume that the body segment accelerations have zero mean [114]:

$$0 = a_{S_i, t}^L + e_{ao, t}^{S_i}, \quad e_{ao, t}^{S_i} \sim \mathcal{N}(0, \Sigma^{ao}) \quad (4.15)$$

where  $a_{S_i, t}^L$  is the linear acceleration and  $e_{ao, t}^{S_i}$  is a Gaussian error term.

#### 4.3.3 Dynamic initialization:

The position ( $p_{S_i, 1}^L$ ) and velocity ( $v_{S_i, 1}^L$ ) states are initialized with zeros. The orientation ( $q_{S_i, 1}^{LS_i}$ ) states are initialized with a unit quaternion. The initial process errors of translations  $w_{i, 1}^{X_S^L}$ , and orientations  $w_{i, 1}^{q^{LS}}$ , are assumed to be iid Gaussian noise terms:

$$w_{i, 1}^{X_S^L} \sim \mathcal{N}(0, \Sigma^{X_1}), \quad X \in \{p, v\}, \quad w_{i, 1}^{q^{LS}} \sim \mathcal{N}(0, \Sigma^{q_1}) \quad (4.16)$$

#### 4.3.4 Dynamic models:

Given the linear acceleration  $a_{S_i}^L$  and angular velocity  $\omega_{S_i, t}^{LS_i}$  for each sensor  $S_i \in S$  at a certain time point  $t$ . Now, the discrete kinematic equations describe the sensor's pose and velocity at  $t + T$ , with sampling time  $T$ :

$$p_{S_i, t+T}^L = p_{S_i, t}^L + T v_{S_i, t}^L + \frac{T^2}{2} a_{S_i, t}^L + w_{i, t}^{p_S^L} \quad (4.17a)$$

$$v_{S_i, t+T}^L = v_{S_i, t}^L + T a_{S_i, t}^L + w_{i, t}^{v_S^L} \quad (4.17b)$$

$$q_{t+T}^{LS_i} = q_{S_i, t}^{LS_i} \odot \exp\left(\frac{T}{2} \omega_{S_i, t}^{S_i, L}\right) + w_{i, t}^{q^{LS}} \quad (4.17c)$$

with the process noises being described by:

$$w_{i, t}^{X_S^L} \sim \mathcal{N}(0, \Sigma^X), \quad X \in \{p, v\}, \quad w_{i, t}^{q^{LS}} \sim \mathcal{N}(0, \Sigma^q) \quad (4.18)$$

#### 4.4 SOLVING

The total cost function is found by rewriting the individual stochastic models such that each is a function of the particular noise variable  $e$  or  $w$ . After neglecting the constant terms of the measurement function and summing all individual terms, this eventually results in the following cost function:

$$\begin{aligned}
 \hat{z} = & \arg \min_z \sum_{S_i \in S} \underbrace{\left( \|w_{i,1}^{p_S^L}\|_{(\Sigma^{p_1})^{-1}}^2 + \|w_{i,1}^{v_S^L}\|_{(\Sigma^{v_1})^{-1}}^2 + \|w_{i,1}^{q^{LS}}\|_{(\Sigma^{q_1})^{-1}}^2 \right)}_{\text{Initialisation of the dynamics (4.3.3)}} \\
 & + \sum_{t \in T} \sum_{S_i \in S} \underbrace{\left( \|w_{i,t}^{p_S^L}\|_{(\Sigma^p)^{-1}}^2 + \|w_{i,t}^{v_S^L}\|_{(\Sigma^v)^{-1}}^2 + \|w_{i,t}^{q^{LS}}\|_{(\Sigma^q)^{-1}}^2 \right)}_{\text{Dynamics (4.3.4)}} \\
 & + \sum_{t \in T} \sum_{S_i \in S} \left( \underbrace{\|e_{g,t}^{S_i}\|_{(\Sigma^g)^{-1}}^2}_{\text{Gyroscopes (4.3.2.1)}} + \underbrace{\|e_{a,t}^{S_i}\|_{(\Sigma^a)^{-1}}^2}_{\text{Accelerometers (4.3.2.2)}} + \underbrace{\|e_{ao,t}^{S_i}\|_{(\Sigma^{ao})^{-1}}^2}_{\text{Zero acc. (4.3.2.8)}} \right) \\
 & + \sum_{t \in T} \sum_{S_i \in S} \left( \underbrace{\|e_t^{q_{S_i} B_i}\|_{(\Sigma^{q_{SB}})^{-1}}^2}_{\text{Sensor To Segment calibration (4.3.2.3)}} + \|e_t^{P_{S_i}^B}\|_{(\Sigma^{P_S^B})^{-1}}^2 \right) \\
 & + \sum_{t \in T} \sum_{J_k \in J} \left( \underbrace{\|e_t^{J_k^p}\|_{(\Sigma^{J_p})^{-1}}^2}_{\text{Joint pos. (4.3.2.4)}} + \underbrace{\|e_t^{J_k^v}\|_{(\Sigma^{J_v})^{-1}}^2}_{\text{Joint vel. (4.3.2.5)}} + \underbrace{\|e_t^{J_k^d}\|_{(\Sigma^{J_d})^{-1}}^2}_{\text{Joint dim. constr. (4.3.2.6)}} \right) \\
 & + \sum_{S_i \in S} \left( \underbrace{\|e_{S_i}^q\|_{(\Sigma^{S_q})^{-1}}^2}_{\text{S2B constr. (4.3.2.7)}} + \underbrace{\|e_{prior}^{S_i}\|_{(\Sigma_{prior}^S)^{-1}}^2}_{\text{Priors (4.3.1)}} \right)
 \end{aligned} \tag{4.19}$$

For convenience reasons all parameter priors, except for the gyro biases, have been captured under a single cost term.

The solution to this non-linear least squares problem can be found by using an iterative [WLS](#) solver like a trust region (e.g. Levenberg-Marquardt) or linesearch method (e.g. Broyden-Fletcher-Goldfarb-Shanno). The covariances matrices determine the weighting between different cost function components and eventually determine the success of convergence when minimizing the cost function.

The accelerometer and gyroscope covariances are determined empirically using a static measurement. Other covariances are somewhat chosen arbitrary as they did not have significant influence on the convergence. Yet, covariances that do have a significant influence are outlined in the next section.

## 4.5 EXPERIMENTAL METHODS AND RESULTS

The functionality, accuracy and repeatability of the proposed algorithm were tested using two different measurement setups.

The first setup uses a 3D printed, manually tendon actuated, finger whereas the second setup comprises an experiment on a real hand, see Fig. 4.2.

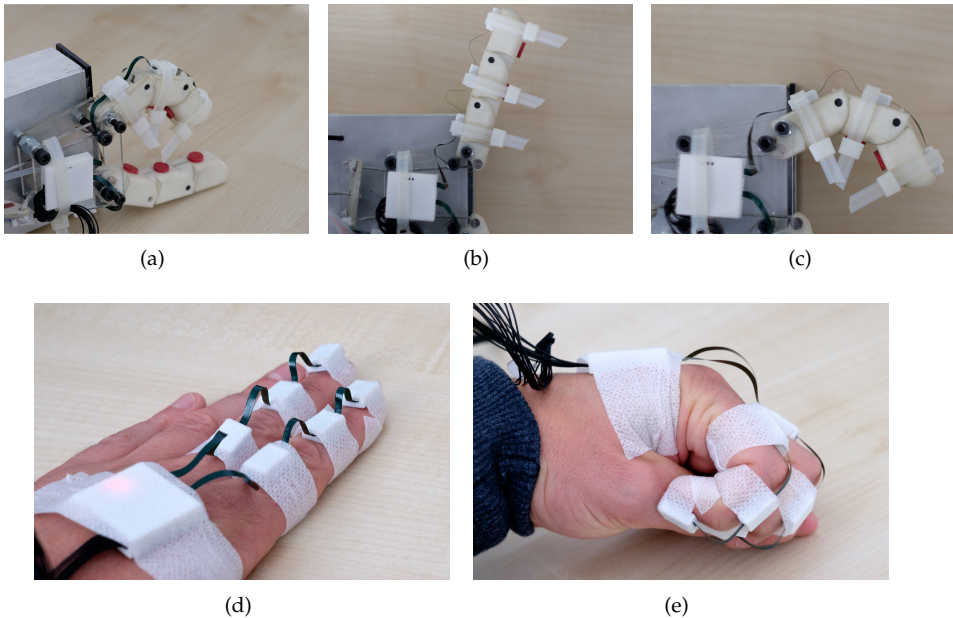


Figure 4.2: Experimental setups: Artificial finger (a-c): consisting of four segments made of 3D printed material. A thread is pulled through all segments and attached to the most distal one. Together with internal springs the wire mimics the tendon actuation of a human finger. Sensors are strapped along the top surface of the finger (small rectangular white boxes) and sideways on the Plexiglas board (larger white square box). The sensor PCB's are electrically connected with flexible PCB material. 2nd setup). In the second setup (d-e) the same system has been strapped to a human hand, index and middle finger using adhesive tape.

Both setups use the same data acquisition hardware as being used in former studies [97, 192] and is referred to as the PowerGlove system. The only difference are the inertial sensors being used, which in this study have been updated to Invensense (MPU9250). Inertial data of four sensors was sampled at 100 Hz and acquired via USB. Custom Python scripts and C++ programs were developed and used for importing, processing, analysis and visualizing. A major role is devoted to the optimization framework of which its details

will be outlined in the next subsection. Experimental setups, procedures and results of both experiments will be reported subsequently.

#### 4.5.1 Signal processing software

The optimization algorithm is written in the C++ language and incorporates some specific libraries. First, the Eigen matrix library [46] was used to perform fast and easy matrix manipulations. In addition, this library allows proper handling of 3D orientations using quaternions and rotation matrices. The quaternion is a 4D parameterization of a 3D orientation, which is appealing because it circumvents singularities as one would have when using a 3D parameterization like Euler angles (famous gimbal lock problem), and its representation is minimal (and therefore fast) compared to rotation matrices.

The second library, named Ceres [2], is a large scale numerical optimization library targeting on solving bundle-adjustment problems [190]. This library has several properties that make it very suitable for our purpose. First, it allows different parameterizations, among which the quaternion parameterization is most valuable. Least Squares solvers, like the ones used in Ceres, cannot handle quaternions in a natural way because of their unit norm constraint. Ceres applies a common solution by letting the solver operate on a local, tangential, space of the particular quaternion. This, so-called boxplus method allows for proper linearization of the quaternion [71]. Typical operations within the solver, like additions, are now correctly performed without violating the norm constraint. The second appealing property of the Ceres solver is its support for automatic differentiation. Gradient based optimization algorithms depends on evaluations of some objective (cost) function and their derivatives. Automatic differentiation is a technique to compute analytic derivatives of such objective functions with almost the same effort one would need for numerical derivatives.

Finally, Ceres supports large and sparse matrices which is crucial as our optimization problem easily contains over 100K variables. As mentioned in the previous section, the algorithm depends on various covariance parameters. For both experiments those initial parameters were set to the following values:

- Dynamics:  $\Sigma^a = 10^{-6} \text{ (m/s}^2\text{)}, \Sigma^q = 10^{-6} \text{ (rad)}$
- Sensors:  $\Sigma^\omega = 10^{-3} \text{ (rad/s)}, \Sigma^a = 8 \times 10^{-2} \text{ (m/s}^2\text{)}$
- Sensor Bias Prior:  $\Sigma^b = 10^{-6} \text{ (rad/s)}$
- S2B calibration:  $\Sigma^{q_{SB}} = 10^{-6} \text{ (rad)}, \Sigma^{P_S^B} = 10^{-6} \text{ (m)}$
- Biomech. contrs.:  $\Sigma^{J^P} = 10^{-6} \text{ (m)}, \Sigma^{J^V} = 1 \text{ (m/s)},$   
 $\Sigma^{J^d} = 10^{-3} \text{ (rad)}, \Sigma^{ao} = 1 \times 10^1 \text{ (m/s}^2\text{)}, \Sigma^{Sq} = 10^{-3} (-)$

All covariance matrices, except  $\Sigma^{Sq}$  which is a scalar, are diagonal  $\mathbb{R}^{3 \times 3}$  matrices with identical values on the diagonal.

Instead of entering the joint positions ( $\Sigma^{J^P}$ ) as a hard constraint in the framework we chose to include them as a soft constraint with relatively low covariance. This is justified by the fact that some joints, like the MCP, do have im-

perfections that makes the position of the joint's center depends on the joint's angle. Hence, small position changes are possible as the joint angle changes.

It should be noted that the algorithm is most sensitive for the soft constraint on this joint position, the sensor to segment calibration, and velocity.

The sensor to segment parameters are directly coupled to the joint position constraints and therefore require also a relative low covariance. The velocity constraint covariance should be set to a relatively large value because the joint velocity error is rather large as it is an accumulation of biomechanical model and sensor errors. This was also mentioned in the studies by Kok and Taetz.

#### 4.5.2 Artificial finger: experimental method and result

The first experiment is conducted using an artificial finger that has been constructed using 3D printing material, see Fig. 4.2. The finger consists of three single DoF (MCP, PIP, DIP) joints. Joint flexion rotations are enabled by tendon means. By pulling a string the finger joints flexes until each individual joint reaches its end stop. Internal rotational springs apply a counter force during flexion such that joint extensions are enabled when the tendon string is released.

IMU sensors were embodied in small 3D printed housings and attached to the underlying segments using fixation straps.

The distance between the origins of the hand and distal sensor was measured using a divider tool. The value for this distance was 140mm during maximum joint flexion. It should be noted that this reference measurement error is uncertain up to several millimeters.

Due to the 3D printed structures, it was impossible to determine the 3D position of the sensor with respect to its segment accurately. Therefore, it was chosen to measure the distance between of the sensor chip origins and the segment's origins ( $\|p_S^B\|$ ). The distances values were 75, 18, 19 and 24 mm for the hand, proximal, medial and distal segments respectively.

The proximal and medial segments were the same and have therefore a similar longitudinal distance, referred as to the segment length ( $\|p_J^{B_i}\|$ ), which was 30 mm.

The orientation between sensor and segment could not be measured reliably and was therefore not given for comparison. However, the sensors are placed flat and almost aligned with the proximal, medial and distal segment as can be seen from Fig. 4.2. In addition, by visual inspection it is known that the sensors have been rotated approximately 90 degrees with respect to the segment.

The segment orientations were defined such that extensions about the joints axis defines the x-axis, perpendicular to that axis directed to the next segment defines the y-axis, and perpendicular to both axes defines the z-axis. Because this setup only has single DoF joints an ambiguity exists with respect to the origin's position of the first segment frame. This has been resolved by defining the segment's frame such that sensor's origin coincides with the  $x = 0$  position of the segment's frame.

#### 4.5.2.1 Procedure

The setup was rested, with PIP and DIP joints extended, on a table top for a couple of seconds. The entire setup was operated manually by hand. First the setup was lifted, then the base was moved in arbitrary directions under arbitrary orientations. Simultaneously, the tendon was pulled repeatedly, such that multiple flexion and extensions were performed while moving the base. This, somewhat arbitrary movement, was continued for about 40 seconds when the setup was placed on the tabletop again. This experiment was repeated 15 times.

#### 4.5.2.2 Results

Estimates of the kinematic calibrations parameters (sensor to segment pose and segments length) obtained after data processing can be found in Table 4.1. Mean and standard deviation are reported for each parameter over 15 trials. Differences between reference measurements are given when reference data was available. In addition, the distributions are graphically depicted in Fig. 4.3.

Distributions of estimated accelerometer and gyroscope biases are depicted in Fig. 4.4. A reference of the gyroscope bias is determined by averaging the initial gyroscope signals prior to lifting the entire setup. The difference between reference and estimate were found to be  $-2.1 \pm 22.4\%$ .

Finally, an example reconstruction of the distance between hand and tip IMU over time is given in Fig 4.5a. The true distance (140mm), as being measured using the divider tool when the tendon was maximally pulled, is indicated by dashed black traces. Each trial consisted of a static and dynamic phase. During the static phase (indicated with a grey shaded area) the finger was fully extended. After this static phase the tendon was repeatedly pulled referred to as the dynamic phase. The distances during the static and dynamic phase (representing full extension) were labeled and averaged. Distributions of both are depicted in Fig. 4.5b.

#### 4.5.3 Human finger: experimental methods and results

An additional experiment was conducted by one subject to illustrate the potential of the proposed method.

The subject's index and middle fingers were equipped with same sensor hardware as in the previous experiment. The sensors were donned along the phalanges, whereas the hand segment was equipped with a single IMU and shared by both fingers, see Fig. 4.2. Segment lengths of both fingers were estimated by palpating the bony landmarks and using anthropometric data to estimate joint centers from the bone lengths [23]. The lengths of the index finger segments were 45 and 24 mm for the proximal and medial segments respectively. For the middle finger the measured values were 46 and 30 mm respectively.

Table 4.1: Artificial finger: Mean and standard deviations of estimated parameter values. Orientation estimates are denoted using Euler’s description for convenience. Percentile differences with respect to reference data is given for the sensor to segment distances ( $\Delta\|p_S^B\|$ ) and segment lengths ( $\Delta\|p_{B_j}^{B_i}\|$ ). The position of the proximal **IMU** was fixated in the x direction and therefore not included. Similarly, only proximal and medial segment lengths are observable and therefore included.

	$p_S^B$ (mm)			$q^{BS}$ (deg)			$\ p_{B_j}^{B_i}\ $			
	x	y	z	$\ p_S^B\ $	$\Delta\ p_S^B\ (\%)$	θ	φ	ψ	(mm)	Δ(%)
Hand	43.5 ± 1.1	-57.0 ± 1.8	19.8 ± 1.6	74.4 ± 1.5	0.8 ± 2.0	0.1 ± 0.3	0.0 ± 0.0	-99.1 ± 0.5	-	-
Proximal	-	15.7 ± 1.4	8.7 ± 0.5	17.9 ± 1.3	-0.4 ± 7.0	0.8 ± 0.2	0.1 ± 0.0	-92.7 ± 0.3	29.5 ± 1.4	-1.7 ± 4.8
Medial	3.1 ± 1.2	16.0 ± 0.9	8.2 ± 0.3	19.0 ± 0.8	0.0 ± 4.3	0.5 ± 0.2	0.0 ± 0.1	-91.4 ± 0.3	30.2 ± 1.2	0.8 ± 4.1
Distal	4.0 ± 1.6	22.2 ± 0.7	6.8 ± 0.5	23.7 ± 0.8	-1.4 ± 3.4	-0.4 ± 0.2	0.0 ± 0.0	-89.1 ± 0.2	-	-

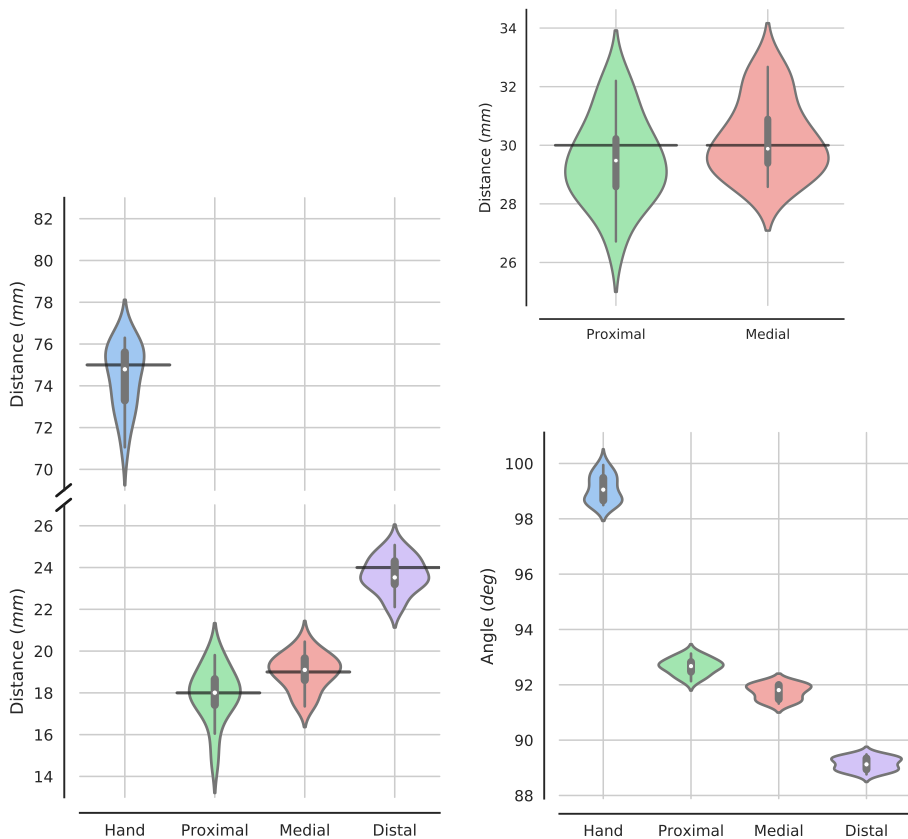


Figure 4.3: Artificial finger results: Estimated distance between the origins of the sensor and corresponding segments (left), estimated proximal and medial segment lengths (top right) and the estimated helical angles between sensor and corresponding segment (bottom right). Manually measured values available are indicated by the horizontal lines. The violin plots illustrate the sample distribution which is based on 15 measurements. Inside the violin plot are the first and third quartiles (thick black vertical line) and median value (white dot) depicted.

The subject was instructed to place the hand down on the tabletop with the palm facing upwards. Then, after some seconds, the subject was instructed to lift the hand and subsequently move and rotate its entire hand in arbitrary positions and directions. While moving the hand, the subject was asked to repeatedly flex and extend the fingers, and when possible, also perform abduction movements with its MCP joint. Each movement period lasted for about 30 seconds when the hand was placed down on the table top again. The

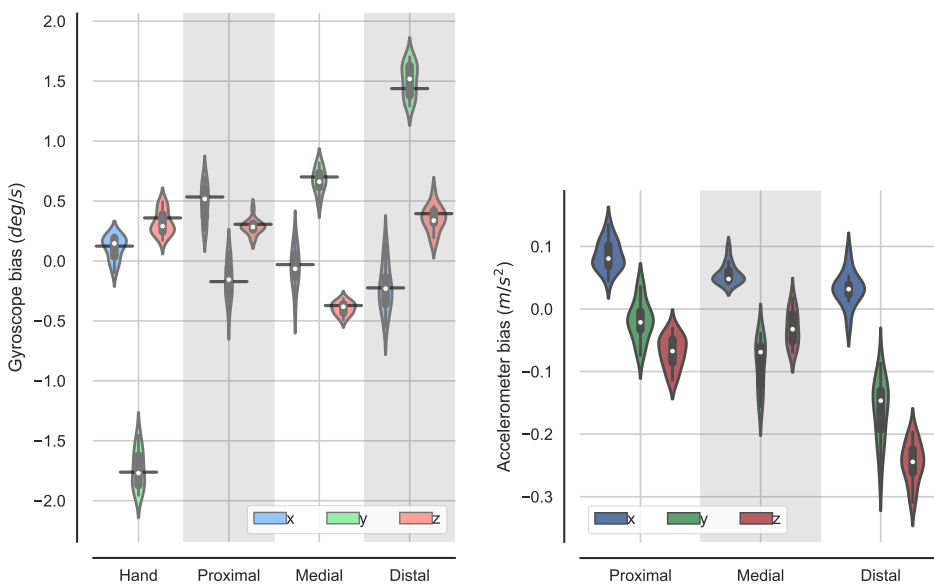


Figure 4.4: Artificial finger results: Estimated biases of the gyroscopes (left) and accelerometers (right). It should be noted that the accelerometer biases are relative with respect to the accelerometer placed on the hand. Manually measured bias values available are indicated by the horizontal lines. The violin plots illustrate the sample distribution which is based on 15 measurements. Inside the violin plot are the first and third quartiles (thick black vertical line) and median value (white dot) depicted.

entire measurement was repeated 3 times with the same subject and without doffing the setup.

An example 3D pose reconstruction is depicted in Fig. 4.6. The pose reflects a snapshot during a flexion of the subject's middle finger.

The estimated sensor to segment positions of both index and middle finger are depicted in Fig. 4.7. The sensor that was placed on the hand segment was used in both linkages. From Fig. 4.2 (d) it is visible that this sensor is placed between the hand phalanges of both fingers, hence the difference in the x-direction of the hand sensor position for both fingers visible in Fig. 4.7.

The estimated helical angles of the sensor to segment orientations are depicted in Fig 4.8. Again, sensors were orientated such that they were rotated approximately 90 degrees about their z-axis. Hence, this is the largest contribution to the helical angle between sensor and segment coordinate frames.

The estimated segment lengths of the proximal and medial phalanx for both index and middle finger are depicted in Fig. 4.9. Reference lengths are indicated by horizontal lines.

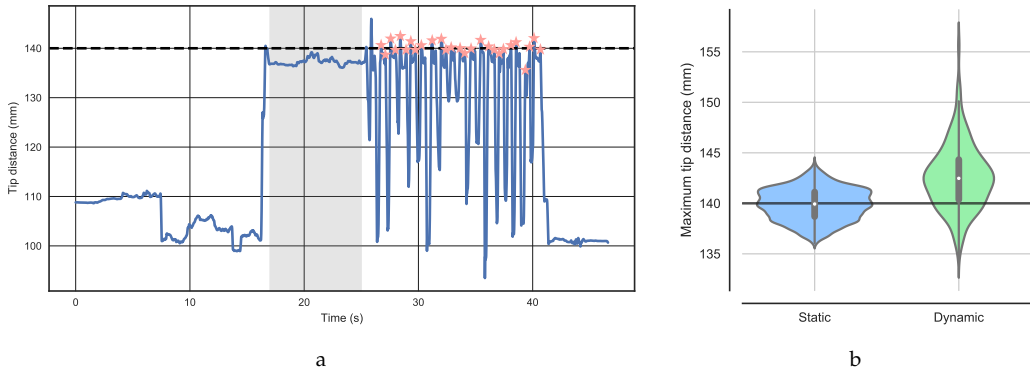


Figure 4.5: Artificial finger results: Estimated tip distances in static and dynamic situations. An example reconstruction of the estimated distance between the sensor placed on the hand segment and the sensor placed on the distal segment (left). The distance during maximal flexion being estimated using a divider tool is indicated (black dashed line). Two distinct phases are indicated: the static phase (grey shaded area) and dynamic phase (peaks indicated by red markers). Distributions of maximum distances during those two phases are visualized using the violin plots (right).

Finally, an exemplary estimate of the distance trajectory over time between the sensor placed on the hand and tip sensors is visualized in Fig. 4.10. The distances between hand and tip sensors was measured when the hand was placed flat on the tabletop and indicated as a reference by the dashed line.

#### 4.6 DISCUSSION AND CONCLUSION

This chapter proposes a new method to calibrate various inertial sensor and model parameters of an inertial hand MoCap system. The algorithm assumes a biomechanical chain of linkages (like the human hand and finger) and has been constructed by stochastic means such that it accounts for sensor errors, joint imperfections and errors due to tissue deformations.

Sensor parameters include the bias parameters of gyroscopes and accelerometers. Model parameters include the poses of the sensor with respect to the segments it has been attached to and the lengths of the segments that have two joints (proximal and medial).

The algorithm is able to, simultaneously with the parameters, estimate the pose of the hand and the fingers over time. However, our method targets the parameter estimation part because the algorithm requires an a-priori dataset of inertial hand movement data and is therefore not suitable for online pose estimation. Nevertheless, other studies have already shown that batched optimization methods have the potential to be used for online MoCap [93, 182]. Yet,

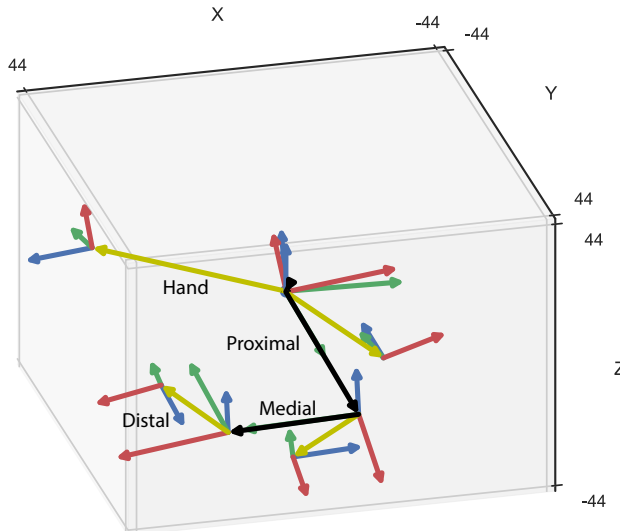


Figure 4.6: Human finger results: Snapshot of the 3D middle finger pose in global reference frame during a full flexion. Visible are the orientations ( $x=$ blue,  $y=$ green,  $z=$ red) of both sensors and segments, the position of the sensor with respect to segment (yellow) and segment lengths (black).

4

further research is required as those studies do assume a-priori model parameters which require calibration interventions by either user or assistant. Small data batches cause a decrease in movement richness as a certain minimum amount of movement is required to ensure convergence in a global minimum. The approach we proposed uses all data available and could replace those intensive calibrations procedures. Alternatively, the method could be used to find proper initials for a batched optimization method which would ease the search for a global minimum.

Two experiments were conducted in this study. The first experiment has shown that the algorithm is robust in its convergence (15 of 15 trial converged correctly) and its ability to accurately estimate model parameters. The artificial finger mimics an ideal situation as the joints can be considered as perfect hinges. Good agreements were found in the position estimates as the errors in sensor to segment distances were  $0.8 \pm 2.0\%$ ,  $-0.4 \pm 7.0\%$ ,  $0.0 \pm 4.3\%$  and  $-1.4 \pm 3.4\%$  for hand, proximal, medial and distal phalanx respectively. In addition, good agreements were found in estimating the segment lengths of the proximal and medial phalanx, proven by a difference of  $-1.7 \pm 4.8\%$ ,  $0.8 \pm 4.1\%$ , respectively.

Our algorithm highly depends on inertial acceleration and angular velocity measurements. Hence, any errors in the accelerometer or gyroscope propa-

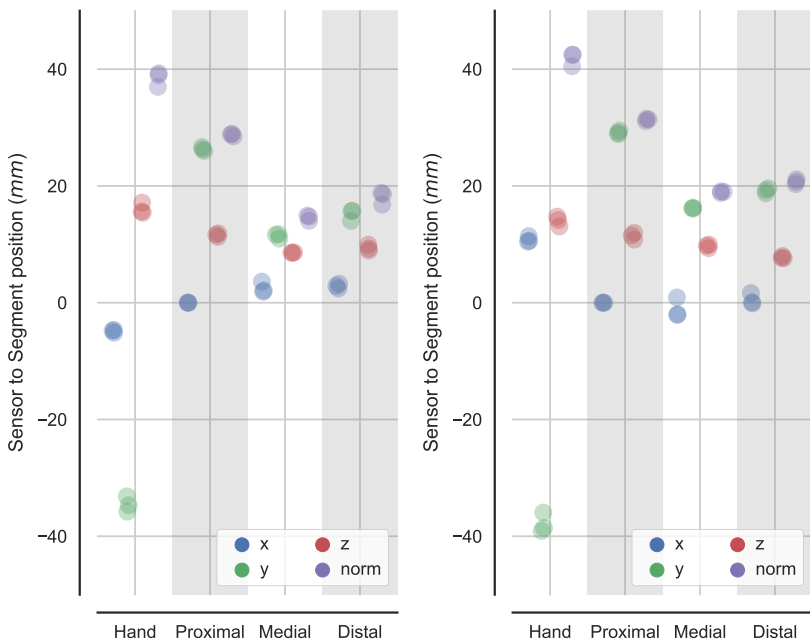


Figure 4.7: Human finger results: Sensor to segment positions. Estimated values (3) for each segment and axis is given for the index finger (left) and middle finger (right). In addition distances values (norm) are given.

gates in the estimates of other variables. Most of the sensor model parameters like internal misalignments and gains can be considered as time invariant and estimated during an onetime sensor calibration procedure. However, others parameters, like the biases are time dependent and should be known prior to usage for correct functioning. Therefore, accelerometer and gyro biases have been included in the framework and could be estimated without the need to be completely still. Good correspondences were found between the reference values (during a no movement period) and estimated values of the gyro biases. Contrary to the gyroscope, the bias of the accelerometer is only observable when some aiding system provides the absolute position or velocity or the sensor is held static under, at least 6, exclusive orientations. However, in kinematic chains, the relative biases become observable again under the influence of any movement and therefore using for the correction of joint accelerations.

In addition, joint velocity constraint enable the observability of the relative heading between segments which makes usage of magnetometers superfluous. Finally, velocity constraints enable the estimation of segment lengths which is traditionally, especially for human body segments, a difficult and time consuming procedure if done manually.

It is inevitable that further research is required regarding the movement dependency of the algorithm. Sensitivity to the amount and type of input move-

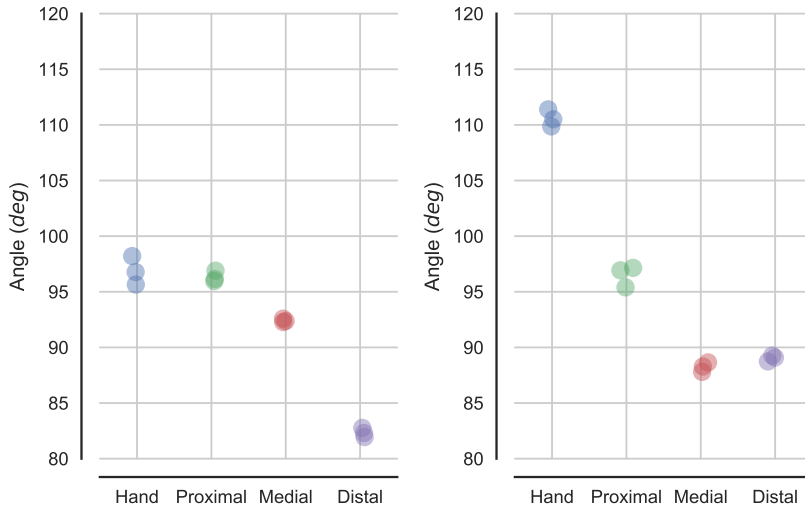


Figure 4.8: Human finger results: Estimated helical angles between sensor and corresponding segment for the index finger (left) and middle finger (right).

ments as well as the excitability of movement with respect to various model parameters are topics that need to be addressed to justify the methods and to demonstrate the potential for clinical, virtual reality, sports or rehabilitation applications.

In addition to the estimation of calibration parameters, our approach also yields the finger's pose over time. During maximal extension of the artificial finger, the distance between hand and most distal sensors showed good correspondence within millimeter level. Therefore, our approach is useful for MoCap applications that require a good accuracy but does not required real time estimates.

Further research topics that could be addressed include the testing of sensor data validity. Clipping of gyroscopes can happen fairly easily during sport activities as most of those sensor have only a range of  $\pm 4000$  (deg/s). The information obtained from the accelerometer could be used to reconstruct angular velocity information when the positions to rotational points are known.

Secondly, depending on the target application, more contextual information could be added to the cost function. Joint angle inter-dependencies, range of motions, contact detection and the finger thumb pad opposition are possible examples which are applicable for the human hand and could improve or facilitate the proposed method.

Furthermore, the priors of various parameter could be adjusted to the specific applications. This could include gyro biases, segmental lengths and sensor to segment orientations. Proper chosen initials with corresponding confidence could improve the eventual processing time.

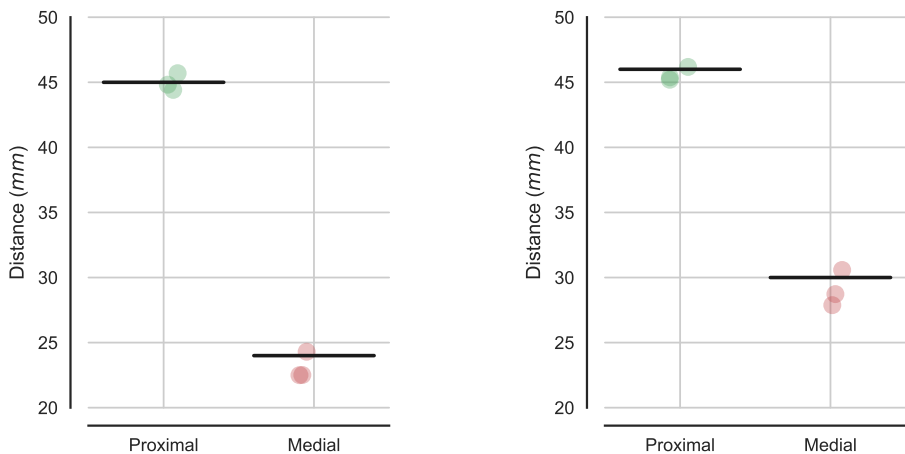


Figure 4.9: Human finger results: Estimated proximal and medial segment lengths of index (left) and middle finger (right). The measured reference lengths are indicated by the horizontal lines.

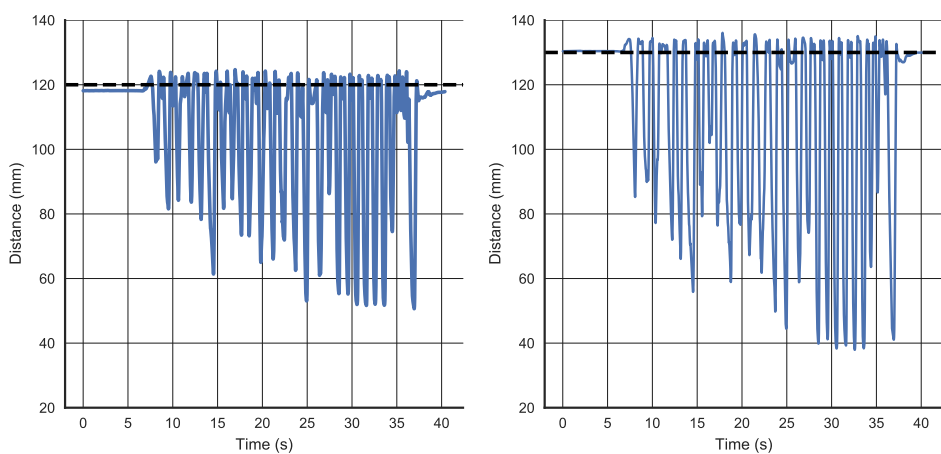


Figure 4.10: Human finger: Example reconstruction of the distance between hand and tip sensor for index (left) and middle (right) finger. The reference distances for the flat hand situation were measured with a ruler and indicated with a dashed black line.

To conclude, this chapter describes a method to automatically calibrate for various parameters which are necessary for the kinematic estimation of the human hand and fingers using inertial sensors. The method has many potentials and makes manual calibration procedures of both sensors and segments superfluous.

## 4.7 APPENDIX

### 4.7.1 Probabilistic modeling

It is the objective to infer knowledge about the state vectors  $x_{1:N}$  and parameter vector  $\theta$  captured by  $z$  using the measurement vectors  $y_{1:N}$ . This can be expressed by the conditional probability function:

$$p(x_{1:N}, \theta | y_{1:N}) \quad (4.20)$$

Expanding this function using Bayes' theorem yields:

$$p(x_{1:N}, \theta | y_{1:N}) = \frac{p(y_{1:N} | x_{1:N}, \theta) p(x_{1:N}, \theta)}{p(y_{1:N})} \quad (4.21)$$

Now we are interested in the point estimate, and corresponding uncertainty of that estimate. By stacking the state and parameter vector as  $z = \{x_{1:N}, \theta\}$  we define this estimate as:

$$\begin{aligned} \hat{z} &= \arg \max_z p(z | y_{1:N}) \\ &= \arg \max_z \frac{p(z, y_{1:N})}{p(y_{1:N})} \\ &= \arg \max_z p(z, y_{1:N}). \end{aligned} \quad (4.22)$$

Where,  $\arg \max$  denotes the operator that returns  $z$  for which the argument attains its maximum. The transition from the first to the second row in [4.20] uses the probability relation:

$$p(z, y_{1:N}) = p(z | y_{1:N}) p(y_{1:N}) \quad (4.23)$$

whereas the transition from the second to third row is allowed because  $y_{1:N}$  is independent of  $z$ . Hence, we seek for the value of  $z$  for which the joint PDF  $p(z, y_{1:N})$  attains its maximum. This estimate is known as the **MAP** value.

Using Bayes' rule and the Markov property we can reformulate the joint PDF  $p(z, y_{1:N})$  as:

$$\begin{aligned} p(z, y_{1:N}) &= p(\theta, x_{1:N}, y_{1:N}) \\ &= \underbrace{p(\theta) p(x_1)}_{\text{priors}} \underbrace{\prod_{t=2}^N p(x_t | x_{t-1}, \theta)}_{\text{dynamics}} \underbrace{\prod_{t=1}^N p(y_t | x_t, \theta)}_{\text{measurements}} \end{aligned} \quad (4.24)$$

where we distinguish between priors, dynamic and measurement PDFs.

Because the logarithm is a monotonic function, finding  $z$  for which  $p(z, y_{1:N})$  is maximal, will be similar as finding  $z$  for which  $\log p(z, y_{1:N})$  is maximal. In

addition, for ease of use, we rewrite [4.24] such that we seek for a minimum instead of a maximum:

$$\begin{aligned}\hat{z} &= \arg \max_z p(z, y_{1:N}) \\ &= \arg \min_{x_{1:N}, \theta} -\log p(\theta) - \log p(x_1) \\ &\quad - \sum_{t=2}^N \log p(x_t | x_{t-1}, \theta) - \sum_{t=1}^N \log p(y_t | x_t, \theta)\end{aligned}\tag{4.25}$$

Various approaches exists to solve such problem, among which optimization methods [216] are interesting as they allow flexibility in the models being used.

We assume all terms in [4.25] as Gaussian distributions. Now, let's consider a general problem which consists of the product of Gaussian PDFs  $p(e_i(z))$ . Where the Gaussian variable  $e_i(z)$  is function of  $z$  and has length  $P$ . Subsequently, its distribution is given by:

$$p(e_i(z)) = \frac{1}{\sqrt{(2\pi)^P \det(\Sigma_i)}} e^{(-\frac{1}{2} e_i(z)^T \Sigma_i^{-1} e_i(z))}\tag{4.26}$$

Hence, we can write the optimization function as:

$$\hat{z} = \arg \min_z - \sum_{i=1}^M \log p(e_i(z)),\tag{4.27}$$

after omitting all terms which are independent of  $z$ , this function reduces to:

$$\hat{z} = \arg \min_z \frac{1}{2} \sum_{i=1}^M \|e_i(z)\|_{\Sigma_i^{-1}}^2\tag{4.28}$$

which is known as the WLS estimate [64].

## HAND POSE ESTIMATION BY USING A PERMANENT MAGNET

### ABSTRACT

Tracking human body motions using inertial sensors has become a well-accepted method in ambulatory applications since the subject is not confined to a lab-bounded volume. However, a major drawback is the inability to estimate relative body positions over time because inertial sensor information only allows position tracking through strapdown integration, but does not provide any information about relative positions. In addition, strapdown integration inherently results in drift of the estimated position over time. We propose a novel method in which a permanent magnet combined with 3D magnetometers and 3D inertial sensors are used to estimate the global trunk orientation and relative pose of the hand with respect to the trunk. An EKF is presented to fuse estimates obtained from inertial sensors with magnetic updates such that the position and orientation between the human hand and trunk as well as the global trunk orientation can be estimated robustly. This has been demonstrated in multiple experiments in which various hand tasks were performed. The most complex task in which simultaneous movements of both trunk and hand were performed resulted in an average RMS position difference with an optical reference system of  $19.7 \pm 2.2$  mm whereas the relative trunk-hand and global trunk orientation error was  $2.3 \pm 0.9$  and  $8.6 \pm 8.7$  deg respectively.

---

Published as:

*H. G. Kortier, J. Antonsson, H. M. Schepers, F. Gustafsson, and P. H. Veltink, "Hand Pose Estimation by Fusion of Inertial and Magnetic Sensing Aided by a Permanent Magnet" IEEE Trans Neural Syst Rehabil Eng, vol. 23, no. 5, pp. 796-806, Sep. 2015. [95]*

## 5.1 INTRODUCTION

Human body motion tracking is of wide interest in various areas, like sports, rehabilitation, ergonomics and entertainment industry [207, 228]. Traditionally, optical tracking systems are used to capture human body motions. However, they suffer from line of sight issues, non-portability, and therefore, operating such devices is often constrained to the volume in which they have been calibrated.

In the last decade, MEMS based inertial sensors became increasingly popular to employ on the human body and formed an alternative for motion tracking purposes [113, 225]. Besides the advantages compared to optical systems, inertial sensors introduce large estimation errors, for both orientation and position, due to integration of inertial signals.

For the estimation of drift free body orientations, several research groups proposed an IMMS which is a filter framework to fuse inertial and magnetic information [154, 162, 230].

However, contrary to estimating 3D orientations, drift free estimates of 3D position over long measurements intervals is much more challenging. This is especially important if non rigid segments as trunk and shoulder are involved.

An example is the assessment of reaching and grasping tasks which are frequently performed in rehabilitation programs to address the severity of a certain disease. Outcome measures include the position accuracy, duration and smoothness of the hand's trajectory which are often determined manually by a physician. Those parameters could be determined using an on-body sensing system which eventually results in a quantitative assessment. This assessment can be carried out in the rehab centre or even at home in daily life situations, for instance in stroke patients [188].

For short time intervals in which the velocity of a certain limb can repeatedly be considered as negligible, for example the foot during walking, suitable initial and final conditions can be applied to mitigate integration drift of the estimated position [165, 176, 194].

Applying forward kinematics for articulated bodies seems to be a suitable method for estimation of positions when the orientation of each segment can be estimated and segmental lengths are known [156, 229]. However, the position error of the end effector accumulates along the articulated chain due to uncertainties in measured segmental lengths, sensor to segment calibration and joint models.

The only robust solution is to fuse inertial sensors with a position aiding system such as optical [155], acoustical [55], Global Positioning System (GPS) [54], Ultra Wide Band (UWB) [75] or visual [76]. A magnetic tracking aiding system offers advantages compared to the other approaches, as indoor environments do not cause a degraded signal and there are no line of sight issues since the human body is transparent for magnetic fields [150].

However, magnetic fields easily get distorted in the vicinity of ferro-magnetic materials. Again, a possible solution is sensor fusion with an aiding system,

which eventually mitigates deviations from the correct state vector during magnetic field disturbances. A solution using an optical system was proposed by Vacarella et al. [191] and a solution using an inertial aiding system was proposed by Roetenberg et al. [154].

Latter method used actuated coils with inertial sensors embodied in a loose fusion filter using a magnetic dipole model. Schepers et al. [166, 167] proposed a similar method but improved the system such that many drawbacks, like coil constellation, energy consumption, loss of stochastic information and short distance measurements were tackled.

Those methods resulted in an accurate position tracking system that can be used in an ambulatory setting. However, some drawbacks still exist. First, energy consumption can be large, especially when large distances are to be covered, and therefore limit the measurement time when the system is used in an ambulatory setting. Second, the coils can be rather large and heavy, which might result in an impaired movement or it could hinder the attachment of the source to specific body locations. Finally, it was impossible to track rapid movements due to the inability of actuating the coils, at a sufficient high rate, in parallel.

The idea of using a permanent magnet for localization and tracking was proposed by Birsan [11]. Using a permanent magnet as a source is beneficial compared to an active source as it can be kept small, works passively and is therefore more suitable for attachment on various body parts. A dipole model of a ferromagnetic object for the detection and tracking of metallic targets, particularly cars, is described by Wahlstrom et.al. [204]. Based on this model Gustafsson and Wahlstrom developed a method to track 3D positions and 2D orientations using a grid of magnetometers and a permanent magnet acting as a source [65].

In this study we propose a new method which combines tracking of a permanent magnet using 3D magnetometers with inertial sensing. Hence, magnetic tracking results in drift free position estimates over long intervals ( $>1$  minute) which is impossible by solely using commercial grade inertial sensors, whereas inertial sensing allows for a robust 3DoF global and relative orientation estimate. In addition, inertial sensing gives pose information during short periods in which magnetometer information is lacking, for instance when the magnet is out of reach.

The aim of this study is to track 3D orientation and 3D position of the hand with respect to the trunk as well as the global orientation of the trunk. This is done by attaching a permanent magnet and an inertial sensor to the hand, and attaching multiple 3D magnetometers and an inertial sensor to the sternum.

## 5.2 METHODS

Figure 5.1 shows the measurement setup which consists of two parts, first the base ( $\Psi_b$ ), comprises a constellation of one or more rigidly connected 3D magnetometers. In addition, inertial information of this constellation is obtained using a 3D gyroscope and 3D accelerometer.



Figure 5.1: Tracking instrumentation attached to trunk and right hand. Visible are four IMMS's (orange) attached to the trunk, each containing a 3D magnetometer. The IMMS that is positioned closest to the right shoulder acts as the primary one and is therefore designated as the trunk's reference frame ( $\Psi_b$ ). Furthermore, accelerometer and gyroscope data is acquired from this IMMS. On the hand, a single IMMS together with a neodymium magnet (silver grey) is visible. The position of the hand ( $p_b^t$ ) and orientation ( $q^{bt}$ ) with respect to the trunk is being estimated. Furthermore the orientation of the trunk with respect to a global frame ( $q^{gb}$ ) is estimated. For each coordinate frame the X (black), Y (white) and Z (dashed) directions are indicated.

Secondly, the target ( $\Psi_t$ ), contains a rigidly connected 3D accelerometer, 3D gyroscope and a permanent magnet. It is the objective to track the position  $p_b^t$ , orientation of the target with respect to the base  $q^{bt}$ , and the orientation of the base with respect to a global frame  $q^{gb}$ .

A general schematic layout is depicted in Fig. 5.2. One can see that it is necessary to have prior knowledge about the constellation. More specifically, the relative position and orientation of all magnetometers with respect to the base frame, as well as the position and orientation of the magnet with respect to the local inertial sensor must be known.

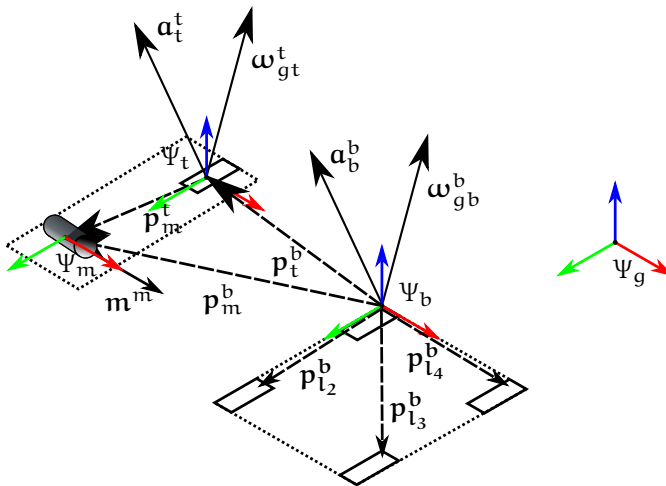


Figure 5.2: Schematic diagram illustrating the global frame  $\Psi_g$ , base frame  $\Psi_b$  and the rigidly attached target frame  $\Psi_t$  and permanent magnet frame  $\Psi_m$ . The relative position  $p_t^b$  and orientation  $q^{bt}$  as well as the global orientation  $q^{bg}$  are estimated by the filter. The base is constellated by 13D magnetometers of which position and orientation with respect to the first magnetometer is invariant and known priorly. In addition, the local magnetic moment ( $m^m$ ), inertial acceleration and angular velocity of target ( $a_t^t, \omega_{gt}^t$ ) and base ( $a_b^b, \omega_{gb}^b$ ) are given.

5

The following sections will describe the filter structure, the measurement models, the process model and finally the experimental methods which are used to validate the accuracy of the proposed system.

### 5.2.1 Filter structure

An EKF has been deployed in order to estimate relative positions as well as relative and absolute orientations [38, 64], see Fig. 5.3.

Inertial measurements are primarily used as input for the process dynamics whereas the magnetic measurements are used for state correction. The state space equations are given by:

$$\begin{aligned} \mathbf{x}_{k+1} &= f(\mathbf{x}_k, \mathbf{u}_k) + \mathbf{w}_k \\ \mathbf{y}_k &= h(\mathbf{x}_k) + \mathbf{v}_k \end{aligned} \quad (5.1)$$

where  $f(\mathbf{x}_k, \mathbf{u}_k)$  denotes the process model,  $\mathbf{y}_k$  the measurements, and  $h(\mathbf{x}_k)$  the measurement model. Process and measurement noise are assumed to be iid Gaussian noise, denoted by  $\mathbf{w}_k$  and  $\mathbf{v}_k$ .

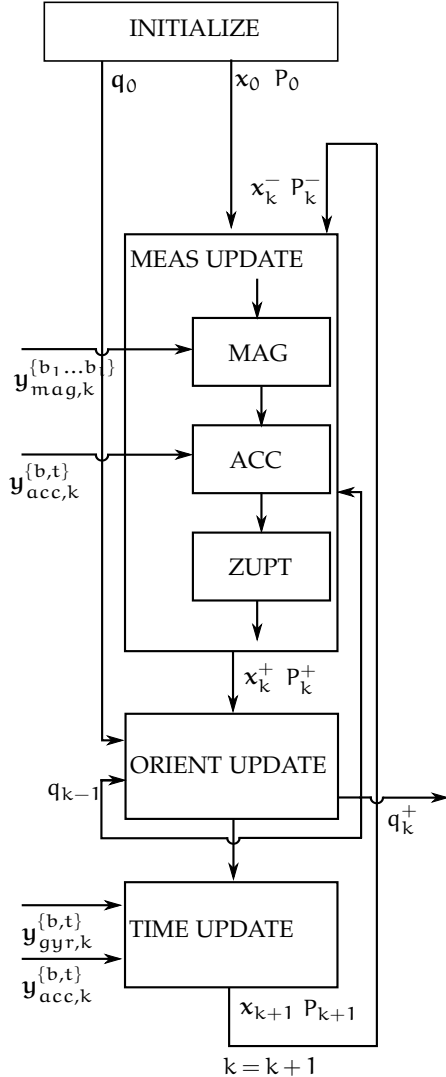


Figure 5.3: Topology of the implemented EKF. After initialisation of both state  $x_0$  and orientation  $q_0$  and corresponding covariance  $P_0$ , a measurement update is performed. This step includes a magnetic update (MAG), acceleration update (ACC) and, when applicable, a zero velocity update (ZUPT). The magnetic update uses information obtained from  $l$  magnetometers expressed in base frame  $\Psi_b$ . The acceleration update step uses accelerometer information of both base and target. Finally the zero velocity update applies an update when either the target velocity is zero with respect to the base or when the target exceeds a pre-defined measurement volume. After the measurement update, the orientation estimates  $q$  of both trunk and target are updated using the estimated error angles  $\delta\theta$ . Subsequently, a time update is performed which includes propagation of the state with corresponding covariance.

The measurement vectors at time  $k$  includes  $l$  magnetometers  $\mathbf{y}_{m,k}^{\{b_1..b_l\}}$  and two accelerometers  $\mathbf{y}_{a,k}^{\{b,t\}}$ . In addition, the accelerometers are used together with two gyroscopes  $\mathbf{y}_{\omega,k}^{\{b,t\}}$  as an input  $\mathbf{u}_k$ .

The state vector includes the following elements:

$$\mathbf{x} = \begin{bmatrix} \mathbf{p}_t^b & \mathbf{v}_t^b & \delta\theta^{bt} & \mathbf{B}^g & \mathbf{b}_g^t & \mathbf{b}_a^t & \delta\theta^{gb} & \mathbf{b}_g^b \end{bmatrix}^T \quad (5.2)$$

where  $\mathbf{p}_t^b$  and  $\mathbf{v}_t^b$  are the position and velocity of the target expressed in the base frame, respectively,  $\mathbf{B}^g$  is the environmental magnetic field experienced by the base expressed in global frame,  $\mathbf{b}_g^t$  and  $\mathbf{b}_a^t$  are the gyroscope and accelerometer bias of the target sensor, respectively, and  $\mathbf{b}_g^b$  is the gyroscope bias attached to the base.

Both orientations are expressed as a unit quaternion  $(q^{bt}, q^{gb})$ , and therefore require the unity norm constraint. Because an EKF is not suitable to handle such constraints properly, the true quaternion is parameterised using a nominal  $\bar{q}$  and error part  $\delta q$  [38]. Under the assumption that the error part is small, we can approximate the error quaternion using an error angle representation  $\delta\theta$ :

$$\begin{aligned} q &= \bar{q} \odot \delta q \\ &\approx \bar{q} \odot [1 \quad \frac{1}{2}\delta\theta]^T \end{aligned} \quad (5.3)$$

where  $\odot$  is the quaternion product operator [100]. The error angles can be handled properly by the EKF filter and therefore included in the state vector  $(\delta\theta^{bt}, \delta\theta^{gb})$ . The corresponding quaternions are adjusted (Fig. 5.3: ORIENT UPDATE) after each measurement update step using the error angle estimates. Because propagation of the error angle (see section 5.2.3) is a function of the gyroscope's error bias, a similar approach for the gyro biases is taken:

$$\mathbf{b}_g = \bar{\mathbf{b}}_g + \delta\mathbf{b}_g \quad (5.4)$$

where  $\mathbf{b}_g$  is the true gyro bias which is modeled by a nominal ( $\bar{\mathbf{b}}_g$ ) and error part ( $\delta\mathbf{b}_g$ ). The latter is included in the state vector and used to update the true bias after the measurement updates. Finally, the error angle and gyro error bias estimates are set to zero before propagated by the process model.

The measurement model is divided in a magnetic update  $\mathbf{h}_{mag}$ , acceleration update  $\mathbf{h}_{acc}$  and zero velocity update  $\mathbf{h}_{zupt}$ . The magnetic update provides information of the relative hand position, 2 DoF of the relative orientation and heading information of the trunk. The acceleration update is required to ensure observability of target and trunk inclination. Finally, the zero velocity update is used to provide additional information in specific conditions. All measurement models will be discussed in detail in section 5.2.2.

The a-posteriori state ( $\mathbf{x}_k^+$ ) and corresponding covariance estimate ( $P_k^+$ ), given the a-priori state and covariance, is determined using the measurement func-

tion ( $h(x_k^-)$ ), its corresponding linearization ( $H_k$ ) and calculated Kalman gain ( $K_k$ ) [64]:

$$\begin{aligned} x_k^+ &= x_k^- + K_k (y_k - h(x_k^-)) \\ P_k^+ &= (I - K_k H_k) P_k^- . \end{aligned} \quad (5.5)$$

Propagation of position and orientation change is obtained by integration of the relative angular velocity and double integration of the relative acceleration, which is described in section 5.2.3. The uncertainty of the corresponding state is propagated according to:

$$P_{k+1}^- = F_k P_k^+ F_k^T + Q_k \quad (5.6)$$

where  $F_k$  the linearized process model  $f(x_k, u_k)$  and  $Q_k$  the covariance matrix of the process noise. The initial covariance  $P_0$  is chosen large for all states except for the relative velocity and orientations because the movement is initiated from rest at an arbitrary position. The process noise covariance  $Q_k$  is experimentally determined by estimating the standard deviation of the inertial sensors.

### 5.2.2 Measurement models

#### Magnetic model

A dipole model is used to track 2 DoF orientation and 3 DoF position of the target [4, 204], and heading information of the trunk. The output of each magnetometer attached to the base is modeled as:

$$\begin{aligned} y_m^l &= h_m^l(x) + e_m \\ &= B + J(r^l)m^l + e_m \end{aligned} \quad (5.7)$$

where the superscript  $l$  indicates the particular magnetometer and  $r^l$  its position with respect to the permanent magnet. The measured field exists of a common component  $B$  and a position dependent component  $J(r)$  which is given by a magnet dipole model:

$$J(r) = \frac{1}{\|r\|_2^5} \left( 3rr^T - \|r\|_2^2 I_3 \right) . \quad (5.8)$$

The position of the target expressed in the base frame is given by (see Fig. 5.2):

$$p_t^b = p_m^b - R^{bt} p_m^t$$

where  $p_m^t$  is the position of the magnet with respect to the local inertial sensor and  $R^{bt}$  the orientation of the target with respect to the base expressed

as a rotation matrix. Subsequently, the position of the magnet measured by magnetometer  $l$  expressed in the frame  $\Psi_b$  is given by:

$$\begin{aligned} \mathbf{r}^b &= \mathbf{p}_m^b - \mathbf{p}_l^b \\ &= \mathbf{p}_t^b + R^{bt} \mathbf{p}_m^t - \mathbf{p}_l^b \end{aligned} \quad (5.10)$$

where  $\mathbf{p}_l^b$  is the position of magnetometer  $l$  with respect to the primary magnetometer expressed in the base frame. The relative orientation between the permanent magnet and local target frame is given by  $R^{tm}$ . This magnetic moment vector  $\mathbf{m}^m$  expressed in the base frame is given by:

$$\mathbf{m}^b = R^{bt} R^{tm} \mathbf{m}^m. \quad (5.11)$$

The global magnetic field  $\mathbf{B}^g$ , which is assumed to be homogeneous within the measurement volume, expressed in the base frame is given by:

$$\mathbf{B}^b = R^{bg} \mathbf{B}^g \quad (5.12)$$

Substituting the parameterized orientation 5.3 into the equations (5.10), (5.11), (5.12) and using the assumption that the magnetometers are equally orientated ( $R^{bl} = I_3$ ) gives:

$$\mathbf{r}^b = \mathbf{p}_t^b + \bar{R}^{bt} \left( I_3 + [\delta\theta]_{\times}^{bt} \right) \mathbf{p}_m^t - \mathbf{p}_l^b \quad (5.13)$$

$$\mathbf{m}^b = \bar{R}^{bt} \left( I_3 + [\delta\theta]_{\times}^{bt} \right) R^{tm} \mathbf{m}^m \quad (5.14)$$

$$\mathbf{B}^b = \bar{R}^{gb,T} \left( I_3 - [\delta\theta]_{\times}^{gb} \right) \mathbf{B}^g \quad (5.15)$$

where the time indices  $k$  have been omitted for clarity and  $[\cdot]_{\times}$  is used to denote a skew symmetric matrix.

In order to construct the Jacobian  $H_{mag}$ , the partial derivatives with respect to the state vector are required. A detailed derivation can be found in appendix 5.5.1.

### *Acceleration model*

The accelerometers on both base and target can be used to obtain a local inclination estimate. This is only valid in a static situation where the inertial acceleration is negligible. Large deviations, i.e. the norm of the measured accelerometer signal is not close to the gravitation constant and the angular velocity norm is not close to zero, can be detected using a Generalized Likelihood Ratio Test (GLRT). This concept has been described by Skog et.al. [176] and has been implemented such that for the "in movement" hypothesis the measurement covariance is adjusted accordingly. The threshold parameters of the GLRT are chosen such that accelerometer measurements are only included if their norm is within five percent of the gravity vector norm.

The measurement model is given by:

$$\mathbf{h}_{\text{acc},b}^{\{b,t\}} = \mathbf{y}_{\text{acc}}^{\{b,t\}} - \bar{\mathbf{R}}^{\{b,t\}g} \left( \mathbf{I}_3 - [\delta\theta]_x^g \right) \mathbf{g}^g + \mathbf{e}_a \quad (5.16)$$

where  $\mathbf{g}^g$  is the known gravitational acceleration vector expressed in the global frame, and  $\mathbf{e}_a$  is the iid Gaussian noise.

However, if both base and target frame experience the same inertial acceleration, additional information about the relative heading can be provided. Therefore a different measurement model is used for the target:

$$\mathbf{h}_{\text{acc},t}^t = \mathbf{y}_{\text{acc}}^t - \bar{\mathbf{R}}^{tb} \left( \mathbf{I}_3 - [\delta\theta]_x^{bt} \right) \mathbf{y}_{\text{acc}}^b + \mathbf{e}_a . \quad (5.17)$$

The difference in magnitude of both measured accelerometer signals is used to test whether this update is applicable.

### *Zero velocity update*

In order to mitigate position diverging, zero velocity updates are applied:

$$\mathbf{h}_{zupt}^b = \mathbf{v}^b + \mathbf{e}_z \quad (5.18)$$

Two different conditions are tested. First, whenever the target or base does not experience an inertial acceleration it is assumed that either is held still which is tested by the same GLRT used for the inclination update. Second, if the target position with respect to the trunk exceeds a predefined cubic volume, the estimate will be kept in this volume by setting the velocity to zero. Latter is used to make the filter more robust such that velocity and position do not drift to infinity when no magnetic information is available for long periods.

#### 5.2.3 Process model

The velocity  $\mathbf{v}_t^b$  and orientations  $\{\mathbf{q}^{gb}, \mathbf{q}^{bt}\}$  are obtained by integration of the difference in measured acceleration  $\mathbf{a}_t^b$  and angular velocity  $\omega_{bt}^t$ . The difference in acceleration  $\mathbf{a}_t^b$  can be expressed as a function of the measured accelerometer signals ( $\mathbf{y}_{\text{acc}}^t, \mathbf{y}_{\text{acc}}^b$ ):

$$\begin{aligned} \mathbf{a}_t^b &= \mathbf{R}^{bt} \mathbf{a}^t - \mathbf{a}^b \\ &= \mathbf{R}^{bt} (\mathbf{y}_{\text{acc}}^t - \mathbf{b}_{a,t}^t - \mathbf{R}^{tg} \mathbf{g}^g) - (\mathbf{y}_{\text{acc}}^b - \mathbf{b}_{a,b}^b - \mathbf{R}^{bg} \mathbf{g}^g) + \mathbf{e}_a \\ &= \mathbf{R}^{bt} (\mathbf{y}_{\text{acc}}^t - \mathbf{b}_{a,t}^t) - (\mathbf{y}_{\text{acc}}^b - \mathbf{b}_{a,b}^b) + \mathbf{e}_a \end{aligned} \quad (5.19)$$

where  $\mathbf{b}_{a,t}^t$  is the accelerometer bias of the target and  $\mathbf{b}_{a,b}^b$  the bias of the base accelerometer which is assumed to be negligible.

The difference in angular velocity expressed in the target frame is given by the difference in measured gyroscope signals of the target  $\mathbf{y}_{gyr}^t$  and base  $\mathbf{y}_{gyr}^b$ :

$$\begin{aligned} \omega_{bt}^t &= \omega_{gt}^t - \mathbf{R}^{bt} \omega_{gb}^b \\ &= (\mathbf{y}_{gyr}^t - \mathbf{b}_{g,t}^t) - \mathbf{R}^{bt,T} (\mathbf{y}_{gyr}^b - \mathbf{b}_{g,b}^b) + \mathbf{e}_g . \end{aligned} \quad (5.20)$$

Propagation of the hand and trunk orientation is given by:

$$\begin{aligned} q_{k+1}^{bt} &= q_k^{bt} \odot \left( \frac{1}{2} T \omega_{k,bt}^t \right) \\ q_{k+1}^{gb} &= q_k^{gb} \odot \left( \frac{1}{2} T \omega_{k,gb}^b \right) \end{aligned} \quad (5.21)$$

where  $k$  indicate the sample,  $T$  is the sample period and  $\odot$  is the quaternion product operator [100]. Subsequently, the linearized state propagation equations which eventually constitute the state transition matrix  $F_k$  are stated as:

$$\begin{aligned} p_{k+1}^b &= p_k^b + T v_k^b + \frac{1}{2} T^2 a_{k,t}^b \\ v_{k+1}^b &= v_k^b + T a_{k,t}^b \\ \delta \theta_{k+1}^{bt} &= \left( I_3 - \left[ T \omega_{k,bt}^b \right] \times \right) \delta \theta_k^{bt} - T (\delta b_g^t - \delta b_g^b) + e_\theta \\ B_{k+1}^g &= B_k^g + e_B \\ b_{a,k+1}^t &= b_{a,k}^t + e_{ba} \\ \delta b_{g,k+1}^t &= \delta b_{g,k}^t + e_{bg} \\ \delta \theta_{k+1}^{gb} &= \left( I_3 - \left[ T \omega_{k,gb}^b \right] \times \right) \delta \theta_k^{gb} - T \delta b_g^b + e_\theta \\ \delta b_{g,k+1}^b &= \delta b_{g,k}^b + e_{bg} . \end{aligned} \quad (5.22)$$

A derivation of the error angle propagation  $\delta \theta$  is given in the appendix 5.5.3.

The local magnetic field  $B^g$ , gyroscope error biases,  $\delta b_g^t$ ,  $\delta b_g^b$ , and accelerometer bias ( $b_a^t$ ) are modelled as random walk processes to account for their low pass behaviour.

#### 5.2.4 Experimental methods

**AMR** magnetometers (Honeywell HMC5883L), each embodied in an **IMMS** (Xsens Technologies B.V. MTw), were rigidly attached to a PMMA panel and strapped to the subject's trunk, see Fig. 5.1. One of the **IMMS**'s was appointed as the primary sensor and designated as the origin of the trunks reference frame ( $\Psi_B$ ). In addition to the magnetometers, inertial sensor signals are obtained from the primary **IMMS**'s accelerometer and gyroscope.

The target, which was placed on the hand, comprises a rigid plaster piece on which a magnet (neodymium rod, length: 2 mm, radius: 7 mm SuperMagne.de) and **IMMS** were attached. The position and orientation of the magnet with respect to the local accelerometer was estimated using a ruler beforehand.

All **IMMS** data was sampled at 60 Hz and transmitted wirelessly to the PC (Xsens Technologies B.V. Awinda). The sensors contain a rechargeable lithium-ion battery which will run for about 4 hours during measurements [221].

Prior to the experiments all magnetometers were calibrated in the volume, in which the experiments was performed, using the magnetic field mapping procedure. All magnetometers were rigidly attached and rotated in any direction, subsequently the magnetic field vectors are mapped onto a unit sphere using a Maximum Likelihood (**ML**) approach described by Kok et al. [91].

As the magnetometer output is normalized during this calibration procedure, we will define the Signal to Noise Ratio ([SNR](#)) of each magnetometer as:

$$\text{SNR}^l = 20 \log \left( \left\| \mathbf{y}_{mag}^l \right\|_2 \right). \quad (5.23)$$

Also both trunk and target accelerometers were calibrated using a fairly simple least squares approach [13]. It should be noted that the bias of the base accelerometer has not been included in the state vector as it is not observable. Finally, the relative position and orientation between magnetometers attached to the plexi panel is required. Because the magnetometer housing also contains inertial sensors of which the position with respect to the local magnetometer is known, it is possible to solve for the relative position and orientation between the rigidly connected magnetometers by expressing the local acceleration as function of the orientation, angular velocity and acceleration and the relative position for each inertial sensor with respect to the other rigidly connected inertial sensors. Now, the required parameters can be obtained if the rigid body is sufficiently accelerated around each axis. A modified version of this algorithm described by Parsa et al. [141] was applied for this purpose.

Both rigid pieces on trunk and hand were accommodated with optical markers (PTI VisualEyes VZ-4000), such that position and orientations could be calculated and subsequently compared to our system.

The inertial sensor system and optical system were synchronized by maximising the correlation between the estimated angular velocities of the hand obtained from both systems.

Possible gaps of the optical system were spline-interpolated with a maximum size of 30 samples.

During the measurement the subject performed various hand tasks while seated at a desk. The total experiment included the following measurements:

1. Static trunk, varying hand: The position and orientation of the trunk were (pseudo) static whereas the position and orientation of the hand were varying cyclically. The subject was asked to maximise the reaching area while seated and minimizing trunk rotations.
2. Varying trunk, static hand: The position and orientation of the trunk were varied by repeated rotations of the trunk around the longitudinal body axis. The subject was asked to keep the hand in a constant relative position and orientation with respect to the trunk.
3. Varying trunk and target. The subject was asked to mimic repeated pick and place actions which required him to change orientation of trunk and hand and relative position between trunk and hand simultaneously. There were no constraints with respect to either trunk or hand movement.

Each measurement lasted 70 seconds, was performed 5 times and were conducted by a single subject. The first 10 seconds of each trial were not taken into account for comparison between our estimates and the optical reference, because this time was required for the filter to recover from an incorrect initial estimate.

### 5.3 RESULTS

A representative trial corresponding to the first measurement condition is depicted in Fig. 5.4. This figure represents the estimate of both distance and total orientation angles (axis-angle representation, [100]) of the hand with respect to the trunk, and the trunk with respect to the global frame. The axes of the trunk are defined such that X points vertically upwards (cranial), Z points in anterior direction (ventral) and Y is chosen such that a right-handed coordinate frame is formed (see Fig. 5.1). The position error is defined as the difference between relative position as estimated by the proposed system and the optical reference system. Similarly, the orientation error is defined as the smallest angle about which the relative orientation of the sensor estimated by the ambulatory system has to be rotated to coincide with the relative orientation estimated by the reference system.

The subject started with the hand far away from the magnetometers, and therefore a low SNR of the magnetic signal induced by the permanent magnet was obtained. In addition, the initial distance estimate was set to zero. For these reasons, the distance and relative orientation estimate up to approximately 5 seconds is unreliable. Periods in which the SNR was above 0.5 dB are indicated using a grey shaded background.

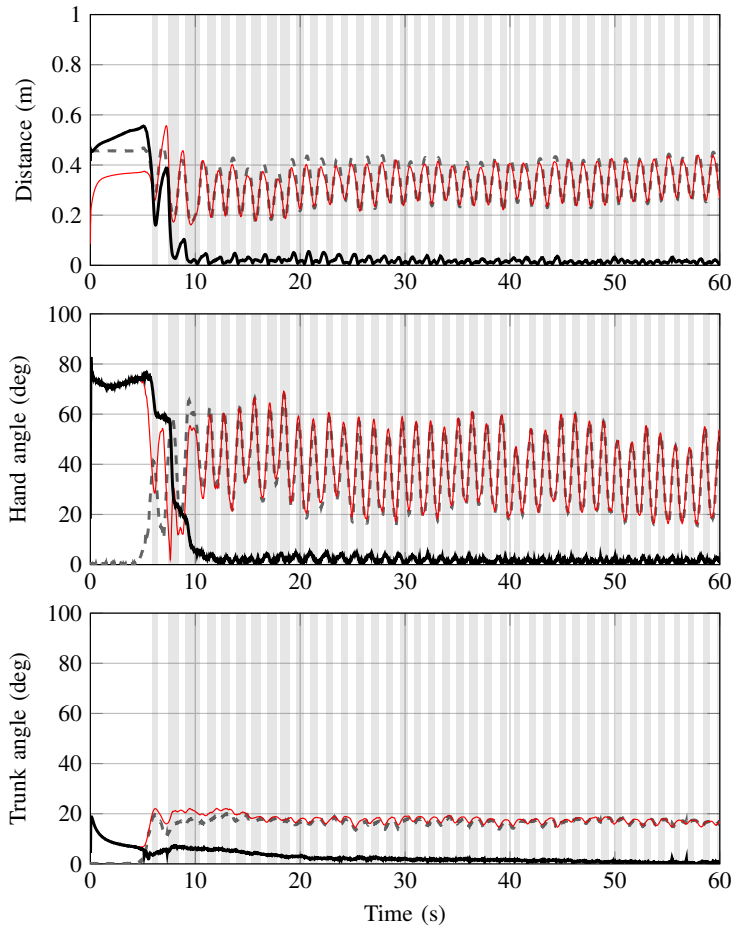
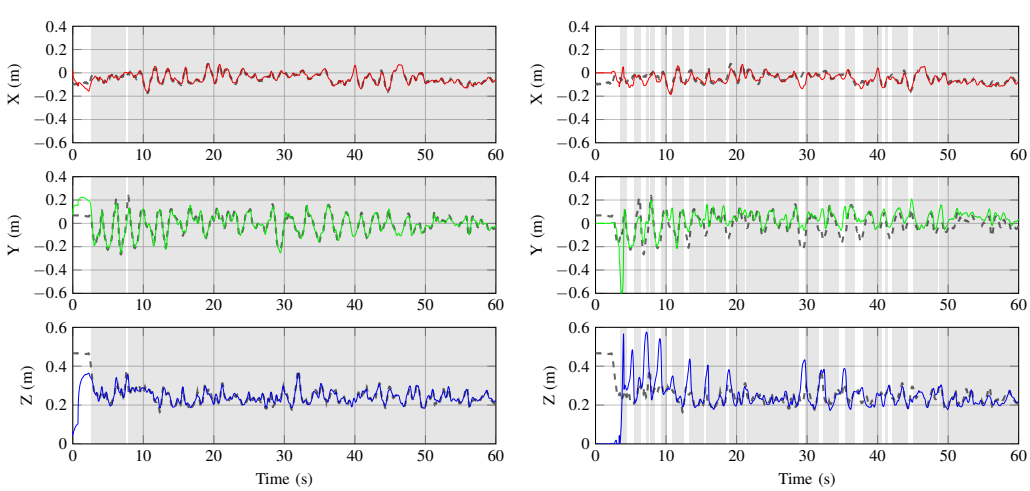


Figure 5.4: Distance (top) and total angle (axis-angle representation) (middle) of the relative orientation (hand with respect to trunk) and global orientation (trunk with respect to the static environment) (bottom) during the reaching task (condition 1). The plots show the estimated values (red), optical reference (grey dashed) as well the corresponding differences (black). A **SNR** above 0.5dB induced by the permanent magnet is indicated (grey background).

From Fig. 5.4 it is noticeable that in many periods minimal information from the permanent magnet was obtained because the magnet was too far away from the trunk. This is certainly the case in the first experiment where the **SNR** was below 0.5 dB for  $50.1 \pm 10.0\%$  of the time compared to the second ( $0.1 \pm 0.0\%$ ) and third experiment ( $8.6 \pm 8.7\%$ ).

A representative trial of the third, and most complex, movement condition is presented in Fig. 5.5a and 5.6. The former figure shows the estimated position of the hand with respect to the trunk together with the optical reference whereas the latter figure shows both the orientation of the trunk with respect to the static global frame and the hand with respect to the trunk. The orientation is represented using Euler angles, in which pitch, roll and yaw represent an angle around the X, Y and Z axis, respectively.

In addition, an estimate of those three kinematic variables using the same measurement trial was made by using only one magnetometer (the one closest to the right shoulder, see Fig. 5.1) instead of four. The position is depicted in Fig. 5.5b and the orientations in Fig. 5.7. Compared to the estimates using four magnetometer it is noticeable that the reconstruction of both position and orientations is worse when a single magnetometer is used, especially in low **SNR** periods. Furthermore, the angle around the vertical is hard to estimate (global yaw, trunk pitch), which can be explained by the fact that is impossible to distinguish between variations in environmental magnetic field and the induced magnetic field by the permanent magnet.



(a) Relative hand trunk position (four magnetometers) (b) Relative hand trunk position (one magnetometer)

Figure 5.5: Estimated position of a varying trunk and hand task (condition 3) using four (left) or one (right) magnetometer. Visible is the estimated position (X,Y,Z) together with the optical reference (grey, dashed). Time periods in which the **SNR** induced by the permanent magnet exceeded 0.5 dB are indicated (grey background).

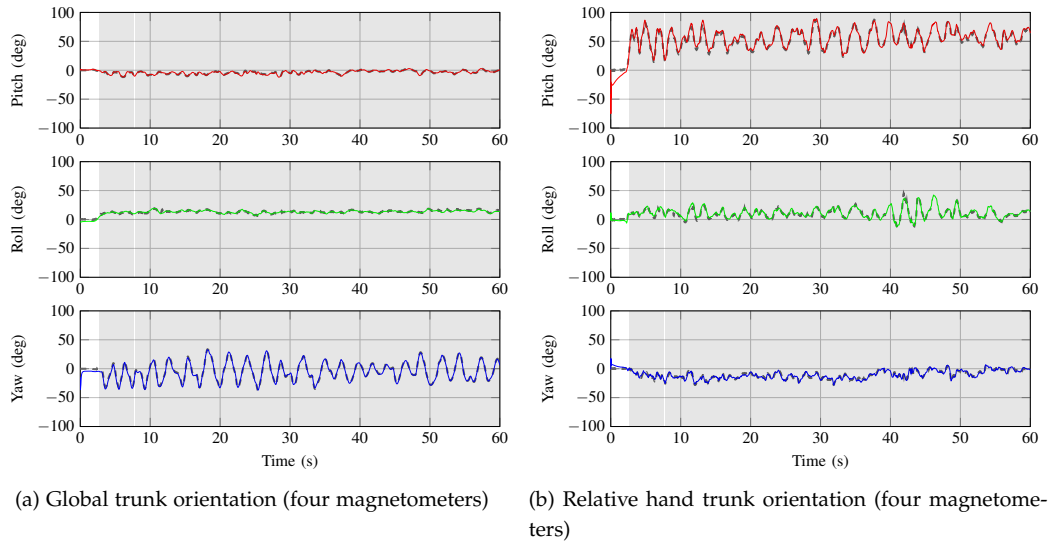


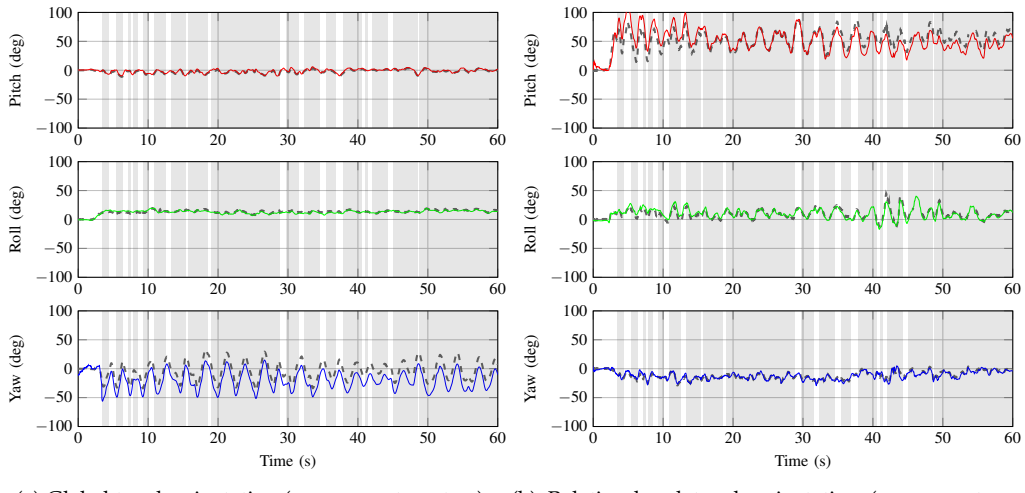
Figure 5.6: Representative trial of a varying trunk and hand task (condition 3) with four magnetometers. Reconstruction of the absolute trunk orientation (left). Reconstruction of hand orientation with respect to the trunk (right). The orientation are expressed in Euler angles (Pitch, Roll, Yaw) A comparison with an optical system is made (grey, dashed). Time periods in which the SNR induced by the permanent magnet exceeded 0.5 dB are indicated (grey background).

In Fig. 5.8 the error distributions of relative positions, orientations and absolute orientation are given for all measurements using box whisker plots. The box plots illustrate that the errors in the position estimate for the second movement condition (varying trunk, static hand) are smaller compared to the other two movement conditions. However, the difference in relative orientation (trunk hand) is larger for this condition, which can be explained by a twice as large magnitude of the trunk's angular velocity compared to the other two conditions. The error in the global trunk orientation estimate is largest for the third measurement condition. This is presumably caused due to the tight filter structure and complexity of movement. Simultaneous trunk and hand movements cause a degraded estimate of the global trunk heading.

#### 5.4 DISCUSSION AND CONCLUSION

This chapter presents a method to accurately estimate the position and orientation of the hand with respect to the trunk and simultaneously estimate the global orientation of the trunk.

Change in position and orientation can be estimated using inertial sensors for short intervals. We aided the inertial sensors by attaching a permanent



(a) Global trunk orientation (one magnetometers) (b) Relative hand trunk orientation (on magnetometers)

Figure 5.7: Representative trial of a varying trunk and hand task (condition 3) with one magnetometer. Reconstruction of the absolute trunk orientation (left). Reconstruction of hand orientation with respect to the trunk (right). The orientation are expressed in Euler angles (Pitch, Roll, Yaw) A comparison with an optical system is made (grey, dashed). Time periods in which the SNR induced by the permanent magnet exceeded 0.5 dB are indicated (grey background).

5

magnet to the hand and measuring the induced field using a set of magnetometers attached to the trunk which allows us to estimate drift free positions and orientations in dynamic tasks over long periods.

The proposed tight filter approach (EKF) is able to compensate for both orientation and position drift. In addition, a good kinematic estimate is still obtained if magnetic information is temporarily unavailable as the filter will rely more on inertial sensing.

The results obtained are promising and can be compared to studies in which an actuated system was used to generate magnetic fields [154, 166]. However, it should be noted that the movement bandwidth was much lower in those studies (approximately 10 times) because the hardware did not allow to generate the magnetic pulses at an adequately high frequency ( $> 2$  Hz). In addition, under more complex movement conditions (varying trunk and hand) our system was able to estimate the positions more accurately whereas the relative orientations estimates were comparable. Finally, using a permanent magnet instead of actuating coils does not require actuation energy, which is an important advantage, bearing in mind that energy capacity is an important aspect when signals must be measured ambulatory.

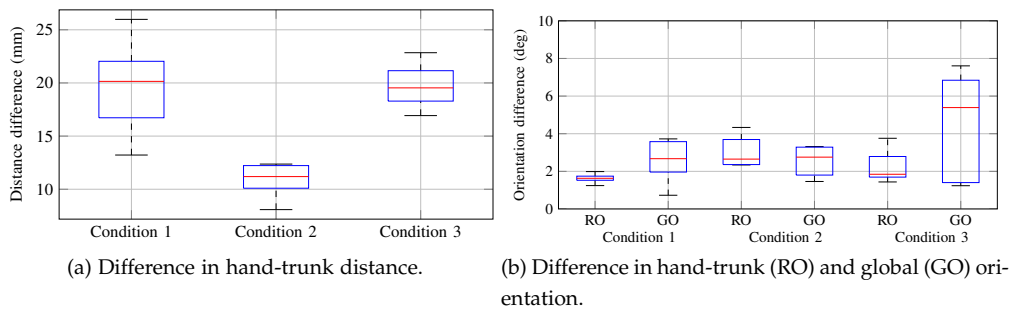


Figure 5.8: Box whisker plots of the estimated kinematic variables. The columns refer to the three different measurement conditions. The box has lines at the lower quartile, median and higher quartile values. The whiskers are the lines showing the extend of the rest of the data. The difference in distance (left) and total orientation (right) are given. The difference in orientation is given for both global (GO) and relative orientation (RO).

The current setup allows for accurate kinematic estimates of hand reaching tasks if the hand trunk distance is repeatedly (intervals less than 4 seconds) below 30 cm. Hence, the accuracy of estimated position strongly depends on the [SNR](#) which is proportional to the distance of the permanent magnet with respect to the magnetometers. This is also demonstrated during the first movement condition in which the subject was asked to reach their arm maximally. The [SNR](#) dropped significantly during those maximum hand position phases ( $50.1 \pm 10.0\%$ ) which subsequently resulted in a relatively low position accuracy ( $19.6 \pm 4.6$  mm).

The accuracy of the relative hand trunk orientation strongly depends on the movement complexity. As indicated by the box plots, a non moving trunk (condition 1) results in the most accurate estimate of the relative hand trunk orientation. Similarly, for the global trunk orientation, an increased movement complexity results in a degraded orientation estimate. However, the first and second movement condition show a similar global trunk performance which can be explained by the fact that a substantial part of the error is contributed by the angle around the global vertical.

Increasing the measurement volume is possible by either adding extra magnetometers or applying a stronger magnet. However, it should be noted that the magnet dimensions become really big with respect to the size of the hand, when a distance over 70 cm is to be covered, because the field strength decreases cubically over distance, whereas the magnet's volume scales linearly.

Only one permanent magnet type was used in this study. Further research should be performed to find the most ideal magnet geometry for the application proposed. In addition, the dipole field approximation is optimal for specifically shaped magnets [144]. Therefore, if the magnet's geometry would be confined, tracking accuracy could be improved presumably.

Another solution to improve the SNR is using more sensitive magnetometers. The next generation magneto resistive (MR) sensors include Giant (GMR) and Tunnel (TMR) magneto resistive sensors which both have a higher sensitivity compared to the AMR based magnetometers that have been used in this study [83].

We used a constellation of four magnetometers, which were rigidly attached to the chest via a Plexiglas plane. However, reducing the number of magnetometers needed would greatly improve the relevance of the proposed method in an ambulatory setting. Wahlstrom et al. [204] demonstrated that only two 3D magnetometers are required to distinguish between changes in magnetic field induced by the permanent magnet or due to environmental field changes. That means the proposed configuration by Wahlstrom et al. obeys observability of the position and orientation states without using inertial sensors. Moreover, the potential of using a single trunk magnetometer aided by inertial sensing is demonstrated and shown in Fig. 5.5b and Fig. 5.7. However, reducing the number of magnetometers requires further research as the accuracy of estimated kinematic variables with a single magnetometer was low compared to a four magnetometer configuration.

If the magnetometers are directly attached to the body, for instance on the sternum, soft tissue artefacts could occur resulting in estimation errors. This could be mitigated when a single trunk magnetometer is used or when the filter is modified such that calibration parameters are estimated online.

Still, further research is required to see the effects of both spatial and temporal magnetic disturbances, soft tissue artefacts as well as the optimal strap location of magnetometers, especially if only one or two magnetometers are used.

Robustness could be further improved by adding biomechanical knowledge of the consecutive links. If the orientation of the shoulder, upper and lower arm is known, forward kinematics can be used to predict the position of the hand with respect to the trunk [156].

The trunk orientation is estimated using the common field component measured by each magnetometer and inclination information measured by the local accelerometer. If environmental magnetic disturbances affect only a part of the magnetometer grid an erroneous trunk heading and eventually relative pose is obtained. Hence, the filter could be improved such that those local disturbances are detected for each magnetometer and discarded if needed.

A final suggestion is to modify the filter such that various parameters can be estimated online. This includes the magnet dipole moment, magnet position with respect to the local inertial sensors and the relative magnetometer poses. A suggestion would be to use an Expectation Maximisation (EM) approach which is able to estimate parameters and states in parallel.

In conclusion, the proposed wearable measurement configuration of inertial and magnetic sensors, combined with a permanent magnet on the hand is able to accurately estimate hand position and orientation with respect to the trunk and the global orientation of the trunk.

## 5.5 APPENDIX

5.5.1 *Partial derivative of the magnetic measurement function w.r.t the position (supercripts are omitted for clarity):*

$$\begin{aligned}\frac{\partial \mathbf{y}_{k,\text{mag}}^l}{\partial \mathbf{r}} &= 3 \frac{\partial}{\partial \mathbf{r}} \|\mathbf{r}\|_2^{-5} (\mathbf{r}^\top \mathbf{m}) \mathbf{r} - \frac{\partial}{\partial \mathbf{r}} \|\mathbf{r}\|_2^{-3} \mathbf{m} \\ &= \frac{3}{\|\mathbf{r}\|_2^5} \left( (\mathbf{r}^\top \mathbf{m}) \mathbf{I}_3 + \mathbf{r} \mathbf{m}^\top - \frac{5(\mathbf{r}^\top \mathbf{m}) \mathbf{r} \mathbf{r}^\top}{\mathbf{r}^\top \mathbf{r}} + \mathbf{m} \mathbf{r}^\top \right)\end{aligned}\quad (5.24)$$

5.5.2 *Partial derivatives of the magnetic measurement with respect to state:*

$$\begin{aligned}\frac{\partial \mathbf{y}_{k,\text{mag}}^l}{\partial \mathbf{p}} &= \frac{3}{\|\mathbf{r}^l\|_2^5} \left( (\mathbf{r}^{l,T} \mathbf{m}) \mathbf{I}_3 + \mathbf{r}^l \mathbf{m}^\top \right) \\ &\quad - \frac{3}{\|\mathbf{r}^l\|_2^5} \left( \frac{5(\mathbf{r}^{l,T} \mathbf{m}) \mathbf{r}^l \mathbf{r}^{l,T}}{\mathbf{r}^{l,T} \mathbf{r}^l} + \mathbf{m} \mathbf{r}^{l,T} \right)\end{aligned}\quad (5.25)$$

$$\frac{\partial \mathbf{y}_{k,\text{mag}}^l}{\partial \mathbf{v}} = 0_3 \quad (5.26)$$

$$\begin{aligned}\frac{\partial \mathbf{y}_{k,\text{mag}}^l}{\partial \delta \theta^{bt}} &= -J(\mathbf{r}_l^b) \bar{R}^{bt} [\mathbf{R}^{tm} \mathbf{m}^m]_{\times} \\ &\quad - \mathbf{R}^{bt} \left( \mathbf{I}_3 + [\theta]_{\times}^{bt} \right) \mathbf{R}^{tm} \mathbf{m}^m \left( J(\mathbf{r}_l^b) \mathbf{R}^{bt} \mathbf{p}_m^b \right)^T\end{aligned}\quad (5.27)$$

$$\frac{\partial \mathbf{y}_{k,\text{mag}}^l}{\partial \mathbf{B}^g} = \mathbf{R}^{gs,T} \quad (5.28)$$

$$\frac{\partial \mathbf{y}_{k,\text{mag}}^l}{\partial \mathbf{b}_a^t} = 0_3 \quad (5.29)$$

$$\frac{\partial \mathbf{y}_{k,\text{mag}}^l}{\partial \delta \mathbf{b}_g^t} = 0_3 \quad (5.30)$$

$$\frac{\partial \mathbf{y}_{k,\text{mag}}^l}{\partial \delta \theta^{gs}} = \bar{R}^{gs,T} [\mathbf{B}^g]_{\times} \quad (5.31)$$

$$\frac{\partial \mathbf{y}_{k,\text{mag}}^l}{\partial \delta \mathbf{b}_g^b} = 0_3 . \quad (5.32)$$

5.5.3 *Expression of the error angle propagation*

One can find the following expression for the error angle dynamics [38] [97]:

$$\dot{\delta \theta} = -[\boldsymbol{\omega}]_{\times} \delta \theta + \delta \boldsymbol{\omega} \quad (5.33)$$

where  $\delta\theta$  is the error angle and  $\hat{\omega}$  is the estimated angular velocity, and  $\delta\omega$  is defined as:

$$\begin{aligned}\delta\omega &= \omega - \hat{\omega} \\ &= (\mathbf{y}_{gyr} - \mathbf{b} - \mathbf{e}) - (\mathbf{y}_{gyr} - \hat{\mathbf{b}}) \\ &= -\delta\mathbf{b} - \mathbf{e}.\end{aligned}\tag{5.34}$$

Discretizing (5.33) using a zero order hold assumption with sample period  $T$  and neglecting the noise term  $e$ , gives:

$$\delta\theta_{k+1} = (I_3 - [T\hat{\omega}_k]_x) \delta\theta_k - T\delta\mathbf{b}.\tag{5.35}$$



## Part II

### ASSESSMENT OF HAND INTERACTIONS USING INERTIAL AND FORCE SENSORS



# 6

## IDENTIFICATION OF OBJECT DYNAMICS

---

### ABSTRACT

Emerging **MEMS** based sensors become much more applicable for on-body measurement purposes lately. Especially, the development of a finger tip-sized tri-axial force sensor provides the opportunity to measure interaction forces between the human hand and environmental objects. We have developed a new prototype device that allows simultaneous 3D force and movement measurements at the finger and thumb tips. The combination of interaction forces and movements makes it possible to identify the dynamical characteristics of the object being handled by the hand. With this device attached to the hand, a subject manipulated mass and spring objects under varying conditions. We were able to identify and estimate the weight of two physical mass objects ( $0.44 \text{ kg}$ :  $29.3\% \pm 18.9\%$  and  $0.28 \text{ kg}$ :  $19.7\% \pm 10.6\%$ ) and the spring constant of a physical spring object ( $16.3\% \pm 12.6\%$ ). The system is a first attempt to quantify the interactions of the hand with the environment and has many potential applications in rehabilitation, ergonomics and sports.

6

---

Published as:

H. G. Kortier, H. M. Schepers, and P. H. Veltink, "Identification of Object Dynamics Using Hand Worn Motion and Force Sensors" *Sensors*, vol. 16, no. 12, Nov. 2016. [96]

## 6.1 INTRODUCTION

A prosperous recovery of arm and hand function after a neuromuscular accident requires adequate training of reach and grasp tasks. It is in many applications desired to evaluate task performances in a quantitative manner. However, the usual procedure is that patients visit the rehabilitation center on a regular basis where either the physical therapist or rehabilitation specialist assesses the patient's performance using subjective measures. Furthermore, such an evaluation is just a snapshot of the patient's capabilities under specific physical and environmental conditions. A continuous monitoring system that informs the physical therapist with quantitative measures obtained in Activities of Daily Living (ADL) would provide more detailed information about the patient's recovery.

A full evaluation of motor task performance during grasp movements requires, besides kinematic, also kinetic measures. Gathering both kinematic and kinetic measures allows for a full dynamic evaluation of tasks in terms of, e.g., movement trajectory, exerted forces, power exchange and the identification of load and body dynamics. In fact, such measures give much more detailed information of the subject's performance compared to solely movement registration and, thus, allow for more specific clinical outcomes.

Previously, we demonstrated the principle feasibility of estimating power exchange by handling passive spring and mass loads [194]. Subsequently, we were able to identify and, moreover, estimate the load characteristics of a system by manipulating its position [94]. However, the instrumentation being used was rather bulky and, therefore, not suitable for on-body attachment.

Measuring interaction forces, tactile information and haptic perception is of interest in many domains [183]. Haptic robots, like DaVinci (Intuitive Surgical, Inc., Sunnyvale, CA, USA) or HapticMaster (Moog Inc., Buffalo, NY, USA), are able to accurately render any kind of contact dynamics, which allow, e.g., surgeons to perform remote operations under minimally-invasive conditions [47]. Those haptic devices require an accurate measure of interaction forces, which are preferably picked up as close as possible to the man-machine interface.

Tactile sensing is important when visual or auditory information is not available or disrupted. Hence, for both humans and robots, tactile information is valuable for identifying and planning strategies during the manipulation of loads [30, 160].

Measuring interaction kinematics and kinetics is essential in the field of neuromuscular modeling [164, 168] and estimation of muscular skeletal loading [218]. Identification of the neuromuscular system in interaction with the environment is in essence a closed-loop identification problem. This imposes several difficulties as most algorithms would estimate the lumped (environment and human body) dynamics. Separation requires known force or movement perturbation signals, such that models can be deduced that represent both active and passive body dynamics, as well as the environmental dynamics. However, it is difficult to simulate situations that mimic ADL because the

human body is able to adapt its internal dynamics for environmental changes easily.

Various groups exploited different force sensing modalities. An in-depth overview and comparison is given by Youssef et al. [224]. They concluded that resistive sensors are still favourable compared to other modalities. However, in the last couple of years, new advances were made for sensors that could be attached to the skin, like strain gauges [139], elastomers [66] or capacitive layers (FingerTPS, PPS Inc., Glasgow, U.K.). A recent review article of Almassri et al. [3] indicated that there is a transition from MEMS kind of solutions towards polymer and piezoresistive solutions in order to improve the haptic sensation. These sensing modalities have high potential, though it is still a major concern to discriminate between different sensing directions. Kurillo et al. [101] developed an isometric force measuring system to quantify grip forces of two fingers and the thumb. Their system used a model to transform the measured tip forces to a total wrench applied to a virtual object. Corresponding movements were subsequently determined by numerical integration. A multi-directional sensitivity is advantageous as it enables one to distinguish between different force components, which are attributed to the total measured force during the grasp of an object. To the authors' knowledge, there is no commercially available sensor that allows measurements of interaction forces in multiple directions and that is suitable for placement on small surfaces, like finger tips.

Recently, Brookhuis et al. [18–21] developed a novel miniaturized six-axis MEMS force/torque (FT) sensor. This sensor is specifically designed for biomedical purposes, such as the measurement of contact forces.

Kinematic estimates can be obtained using widely-available MEMS-based inertial and magnetic sensors. By applying a suitable sensor fusion algorithm, they allow an accurate estimate of the sensors' orientation with respect to a global coordinate frame [152, 161, 220]. Subsequently, by applying forward kinematics, an estimate of the finger and thumb tip positions, velocities and accelerations are obtained, which is demonstrated in chapter 2. More recently, this kinematic hardware (PowerGlove) was used in clinical tests for the assessment of patients suffering from Parkinson's disease and monitoring the hand functioning of aging people [134].

The contribution of this chapter is two-fold. First, an experimental system capable of measuring 3D hand and finger kinetics and kinematics is presented. The system combines a small, commercially available, inertial/magnetic sensor with a novel 6D force torque sensor, as described in the previous paragraph. The sensors are attached to the human hand and allow the measurement of interaction forces and movements simultaneously. Second, a method is presented to estimate the dynamic characteristic of a load being manipulated by the user's hand. The method uses a recursive parametric approach, which is able to identify various properties of dynamic loads under time-varying conditions.

## 6.2 METHOD

The instrumentation setup comprises 3D accelerometers and 3D gyroscopes modules embodied in a single chip (ST LSM330DLC), which are distributed along the dorsal side of the hand. On each of the index and thumb phalanges a single inertial sensor module was attached. In addition, custom-made cuffs (3D printed plastic material) are attached to tips of the index finger and the thumb. Each cuff holds a 6D force/torque sensor on the palmar side of the tip, see Fig. 6.1.

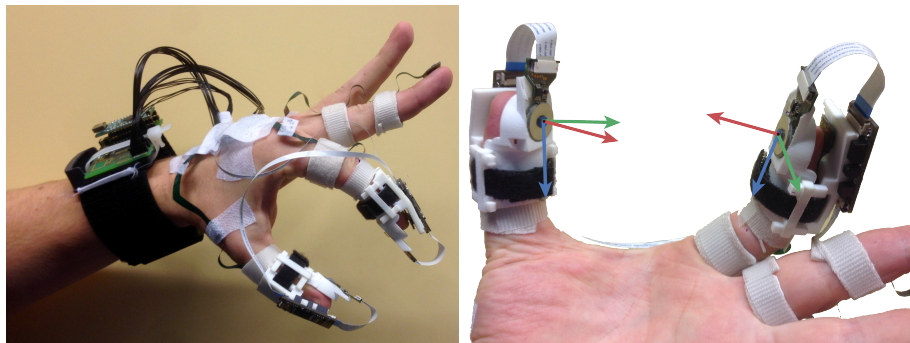


Figure 6.1: Force sensor instrumentation attached to the hand, index finger and thumb.

The inertial kinematic instrumentation (described in chapter 2) is attached to the dorsal side of the hand, index finger and thumb (left). Flexible PCBs allow the connection between the rigid sensor PCBs, which are placed on every digit. Custom-made cuffs (white 3D printed material) secure the force sensor attached to the tips and enforces a rigid connection to the local inertial sensor (right). Applied forces are transferred to the MEMS 6D force/-torque sensor via a cylindrical (height = 3 mm,  $\varnothing$  = 4 mm) glass stylus with rubber coating (blue, origin of the coordinate frames). The force sensor coordinate system is visualized with the x-axis (blue), y-axis (green) and z-axis (red).

The force/torque sensor was developed and built by Brookhuis et al. [21]. Two silicon layers, suspended with a spring-like construction with a known stiffness, can be displaced with respect to each other. Any displacement results in a change of capacity, which gives a direct measure of the forces applied. Using a differential measurement approach, which is realized by comb structures, one can discriminate between various sensing directions. Eventually, capacity change is transformed via a modified martin oscillator to voltages, which are further processed by an Atmel ATmega16 microcontroller.

The custom-made cuffs enforce a rigid connection between the dorsal (inertial sensor) and palmar (force sensor) side of the tip. Hence, the relative

orientation between the inertial and force sensor placed on the same tip is known at all times.

The inertial sensors are used to estimate both the global orientation of the hand and the hand's internal pose (relative orientations of the phalanges). These orientation estimates are used to express all measured signals in a common reference frame (coordinate transformation). In addition, the inertial sensor outputs are used to estimate (relative) translational movements of finger and thumb tips by applying forward kinematics.

Kinetic outputs are used to measure the interaction forces between fingers and the object and to detect the contact between the finger and thumb with an arbitrary object.

Eventually, both kinematic and kinetic estimates are used as an input of the identification algorithm to estimate the dynamic characteristics of the objects manipulated by the hand.

In the next subsections, system identification methods (Section 6.2.1) and the methods for estimating all relevant kinematic and kinetic variables (Section 6.2.2) will be outlined.

### 6.2.1 System Identification

It should be noted that the relation between interaction force and movements at the interface of two bodies is, in general, determined by the dynamic characteristics of both bodies. Identification of such a system is a typical closed loop identification problem [53, 94]. However, if the following conditions are met (a mathematical derivation can be found in Appendix 6.5.1), forces applied by the human body divided by the common velocity yield an approximation of the load's impedance:

1. The human body is an active generator of force:
  - a) The force generated by the human body and applied to an environmental object is minimally influenced by the joint movement of both bodies and can, therefore, be considered as an independent input.
  - b) The force generated by the human body and applied to an environmental object has a sufficiently high bandwidth, that is a larger bandwidth than the load.
2. The load is passive with a relatively low bandwidth.

These conditions are often satisfied in our daily-life interactions with the environment. We will demonstrate that identification of the load characteristics is indeed possible under the above conditions.

Consider a load with unknown internal dynamics being pinched by the index finger and thumb, see Fig. 6.2. According to Newton's second law, the sum of forces acting on the mass when the object is pinched between index and thumb is given by:

$$\sum \mathbf{f} = \mathbf{f}_p + \mathbf{f}_f + \mathbf{f}_g = m\mathbf{a} \quad (6.1)$$

where  $f_p$  is the pinching force,  $f_f$  is the friction force,  $f_g$  the gravitational force,  $m$  is the mass and  $a$  is the acceleration of the mass.

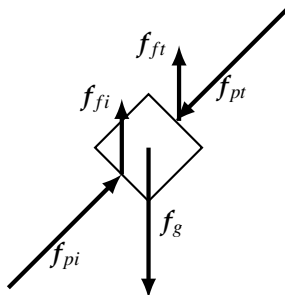


Figure 6.2: Force diagram of a stationary unknown load configuration grasped by the index finger and thumb. The index finger and thumb apply a pinching force indicated by  $f_{p\{i,t\}}$ . Friction  $f_{f\{i,t\}}$  compensates for the gravity  $f_g$  force acting on the load's mass.

In general, the load can be manipulated in two different ways:

1. Inertial and gravitational perturbations act on the load, referred to as external dynamics; for instance, gravitational force (low bandwidth) or inertial displacements introduced by the arm. In addition, viscous and or elastic elements might be present. A non-zero net force would result in an acceleration of the whole object.
2. Internal perturbations of the dynamics; for instance, grasping or pinching, are referred to as internal dynamics. The difference in pinch forces is related to the load dynamics according to Newton's third law. The object exerts equal, but opposite forces.

In order to demonstrate the principle of load identification, rather simple environmental loads will be used that can be manipulated by the index finger and thumb. These loads can be modeled as a mass, which is suspended by a spring-damper pair, see Fig. 6.3.  $f_i$  and  $f_t$  are the measured forces at the contact interface of index finger and thumb, respectively. It is assumed that both springs ( $K_1$  and  $K_2$ ) and dampers ( $D_1$  and  $D_2$ ) have equal characteristics and are only defined in one direction, corresponding to the shortest vector between the application points of both tips. We assume that the internal dynamics obey a large bandwidth compared to the movement bandwidth. That is, either the stiffness is assumed infinitely large or the mass' inertia is assumed to be negligible. Therefore, it is allowed to assume that the distance of the mass is approximately equal to both tips.

$$\|\mathbf{p}_t - \mathbf{p}_m\|_2 \approx \|\mathbf{p}_m - \mathbf{p}_i\|_2 \quad (6.2)$$

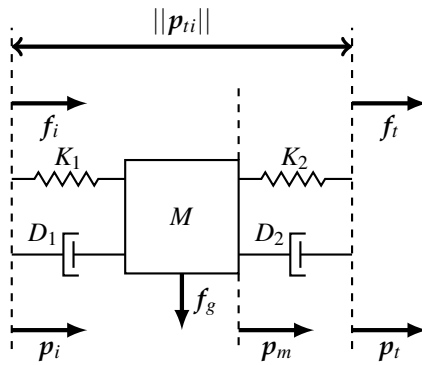


Figure 6.3: Model of the load configuration grasped by the index finger and thumb. A mass ( $M$ ) is suspended by two spring ( $K_{\{1,2\}}$ ) and damper ( $D_{\{1,2\}}$ ) pairs. The index finger and thumb apply forces indicated by  $f_i$  and  $f_t$ . The positions of the mass, index finger and thumb are indicated by  $p_m$ ,  $p_i$  and  $p_t$ , respectively.

The total force exerted by springs and dampers is summed and modeled in a simple linear fashion:

$$f_s = -K(p_{ti} - p_0) \quad (6.3)$$

$$f_d = -D\dot{p}_{ti} \quad (6.4)$$

Now, for the first situation, i.e., when the (mass)load is accelerated, we assume that the relative acceleration of the mass with respect to the tips is negligible compared to the gravitational acceleration, see (6.2) ( $\ddot{p}_{tm} = \ddot{p}_{mi} \approx 0$ ). The summed forces can be rewritten as:

$$f_i^g + f_t^g = f_{tot}^g = M(g^g + a^g) \quad (6.5)$$

where  $g$  and  $a$  are the gravitational and inertial accelerations, respectively. The superscript  $g$  implies that the vector is expressed in the global inertial reference frame.

The second situation, i.e., internal force perturbations, requires the difference in tip forces, which can be expressed as:

$$f_i - f_t = f_{diff} = D\dot{p}_{ti} + K(p_{ti} - p_0). \quad (6.6)$$

Equations (6.5) and (6.6) can be written in a linear fashion for each time instance  $k$ :

$$\mathbf{y}_k = \mathbf{H}_k \boldsymbol{\theta} + \mathbf{e}, \quad (6.7)$$

where  $H_k$  is the measurement matrix,  $\theta = [M \ D \ K]^T$  the parameter vector and  $e$  is an independent error term. Subsequently, Equation (6.7) can be stated as a linear optimization problem:

$$\hat{\theta} = \arg \min_{\theta} \sum_{k=0}^N (\mathbf{y}_k - H_k \theta)^T R_k^T (\mathbf{y}_k - H_k \theta) \quad (6.8)$$

where we seek for the optimal parameter vector  $\hat{\theta}$ , such that the above function is minimized. Equation (6.8) can be solved easily using a weighted least squares solver. The covariance  $R$  matrix defines the uncertainty of different measured signals. Alternatively, equation (6.8) can be written as a batched form, such that the parameter values are found recursively. This is advantageous because not all input data has to be collected prior to the start of the system identification process, and changes of the parameter values, which often occur in [ADL](#) tasks, can be estimated over time. A popular and robust algorithm to solve for varying parameter values is the Recursive Least Squares ([RLS](#)) solution [64] and has therefore been applied.

### 6.2.2 Kinematics and Kinetics

As mentioned in the introduction of the Methods section, the kinematics estimates are necessary for two purposes.

1. Expressing all 3D sensor signals in the same coordinate frame. This allows further processing during the system identification step, and requires the relative orientation between different segments and the global frame.
2. Having a kinematic estimate of both the finger and thumb tip.

An [EKF](#) approach was deployed to estimate the optimal orientation between the sensor frame ( $\Psi_b$ ) and global frame ( $\Psi_g$ ) being expressed by an unit quaternion ( $q^{gb}$ ). Such an approach has a good reputation as a sensor fusion strategy in terms of accuracy and computational load [38]. It uses the 3D gyroscope ( $\mathbf{y}^g$ ) as the primary input for the one step ahead predictor of the orientation:

$$q_{k+1}^{gb} = q_k^{gb} \odot \left( \frac{T}{2} \omega_{k,gb}^b \right) \quad (6.9)$$

where  $T$  is the sample period,  $\odot$  the quaternion product operator and  $\omega_{k,gb}^b$  the angular velocity, which is directly derived from the gyroscope output:

$$\omega_{k,gb}^b = \mathbf{y}_k^g - e_\omega \quad (6.10)$$

where  $e_\omega$  is an [iid](#) Gaussian noise source.

Next, using vector measures of the accelerometers, an independent orientation estimate is obtained and can be used to correct for errors caused by integration drift [152].

Prior to transforming to the global frame, the force sensor output  $\mathbf{y}_f$  needs to be expressed in the coordinate frame of the local inertial sensors  $\Psi_b$ , which has been done by the knowledge of the finger cuffs' geometry.

Summarizing, for the force sensor output ( $\mathbf{y}_f^f$ ), the total transformation of the force sensor output is given by:

$$\mathbf{y}_f^g = R(q^{gb})R(q^{bf})\mathbf{y}_f^f \quad (6.11)$$

where the orientations are expressed using rotation matrices  $R$  [100], and the force sensor output is modeled as:

$$\mathbf{y}_f^f = \mathbf{f}^f + \mathbf{e}_f^f \quad (6.12)$$

where  $\mathbf{e}_f^f$  is modeled as an iid Gaussian noise source.

Besides orientations, the relative acceleration ( $\ddot{\mathbf{p}}_{ti}$ ), velocity ( $\dot{\mathbf{p}}_{ti}$ ) and position ( $\mathbf{p}_{ti}$ ) between the thumb and index finger tips are required as input for the system identification calculations. This is established using forward kinematics combined with the estimated orientation of different finger and thumb segments, explained in the previous chapter 2, but with a slight modification because the magnetometer readings are not used to estimate the relative heading. Two different approaches have been used to ensure the observability of the relative orientation during grasp.

1. Global force during manipulations: When an object is grasped with the index finger and thumb and is not displaced by the hand or arm, only a single external force, hence gravity, acts on the object. All other forces cancel each other out, otherwise the object would be accelerated. This gives the ability to perform an update of the relative orientation update between both tip frames.

With the assumption that the horizontal components of the average net force in the global frame are negligible, the following equation holds:

$$\mathbf{y}_{\text{force}} = A R^{gh} \left( R^{hi} \mathbf{y}_f^i + R^{ht} \mathbf{y}_f^t \right) + \mathbf{e}_{\text{force}} \quad (6.13)$$

with  $\mathbf{y}_f$  being the force measured on the tip of the thumb and index finger and  $R$  the rotation matrix describing the relative orientation between either the hand (h), thumb tip (t), index finger tip (i) and global frame (g). An iid Gaussian noise source is indicated with  $\mathbf{e}_{\text{force}}$ , and  $A$  are the directions of the horizontal force component:

$$A = \begin{bmatrix} 1 & 0 & 0 \\ 0 & 1 & 0 \end{bmatrix}.$$

2. Relative orientation obtained during movements: Under certain conditions, for instance picking up an object after it has been grasped, it is only the subject's arm that is moving. That means that all digits are not or only relatively slowly moving with respect to each other. This makes it possible to use the relative accelerations and angular velocities as a measurement update. Both signals are measured in a different sensor frame, but have the same magnitude. This allows us to update the relative orientation between segments during those pseudo static intervals.
- This can be modeled as:

$$\mathbf{y}_{\text{movement}} = \mathbf{R}^{12} \mathbf{y}_{\{g,a\}}^2 - \mathbf{y}_{\{g,a\}}^1 + \mathbf{e}_{\text{movement}} \quad (6.14)$$

where  $\mathbf{R}^{12}$  is the orientation between two arbitrary frames and  $\mathbf{e}_{\text{movement}}$  an iid Gaussian noise term. Hence, this update is only applicable under strict conditions. Testing for these conditions can be done using a test statistics on the measured gyroscope and acceleration signals. Large deviations, i.e., the norm of the difference in measured acceleration or angular velocity signals is not close to zero, are detected using a GLRT described by Skog et al. [176].

A schematic overview of the implemented kinematic estimation algorithm is given in Fig. 6.4. Hence, this approach is similar as described in chapter 2 with the difference that: (1) there is no inclusion of magnetometers as their output would have been distorted by the objects that have been grasped; (2) force and gyroscope information is used to update relative orientations during specific phases of the grasp.

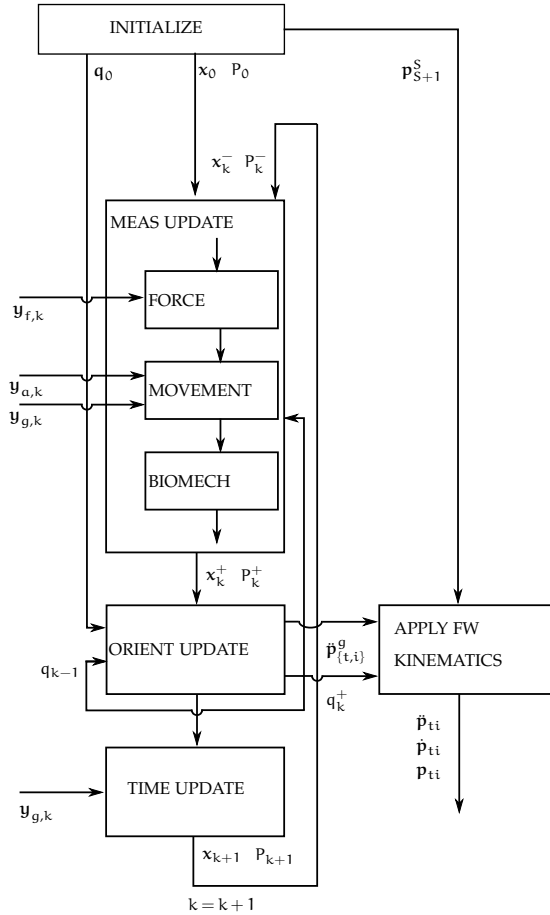


Figure 6.4: Topology of the kinematic estimation filter embodied in an EKF that operates on the error states (also known as a MEKF [38]). The inputs consist of the sensor data ( $y_f, y_a, y_g$ ) and the lengths of the finger and thumb segments ( $P_{S+1}^S$ ). The output consists of the relative kinematics ( $p_{t,i}, \dot{p}_{t,i}, \ddot{p}_{t,i}$ ) and inertial acceleration of the tips ( $\ddot{p}_{\{t,i\}}^g$ ). After initialization of both the state ( $x$ ), error state ( $\delta x$ ) and corresponding covariances ( $P$ ), a measurement update of error states according to the measured forces, accelerations, angular velocities ( $y_f, y_a, y_g$ ) and biomechanical dimensionality information is performed. Information of the force and movement updates can be found in Section 6.2.2 and equations (6.13) and (6.14). Information of applying biomechanical constraints as a measurement update can be found in our previous article [97]. The orientation states are subsequently used to perform the forward kinematics. Given the set of segmental lengths ( $P_{S+1}^S$ ) of the finger and thumb, one can calculate the position, velocity and accelerations of the tips, see also equation (2.1) from [97]. Subsequently, gyroscope information  $y_g$  is used as an input along with a motion model to predict the next state (time update). Finally, the next iteration is initiated ( $k = k + 1$ ), and the described procedure is repeated.

### 6.2.3 Experimental Method

Two different experiments were conducted, each with a different load configuration being handled by the subject.

A subject was seated at a desk with the PowerSensor hardware put on the left hand using Velcro straps, see Fig. 6.1. The forearm and wrist were in a position such that the palm was faced tangential with respect to the table top.

The PowerSensor hardware deploys three triaxial gyroscope ( $\pm 2000$  deg/s) and accelerometer ( $\pm 4$  G) pairs (ST LSM330DLC), one for each finger and thumb segment. In addition, the tips of the index finger and thumb were equipped with the force sensor. Sensor data are sampled (200 Hz for the gyroscope, 100 Hz for the accelerometer, 12 Hz for the force/torque sensors) by a microcontroller (Atmel XMEGA), collected by a master microcontroller (Atmel XMEGA) and subsequently transmitted via USB to the computer. After collecting the sensor data, a sensor to segment calibration was performed as described in chapter 2. Then, the kinematics filter and system identification algorithm were executed consecutively. All algorithms are written and executed in customized MATLAB and Python scripts.

In the first experiment, two cylindrical (radius of 3 cm) mass loads (with different mass weights: 0.28 kg and 0.44 kg) were manipulated. The load was initially resting on the table, then grasped by the index finger and thumb, lifted for about 3 s at a height of 0.5 m and eventually placed on the table again. It is assumed that this load corresponds to an infinite stiff internal load, whereas the mass weight parameter is assumed to be finite. There is a change in applied forces on the load as the table exerts a normal force to compensate for the gravitational force at the start and finish of the experiment.

In the second experiment, a passive linear compression spring (spring constant = 0.6 N/mm, zero force length = 4 cm, weight =  $10 \times 10^{-3}$  kg) was handled. This load corresponds to a finite stiff internal load and a negligible external mass load. The load was handled in a similar way as the mass load; initially resting on the tabletop, picked up and lifted to a height of approximately 20 cm. Then, the spring was repeatedly compressed eight times by the index finger and thumb. Finally, the subject placed the spring load back on the table top. The total force applied by the fingers is assumed to be equal, but opposite (the weight and inertia of the spring are neglected) to the force exerted by the spring. The spring offset position  $p_0$  was determined at the moment the spring was grasped.

Each experiment was performed by a single subject and repeated 10 times. The medical ethical committee of the Medisch Spectrum Twente (Enschede, NL, The Netherlands) confirmed that no further ethical approval concerning the Medical Research Involving Human Subjects Act (WMO) was required, due to the nature of the study.

### 6.3 RESULTS

An example reconstruction of the measured 3D forces during the first experiment, i.e., lifting a mass load (0.44 kg), is depicted in Fig. 6.5. Visible are the measured forces starting from grasping the mass load until releasing the load back on the table top. The sum of measured forces expressed in the global reference frame is visible in the right plot. The z-component is primarily determined by the gravitational force exerted on the mass load because inertial accelerations were not dominant compared to the gravitational acceleration acting in the vertical (z) direction.

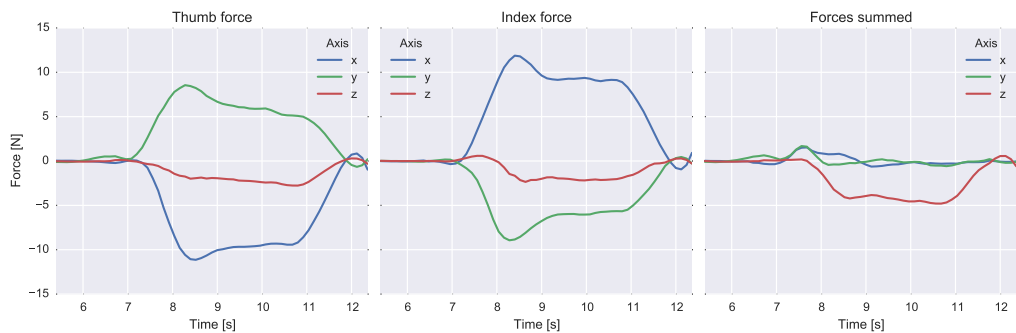


Figure 6.5: Experiment 1: lifting a mass load (0.44 kg); the forces of the index finger (left) and thumb (middle). In addition, the summed forces are displayed (right). All signals are expressed in the global coordinate frame.

A time snapshot, at 11 seconds, of the same trial is used to reconstruct the measured forces in 3D, see Fig. 6.6. Both measured force vectors are expressed in a global reference frame. It can be seen that both vectors have opposite horizontal and positive vertical components. This indicates that, besides normal forces, also shear forces are present during the grasp.

The mass's weight is estimated online using the RLS algorithm. A point estimate of the estimated weight value is determined at 0.5 s before the release of the object, where it should be noticed that the grasp and release of the object have been determined using a threshold detector acting on the sum of measured forces. An example time series of the, recursively, estimated mass's weight is depicted in Fig. 6.7.

Fig. 6.8 represents a trial of the second experiment (spring compressions). The 3D forces of the thumb and index finger are depicted, as well as, the total force magnitudes and relative distance between both tips. During the experiment, the subject imposed minimal hand accelerations. This has been empirically observed by testing for the difference in the norms of the measured accelerations and the known gravitational acceleration.

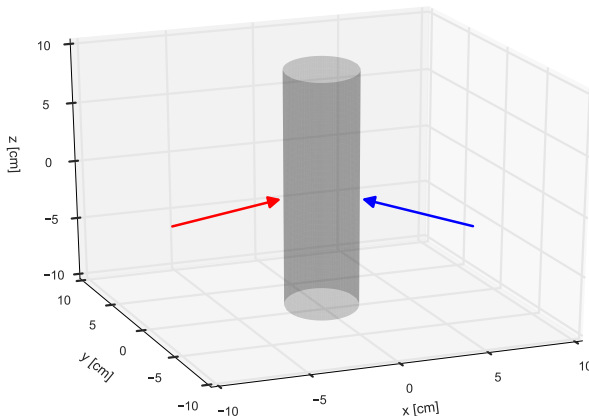


Figure 6.6: Experiment 1: lifting a cylindrical (radius = 3 cm) mass load (0.44 kg); the force vectors for thumb (red) and index finger (blue) are displayed when the load was grasped and held still in the air. Both vectors are expressed in the global reference frame.

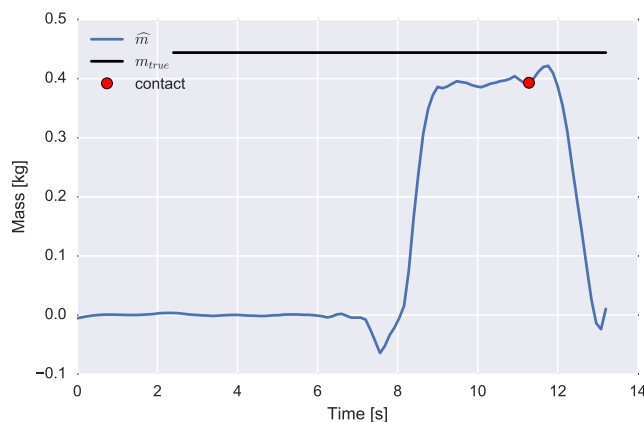


Figure 6.7: Experiment 1: lifting the cylindrical mass load (0.44 kg). The estimated (blue) and true (black) mass weight parameter value are displayed. The load has been grasped at approximately  $t = 7$  s. A point estimate of the mass value used for further analysis is indicated by a red dot.

The estimation error is defined as the absolute difference between the estimated and true value of the mass weight parameter (first experiment) and spring stiffness parameter (second experiment). The experiments were repeated 10 times for both mass weights loads and the spring load. Absolute differences are given in box-plots (see Fig. 6.9) and were  $0.13 \pm 0.08$  kg ( $29.3\% \pm 18.9\%$ ) for the large mass load (0.44 kg) and  $0.06 \pm 0.03$  kg ( $19.7\% \pm 10.6\%$ ) for the smaller

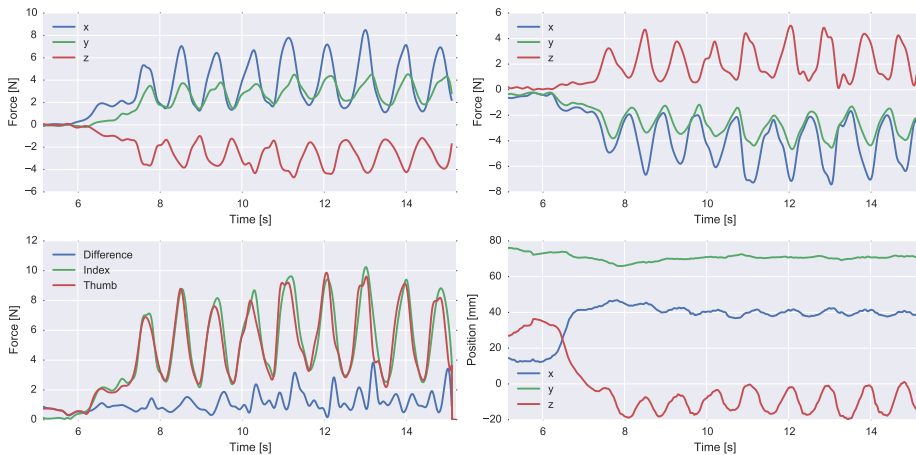


Figure 6.8: Example reconstruction of Experiment 2 where a spring load was manipulated. A force has been applied to the spring by index finger (top left) and thumb (top right). The magnitude of both index finger and thumb forces and the magnitude of the sum are depicted in the (lower left) graph. The (lower right) plot depicts the relative tip position. All signals are expressed in the global coordinate frame.

mass load (0.28 kg). Like the first experiment, an RLS algorithm was used to estimate the spring stiffness online. A point estimate of the parameter value was, arbitrarily, determined 0.5 s before the release of the spring object. The absolute error values of the estimated spring constant are  $8.9 \pm 5.7 \times 10^{-2}$  (N/mm) ( $14.8\% \pm 9.6\%$ ). The variation of differences are visualized in the box-plot, see Fig. 6.9.

#### 6.4 DISCUSSION AND CONCLUSION

We have demonstrated a novel device that allows the simultaneous measurement of thumb and finger movements and interaction forces with the environment. The system was tested during fairly simple hand motor tasks and was able to reconstruct the important dynamic characteristics of loads being manipulated by the index finger and thumb.

Yet, the proposed device is a prototype and therefore in an experimental status that copes with various, mostly practical, issues. Those issues reflect the quality of the estimated parameters. It is our intention to show the feasibility of such a system. Further sensitivity analyses of different subsystems are required to improve the quality of the output data.

First, attachment of the force sensors to the skin is a major concern. Human tissue deforms easily, especially when it is in contact with external objects. These deformations deteriorate kinematic estimates of MoCap systems, often

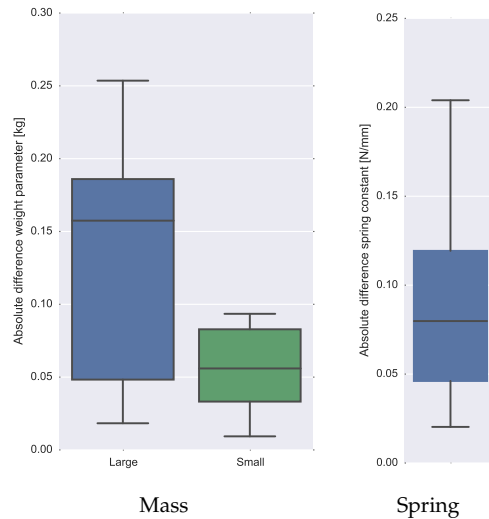


Figure 6.9: Boxplots of the absolute difference measures of the mass parameter (kg) estimated during Experiment 1 for two different loads (left), and a boxplot of the stiffness parameter (N/mm) estimated during Experiment 2 (right). The median, upper and lower quartiles and outliers are visualized. All experiments were conducted 10 times.

indicated as Soft tissue artifacts (STA) [28, 107]. Soft tissue artifacts can be reduced if forces induced by movement accelerations are small compared to the forces causing skin deformations. This can be achieved by keeping the sensor lightweight and small.

Second, measuring interaction forces requires a proper coupling between the human tissue, force sensor and the environmental load. Force sensors are inherently stiff, which makes a good skin to sensor attachment rather difficult as the sensor easily tends to shift when forces are applied (STA). In our study, custom-made cuffs were designed and used to attach both force and movement sensors to the tips. The combination of cuff and stiff sensors results in the loss of touch and causes major difficulties in proper handling of the load. In this study, only two force sensors were used. Hence, grasping an object forces the subject to pinch with the index and thumb finger tips. If the Center of Mass (CoM) of the object is not positioned between the application points, an undesired moment is applied around the force sensor's normal sensitive axis. Stability could be improved significantly when three or more fingers are used for grasping.

Third, the electronic data acquisition circuitry requires improvements as it is currently sensitive for power supply fluctuations, which especially affects the daisy-chained force sensors. All force sensor data have been low pass filtered prior to further processing in order to minimize this effect as much as possible.

Further improvements can be made in the sampling rate of the force sensor, which has been capped as the sensor used a 100-Hz clock to read each of the 12 force channels serially. The effective sample frequency is restricted to 8.3 Hz, whereas the individual channels should preferably be sampled at a much higher rate ( $>100$  Hz). In our study, a cubic interpolator was used in order to feed the Kalman filter with force updates at a sufficient rate.

Fourth, as mentioned in the Methods section, it is necessary to express both force sensors in a common coordinate frame. The inertial sensors were used for this purpose. Prior to using the inertial sensors for kinematic estimates, a mapping (sensor to segment calibration) is required. Obtaining a proper calibration is a bit difficult because the subject is constrained in his/her movements due to the apparatus being attached to the subject's hand. Another drawback of the inertial sensors is that the gyroscope and accelerometer pair provide only the relative orientation during sufficient common movement. In the static situation, only the relative inclination is provided. A traditional IMMU provides heading information using a magnetometer. However, large disturbances due to the vicinity of magnetic materials make this approach challenging. In addition, the relative orientation between the rigid force and inertial sensor should be known. An improved version of the kinematic estimator is currently under development, which avoids the usage of the magnetometers, but still provides robust heading estimates.

Any of the mentioned errors could have been accumulated, which resulted in a fairly large mismatch between the true and estimated parameter values.

Two different loads, indicated as a mass and a spring, were manipulated. They do not only differ in dynamic characteristics, but also in the way they were handled; the mass was primarily perturbed by an external gravitational force, whereas the spring was perturbed by internally-applied finger forces. Those two distinct load types are common in ADL tasks where grasping and releasing a load involves gripping forces and displacing a load involves one or more external force sources. The way forces act differently on both loads could also be an explanation for the relatively large errors of the spring's constant estimate compared to the mass' parameter estimates. The estimation quality of the spring relies heavily on the relative kinematics, whereas the mass estimate only requires a good estimate of the inclination during static, that is minimal movement, periods. The estimate of the relative orientation between the thumb and index finger tips could be improved when heading information is available during the complete movement and not only during the limited periods of the contact.

In our study, the external dynamics were assumed to be rather simple, as only the gravitational acceleration was dominant. Higher order dynamics could be implemented fairly easily for various loads, like drag frictions and inertial accelerations. The latter would be practically easy, but requires either a fairly large mass or a large force sensor bandwidth, which are both troublesome for the current setup.

Independent perturbations are required to identify parts of the closed loop system. Depending on the type (movement or force) and location where the perturbation enters the loop, different parts of the loop will be identified. Further research is required to analyze the estimation validity using measures of interaction forces and movement under such various conditions and excitations.

A possible application in the rehabilitation field of the proposed device is the classification and quantification of various hand motor tasks. Especially in neurological diseases, it is often the case that the disease results in spasticity of the arm and hand muscles. Not only the grasps (e.g., power grip, pinching, span) could be assessed, but also the planning of the tasks and, hence, the strategy of different subjects aimed at performing a single task could be monitored using our device. Quantitative measures of not only the forces applied to an environmental object, but also measures from the corresponding arm and hand movements give much more information (e.g., power exchange) about the efficiency with which the subject is performing the specific task.

Further application areas can be found in machine learning, like the classification of various handled objects. Obviously, a physical interpretation of the quantitative outcomes might be impossible, but the requirements of the sensing hardware could be less strict.

The current hardware has a large advantage, as it measures in multiple directions and, therefore, might enable the estimation of complex load dynamics, like a mug with a viscous or granular content.

## CONCLUSION

Body-worn unobtrusive sensing systems are of utmost importance for interaction measurements in [ADL](#) tasks.

The development and preliminary validation of a hand-worn 3D force and movement setup has been presented. The setup allows for measurements of independent finger movements and forces using a custom-made hardware that includes 3D [MEMS](#)-based force and inertial sensors, which can be worn on small body surfaces, like finger tips.

Two loads were manipulated by the hand, and their dynamic characteristics were estimated by simultaneously measuring kinematic and kinetic sensor data, applying orientation filters and subsequently applying a recursive system identification algorithm.

The system goes beyond pressure sensing and gesture recognition and, therefore, opens up the ability to gather profound insights into interaction optimization between the human body and its environment.

## 6.5 APPENDIX

## 6.5.1 Closed Loop System Identification

Fig. 6.10 models the closed loop coupling between the human body (dashed rectangle) and environmental load (P). The human body (dashed box) consists of a set-point controller with reference position signal ( $r$ ), dynamics ( $H$ ) and an independent force source ( $w$ ). External force ( $n$ ) and position disturbances ( $m$ ) and both inputs are assumed independent. Hence, this can be shown in the frequency domain with the cross-spectral densities being zero:

$$S_{rn} = S_{rw} = S_{rm} = \dots = 0. \quad (6.15)$$

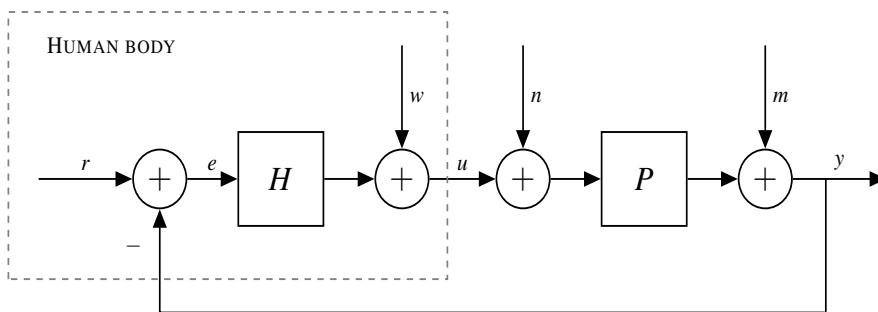


Figure 6.10: Closed loop representation of human (H) load (P) interaction. The human body (dashed) is modeled as a setpoint controller, dynamics (H) and an independent active force generator (w). Independent force (n) and position disturbances (m) are given.

We measure both positions  $y$  and forces  $u$ . Now, the frequency response function (FRF) of the load is given by:

$$\hat{P} = \frac{S_{uy}}{S_{uu}} \quad (6.16)$$

The Fourier transforms of  $u$  and  $y$  are given by:

$$U(\omega) = S_{HR} + SW - SHM - SHPN \quad (6.17)$$

$$Y(\omega) = SHPR + SPW + SPN + SM \quad (6.18)$$

where the sensitivity  $S$  is given by:

$$S(\omega) = \frac{1}{1 + H(\omega)P(\omega)} \quad (6.19)$$

Now, the cross- and auto-spectral density are given by:

$$\begin{aligned} S_{uy} &= \frac{1}{T} U^* Y \\ &= \frac{|S|^2}{T} \left( |H_0|^2 P S_{rr} + P S_{ww} - H^* S_{mn} - H^* |P_0|^2 S_{nn} \right) \end{aligned} \quad (6.20)$$

$$\begin{aligned} S_{uu} &= \frac{1}{T} U^* U \\ &= \frac{|S|^2}{T} \left( |H_0|^2 S_{rr} + S_{ww} - |H_0|^2 S_{mn} - |H_0|^2 |P_0|^2 S_{nn} \right) \end{aligned} \quad (6.21)$$

where the asterisk symbol indicates the complex conjugate and:

$$S^* S = |S|^2 \quad (6.22)$$

Finally, one yields the FRF estimate of the plant [110, 146]:

$$\begin{aligned} \hat{P} &= \frac{S_{uy}}{S_{uu}} \\ &= \frac{|H_0|^2 P S_{rr} + P S_{ww} - H^* S_{mn} - H^* |P_0|^2 S_{nn}}{|H_0|^2 S_{rr} + S_{ww} - |H_0|^2 S_{mn} - |H_0|^2 |P_0|^2 S_{nn}} \end{aligned} \quad (6.23)$$

If  $S_{ww}$  dominates with respect to other noise sources,  $\hat{P}$  approximates  $P$ . However, if any other noise source dominates, the estimate  $\hat{P}$  approximates  $-\frac{1}{H}$ .

## GENERAL DISCUSSION

---

This thesis reports the findings according to the two research objectives. The first objective, the development and validation of an inertial and magnetic sensing system for the measurement of hand and finger kinematics is the topic of chapters 2 to 5. The second objective, the assessment of the dynamic interaction between the human hand and its environment using combined force and movement sensing is the topic of chapter 6.

In the remainder of this chapter, specific aspects of each research objective as well as future directions on associated research topics are discussed.

### 7.1 DISCUSSION AND OUTLOOK

The hand is one of the most versatile and complex instruments of our body and plays a major role in our daily life. It is in many ways involved with the execution of a wide variety of tasks like grasping, holding and moving objects, pointing, reaching and touching. Furthermore, many labour and leisure activities require the precise and gentle, yet powerful abilities of the hands. Hand functioning is therefore an important factor to determine the quality of life and conveyed by a growing number of devices and methods to asses the functioning [45].

Manipulating objects usually requires a combination of different grip types, which are predominantly a full hand grasp and a pinch involving fingers and thumb. A successful performance requires an adequate RoM and grip strength of both fingers and thumb.

However, RoM and strength assessments alone do not demonstrate how a healthy person, or a patient with motor impairments, performs functional tasks. In fact there is little direct correlation between hand RoM and the patient's ability to perform functional activities [45].

In addition, activities like handwriting and instrument playing, rely more on the dexterity of the hand and individual fingers and the thumb. Assessment of these tasks requires a combination of RoM, speed and accuracy measures [145].

Therefore, it is desirable to have an assessment tool that provides the pose of the hand and fingers for reconstruction of RoM, 3D finger and thumb tip positions. Furthermore, it should provide information of the whole hand and individual joint velocities, and finally, incorporate grip forces such that a dynamic assessment is possible. In addition, including knowledge about the task, either by instruction or by estimation using an activity monitor, enables assessment at a functional level.

This thesis is the result of hardware and algorithm development of a system that is able to provide these measures using on-body inertial and force sensing. In this section we will outline the strengths and weaknesses of the system and propose some guidelines for future research.

### 7.1.1 *Sensing the kinematics of the human hand using a non-obtrusive on-body sensing system*

The reconstruction of hand and finger kinematics using on-body sensing entails multiple user interventions and processing steps. Sensors need to be calibrated and attached properly to the skin. Furthermore, an anatomical calibration is required to ensure sensor outputs represent the motion of the underlying skeletal bones. Finally, limits of the sensing system should be taken into account to avoid disturbances and saturated sensor readings. Hence, the reconstruction quality is in many aspects dependent on the establishment of various processing stages.

Different studies already presented the clinical relevance of adopting inertial sensors for gait analysis [12, 29]. It has been argued that inertial sensors enable online calibrations, provide self contained measurements, are location independent, and do not constrain mobility during complex functional motor tasks.

In this thesis, we have focused on the development of a system for clinical measurement purposes [132] which requires accurate and reliable full 3D pose estimates of different fingers and the hand in an unobtrusive manner.

Chapter 3 concludes that our inertial hand sensing system has the potential to be used in clinical practice, however care should be taken when considering such system for clinical use. The comparison with an optical system does not provide adequate evidence about reliability and accurateness of our inertial sensing system. We could only partly explain the, rather large, differences found in the estimated angles and positions and therefore not attribute the errors to a single element of the processing sequence mentioned. Comprehensive experiments involving a larger subject group are necessary to test for both the consistency in the anatomical calibrations and the reconstruction quality during the execution of different functional tasks. In addition, the limited space on the hand available for optical marker attachment compromises the reference orientation estimates and freedom of finger movements. It is therefore also necessary to elaborate on the validity of using an optical system as an evaluation tool for estimation hand and finger kinematics.

Different types of motion tasks have been evaluated, including individual finger tapping, full flex/extensions, circular pointing motions and full hand grasping tasks. The ability to pursue this large variety of motions has implications on the functionality and complexity of the inertial sensing system and requires additional research and evaluations in different trial studies before it is applicable in clinical practice. However, rather simple evaluation methods, like the tapping frequency or RoM analysis in 1 DoF flex-extension tasks

could already benefit from the presented technology, meaning that parts of the system could be adopted in clinical practice.

The inertial sensors used for the finger tracking system reported in chapter 2, 3 and 6 differ from the one used in chapter 4, where the latter is more state-of-the-art. This is manifested in better noise characteristics, which is primarily devoted to the 16 bits Analog to Digital Converter ([ADC](#)) instead of the 12 bits [ADC](#) used in the former sensors. Both sensor models allowed flexibility by trading off sensing range and sensitivity. Especially the sensing range should be taken into account when performing rapid dexterous finger tasks. Not only the experienced angular velocities during such tasks could saturate the gyroscope sensor but also the impact accelerations could cause saturated accelerometer signals. It is therefore important to detect saturated sensor outputs to prevent the inclusion and processing of erroneous signals by the estimation filter.

In addition, inertial sensor data was sampled at 100 Hz. This might be too slow, especially during impact situations that cause large accelerations. Therefore, capturing these high dynamic situations requires much higher sample rates ( $> 1 \text{ kHz}$ ). Fortunately, inertial sensor data is usually integrated yielding the difference in translational velocity from the accelerometer and orientation difference from the gyroscope. Hence, sensor data can be sampled locally at a high rate, integrated, and subsequently transmitted at a much lower rate without losing kinematic information.

#### *Anatomical calibration procedures*

Pose reconstructions require a mapping from the sensor coordinate frame to the anatomical coordinate frame such that the signals can be attributed to the motion of the underlying segment. The [ISB](#) provides recommendations for definitions of joint coordinate frames of various upper body segments. For the hand (carpals, metacarpals) and fingers (phalanges), [ISB](#) recommends to place the orthogonal triad at the axial centre or volumetric centroid of the bones [217]. The axes for the metacarpal and phalangeal bones are defined such that one of the axes is parallel to the line from the centre of distal head to base of the bone. This makes it an impractical definition because it requires a precise estimate of base and head centre positions, which can only be achieved by radiological means. Goislard de Monsabert et.al. state that the estimation of joint centres by palpation results in large discrepancies (up to 15 deg) for the eventual coordinate frame definition [60]. Furthermore, the authors conclude that an anatomical calibration based on rotations about the functional axes is generally more consistent and therefore used in our studies.

Triaxial gyroscopes become particularly useful for an easy and practical determination of the functional axes directions. However, using functional axes is not always preferred or even possible. Rheumatoid patients for example can have troubles with flexion movements due to joint deformities. Additional research is required for the development and adoption of more specific biomechanical models. One of the directions is replacing ball socket joints by

individual joint axes which are non-orthogonally directed and do not intersect [171]. Incorporating these, less constrained, anatomical relations require more generic estimation methods like an optimization framework.

#### *Kinematic calibration and estimation using an optimization approach*

The proposed anatomical calibration method in chapter 4 is based on the performance of functional movements. The underlying model poses minimal restrictions on the anatomical joint composition as some joint laxity is allowed by using a stochastic model for the joint position constraints.

In our opinion, optimization based methods are most promising whenever a detailed and robust reconstruction of the hand and fingers is desired. Studies that have performed a survey of algorithms for human motion of the upper limb [51, 92, 124] also concluded that optimization-based systems have the highest potential for inertial MoCap applications. It was concluded that these methods offer a large flexibility, yet a great robustness against erroneous sensor read-outs or biomechanical model inaccuracies.

We exploited the kinematic constraints, both temporal by including the motion dynamics, and spatial by including position and dimensionality constraints, to correctly estimate parameter and state values. In addition, such relations allow us to exclude the magnetometers for heading estimates, which is advantageous as their outputs require extra processing steps because the measured field could be disturbed unexpectedly [103].

Another big advantage is the inclusion of additional, non sensory, information sources. For example, rather complex information like the shape of the skin surface or custom skeleton rig models could be included [119, 182]. Hence, adding redundancies by using stochastic constraints is one possibility to address unavoidable errors in the biomechanical model parameters.

The promising results we obtained are steps in the right direction, but not yet the solution for every on-body MoCap application. The observability and identifiability of parameters still requires attention, that is, do the estimates converge to the correct parameter values given the measurement data. Especially, when convergence strongly depends on the excitation in terms of change of positions and orientations. The choice initial values, number of included unknowns, and validity of models used, are some of the aspects that influence the convergence behaviour. Simulation studies could assist in the examination [182] but a more legitimate understanding of the observability, preferably as function of different motions, is desired.

Furthermore, it is questionable whether we should focus on a clear dividing line between calibration and actual MoCap. A system that is able to perform auto calibration, thus, taking into account changes of sensor behaviour over time, location and temperature, movements of sensor position with respect to the attached body segment, and pays attention to excitability would greatly enhance the MoCap experience.

Obviously, every redundancy added to the optimization problem increases the dimensionality of the problem and, hence, the computational complexity.

In addition, our approach is an offline method which is suitable for calibration purposes but less appropriate for pose estimation over time. Some studies already investigated online methods, based on a sliding window approach or message passing [93, 124]. Still, an investigation in terms of eventual real-time behaviour, accuracy and robustness is necessary.

Challenges and questions remain, including the specificity, robustness, reliability and validity of these algorithms. Additional research that goes beyond technical evaluations, in a small subject pool performing simple movements, is desired to close the gap from technical principles to practicable tools.

### *Using a permanent magnet for positions measurements*

Many clinical assessments, but also other MoCap applications, desire a position measurement of the hand with respect to the trunk. For instance, in stroke survivors it is tested whether they involve their arm or trunk for directed movements during the performance of reach and grasp tasks. Evaluations are based on the determination of the RoM between hand and trunk and orientation changes of the trunk. Measuring these relative positions with only IMUs requires additional information to correct for position drift. This could be done either by restricting the performed motion, see e.g. Van Meulen et.al. [122], but preferably by measuring relative positions with an aiding system. In chapter 5 we proposed a new method, using a permanent magnet, that can be used as a time independent distance and position estimate. The proposed system is however limited in tracking range which could be mitigated by applying a magnet with a larger magnetic moment. However, such modifications could obstruct the freedom of movements due to the magnet's weight and size. Alternatively, one could rely more on IMU data during periods in which no magnetic information is available and incorporate the kinematic articulations of the upper body to reduce the set of position solutions in 3D space.

Our method uses a dipole model of the magnet, assuming that the distance between the magnet and the point of measurement is large compared to the magnets' dimensions, which could be violated when the hand is close to the chest. Further research could adopt more generic, but complex, models based on Maxwell's equations as already exploited for actuated coil systems [167].

Besides applications in measuring upper extremity movements, the system could be used for estimating the relative foot position during gait as an alternative to optical or acoustic sensing principles [206].

### *Increasing the wearability*

Reducing the number of sensors is an important aspect considering the wearability of an on-body sensing system and possible usage during ADL tasks. In chapter 5 we demonstrated the use of a single IMU attached to the chest combined with a permanent magnet and an IMU attached to the hand to reconstruct the pose of the hand with respect to the upper body. Hence, a reduced set of magnetometers in combination with a tiny permanent magnet enables

tracking of body part positions that have minimal space for attachment, like the finger tips.

Furthermore, the reduction of IMUs in MoCap systems is steadily gaining attention due to the computational abilities of computers and micro controllers. Explorative studies apply machine learning methods to estimate the full body postures with IMUs only attached to the extremities of the body [119, 126, 214].

Despite the potential, this approach is fundamentally different compared to our algorithms as we infer kinematic relations from measured signals, whereas machine learning methods are often focussed on finding a solution within the user's task space given the correlations found in the measurements. Nevertheless, this could be interesting for tracking hand motions, because the typical movements in functional reach and grasping tasks are duly limited.

Not only the reduction of sensors, but also minimizing the dimensions of sensors does increase the unobtrusiveness and eases the embodiment of sensors in garment [8, 31, 118]. Still, the challenge will be in the definition, and eventual estimation, of effective metrics such that relevant questions can be answered within devised protocols.

### 7.1.2 Assessing dynamic interactions between the human hand and its environment

#### Force sensing between the human hand and environment

Friction and normal forces are what allows one to change an object's configuration and hold it against gravity and other disturbances. It is therefore relevant to measure contact force in multiple directions to evaluate grip and grasping strategies. We experienced that measuring these forces at the finger tips imposes major practical difficulties. The skin of the hand and finger allow relatively large deformations to provide us with the optimal grip whenever fingers are in contact with irregular surfaces. Despite the diameter of less than one centimeter, the presence of the force sensor at the finger or thumb tip does affect the actual skin sensation. The force sensor we used was made of a silicon chip that has been annealed to a PCB layer, resulting in a thickness of just a few millimeters. Still, the rigidity and size of the force sensor deteriorate the actual gripping performance. In addition, any additional thickening layer imposes a moment arm to the finger tip, resulting in an even more unnatural feeling and undesired force components. Further research is required to investigate an optimal sensor layout for finger tip purposes.

Ideally, this sensor should be very flexible, such that it adapts to the compliant contours of the skin whenever it is in contact with objects. Yet, the sensor should be sufficiently stiff to prevent energy loss due to damping of the skin. It is questionable whether the silicon material used could accommodate for such adaptions, or that a sensor made from a different material, possible with fewer sensitive measurement directions, would be more suitable. Many groups already investigate potential materials to estimate interaction forces or, rather, pressure from changes in material properties [8, 31, 109, 157]. Different kinds

of stretchable sensors emerge from the development of smart garments applicable for the assessment of clinical outcomes in daily life [188, 205] or for physical assistance during the rehabilitation of a particular disorder [148]. Yet, those sensing systems are not comparable to the force and moment sensors used in our study which allow for measurements in normal direction, shear directions, and different rotational directions resulting in 6 DoF's. It is, however, questionable whether the measurements of moments is needed because any possible induced moment will be decoupled in shear forces for the majority of functional grip and grasping tasks involving multiple fingers. Nevertheless, it is certainly important to have a decoupled measure of normal and shear forces due to the mutual difference of holding objects by either applying normally directed tip forces or relying more on the friction characteristics of the skin [209].

Besides the limitations of sensors' mechanical properties, further development of the data acquisition circuitry is required such that a higher sampling rate ( $>12$  Hz) and an improved synchronisation with inertial sensors is possible to accommodate for rapid or sudden changes in contact forces. Furthermore, in our study we considered hand tasks with only index and thumb pinching motions. An improved version of instrumentation should allow measurements at additional contact points, e.g. at the various finger tips and palm of the hand, to be able to examine the performance of a vast set of hand tasks.

#### *Evaluation of hand tasks performances and the dynamic interaction*

Assessment of hand tasks performances requires both the understanding of underlying mechanisms that the human body applies before and during the execution of a task, and the means to measure and quantify those tasks. In many functional ADL tasks it is the dynamic interaction between hand and environment that regulates eventual performance. The human body applies different control strategies for task executions [212]. First, predictive or feed-forward control make use of learned patterns and is the most important strategy for fast and dexterous, hence, skilled actions. Second, our sensory (visual, tactile, proprioceptive) system is used in a feedback control loop and allows online adaption of our control strategy. Finally, our body is able to change its biomechanical dynamics of our system. Both intrinsic or stiffness and reflexive properties can be adapted or deployed to optimally accommodate for a certain task.

On a functional level, humans aim at performing a task in such a way that it can be explained by optimal feedback control principles [186]. Depending on the context, a control strategy is selected, often based on a trade-off between energy consumption (effort) and accuracy constraints [187, 213]. Task planning includes the kinematic trajectories as well as the interaction with the environment by means of contact. For example, in manipulation tasks, besides the posture of the arm, friction is of great importance. Hence, appointed tasks can be quantified when kinematic and kinetic measures of the trajectories and interac-

tions are available. Postural estimates and trajectory smoothness measures can be provided by the inertial and magnetic sensors, whereas interaction forces can be measured by the force sensors we have introduced. In addition, the product of velocity and movement at any time yields the momentary power transferred between body and environment which, after integration over time, results in the energy exchanged [194]. Hence, the kinematic sensing including the pose of the finger and absolute hand position combined with 3D force sensors enables the evaluation of functional, a-priori known, tasks.

Deeper understanding of sensory and biomechanical motor control paradigms puts additional constraints on the task, and might, require additional sensors and external perturbations. During interactions, measured forces and movements at the interface of the human body and environment expose the lumped dynamic characteristics of both bodies. A proper distinctive dynamic estimate of both systems requires an independent perturbation signal, imposed at the contact interface, and a proper method that allows the identification of systems when measuring within a closed loop condition [169, 201]. These methods are often based on assumptions that require the execution of fairly simple and constrained tasks and therefore are not comparable with functional [ADL](#) tasks.

Nevertheless, it would be interesting to know what dynamic information can be extracted when open loop system identification methods are applied on signals measured during [ADL](#) tasks. During an interaction, where the human body dictates the force and expresses a compliant behaviour, it is likely that the force-movement relation provides information about the environmental load, as shown in chapter 6. However, in our study it has not been investigated whether this assumption is valid, nor what type and duration of excitation signals are required for the identification of various properties. It is furthermore certain that information richness of interface signals during interactions depend to a great extend on the instructed task. Therefore, it is necessary to conduct research to investigate what characteristics under which specific conditions can be estimated using the interface force and movement measures.

Besides identifying load characteristics, it is interesting to gain knowledge of the exhibited motor control strategy. In particular, dynamic adaptions of the body during the task execution, which could be interpreted as a conservative control strategy, might give valuable information. Furthermore, by adding [EMG](#) measurements for the assessment of muscular co-contractions, and having a full posture estimate over time might enable estimation of the endpoint stiffness ellipsoid parameters [61] and impedance control strategies in general [56].

## 7.2 CONCLUSION

The presented systems and algorithms in this thesis contribute to new methods for the assessment of human hand tasks. In particular, algorithms were developed to accurately estimate various important kinematics quantities of the hand and fingers. Furthermore, first efforts were presented to combine on-body force and movement sensing on the hand for the assessment of dynamic interactions. These principles do not require ambient measurement systems and are therefore intended for use in daily life situations without impeding natural task executions.



## BIBLIOGRAPHY

---

- [1] 5DT dataglove. 2017. URL: <http://www.5dt.com>.
- [2] Sameer Agarwal, Keir Mierle, et al. Ceres Solver (<http://ceres-solver.org>). 2017.
- [3] A M Almassri, WZ Wan Hasan, S A Ahmad, and A J Ishak. "Pressure sensor: state of the art, design, and application for robotic hand." In: *Journal of Sensors* (2015). doi: [10.1155/2015/846487](https://doi.org/10.1155/2015/846487).
- [4] Jacob Antonsson. *Motion tracking using a permanent magnet*. 2013.
- [5] Daniel Ashbrook, Patrick Baudisch, and Sean White. "Nenya: subtle and eyes-free mobile input with a magnetically-tracked finger ring." In: *CHI '11: Proceedings of the SIGCHI Conference on Human Factors in Computing Systems*. New York, New York, USA: ACM Request Permissions, May 2011, p. 2043. doi: [10.1145/1978942.1979238](https://doi.org/10.1145/1978942.1979238).
- [6] S Beauregard and M Klepal. "Indoor PDR performance enhancement using minimal map information and particle filters." In: *2008 IEEE/ION Position* (2008). doi: [10.1109/plans.2008.4570050](https://doi.org/10.1109/plans.2008.4570050).
- [7] N van Beek, J C van den Noort, P.H. Veltink, R Selles, H E Veeger, H Maas, and D Stegeman. "Mechanical constraints of finger independence: linking tendon displacement with joint movement." In: *In Proceedings of 25th congress of the International Society of Biomechanics*. 2015.
- [8] Matteo Bianchi, Robert Haschke, Gereon Büscher, Simone Ciotti, Nicola Carbonaro, and Alessandro Tognetti. "A multi-modal sensing glove for human manual-interaction studies." In: *Electronics (Switzerland)* 5.3 (July 2016). doi: [10.3390/electronics5030042](https://doi.org/10.3390/electronics5030042).
- [9] O Birbach, B Bäuml, and U Frese. "Automatic and self-contained calibration of a multi-sensorial humanoid's upper body." In: *Robotics and Automation (ICRA)* (2012), pp. 3103–3108. doi: [10.1109/icra.2012.6225004](https://doi.org/10.1109/icra.2012.6225004).
- [10] Oliver Birbach and Berthold Bauml. "Calibrating a pair of inertial sensors at opposite ends of an imperfect kinematic chain." In: *Intelligent Robots and Systems (IROS 2014), 2014 IEEE/RSJ International Conference on*. IEEE, 2014, pp. 422–428. doi: [10.1109/iros.2014.6942594](https://doi.org/10.1109/iros.2014.6942594).
- [11] M Birsan. "Unscented particle filter for tracking a magnetic dipole target." In: *Proceedings of MTS/IEEE OCEANS*, 2005. 2005. doi: [10.1109/oceans.2005.1639993](https://doi.org/10.1109/oceans.2005.1639993).
- [12] Gabriele Bleser, Bertram Taetz, Markus Miezal, Corinna A Christmann, Daniel Steffen, and Katja Regensperger. "Development of an Inertial Motion Capture System for Clinical Application." In: *i-com* (Aug, 2017), pp. 1–17.

- [13] S Bonnet, C Bassompierre, C Godin, S Lesecq, and A Barraud. "Calibration methods for inertial and magnetic sensors." In: *Sensors and Actuators A: Physical* 156.2 (2009), pp. 302–311. doi: [10.1016/j.sna.2009.10.008](https://doi.org/10.1016/j.sna.2009.10.008).
- [14] Michela Borghetti, Emilio Sardini, and Mauro Serpelloni. "Sensorized Glove for Measuring Hand Finger Flexion for Rehabilitation Purposes." In: *IEEE Transactions on Instrumentation and Measurement* 62.12 (Oct. 2013), pp. 3308–3314. doi: [10.1109/tim.2013.2272848](https://doi.org/10.1109/tim.2013.2272848).
- [15] JE Bortz. "A new mathematical formulation for strapdown inertial navigation." In: *Aerospace and Electronic Systems, IEEE Transactions on* 1 (2007), pp. 61–66. doi: [10.1109/taes.1971.310252](https://doi.org/10.1109/taes.1971.310252).
- [16] Paul W Brand and Anne Hollister. *Clinical mechanics of the hand*. Mosby Incorporated, 1999.
- [17] Peter C Breedveld. "Port-based modeling of mechatronic systems." In: *Mathematics and Computers in Simulation* 66.2-3 (June 2004), pp. 99–128. doi: [10.1016/j.matcom.2003.11.002](https://doi.org/10.1016/j.matcom.2003.11.002).
- [18] R A Brookhuis, H Droogendijk, M J de Boer, R G P Sanders, T S J Lammerink, R J Wiegerink, and G J M Krijnen. "Six-axis force-torque sensor with a large range for biomechanical applications." In: *Journal of Micromechanics and Microengineering* 24.3 (Jan. 2014). doi: [10.1088/0960-1317/24/3/035015](https://doi.org/10.1088/0960-1317/24/3/035015).
- [19] R A Brookhuis, T S J Lammerink, R J Wiegerink, M J de Boer, and M C Elwenspoek. "3D force sensor for biomechanical applications." In: *Sensors and Actuators A: Physical* 182 (Aug. 2012), pp. 28–33. doi: [10.1016/j.sna.2012.04.035](https://doi.org/10.1016/j.sna.2012.04.035).
- [20] R A Brookhuis, R G P Sanders, K Ma, T S J Lammerink, M J de Boer, G J M Krijnen, and R J Wiegerink. "Miniature large range multi-axis force-torque sensor for biomechanical applications." In: *Journal of Micromechanics and Microengineering* 25.2 (Feb. 2015), p. 025012. doi: [10.1088/0960-1317/25/2/025012](https://doi.org/10.1088/0960-1317/25/2/025012).
- [21] R A Brookhuis, R J Wiegerink, T S J Lammerink, K Ma, and G J M Krijnen. "Large range multi-axis fingertip force sensor." In: *2013 Transducers & Eurosensors XXVII: The 17th International Conference on Solid-State Sensors, Actuators and Microsystems (TRANSDUCERS & EUROSENSORS XXVII)* (2013), pp. 2737–2740. doi: [10.1109/transducers.2013.6627372](https://doi.org/10.1109/transducers.2013.6627372).
- [22] Robert Anton Brookhuis. "Miniature force-torque sensors for biomechanical applications." PhD thesis. Twente University Press, 2014.
- [23] B Buchholz. "A kinematic model of the human hand to evaluate its prehensile capabilities." In: *Journal of Biomechanics* (1992). doi: [10.1016/0021-9290\(92\)90272-3](https://doi.org/10.1016/0021-9290(92)90272-3).
- [24] Bryan Buchholz, Thomas J Armstrong, and Steven A Goldstein. "Anthropometric data for describing the kinematics of the human hand." In: *Ergonomics* 35.3 (1992), pp. 261–273.

- [25] Frank L Buczak, Erik W Sinsel, Daniel S Gloekler, Bryan M Wimer, Christopher M Warren, and John Z Wu. "Kinematic performance of a six degree-of-freedom hand model (6DHand) for use in occupational biomechanics." In: *Journal of Biomechanics* 44.9 (June 2011), pp. 1805–1809. doi: [10.1016/j.jbiomech.2011.04.003](https://doi.org/10.1016/j.jbiomech.2011.04.003).
- [26] I M Bullock, J Borras, and A M Dollar. "Assessing assumptions in kinematic hand models: A review." In: *Biomedical Robotics and Biomechatronics (BioRob), 2012 4th IEEE RAS & EMBS International Conference on*. IEEE, 2012, pp. 139–146. doi: [10.1109/biorob.2012.6290879](https://doi.org/10.1109/biorob.2012.6290879).
- [27] Yongyao Cai, Yang Zhao, Xianfeng Ding, and James Fennelly. "Magnetometer basics for mobile phone applications." In: *Electron. Prod.(Garden City, New York)* 54.2 (2012).
- [28] P Cerveri, N Lopomo, A Pedotti, and G Ferrigno. "Derivation of centers and axes of rotation for wrist and fingers in a hand kinematic model: Methods and reliability results." In: *Annals of Biomedical Engineering* 33.3 (2005), pp. 402–412. doi: [10.1007/s10439-005-1743-9](https://doi.org/10.1007/s10439-005-1743-9).
- [29] Shanshan Chen, John Lach, Benny Lo, and Guang-Zhong Yang. "Toward Pervasive Gait Analysis With Wearable Sensors: A Systematic Review." In: *IEEE journal of biomedical and health informatics* 20.6 (Nov. 2016), pp. 1521–1537. doi: [10.1109/jbhi.2016.2608720](https://doi.org/10.1109/jbhi.2016.2608720).
- [30] S Chitta, J Sturm, M Piccoli, and W Burgard. "Tactile sensing for mobile manipulation." In: *IEEE Transactions on Robotics* 27.3 (2011), pp. 558–568. doi: [10.1109/tro.2011.2134130](https://doi.org/10.1109/tro.2011.2134130).
- [31] J B Chossat, Y Tao, V Duchaine, and Y L Park. "Wearable soft artificial skin for hand motion detection with embedded microfluidic strain sensing." In: *Proceedings - IEEE International Conference on Robotics and Automation*. IEEE, 2015, pp. 2568–2573. doi: [10.1109/icra.2015.7139544](https://doi.org/10.1109/icra.2015.7139544).
- [32] K J Cole, K M Cook, S M Hynes, and W G Darling. "Slowing of dexterous manipulation in old age: force and kinematic findings from the 'nut-and-rod' task." In: *Exp. Brain Res* 201.2 (2010), pp. 239–247. doi: [10.1007/s00221-009-2030-z](https://doi.org/10.1007/s00221-009-2030-z).
- [33] R Colombo, F Pisano, S Micera, A Mazzone, C Delconte, M C Carrozza, P Dario, and G Minuco. "Assessing Mechanisms of Recovery During Robot-Aided Neurorehabilitation of the Upper Limb." In: *Neurorehabilitation and Neural Repair* 22.1 (Jan. 2008), pp. 50–63. doi: [10.1177/1545968307303401](https://doi.org/10.1177/1545968307303401).
- [34] Roberto Colombo, Fabrizio Pisano, Silvestro Micera, Alessandra Mazzone, Carmen Delconte, Chiara M Carrozza, Paolo Dario, and Giuseppe Minuco. "Robotic techniques for upper limb evaluation and rehabilitation of stroke patients." In: *IEEE Transactions on neural systems and rehabilitation engineering* 13.3 (2005), pp. 311–324. doi: [10.1109/tnsre.2005.848352](https://doi.org/10.1109/tnsre.2005.848352).

- [35] D A Commissaris and H M Toussaint. "Load knowledge affects low-back loading and control of balance in lifting tasks." In: *Ergonomics* 40.5 (May 1997), pp. 559–575. doi: [10.1080/001401397188035](https://doi.org/10.1080/001401397188035).
- [36] Wikimedia Commons. *Dip Needle*. File: LambdaPlaques.jpg. 2014. URL: [https://commons.wikimedia.org/wiki/File:Dip\\_needle,\\_by\\_W.\\_Wilson,\\_1\\_Belmont\\_St.,\\_London,\\_NW,\\_for\\_measuring\\_vertical\\_aspect\\_of\\_Earth%27s\\_magnetic\\_field,\\_c.\\_1900\\_-\\_Museum\\_of\\_Science\\_and\\_Industry\\_\(Chicago\)\\_-\\_DSC06529.JPG](https://commons.wikimedia.org/wiki/File:Dip_needle,_by_W._Wilson,_1_Belmont_St.,_London,_NW,_for_measuring_vertical_aspect_of_Earth%27s_magnetic_field,_c._1900_-_Museum_of_Science_and_Industry_(Chicago)_-_DSC06529.JPG).
- [37] J Coupier, F Moiseev, V Feipel, M Rooze, and Jan S Van Sint. "Motion representation of the long fingers: a proposal for the definitions of new anatomical frames." In: *J. Biomech* 47.6 (2014), pp. 1299–1306. doi: [10.1016/j.jbiomech.2014.02.017](https://doi.org/10.1016/j.jbiomech.2014.02.017).
- [38] JL Crassidis, FL Markley, and Y Cheng. "Survey of nonlinear attitude estimation methods." In: *Journal of Guidance Control and Dynamics* 30.1 (2007), p. 12. doi: [10.2514/1.22452](https://doi.org/10.2514/1.22452).
- [39] M.R. Cutkosky and R D Howe. "Human grasp choice and robotic grasp analysis." In: *Dextrous robot hands* (1990). doi: [10.1007/978-1-4613-8974-3\\_1](https://doi.org/10.1007/978-1-4613-8974-3_1).
- [40] A G Cutti, A Giovanardi, L Rocchi, A Davalli, and R Sacchetti. "Ambulatory measurement of shoulder and elbow kinematics through inertial and magnetic sensors." In: *Med. Biol. Eng. Comput* 46.2 (2008), pp. 169–178. doi: [10.1007/s11517-007-0296-5](https://doi.org/10.1007/s11517-007-0296-5).
- [41] *Cyberglove systems*. 2017. URL: <http://www.cyberglovesystems.com/>.
- [42] L Dipietro, AM Sabatini, and P Dario. "A survey of glove-based systems and their applications." In: *Systems, Man, and Cybernetics, Part C: Applications and Reviews, IEEE Transactions on* 38.4 (2008), pp. 461–482. doi: [10.1109/tsmcc.2008.923862](https://doi.org/10.1109/tsmcc.2008.923862).
- [43] Laura Dipietro, Angelo M Sabatini, and Paolo Dario. "Evaluation of an instrumented glove for hand-movement acquisition." In: *Journal of Rehabilitation Research and Development* 40.2 (2003), pp. 179–190. doi: [10.1682/jrrd.2003.03.0181](https://doi.org/10.1682/jrrd.2003.03.0181).
- [44] Milica D Djurić-Jovičić, Nenad S Jovičić, Dejan B Popović, and Antonije R Djordjević. "Nonlinear optimization for drift removal in estimation of gait kinematics based on accelerometers." In: *Journal of Biomechanics* 45.16 (Nov. 2012), pp. 2849–2854. doi: [10.1016/j.jbiomech.2012.08.028](https://doi.org/10.1016/j.jbiomech.2012.08.028).
- [45] Mehmet Tuncay Duruöz. *Hand function: a practical guide to assessment*. Springer Science & Business Media, 2014.
- [46] *Eigen C++ Matrix libraries* (<http://eigen.tuxfamily.org/>). 2017.
- [47] D Erickson, M Weber, and I Sharf. "Contact stiffness and damping estimation for robotic systems." In: *International Journal of Robotics Research*. McGill University, Montreal, Canada. Jan. 2003, pp. 41–57. doi: [10.1177/027836403128964700](https://doi.org/10.1177/027836403128964700).

- [48] Ali Erol, George Bebis, Mircea Nicolescu, Richard D Boyle, and Xander Twombly. "Vision-based hand pose estimation: A review." In: *Computer Vision and Image Understanding* 108.1-2 (Oct. 2007), pp. 52–73. doi: [10.1016/j.cviu.2006.10.012](https://doi.org/10.1016/j.cviu.2006.10.012).
- [49] Chin-Shyurng Fahn and Herman Sun. "Development of a fingertip glove equipped with magnetic tracking sensors." In: *Sensors (Switzerland)* 10.2 (Feb. 2010), pp. 1119–1140. doi: [10.3390/s100201119](https://doi.org/10.3390/s100201119).
- [50] S Fahn and R L Elton. "The UPDRS development Committee, 'Unified Parkinson's Disease Rating Scale'." In: *Recent Developments in Parkinson's Disease*. Ed. by S Fahn, C D Marsden, D B Calne, and M Goldstein. Florham Park, NJ: Macmillan Healthcare Information, 1987, pp. 153–163.
- [51] Alessandro Filippeschi, Norbert Schmitz, Markus Miezal, Gabriele Bleser, Emanuele Ruffaldi, and Didier Stricker. "Survey of Motion Tracking Methods Based on Inertial Sensors: A Focus on Upper Limb Human Motion." In: *Sensors* 17.6 (June 2017), p. 1257. doi: [10.3390/s17061257](https://doi.org/10.3390/s17061257).
- [52] A Forner-Cordero, H J F M Koopman, and F C T Van der Helm. "Inverse dynamics calculations during gait with restricted ground reaction force information from pressure insoles." In: *Gait & posture* 23.2 (Feb. 2006), pp. 189–199. doi: [10.1016/j.gaitpost.2005.02.002](https://doi.org/10.1016/j.gaitpost.2005.02.002).
- [53] Urban Forssell and Lennart Ljung. "Closed-loop identification revisited." In: *Automatica* 35.7 (1999), pp. 1215–1241.
- [54] E Foxlin. "Pedestrian tracking with shoe-mounted inertial sensors." In: *Computer Graphics and Applications* (2005). doi: [10.1109/mcg.2005.140](https://doi.org/10.1109/mcg.2005.140).
- [55] E Foxlin, M Harrington, and G Pfeifer. "Constellation: A wide-range wireless motion-tracking system for augmented reality and virtual set applications." In: *Proceedings of the 25th annual conference on Computer graphics and interactive techniques. Siggraph 98*. New York, 1998, pp. 371–378. doi: [10.1145/280814.280937](https://doi.org/10.1145/280814.280937).
- [56] David W Franklin. "Impedance control: Learning stability in human sensorimotor control." In: *Conf. Proc. IEEE Eng Med. Biol. Soc* 2015 (Aug. 2015), pp. 1421–1424. doi: [10.1109/embc.2015.7318636](https://doi.org/10.1109/embc.2015.7318636).
- [57] M Gabiccini, G Stillfried, H Marino, and M Bianchi. "A data-driven kinematic model of the human hand with soft-tissue artifact compensation mechanism for grasp synergy analysis." In: *IEEE International Conference on Intelligent Robots and Systems. 2013*, pp. 3738–3745. doi: [10.1109/iros.2013.6696890](https://doi.org/10.1109/iros.2013.6696890).
- [58] R Gentner and J Classen. "Development and evaluation of a low-cost sensor glove for assessment of human finger movements in neurophysiological settings." In: *Journal of neuroscience methods* 178.1 (2009), pp. 138–147. doi: [10.1016/j.jneumeth.2008.11.005](https://doi.org/10.1016/j.jneumeth.2008.11.005).
- [59] Ray C Goertz. *Master-slave manipulator*. Tech. rep. ANL (Argonne National Laboratory (ANL), Argonne, IL (United States)), 1949.

- [60] B Goislard de Monsabert, J M A Visser, L Vigouroux, F C T Van der Helm, and H E J Veeger. "Comparison of three local frame definitions for the kinematic analysis of the fingers and the wrist." In: *Journal of Biomechanics* 47.11 (Aug. 2014), pp. 2590–2597. doi: [10.1016/j.jbiomech.2014.05.025](https://doi.org/10.1016/j.jbiomech.2014.05.025).
- [61] H Gomi and R Osu. "Task-dependent viscoelasticity of human multijoint arm and its spatial characteristics for interaction with environments." In: *The Journal of neuroscience : the official journal of the Society for Neuroscience* 18.21 (Nov. 1998), pp. 8965–8978.
- [62] G Grisetti, R Kummerle, C Stachniss, U Frese, and C Hertzberg. "Hierarchical optimization on manifolds for online 2D and 3D mapping." In: *Robotics and Automation (ICRA), 2010 IEEE International Conference on*. IEEE, 2010, pp. 273–278. doi: [10.1109/robot.2010.5509407](https://doi.org/10.1109/robot.2010.5509407).
- [63] Jože Guna, Grega Jakus, Matevž Pogačnik, Sašo Tomažič, and Jaka Sodnik. "An Analysis of the Precision and Reliability of the Leap Motion Sensor and Its Suitability for Static and Dynamic Tracking." In: *Sensors* 14.2 (Feb. 2014), pp. 3702–3720. doi: [10.3390/s140203702](https://doi.org/10.3390/s140203702).
- [64] Fredrik Gustafsson. *Statistical sensor fusion*. Studentlitteratur, 2010.
- [65] Fredrik Gustafsson and Niklas Wahlstrom. "Method and device for pose tracking using vector magnetometers." 13/427,118. 2012.
- [66] Frank L Hammond, Yigit Menguc, and Robert J Wood. "Toward a modular soft sensor-embedded glove for human hand motion and tactile pressure measurement." In: *Intelligent Robots and Systems (IROS 2014), 2014 IEEE/RSJ International Conference on*. IEEE, 2014, pp. 4000–4007. doi: [10.1109/iros.2014.6943125](https://doi.org/10.1109/iros.2014.6943125).
- [67] Ernst A Hansen and Harry Waldestrand. "Seated versus standing position for maximization of performance during intense uphill cycling." In: *Journal of sports sciences* 26.9 (June 2008), pp. 977–984. doi: [10.1080/02640410801910277](https://doi.org/10.1080/02640410801910277).
- [68] T Harada, T Mori, and T Sato. "Development of a tiny orientation estimation device to operate under motion and magnetic disturbance." In: *The International Journal of Robotics Research* 26.6 (2007), p. 547. doi: [10.1177/0278364907079272](https://doi.org/10.1177/0278364907079272).
- [69] R Harle. "A survey of indoor inertial positioning systems for pedestrians." In: *IEEE Communications Surveys & Tutorials* 15.3 (2013), pp. 1281–1293. doi: [10.1109/surv.2012.121912.00075](https://doi.org/10.1109/surv.2012.121912.00075).
- [70] Jose L Hernandez-Rebollar, Nicholas Kyriakopoulos, and Robert W Lindeman. "The AcceleGlove: a whole-hand input device for virtual reality." In: *SIGGRAPH '02: SIGGRAPH 2002 conference abstracts and applications*. New York, New York, USA: ACM, July 2002, p. 259. doi: [10.1145/1242073.1242272](https://doi.org/10.1145/1242073.1242272).
- [71] C Hertzberg, R Wagner, U Frese, and L Schröder. "Integrating generic sensor fusion algorithms with sound state representations through encapsulation of manifolds." In: *Information Fusion* 14.1 (2013), pp. 57–77. doi: [10.1016/j.inffus.2011.08.003](https://doi.org/10.1016/j.inffus.2011.08.003).

- [72] Frédérique Hintzy and Nicolas Tordi. "Mechanical efficiency during hand–rim wheelchair propulsion: effects of base-line subtraction and power output." In: *Clinical Biomechanics* 19.4 (May 2004), pp. 343–349. doi: [10.1016/j.clinbiomech.2004.01.001](https://doi.org/10.1016/j.clinbiomech.2004.01.001).
- [73] M J Hofmijster and A J Van Soest. "Rowing skill affects power loss on a modified rowing ergometer." In: *Medicine Science in Sports Exercise* (2008). doi: [10.1249/mss.0b013e3181668671](https://doi.org/10.1249/mss.0b013e3181668671).
- [74] Neville Hogan, Hermano Igo Krebs, J Charnnarong, P Srikrishna, and Andre Sharon. "MIT-MANUS: a workstation for manual therapy and training. I." In: *Robot and Human Communication, 1992. Proceedings., IEEE International Workshop on*. IEEE. 1992, pp. 161–165.
- [75] J.D Hol, F Dijkstra, H Luinge, and T B Schon. "Tightly coupled UWB/IMU pose estimation." In: *Ultra-Wideband, 2009. ICUWB 2009. IEEE International Conference on*. IEEE, 2009, pp. 688–692. doi: [10.1109/icuwb.2009.5288724](https://doi.org/10.1109/icuwb.2009.5288724).
- [76] J.D Hol, T B Schon, H Luinge, P J Slycke, and F Gustafsson. "Robust real-time tracking by fusing measurements from inertial and vision sensors." In: *Journal of Real-Time Image Processing* 2.2-3 (2007), pp. 149–160. doi: [10.1007/s11554-007-0040-2](https://doi.org/10.1007/s11554-007-0040-2).
- [77] Jeroen D Hol. "Sensor fusion and calibration of inertial sensors, vision, ultra-wideband and GPS." PhD thesis. Linköping University Electronic Press, 2011.
- [78] Berthold K P Horn. "Closed-form solution of absolute orientation using unit quaternions." In: *JOSA A* 4.4 (Apr. 1987), pp. 629–642. doi: [10.1364/josaa.4.000629](https://doi.org/10.1364/josaa.4.000629).
- [79] Maaike A Huysmans, Marco J M Hoozemans, Bart Visser, and Jaap H van Dieën. "Grip force control in patients with neck and upper extremity pain and healthy controls." In: *Clinical Neurophysiology* 119.8 (Aug. 2008), pp. 1840–1848. doi: [10.1016/j.clinph.2008.04.290](https://doi.org/10.1016/j.clinph.2008.04.290).
- [80] J M Iaquinto, R Tsai, D R Haynor, M J Fassbind, B J Sangeorzan, and W R Ledoux. "Marker-based validation of a biplane fluoroscopy system for quantifying foot kinematics." In: *Med. Eng Phys* 36.3 (2014), pp. 391–396. doi: [10.1016/j.medengphy.2013.08.013](https://doi.org/10.1016/j.medengphy.2013.08.013).
- [81] Thea Iberall. "The nature of human prehension: Three dextrous hands in one." In: *1987 IEEE International Conference on Robotics and Automation* 4 (Mar. 1987), pp. 396–401. doi: [10.1109/robot.1987.1087813](https://doi.org/10.1109/robot.1987.1087813).
- [82] S Ingham, G Whyte, K Jones, and A Nevill. "Determinants of 2,000 m rowing ergometer performance in elite rowers." In: *European Journal of Applied Physiology* 88.3 (2002), pp. 243–246. doi: [10.1007/s00421-002-0699-9](https://doi.org/10.1007/s00421-002-0699-9).
- [83] Albrecht Jander, Carl Smith, and Robert Schneider. "Magnetoresistive sensors for nondestructive evaluation (Invited Paper)." In: *Nondestructive Evaluation for Health Monitoring and Diagnostics* 5770 (2005), pp. 1–13. doi: [10.1117/12.601826](https://doi.org/10.1117/12.601826).

- [84] Rudolph Emil Kalman et al. "A new approach to linear filtering and prediction problems." In: *Journal of basic Engineering* (1960).
- [85] G D Kessler, L F Hodges, and N Walker. "Evaluation of the CyberGlove as a whole hand input device." In: *ACM Trans. Comput.-Human Interaction* 2.4 (1995), pp. 263–283. doi: [10.1145/212430.212431](https://doi.org/10.1145/212430.212431).
- [86] YS Kim, BS Soh, and SG Lee. "A new wearable input device: SCURRY." In: *Industrial Electronics, IEEE Transactions on* 52.6 (2005), pp. 1490–1499. doi: [10.1109/tie.2005.858736](https://doi.org/10.1109/tie.2005.858736).
- [87] Idsart Kingma, Chris T M Baten, Patricia Dolan, Huub M Toussaint, Jaap H van Dieën, Michiel P de Looze, and Michael A Adams. "Lumbar loading during lifting: a comparative study of three measurement techniques." In: *Journal of Electromyography and Kinesiology* 11.5 (Oct. 2001), pp. 337–345. doi: [10.1016/s1050-6411\(01\)00011-6](https://doi.org/10.1016/s1050-6411(01)00011-6).
- [88] Idsart Kingma, Tim Bosch, Louis Bruins, and Jaap van Dieën. "Foot positioning instruction, initial vertical load position and lifting technique: effects on low back loading." In: *Ergonomics* 47.13 (Oct. 2004), pp. 1365–1385. doi: [10.1080/00140130410001714742](https://doi.org/10.1080/00140130410001714742).
- [89] Idsart Kingma, Jaap H van Dieën, Michiel de Looze, Huub M Toussaint, Patricia Dolan, and Chris T M Baten. "Asymmetric low back loading in asymmetric lifting movements is not prevented by pelvic twist." In: *Journal of Biomechanics* 31.6 (June 1998), pp. 527–534. doi: [10.1016/s0021-9290\(98\)00045-1](https://doi.org/10.1016/s0021-9290(98)00045-1).
- [90] M Kok, J.D Hol, and T B Schon. "An optimization-based approach to human body motion capture using inertial sensors." In: *IFAC Proceedings Volumes* 47.3 (2014), pp. 79–85. doi: [10.3182/20140824-6-za-1003.02252](https://doi.org/10.3182/20140824-6-za-1003.02252).
- [91] M Kok, J.D Hol, T B Schon, F Gustafsson, and H Luinge. "Calibration of a magnetometer in combination with inertial sensors." In: *15th International Conference on Information Fusion, FUSION 2012.* 2012, pp. 787–793.
- [92] Manon Kok, Jeroen D Hol, and Thomas B Schon. "Using Inertial Sensors for Position and Orientation Estimation." In: *arXiv.org* (Apr. 2017). doi: [10.1561/2000000094](https://doi.org/10.1561/2000000094). arXiv: [1704.06053v1 \[cs.RO\]](https://arxiv.org/abs/1704.06053v1).
- [93] Manon Kok, Thomas B Schon, n, Thomas B Schon, Anders Hansson, and Jeroen D Hol. "A scalable and distributed solution to the inertial motion capture problem." In: *2016 19th International Conference on Information Fusion (FUSION.* IEEE, 2016, pp. 1348–1355.
- [94] H. G Kortier and P.H. Veltink. "Load identification during object handling." In: *Engineering in Medicine and Biology Society, EMBC, 2011 Annual International Conference of the IEEE.* IEEE, 2011, pp. 3500–3502. doi: [10.1109/iembs.2011.6090945](https://doi.org/10.1109/iembs.2011.6090945).

- [95] H.G. Kortier, J. Antonsson, H.M. Schepers, F. Gustafsson, and P.H. Veltink. "Hand pose estimation by fusion of inertial and magnetic sensing aided by a permanent magnet." In: *IEEE transactions on neural systems and rehabilitation engineering* 23.5 (Sept. 2015). eemcs-eprint-25437, pp. 796–806. doi: [10.1109/TNSRE.2014.2357579](https://doi.org/10.1109/TNSRE.2014.2357579).
- [96] H.G. Kortier, H.M. Schepers, and P.H. Veltink. "Identification of Object Dynamics Using Hand Worn Motion and Force Sensors." In: *Sensors* 16.12 (2016). issn: 1424-8220. doi: [10.3390/s16122005](https://doi.org/10.3390/s16122005).
- [97] H.G. Kortier, V.I. Sluiter, D. Roetenberg, and P.H. Veltink. "Assessment of hand kinematics using inertial and magnetic sensors." In: *Journal of neuroengineering and rehabilitation* 11 (Apr. 2014). Open access, 70:1–70:14. issn: 1743-0003. doi: [10.1186/1743-0003-11-70](https://doi.org/10.1186/1743-0003-11-70).
- [98] H I Krebs, J J Palazzolo, L Dipietro, M Ferraro, J Krol, K Rannekleiv, B T Volpe, and N Hogan. "Rehabilitation Robotics: Performance-Based Progressive Robot-Assisted Therapy." In: *Autonomous Robots* 15.1 (2003), pp. 7–20.
- [99] Hermano Igo Krebs, Stephen Mernoff, Susan E Fasoli, Richard Hughes, Joel Stein, and Neville Hogan. "A comparison of functional and impairment-based robotic training in severe to moderate chronic stroke: a pilot study." In: *NeuroRehabilitation* 23.1 (2008), pp. 81–87.
- [100] Jack B Kuipers et al. *Quaternions and rotation sequences*. Vol. 66. Princeton university press Princeton, 1999.
- [101] Gregorij Kurillo, Matjaž Mihelj, Marko Munih, and Tadej Bajd. "Multi-Fingered Grasping and Manipulation in Virtual Environments Using an Isometric Finger Device." In: *Presence* 16.3 (June 2007), pp. 293–306. doi: [10.1162/pres.16.3.293](https://doi.org/10.1162/pres.16.3.293).
- [102] Gert Kwakkel, Boudewijn J Kollen, and Hermano I Krebs. "Effects of Robot-Assisted Therapy on Upper Limb Recovery After Stroke: A Systematic Review." In: *Neurorehabilitation and Neural Repair* 22.2 (Sept. 2007), pp. 111–121. doi: [10.1177/1545968307305457](https://doi.org/10.1177/1545968307305457).
- [103] Daniel Laidig, Thomas Schauer, and Thomas Seel. "Exploiting kinematic constraints to compensate magnetic disturbances when calculating joint angles of approximate hinge joints from orientation estimates of inertial sensors." In: *Rehabilitation Robotics ICORR, International Conference on* 2017 (July 2017), pp. 971–976. doi: [10.1109/icorr.2017.8009375](https://doi.org/10.1109/icorr.2017.8009375).
- [104] C E Lang and M H Schieber. "Human finger independence: Limitations due to passive mechanical coupling versus active neuromuscular control." In: *Journal of Neurophysiology* 92.5 (2004), pp. 2802–2810. doi: [10.1152/jn.00480.2004](https://doi.org/10.1152/jn.00480.2004).
- [105] M L Latash, J K Shim, M Shinohara, and V M Zatsiorsky. "Changes in finger co-ordination and hand function with advanced age." In: *Motor control and learning*. Ed. by Springer US. 2006, pp. 141–159. doi: [10.1007/0-387-28287-4\\_13](https://doi.org/10.1007/0-387-28287-4_13).

- [106] *LEAP Motion*. 2017. URL: <https://www.leapmotion.com>.
- [107] Alberto Leardini, Lorenzo Chiari, Ugo Della Croce, and Aurelio Cappozzo. "Human movement analysis using stereophotogrammetry. Part 3. Soft tissue artifact assessment and compensation." In: *Gait & posture* 21.2 (Feb. 2005), pp. 212–225.
- [108] G Ligorio and A M Sabatini. "Dealing with Magnetic Disturbances in Human Motion Capture: A Survey of Techniques." In: *Micromachines* 7.3 (2016). doi: [10.3390/mi7030043](https://doi.org/10.3390/mi7030043).
- [109] Hangxin Liu, Xu Xie, Matt Millar, Mark Edmonds, Feng Gao, Yixin Zhu, Veronica J Santos, Brandon Rothrock, and Song-Chun Zhu. "A Glove-based System for Studying Hand-Object Manipulation via Joint Pose and Force Sensing." In: *International Conference on Intelligent Robots and Systems (IROS)*. 2017.
- [110] Lennart Ljung. "System identification." In: *Signal analysis and prediction*. Ed. by Springer. Springer, 1998, pp. 163–173.
- [111] Rui Loureiro, Farshid Amirabdollahian, Michael Topping, Bart Driessens, and William Harwin. "Upper Limb Robot Mediated Stroke Therapy—GENTLE/s Approach." In: *Autonomous Robots* 15.1 (2003), pp. 35–51.
- [112] H.J. Luinge and P.H. Veltink. "Measuring orientation of human body segments using miniature gyroscopes and accelerometers." In: *Medical and Biological Engineering and Computing* 43.2 (Mar. 2005), pp. 273–282. doi: [10.1007/bf02345966](https://doi.org/10.1007/bf02345966).
- [113] H.J. Luinge, P.H. Veltink, and C T M Baten. "Ambulatory measurement of arm orientation." In: *Journal of Biomechanics* 40.1 (2007), pp. 78–85. doi: [10.1016/j.jbiomech.2005.11.011](https://doi.org/10.1016/j.jbiomech.2005.11.011).
- [114] H Luinge and PH Veltink. "Inclination measurement of human movement using a 3-D accelerometer with autocalibration." In: *IEEE Transactions on neural systems and rehabilitation engineering* 12.1 (2004), pp. 112–121. doi: [10.1109/tnsre.2003.822759](https://doi.org/10.1109/tnsre.2003.822759).
- [115] Paweł Maciejasz, Jörg Eschweiler, Kurt Gerlach-Hahn, Arne Jansen-Troy, and Steffen Leonhardt. "A survey on robotic devices for upper limb rehabilitation." In: *Journal of NeuroEngineering and Rehabilitation* 11.1 (Jan. 2014), p. 3. doi: [10.1186/1743-0003-11-3](https://doi.org/10.1186/1743-0003-11-3).
- [116] Jeffrey R Mackey and Brian L Davis. "Simultaneous shear and pressure sensor array for assessing pressure and shear at foot/ground interface." In: *Journal of Biomechanics* 39.15 (Jan. 2006), pp. 2893–2897. doi: [10.1016/j.jbiomech.2005.10.001](https://doi.org/10.1016/j.jbiomech.2005.10.001).
- [117] Sebastian O H Madgwick, Andrew J L Harrison, and Andrew Vaidyanathan. "Estimation of IMU and MARG orientation using a gradient descent algorithm." In: *Rehabilitation Robotics ICORR, IEEE International Conference on* 2011 (2011), pp. 5975346–7. doi: [10.1109/icorr.2011.5975346](https://doi.org/10.1109/icorr.2011.5975346).

- [118] Carmel Majidi. "Soft Robotics: A Perspective—Current Trends and Prospects for the Future." In: *Soft Robotics* 1.1 (Mar. 2014), pp. 5–11. doi: [10.1089/soro.2013.0001](https://doi.org/10.1089/soro.2013.0001).
- [119] T von Marcard, B Rosenhahn, M J Black, and G Pons-Moll. "Sparse Inertial Poser: Automatic 3D Human Pose Estimation from Sparse IMUs." In: *Computer Graphics Forum* 36.2 (May 2017), pp. 349–360. doi: [10.1111/cgf.13131](https://doi.org/10.1111/cgf.13131).
- [120] Elaine Nicpon Marieb and Katja Hoehn. *Human anatomy & physiology*. Pearson Education, 2007.
- [121] Stefano Masiero, Patrizia Poli, Giulio Rosati, Damiano Zanotto, Marco Iosa, Sefano Paolucci, and Giovanni Morone. "The value of robotic systems in stroke rehabilitation." In: *Expert Review of Medical Devices* 11.2 (Nov. 2013), pp. 187–198. doi: [10.1586/17434440.2014.882766](https://doi.org/10.1586/17434440.2014.882766).
- [122] Fokke B van Meulen, Bert-Jan F van Beijnum, Jaap H Buurke, and Peter H Veltink. "Assessment of lower arm movements using one inertial sensor." In: *Rehabilitation Robotics ICORR, International Conference on* 2017 (July 2017), pp. 1407–1412. doi: [10.1109/icorr.2017.8009445](https://doi.org/10.1109/icorr.2017.8009445).
- [123] S Micera et al. "A Simple Robotic System for Neurorehabilitation." In: *Autonomous Robots* 19.3 (2005), pp. 271–284. doi: [10.1007/s10514-005-4749-0](https://doi.org/10.1007/s10514-005-4749-0).
- [124] Markus Miezal, Bertram Taetz, and Gabriele Bleser. "On Inertial Body Tracking in the Presence of Model Calibration Errors." In: *Sensors* 16.7 (2016). doi: [10.3390/s16071132](https://doi.org/10.3390/s16071132).
- [125] T B Moeslund, A Hilton, and V Krüger. "A survey of advances in vision-based human motion capture and analysis." In: *Computer Vision and Image Understanding* 104.2-3 SPEC. ISS. (2006), pp. 90–126. doi: [10.1016/j.cviu.2006.08.002](https://doi.org/10.1016/j.cviu.2006.08.002).
- [126] Mostafa Mohammadi, Tommaso Lisini Baldi, Stefano Scheggi, and Domenico Prattichizzo. "Fingertip force estimation via inertial and magnetic sensors in deformable object manipulation." In: *IEEE Haptics Symposium, HAPTICS*. Universita degli Studi di Siena, Siena, Italy. IEEE, Apr. 2016, pp. 284–289. doi: [10.1109/haptics.2016.7463191](https://doi.org/10.1109/haptics.2016.7463191).
- [127] *Motion Workshop* (<https://www.motionnode.com>). 2017.
- [128] Philipp Muller, Marc Andre Begin, Thomas Schauer, and Thomas Seel. "Alignment-free, self-calibrating elbow angles measurement using inertial sensors." In: *3rd IEEE EMBS International Conference on Biomedical and Health Informatics, BHI 2016*. Technische Universitat Berlin, Berlin, Germany. IEEE, Apr. 2016, pp. 583–586. doi: [10.1109/bhi.2016.7455965](https://doi.org/10.1109/bhi.2016.7455965).
- [129] Raviraj Nataraj and Zong-Ming Li. "Robust Identification of Three-Dimensional Thumb and Index Finger Kinematics With a Minimal Set of Markers." In: *Journal of Biomechanical Engineering* 135.9 (2013), p. 091002. doi: [10.1115/1.4024753](https://doi.org/10.1115/1.4024753).

- [130] Tobias Nef, Matjaz Mihelj, Gery Colombo, and Robert Riener. "ARMin-robot for rehabilitation of the upper extremities." In: *Robotics and Automation, 2006. ICRA 2006. Proceedings 2006 IEEE International Conference on*. IEEE. 2006, pp. 3152–3157.
- [131] Michiko Nishiyama and Kazuhiro Watanabe. "Wearable sensing glove with embedded hetero-core fiber-optic nerves for unconstrained hand motion capture." In: *IEEE Transactions on Instrumentation and Measurement* 58.12 (Dec. 2009), pp. 3995–4000. doi: [10.1109/tim.2009.2021640](https://doi.org/10.1109/tim.2009.2021640).
- [132] J C van den Noort, K van Dijk, H. G Kortier, N van Beek, R Verhagen, L Bour, and P.H. Veltink. "Applications of the PowerGlove for Measurement of Finger Kinematics." In: *In 11th International Conferences on Wearable and Implantable Body Sensor Networks Workshops*. IEEE, Proceedings of 11th International Conferences on Wearable and Implantable Body Sensor Networks Workshops (BSN Workshops), 2014, pp. 6–10. doi: [10.1109-bsn.workshops.2014.19](https://doi.org/10.1109-bsn.workshops.2014.19).
- [133] J C van den Noort, A Ferrari, A G Cutti, J G Becher, and J Harlaar. "Gait analysis in children with cerebral palsy via inertial and magnetic sensors." In: *Med. Biol. Eng Comput* 51.4 (2013), pp. 377–386. doi: [10.1007/s11517-012-1006-5](https://doi.org/10.1007/s11517-012-1006-5).
- [134] J C Noort et al. "Applications of the PowerGlove." In: *Proceedings of 3D-AHM* (2014).
- [135] Josien van den Noort, Kees van Dijk, Henk Kortier, Nathalie van Beek, Rens Verhagen, Lo Bour, and Peter Veltink. "Applications of the powerglove for measurement of finger kinematics." In: *Wearable and Implantable Body Sensor Networks Workshops (BSN Workshops), 2014 11th International Conference on*. IEEE. 2014, pp. 6–10.
- [136] N Oess, J Wanek, and A Curt. "Design and evaluation of a low-cost instrumented glove for hand function assessment." In: *Journal of NeuroEngineering and Rehabilitation* 9.1 (2012), p. 2. doi: [10.1186/1743-0003-9-2](https://doi.org/10.1186/1743-0003-9-2).
- [137] Bjorn Olofsson, Jacob Antonsson, Henk G Kortier, Bo Bernhardsson, Anders Robertsson, and Rolf Johansson. "Sensor Fusion for Robotic Workspace State Estimation." In: *IEEE/ASME Transactions on Mechatronics* 21.5 (Oct. 2016), pp. 2236–2248. doi: [10.1109/tmech.2015.2506041](https://doi.org/10.1109/tmech.2015.2506041).
- [138] Optotrak. 2017. URL: <https://www.ndigital.com>.
- [139] L Paredes-Madrid and P Gonzalez De Santos. "Dataglove-based interface for impedance control of manipulators in cooperative human-robot environments." In: *Measurement Science and Technology* 24.2 (Feb. 2013), p. 025005. doi: [10.1088/0957-0233/24/2/025005](https://doi.org/10.1088/0957-0233/24/2/025005).
- [140] W L Parker. "Evidence-based medicine: thumb carpometacarpal arthroplasty." In: *Plast. Reconstr. Surg* 132.6 (2013), pp. 1706–1719. doi: [10.1097/prs.0b013e3182a807af](https://doi.org/10.1097/prs.0b013e3182a807af).

- [141] K Parsa, J Angeles, and A K Misra. "Rigid-body pose and twist estimation using an accelerometer array." In: *Archive of Applied Mechanics* 74.3-4 (2004), pp. 223–236. DOI: [10.1007/s00419-004-0345-6](https://doi.org/10.1007/s00419-004-0345-6).
- [142] S K Patrick, A A Denington, M J A Gauthier, D M Gillard, and A Prochazka. "Quantification of the UPDRS rigidity scale." In: *IEEE Transactions on neural systems and rehabilitation engineering* 9.1 (2001), pp. 31–41. DOI: [10.1109/7333.918274](https://doi.org/10.1109/7333.918274).
- [143] *Perception Neuron (<https://neuronmocap.com>)*. 2017.
- [144] A J Petruska and J J Abbott. "Optimal permanent-magnet geometries for dipole field approximation." In: *IEEE Transactions on Magnetics* 49.2 (2013), pp. 811–819. DOI: [10.1109/tmag.2012.2205014](https://doi.org/10.1109/tmag.2012.2205014).
- [145] Trieu H Pham. "A Quantifiable Kinematic Characterisation of Hand Function." In: *Deakin University* (Nov. 2016), pp. 1–119.
- [146] Rik Pintelon and Johan Schoukens. *System identification: a frequency domain approach*. John Wiley & Sons, 2012.
- [147] *Polhemus*. 2017. URL: <http://polhemus.com>.
- [148] Panagiotis Polygerinos, Zheng Wang, Kevin C Galloway, Robert J Wood, and Conor J Walsh. "Soft robotic glove for combined assistance and at-home rehabilitation." In: *Robotics and Autonomous Systems* 73 (Nov. 2015), pp. 135–143. DOI: [10.1016/j.robot.2014.08.014](https://doi.org/10.1016/j.robot.2014.08.014).
- [149] B Post, M P Merkus, R M A De Bie, R J De Haan, and J D Speelman. "Unified Parkinson's disease rating scale motor examination: Are ratings of nurses, residents in neurology, and movement disorders specialists interchangeable?" In: *Movement Disorders* 20.12 (2005), pp. 1577–1584. DOI: [10.1002/mds.20640](https://doi.org/10.1002/mds.20640).
- [150] F H Raab, E B Blood, T O Steiner, and H R Jones. "Magnetic Position and Orientation Tracking System." In: *Aerospace and Electronic Systems, IEEE Transactions on* 5 (1979), pp. 709–718. DOI: [10.1109/taes.1979.308860](https://doi.org/10.1109/taes.1979.308860).
- [151] Mohammad A Razian and Matthew G Pepper. "Design, development, and characteristics of an in-shoe triaxial pressure measurement transducer utilizing a single element of piezoelectric copolymer film." In: *IEEE Transactions on neural systems and rehabilitation engineering* 11.3 (2003), pp. 288–293. DOI: [10.1109/tnsre.2003.818185](https://doi.org/10.1109/tnsre.2003.818185).
- [152] D Roetenberg, HJ Luinge, CTM Baten, and PH Veltink. "Compensation of magnetic disturbances improves inertial and magnetic sensing of human body segment orientation." In: *Neural Systems and Rehabilitation Engineering, IEEE Transactions on* 13.3 (2005), pp. 395–405. DOI: [10.1109/tnsre.2005.847353](https://doi.org/10.1109/tnsre.2005.847353).
- [153] D Roetenberg, L Schipper, P Garofalo, and A G Cutti. *Joint angles and segment length estimation using inertial sensors*. Proceedings of the 3dMA, 2010.

- [154] D Roetenberg, PJ Slycke, and PH Veltink. "Ambulatory position and orientation tracking fusing magnetic and inertial sensing." In: *IEEE Transactions on Biomedical Engineering* 54.5 (Jan. 2007), pp. 883–890. doi: [10.1109/tbme.2006.889184](https://doi.org/10.1109/tbme.2006.889184).
- [155] D Roetenberg and P.H. Veltink. "Camera-marker and inertial sensor fusion for improved motion tracking." In: *Gait & posture* 22 (2005), pp. 1–53.
- [156] Daniel Roetenberg, Henk Luinge, and Per Slycke. "Xsens MVN: full 6DOF human motion tracking using miniature inertial sensors." In: *Xsens Motion Technologies BV, Tech. Rep* (2009).
- [157] Paulo Roriz, Lidia Carvalho, Orlando Frazão, José Luis Santos, and José António Simões. "From conventional sensors to fibre optic sensors for strain and force measurements in biomechanics applications: A review." In: *Journal of Biomechanics* 47.6 (Apr. 2014), pp. 1251–1261. doi: [10.1016/j.jbiomech.2014.01.054](https://doi.org/10.1016/j.jbiomech.2014.01.054).
- [158] J B Rowe, N Friedman, M Bachman, and D J Reinkensmeyer. "The Manumeter: A non-obtrusive wearable device for monitoring spontaneous use of the wrist and fingers." In: *Rehabilitation Robotics (ICORR), 2013 IEEE International Conference on*. IEEE, 2013, pp. 1–6. doi: [10.1109/icorr.2013.6650397](https://doi.org/10.1109/icorr.2013.6650397).
- [159] J H Ryu, N Miyata, M Kouchi, M Mochimaru, and K H Lee. "Analysis of skin movement with respect to flexional bone motion using MR images of a hand." In: *J. Biomech* 39.5 (2006), pp. 844–852. doi: [10.1016/j.jbiomech.2005.02.001](https://doi.org/10.1016/j.jbiomech.2005.02.001).
- [160] H P Saal, Jo-Anne Ting, and S Vijayakumar. "Active estimation of object dynamics parameters with tactile sensors." In: *Intelligent Robots and Systems (IROS), 2010 IEEE/RSJ International Conference on*. IEEE, 2010, pp. 916–921. doi: [10.1109/iros.2010.5649191](https://doi.org/10.1109/iros.2010.5649191).
- [161] AM Sabatini. "Quaternion-based extended Kalman filter for determining orientation by inertial and magnetic sensing." In: *Biomedical Engineering, IEEE Transactions on* 53.7 (2006), pp. 1346–1356. doi: [10.1109/tbme.2006.875664](https://doi.org/10.1109/tbme.2006.875664).
- [162] Angelo Maria Sabatini. "Estimating Three-Dimensional Orientation of Human Body Parts by Inertial/Magnetic Sensing." In: *Sensors* 11.2 (Feb. 2011), pp. 1489–1525. doi: [10.3390/s110201489](https://doi.org/10.3390/s110201489).
- [163] Sarvenaz Salehi, Gabriele Bleser, Attila Reiss, and Didier Stricker. *Body-IMU autocalibration for inertial hip and knee joint tracking*. ICST (Institute for Computer Sciences, Social-Informatics and Telecommunications Engineering), Sept. 2015. doi: [10.4108/eai.28-9-2015.2261522](https://doi.org/10.4108/eai.28-9-2015.2261522).
- [164] E M Schearer, Yu-Wei Liao, E J Perreault, M C Tresch, W D Memberg, R F Kirsch, and K M Lynch. "Identifying inverse human arm dynamics using a robotic testbed." In: *2014 IEEE/RSJ International Conference on Intelligent Robots and Systems (IROS 2014)* (2014), pp. 3585–3591. doi: [10.1109/iros.2014.6943064](https://doi.org/10.1109/iros.2014.6943064).
- [165] H Martin Schepers, H F J M Koopman, and Peter H Veltink. "Ambulatory assessment of ankle and foot dynamics." In: *IEEE Transactions on Biomedical Engineering* 54.5 (May 2007), pp. 895–902. doi: [10.1109/tbme.2006.889769](https://doi.org/10.1109/tbme.2006.889769).

- [166] H.M. Schepers, D Roetenberg, and P.H. Veltink. "Ambulatory human motion tracking by fusion of inertial and magnetic sensing with adaptive actuation." In: *Medical and Biological Engineering and Computing* 48.1 (2010), pp. 27–37. doi: [10.1007/s11517-009-0562-9](https://doi.org/10.1007/s11517-009-0562-9).
- [167] HM Schepers and PH Veltink. "Stochastic magnetic measurement model for relative position and orientation estimation." In: *Measurement Science and Technology* 21 (2010), p. 065801. doi: [10.1088/0957-0233/21/6/065801](https://doi.org/10.1088/0957-0233/21/6/065801).
- [168] AC Schouten, E de Vlugt, FCT van der Helm, and GG Brouwn. "Optimal posture control of a musculo-skeletal arm model." In: *Biological Cybernetics* 84.2 (2001), pp. 143–152. doi: [10.1007/s004220000202](https://doi.org/10.1007/s004220000202).
- [169] AC Schouten, E de Vlugt, JJB van Hiltén, and FCT van der Helm. "Quantifying Proprioceptive Reflexes During Position Control of the Human Arm." In: *Biomedical Engineering, IEEE Transactions on* 55.1 (2008), pp. 311–321. doi: [10.1109/tbme.2007.899298](https://doi.org/10.1109/tbme.2007.899298).
- [170] T Seel, J Raisch, and T Schauer. "IMU-based joint angle measurement for gait analysis." In: *Sensors (Switzerland)* 14.4 (2014), pp. 6891–6909. doi: [10.3390/s140406891](https://doi.org/10.3390/s140406891).
- [171] T Seel, T Schauer, and J Raisch. "Joint axis and position estimation from inertial measurement data by exploiting kinematic constraints." In: *Proceedings of the IEEE International Conference on Control Applications*. 2012, pp. 45–49. doi: [10.1109/cca.2012.6402423](https://doi.org/10.1109/cca.2012.6402423).
- [172] Helaine Selin. *Encyclopaedia of the history of science, technology, and medicine in non-western cultures*. Springer Science & Business Media, 2013.
- [173] T Sharp, C Keskin, D Robertson, and J Taylor. "Accurate, robust, and flexible real-time hand tracking." In: *Proceedings of the 33rd Annual ACM Conference on Human Factors in Computing Systems*. 2015, pp. 3633–3642. doi: [10.1145/2702123.2702179](https://doi.org/10.1145/2702123.2702179).
- [174] Z L Shen, T A Mondello, R Nataraj, M F Domalain, and Z M Li. "A digit alignment device for kinematic analysis of the thumb and index finger." In: *Gait Posture* 36.3 (2012), pp. 643–645. doi: [10.1016/j.gaitpost.2012.04.012](https://doi.org/10.1016/j.gaitpost.2012.04.012).
- [175] L K Simone, N Sundarajan, X Luo, Y Jia, and D G Kamper. "A low cost instrumented glove for extended monitoring and functional hand assessment." In: *Journal of neuroscience methods* 160.2 (2007), pp. 335–348. doi: [10.1016/j.jneumeth.2006.09.021](https://doi.org/10.1016/j.jneumeth.2006.09.021).
- [176] I Skog, P Händel, J Nilsson, and J Rantakokko. "Zero-velocity detection — an algorithm evaluation." In: *IEEE transactions on bio-medical engineering* 57.11 (Nov. 2010), pp. 2657–2666.
- [177] J H Skotte, M Essendrop, A F Hansen, and B Schibye. "A dynamic 3D biomechanical evaluation of the load on the low back during different patient-handling tasks." In: *Journal of Biomechanics* 35.10 (Oct. 2002), pp. 1357–1366. doi: [10.1016/s0021-9290\(02\)00181-1](https://doi.org/10.1016/s0021-9290(02)00181-1).

- [178] I Soderkvist and P A Wedin. "Determining the movements of the skeleton using well-configured markers." In: *J. Biomech* 26.12 (1993), pp. 1473–1477. doi: [10.1016/0021-9290\(93\)90098-y](https://doi.org/10.1016/0021-9290(93)90098-y).
- [179] B Stenger, A Thayananthan, and PHS Torr. "Model-based hand tracking using a hierarchical bayesian filter." In: *IEEE Transactions on pattern analysis and machine intelligence* (2006). doi: [10.1109/tpami.2006.189](https://doi.org/10.1109/tpami.2006.189).
- [180] DJ Sturman and D Zeltzer. "A survey of glove-based input." In: *IEEE Computer Graphics and Applications* 14.1 (1994), pp. 30–39. doi: [10.1109/38.250916](https://doi.org/10.1109/38.250916).
- [181] S S Sultana, J C MacDermid, R Grewal, and S Rath. "The effectiveness of early mobilization after tendon transfers in the hand: a systematic review." In: *J. Hand Ther* 26.1 (2013), pp. 1–20. doi: [10.1016/j.jht.2012.06.006](https://doi.org/10.1016/j.jht.2012.06.006).
- [182] B Taetz, G Bleser, and M Miezal. "Towards self-calibrating inertial body motion capture." In: *Information Fusion (FUSION)* (2016), pp. 1751–1759.
- [183] S Takamuku, G Gomez, and K Hosoda. "Haptic discrimination of material properties by a robotic hand." In: *Development and Learning, 2007. ICDL 2007. IEEE 6th International Conference on* (2007), pp. 1–6. doi: [10.1109/devlrn.2007.4354057](https://doi.org/10.1109/devlrn.2007.4354057).
- [184] Jonathan Taylor et al. "Efficient and precise interactive hand tracking through joint, continuous optimization of pose and correspondences." In: *ACM Transactions on Graphics*. Microsoft Research, Redmond, United States. July 2016. doi: [10.1145/2897824.2925965](https://doi.org/10.1145/2897824.2925965).
- [185] E Todorov. "Probabilistic Inference of Multijoint Movements, Skeletal Parameters and Marker Attachments From Diverse Motion Capture Data." In: *IEEE Transactions on Biomedical Engineering* 54.11 (2007), pp. 1927–1939. doi: [10.1109/tbme.2007.903521](https://doi.org/10.1109/tbme.2007.903521).
- [186] E Todorov and MI Jordan. "Optimal feedback control as a theory of motor coordination." In: *Nature neuroscience* 5.11 (2002), pp. 1226–1235. doi: [10.1038/nn963](https://doi.org/10.1038/nn963).
- [187] Emanuel Todorov. "Optimality principles in sensorimotor control." In: *Nature neuroscience* 7.9 (Sept. 2004), pp. 907–915. doi: [10.1038/nn1309](https://doi.org/10.1038/nn1309).
- [188] A Tognetti et al. "Daily-life monitoring of stroke survivors motor performance: The INTERACTION sensing system." In: *2014 36th Annual International Conference of the IEEE Engineering in Medicine and Biology Society*. IEEE, 2014, pp. 4099–4102. doi: [10.1109/embc.2014.6944525](https://doi.org/10.1109/embc.2014.6944525).
- [189] José Torres-Moreno, José Blanco-Claraco, Antonio Giménez-Fernández, Emilio Sanjurjo, and Miguel Naya. "Online Kinematic and Dynamic-State Estimation for Constrained Multibody Systems Based on IMUs." In: *Sensors* 16.3 (Mar. 2016), pp. 333–19. doi: [10.3390/s16030333](https://doi.org/10.3390/s16030333).

- [190] Bill Triggs, Philip F McLauchlan, Richard I Hartley, and Andrew W Fitzgibbon. "Bundle Adjustment — A Modern Synthesis." In: *Vision Algorithms: Theory and Practice*. Ed. by Springer. Berlin, Heidelberg: Springer Berlin Heidelberg, Sept. 1999, pp. 298–372. doi: [10.1007/3-540-44480-7\\_21](https://doi.org/10.1007/3-540-44480-7_21).
- [191] A Vaccarella, E de Momi, A Enquobahrie, and G Ferrigno. "Unscented Kalman filter based sensor fusion for robust optical and electromagnetic tracking in surgical navigation." In: *IEEE Transactions on Instrumentation and Measurement* 62.7 (2013), pp. 2067–2081. doi: [10.1109/tim.2013.2248304](https://doi.org/10.1109/tim.2013.2248304).
- [192] J.C. van den Noort, H.G. Kortier, N. van Beek, H.E.J. Veeger, and P.H. Veltink. "Measuring 3D hand and finger kinematics - a comparison between inertial sensing and an opto-electronic marker system." In: *PLoS ONE* 11.11 (Nov. 2016). Henk G Kortier contributed in: Conceiving and designing the experiments, Performing the experiments, Analyzing the data, Contributing materials/analysis tools, Writing the paper, Designed the software used in analysis, p. e0164889. ISSN: 1932-6203. doi: [10.1371/journal.pone.0164889](https://doi.org/10.1371/journal.pone.0164889).
- [193] Richard Q Van der Linde, Piet Lammertse, Erwin Frederiksen, and B Ruiter. "The HapticMaster, a new high-performance haptic interface." In: *Proc. Eurohaptics*. 2002, pp. 1–5.
- [194] P.H. Veltink, H.G. Kortier, and H.M. Schepers. "Sensing power transfer between the human body and the environment." In: *IEEE Transactions on Biomedical Engineering* 56.6 (June 2009). H Kortier contributed in: Conceiving and designing the experiments, Performing the experiments, Analyzing the data, Writing the paper, Designed the software used in analysis, pp. 1711–1718. doi: [10.1109/TBME.2009.2014963](https://doi.org/10.1109/TBME.2009.2014963).
- [195] P.H. Veltink, P Slycke, J Hemssems, R Buschman, G Bultstra, and H Hermens. "Three dimensional inertial sensing of foot movements for automatic tuning of a two-channel implantable drop-foot stimulator." In: *Medical Engineering and Physics* 25.1 (Jan. 2003), pp. 21–28. doi: [10.1016/s1350-4533\(02\)00041-3](https://doi.org/10.1016/s1350-4533(02)00041-3).
- [196] Peter H Veltink, Christian Liedtke, Ed Droog, and Herman van der Kooij. "Ambulatory measurement of ground reaction forces." In: *IEEE Transactions on neural systems and rehabilitation engineering* 13.3 (2005), pp. 423–427. doi: [10.1109/icsmc.2004.1398383](https://doi.org/10.1109/icsmc.2004.1398383).
- [197] Petrus Hermanus Veltink. *Device and method for measuring the dynamic interaction between bodies*. 2008.
- [198] Jan F Veneman, Rik Kruidhof, Edsko E G Hekman, Ralf Ekkelenkamp, Edwin H F Van Asseldonk, and Herman van der Kooij. "Design and Evaluation of the LOPES Exoskeleton Robot for Interactive Gait Rehabilitation." In: *IEEE Transactions on neural systems and rehabilitation engineering* 15.3 (2007), pp. 379–386. doi: [10.1109/tnsre.2007.903919](https://doi.org/10.1109/tnsre.2007.903919).
- [199] Vicon. 2017. URL: <https://www.vicon.com>.
- [200] VisualEyes. 2017. URL: <http://www.ptiphoenix.com>.

- [201] E de Vlugt, AC Schouten, and FCT van der Helm. "Closed-loop multivariable system identification for the characterization of the dynamic arm compliance using continuous force disturbances: a model study." In: *Journal of neuroscience methods* 122.2 (2003), pp. 123–140. doi: [10.1016/s0165-0270\(02\)00303-5](https://doi.org/10.1016/s0165-0270(02)00303-5).
- [202] Bruce T Volpe, Daniel Lynch, Avrielle Rykman-Berland, Mark Ferraro, Michael Galgano, Neville Hogan, and Hermano I Krebs. "Intensive Sensorimotor Arm Training Mediated by Therapist or Robot Improves Hemiparesis in Patients With Chronic Stroke." In: *Neurorehabilitation and Neural Repair* 22.3 (May 2008), pp. 305–310. doi: [10.1177/1545968307311102](https://doi.org/10.1177/1545968307311102).
- [203] W H de Vries, H E Veeger, A G Cutti, C. Baten, and F C Van der Helm. "Functionally interpretable local coordinate systems for the upper extremity using inertial & magnetic measurement systems." In: *J. Biomech* 43.10 (2010), pp. 1983–1988. doi: [10.1016/j.jbiomech.2010.03.007](https://doi.org/10.1016/j.jbiomech.2010.03.007).
- [204] N Wahlstrom, J Callmer, and F Gustafsson. "Magnetometers for tracking metallic targets." In: *Information Fusion (FUSION), 2010 13th Conference on*. 2010, pp. 1–8. doi: [10.1109/icif.2010.5711900](https://doi.org/10.1109/icif.2010.5711900).
- [205] Qi Wang, Panos Markopoulos, Bin Yu, Wei Chen, and Annick Timmermans. "Interactive wearable systems for upper body rehabilitation: a systematic review." In: *Journal of NeuroEngineering and Rehabilitation* 14.1 (Mar. 2017), pp. 1–21. doi: [10.1186/s12984-017-0229-y](https://doi.org/10.1186/s12984-017-0229-y).
- [206] D Weenk, D Roetenberg, B van Beijnum, and H Hermens. "Ambulatory Estimation of Relative Foot Positions by Fusing Ultrasound and Inertial Sensor Data." In: *IEEE transactions on neural systems and rehabilitation engineering* (2014). doi: [10.1109/tnsre.2014.2357686](https://doi.org/10.1109/tnsre.2014.2357686).
- [207] G Welch and E Foxlin. "Motion tracking survey." In: *IEEE Computer Graphics and Applications* (2002), pp. 24–38.
- [208] F Wenk and U Frese. "Posture from motion." In: *Intelligent Robots and Systems (IROS)* (2015), pp. 280–285. doi: [10.1109/iros.2015.7353386](https://doi.org/10.1109/iros.2015.7353386).
- [209] Nkenge Wheatland, Yingying Wang, Huaguang Song, Michael Neff, Victor Zordan, and Sophie Jörg. "State of the Art in Hand and Finger Modeling and Animation." In: *Computer Graphics Forum* 34.2 (May 2015), pp. 735–760. doi: [10.1111/cgf.12595](https://doi.org/10.1111/cgf.12595).
- [210] NW Williams, JMT Penrose, CM Caddy, E Barnes, DR Hose, and P Harley. "A goniometric glove for clinical hand assessment." In: *Journal of Hand Surgery (British and European Volume)* 25.2 (2000), p. 200. doi: [10.1054/jhsb.1999.0360](https://doi.org/10.1054/jhsb.1999.0360).
- [211] S Wise, W Gardner, E Sabelman, E Valainis, Y Wong, J Drace, and JM Rosen. "Evaluation of a fiber optic glove for se-automated goniometric measurements." In: *Journal of Rehabilitation Research and Development* 27.4 (1990). doi: [10.1682/jrrd.1990.10.0411](https://doi.org/10.1682/jrrd.1990.10.0411).

- [212] Daniel M Wolpert, Jörn Diedrichsen, and J Randall Flanagan. "Principles of sensorimotor learning." In: *Nature Reviews Neuroscience* (Oct. 2011), pp. 1–13. doi: [10.1038/nrn3112](https://doi.org/10.1038/nrn3112).
- [213] DM Wolpert. "Probabilistic models in human sensorimotor control." In: *Human movement science* 26.4 (2007), pp. 511–524. doi: [10.1016/j.humov.2007.05.005](https://doi.org/10.1016/j.humov.2007.05.005).
- [214] Frank Wouda, Matteo Giuberti, Giovanni Bellusci, and Peter Veltink. "Estimation of Full-Body Poses Using Only Five Inertial Sensors: An Eager or Lazy Learning Approach?" In: *Sensors* 16.12 (Dec. 2016), pp. 2138–17. doi: [10.3390/s16122138](https://doi.org/10.3390/s16122138).
- [215] Lucas H V van der Woude, Astrid Horstman, Paul Faas, Sander Mechielsen, Hamid Abbasi Bafghi, and Jos J de Koning. "Power output and metabolic cost of synchronous and asynchronous submaximal and peak level hand cycling on a motor driven treadmill in able-bodied male subjects." In: *Medical Engineering and Physics* 30.5 (June 2008), pp. 574–580. doi: [10.1016/j.medengphy.2007.06.006](https://doi.org/10.1016/j.medengphy.2007.06.006).
- [216] Stephen J Wright and Jorge Nocedal. "Numerical optimization." In: *Springer Science* 35.67–68 (1999), p. 7.
- [217] G Wu, FCT van der Helm, HEJ Veeger, M Makhsous, P van Roy, C Anglin, J Nagels, AR Karduna, and K McQuade. "ISB recommendation on definitions of joint coordinate systems of various joints for the reporting of human joint motion—Part II: shoulder, elbow, wrist and hand." In: *Journal of Biomechanics* 38.5 (2005), pp. 981–992. doi: [10.1016/j.jbiomech.2004.05.042](https://doi.org/10.1016/j.jbiomech.2004.05.042).
- [218] John Z Wu, Kai-Nan An, Robert G Cutlip, Kristine Krajnak, Daniel Welcome, and Ren G Dong. "Analysis of musculoskeletal loading in an index finger during tapping." In: *Journal of Biomechanics* 41.3 (2008), pp. 668–676. doi: [10.1016/j.jbiomech.2007.09.025](https://doi.org/10.1016/j.jbiomech.2007.09.025).
- [219] Tingfan Wu, Yuval Tassa, Vikash Kumar, Javier Movellan, and Emanuel Todorov. "STAC: Simultaneous tracking and calibration." In: *IEEE-RAS International Conference on Humanoid Robots*. University of California, San Diego, United States. IEEE, Jan. 2015, pp. 469–476. doi: [10.1109/humanoids.2013.7030016](https://doi.org/10.1109/humanoids.2013.7030016).
- [220] Y Xiaoping, ER Bachmann, and RB McGhee. "A simplified quaternion-based algorithm for orientation estimation from earth gravity and magnetic field measurements." In: *Instrumentation and Measurement, IEEE Transactions on* 57.3 (2008), pp. 638–650. doi: [10.1109/tim.2007.911646](https://doi.org/10.1109/tim.2007.911646).
- [221] Xsens Technologies B.V. (<http://www.xsens.com>). 2017.
- [222] Takeo Yamada, Yuhei Hayamizu, Yuki Yamamoto, Yoshiki Yomogida, Ali Izadi-Najafabadi, Don N Futaba, and Kenji Hata. "A stretchable carbon nanotube strain sensor for human-motion detection." In: *Nature nanotechnology* 6.5 (May 2011), pp. 296–301. doi: [10.1038/nnano.2011.36](https://doi.org/10.1038/nnano.2011.36).

- [223] AD Young. "Use of Body Model Constraints to Improve Accuracy of Inertial Motion Capture." In: *2010 International Conference on Body Sensor Networks* (2010), pp. 180–186. doi: [10.1109/bsn.2010.549030](https://doi.org/10.1109/bsn.2010.549030).
- [224] Hanna Yousef, Mehdi Boukallel, and Kaspar Althoefer. "Tactile sensing for dexterous in-hand manipulation in robotics - A review." In: *Sensors and Actuators A: Physical* 167.2 (June 2011), pp. 171–187. doi: [10.1016/j.sna.2011.02.038](https://doi.org/10.1016/j.sna.2011.02.038).
- [225] X Yun and ER Bachmann. "Design, implementation, and experimental results of a quaternion-based Kalman filter for human body motion tracking." In: *Robotics, IEEE Transactions on* 22.6 (2006), pp. 1216–1227. doi: [10.1109/tro.2006.886270](https://doi.org/10.1109/tro.2006.886270).
- [226] V M Zatsiorsky, Z M Li, and M L Latash. "Enslaving effects in multi-finger force production." In: *Exp. Brain Res* 131.2 (2000), pp. 187–195. doi: [10.1007/s002219900261](https://doi.org/10.1007/s002219900261).
- [227] Jun-Tian Zhang, Alison C Novak, Brenda Brouwer, and Qingguo Li. "Concurrent validation of Xsens MVN measurement of lower limb joint angular kinematics." In: *Physiological Measurement* 34.8 (Aug. 2013), N63–N69. doi: [10.1088/0967-3334/34/8/n63](https://doi.org/10.1088/0967-3334/34/8/n63).
- [228] H Zhou and H Hu. "Human motion tracking for rehabilitation–A survey." In: *Biomedical Signal Processing and Control* 3.1 (2008), pp. 1–18. doi: [10.1016/j.bspc.2007.09.001](https://doi.org/10.1016/j.bspc.2007.09.001).
- [229] H Zhou and H Hu. "Reducing drifts in the inertial measurements of wrist and elbow positions." In: *Instrumentation and Measurement, IEEE Transactions on* 59.3 (2010), pp. 575–585. doi: [10.1109/tim.2009.2025065](https://doi.org/10.1109/tim.2009.2025065).
- [230] R Zhu and Z Zhou. "A real-time articulated human motion tracking using tri-axis inertial/magnetic sensors package." In: *Neural Systems and Rehabilitation Engineering, IEEE Transactions on* 12.2 (2004), pp. 295–302. doi: [10.1109/tnsre.2004.827825](https://doi.org/10.1109/tnsre.2004.827825).
- [231] J Žumer, J Slavič, and M Boltežar. "Minimization of the positional errors for an accurate determination of the kinematic parameters of a rigid-body system with miniature inertial sensors." In: *Mechanism and Machine Theory* 81 (2014), pp. 193–208. doi: [10.1016/j.mechmachtheory.2014.07.008](https://doi.org/10.1016/j.mechmachtheory.2014.07.008).
- [232] A Zyluk and K Skala. "Hand disorders in the course of systemic and chronic diseases: a review." In: *Pol. Orthop. Traumatol* 79 (2014), pp. 30–36.

## JOURNAL PUBLICATIONS

---

- [1] H.G. Kortier, J. Antonsson, H.M. Schepers, F. Gustafsson, and P.H. Veltink. "Hand pose estimation by fusion of inertial and magnetic sensing aided by a permanent magnet." In: *IEEE transactions on neural systems and rehabilitation engineering* 23.5 (Sept. 2015). eemcs-eprint-25437, pp. 796–806. doi: [10.1109/TNSRE.2014.2357579](https://doi.org/10.1109/TNSRE.2014.2357579).
- [2] H.G. Kortier, H.M. Schepers, and P.H. Veltink. "Identification of Object Dynamics Using Hand Worn Motion and Force Sensors." In: *Sensors* 16.12 (2016). issn: 1424-8220. doi: [10.3390/s16122005](https://doi.org/10.3390/s16122005).
- [3] H.G. Kortier, V.I. Sluiter, D. Roetenberg, and P.H. Veltink. "Assessment of hand kinematics using inertial and magnetic sensors." In: *Journal of neuroengineering and rehabilitation* 11 (Apr. 2014). Open access, 70:1–70:14. issn: 1743-0003. doi: [10.1186/1743-0003-11-70](https://doi.org/10.1186/1743-0003-11-70).
- [4] B. Olofsson, J. Antonsson, H. G. Kortier, B. Bernhardsson, A. Robertsson, and R. Johansson. "Sensor Fusion for Robotic Workspace State Estimation." In: *IEEE/ASME Transactions on Mechatronics* 21.5 (Oct. 2016). Henk G Kortier contributed in: Writing the paper, Designed the software used in analysis, pp. 2236–2248. issn: 1083-4435. doi: [10.1109/TMECH.2015.2506041](https://doi.org/10.1109/TMECH.2015.2506041).
- [5] J.C. van den Noort, H.G. Kortier, N. van Beek, H.E.J. Veeger, and P.H. Veltink. "Measuring 3D hand and finger kinematics - a comparison between inertial sensing and an opto-electronic marker system." In: *PLoS ONE* 11.11 (Nov. 2016). Henk G Kortier contributed in: Conceiving and designing the experiments, Performing the experiments, Analyzing the data, Contributing materials/analysis tools, Writing the paper, Designed the software used in analysis, p. 0164889. issn: 1932-6203. doi: [10.1371/journal.pone.0164889](https://doi.org/10.1371/journal.pone.0164889).
- [6] P.H. Veltink, H.G. Kortier, and H.M. Schepers. "Sensing power transfer between the human body and the environment." In: *IEEE Transactions on Biomedical Engineering* 56.6 (June 2009). H Kortier contributed in: Conceiving and designing the experiments, Performing the experiments, Analyzing the data, Writing the paper, Designed the software used in analysis, pp. 1711–1718. doi: [10.1109/TBME.2009.2014963](https://doi.org/10.1109/TBME.2009.2014963).



## CONFERENCE PUBLICATIONS

---

- [1] H.G. Kortier, O. Schenk, H.J. Luinge, and P.H. Veltink. "A method to estimate relative orientations of body segments during movement using accelerometry." In: *Book of Abstracts of ICAMPAM 2011: the 2nd International Conference on Ambulatory Monitoring of Physical Activity and Movement.* eemcs-eprint-21409. ICAMPAM, May 2011.
- [2] H.G. Kortier, O. Schenk, H.J. Luinge, and P.H. Veltink. "Estimation of relative body segment orientation during movement using accelerometry." In: *Proceedings of Annual Symposium of the Benelux Chapter of the IEEE Engineering in Medicine and Biology Society, IEEE-EMBS 2011 - Leuven and Brussels, Belgium.* IEEE EMBS Benelux chapter, 2011.
- [3] H.G. Kortier, H.M. Schepers, V.I. Sluiter, and P.H. Veltink. "Ambulatory Assessment of Hand Kinematics, using an instrumented glove." In: *Proceedings of XII International Symposium on 3D Analysis of Human Movement.* Ed. by A. Leardini and R. Stagni. Universita di Bologna, July 2012, pp. 15–18.
- [4] H.G. Kortier, H.M. Schepers, V.I. Sluiter, and P.H. Veltink. "Estimation of hand and finger kinematics using inertial sensors." In: *4th Dutch Bio-Medical Engineering Conference, BME 2013.* BME2013, Jan. 2013.
- [5] H.G. Kortier, H.M. Schepers, and P.H. Veltink. "On-body inertial and magnetic sensing for assessment of hand and finger kinematics." In: *Proceedings of the 5th IEEE RAS & EMBS Interantional Conference on Biomedical Robotics and Biomechatronics.* IEEE ROBOTICS and AUTOMATION SOCIETY, Aug. 2014, pp. 555–560. doi: [10.1109/BIOROB.2014.6913836](https://doi.org/10.1109/BIOROB.2014.6913836).
- [6] H.G. Kortier and P.H. Veltink. "Assessment of daily-life dynamic interactions between human body and environment using movement and force sensing on the interface." In: *3rd Dutch Conference on Bio-Medical Engineering.* BME, Jan. 2011.
- [7] H.G. Kortier and P.H. Veltink. "Load identification during object handling." In: *33rd Annual International Conference of the IEEE Engineering in Medicine and Biology Society (EMBC '11).* IEEE Engineering in Medicine & Biology Society, Aug. 2011, pp. 3500–3502. ISBN: 978-1-4244-4122-8. doi: [10.1109/IEMBS.2011.6090945](https://doi.org/10.1109/IEMBS.2011.6090945).
- [8] J.C. van den Noort, K.J. van Dijk, H.G. Kortier, P.H. Veltink, N. van Beek, R. Verhagen, and L.J. Bour. "Applications of the PowerGlove for measurement of finger kinematics." In: *11th International Conference on Wearable and Implantable Body Sensor Networks, BSN 2014.* Ed. by G. Troster and G. Cantarella. Wearable and Implantable Body Sensor Networks (BSN) International Conference.

IEEE Xplore, June 2014, pp. 6–10. ISBN: 978-1-4799-6135-1. DOI: [10.1109/BSN.2014.700019](https://doi.org/10.1109/BSN.2014.700019).

- [9] J.C. van den Noort et al. “Applications of the PowerGlove.” In: *13th International Symposium on 3D Analysis of Human Movement, 3D-AHM 2014*. Ed. by K. Aminian. Internation Symposium on 3D Analysis of Human Movement O35. Ecole Polytechnique Federale de Lausanne, July 2014, pp. 381–384.
- [10] P.H. Veltink, H.G. Kortier, and H.M. Schepers. “Sensing dynamic interaction with the environment.” In: *Annual symposium of the IEEE/EMBS Benelux chapter*. Annual Symposium of the IEEE/EMBS Benelux chapter 7. IEEE Benelux Signal Processing Chapter, Dec. 2007, p. 13.
- [11] P.H. Veltink, H.G. Kortier, and H.M. Schepers. “Sensing dynamic interaction with the environment.” In: *International conference on ambulatory monitoring of physical activity and movement, conference book*. Ed. by J.B.J. Bussmann, H.L.D. Horemans, and H.L.P. Hurkmans. Dept. of Rehabilitation Medicine Erasmus MC, May 2008. ISBN: 978-90-813154-1-8.
- [12] P.H. Veltink, H.G. Kortier, H.M. Schepers, V.I. Sluiter, R.A. Brookhuis, T.S.J. Lammerink, and R.J. Wiegerink. “PowerGlove, Concepts and current results.” In: *Proceedings of XII International Symposium on 3D Analysis of Human Movement, DAHM 2012*. Ed. by A. Leardini and R. Stagni. Universita di Bologna, July 2012, pp. 42–45.
- [13] D. Weenk, M. van der Coelen, A.A.G Geessink, F.J. van der Hoek, B. Verstoep, H.G. Kortier, F. van Meulen, B.J.F. van Beijnum, and P.H. Veltink. “Ambulatory Estimation of Relative Foot Positions using Ultrasound.” In: *4th Dutch Bio-Medical Engineering Conference, BME 2013*. BME. 2013.

## DANKWOORD

---

Het is 06u16 en ik bevind me in de trein naar Schiphol voor een korte trip naar Wales. Mijn plan is om in de komende twee uur het laatste, al dan niet meest gelezen, deel van mijn proefschrift te schrijven. Echter vallen de oogleden dicht en dwalen mijn gedachten af naar de periode die aan het schrijven van dit proefschrift voorafging.

Aan het Zurriola strand, liggend met enkele huisgenoten niet ver van ons appartement waar ik tijdens mijn stageperiode bivakkeer, gaat mijn telefoon over. Je spreekt met Peter Veltink. Je sollicitatie voor een PhD plek binnen het PowerSensor project is in goede orde ontvangen, we denken dat je een geschikte kandidaat bent, en ik vroeg me af of je tijd hebt om even af te stemmen over je aanvang. Dolblij werd mijn stranddag voortgezet in de verschillende barretjes van Parte Vieja...

Feit is wel dat ik nog met mijn stage bezig was en dus nog aan het afstuderen moest beginnen. Dat afstuderen ging over het kwantitatief evalueren van mensen die eenvoudige handtakken uitvoeren. We maakten gebruik van een hippe haptische robot die ik, na veel werk, trots in C++ geprogrammeerd had. Leuk om te doen, echter bleek het nabootsen, of renderen, van dynamische lasten nog wel een dingetje en werd er uiteindelijk toch teruggevallen op het gebruik van *old school* massa's en veren.

Eind 2010 kon ik dan daadwerkelijk de aftrap van mijn promotietraject nemen. Een periode waarin ik veel nieuwe, zowel inhoudelijk alsmede de sociaal culturele, ervaringen heb opgedaan. Het werd een lange periode... Nu zo aan het eind terugkijkend ben ik erg benieuwd hoe veel het lood bij mij uiteindelijk woog. Dit alles heeft er wel voor gezorgd dat ik veel mensen heb leren kennen en zo doende een ontzettend leuke tijd heb gehad! Ik ben dan ook veel mensen dankbaar dat dit traject, uiteindelijk, tot een succesvolle afronding geleid heeft.

Iedereen persoonlijk benoemen gaat in de papieren lopen, toch wil ik enkele personen uitlichten.

Vanaf mijn bacheloropdracht tot en met de gehele promotieperiode was jij, Peter, mijn begeleider. Ik wil je ontzettend danken voor al die tijd en energie die jij in mij gestopt hebt. De kennis, enthousiasme en enorme toewijding maken je een heel bijzonder persoon. Enorm dank!

Nadat Henk, Daniël en jij, Martin, bij [BSS](#) aan inertial sensing gewerkt hebben mocht ik het stokje overnemen. Intussen had de vakgroep op dit vlak een goede reputatie opgebouwd en was het dus een eer om hier vervolgstappen in te mogen zetten. Jij als ze begeleider, weliswaar extern bij Xsens, wist altijd tijd voor me te maken, mee te sparren, en feedback op mijn zoveelste concept paper te geven. Martin, veel dank daarvoor!

Ik wil bovendien de overig betrokkenen bij Xsens bedanken voor de support en nuttige bijdragen tijdens meetings en lezingen.

De goede, en vooral gezellige, tijd bij BSS heeft mede gezorgd voor het toenemende gewicht van het loodje. Vanaf het moment dat ik startte waren de gemeenschappelijk lunchwandelingen, pauzes, donderdagmiddagborrels, pizza momenten, sinterkerstborrels en vakgroepuitjes altijd erg gezellig en leuk om aan deel te nemen.

In het bijzonder wil ik Wies, en later Sandra, danken voor de morele support en de vele administratieve taken die ze voor mij uitgevoerd hebben.

Mijn 'langstzittende' kamergenoten Dirk en Fokke wil ik danken voor de goede sfeer die er altijd op *de zaak* heerste. De vele bakjes, de slechte muziek, kansloze quotes, en het eindeloos geouwehoer en gezeur over van alles en nog wat hoop ik snel te vergeten ;) Desalniettemin hoop ik dat we de vriendschap en het contact nog lang in stand kunnen houden!

Het project zou nooit succesvol geweest zijn zonder de hulp van mensen met goede praktijk skills. Victor, jou wil ik enorm bedanken voor de grote bijdrage die je geleverd hebt in het ontwikkelen en fabriceren van hard en software. Nu ik zo terugblik besef ik me hoeveel ik van je engineering skills wel niet heb opgestoken. Dank daarvoor! Ook de overige technici: Ed, droog van karakter maar altijd met veel tromgeroffel aanwezig. Gelukkig was er dan Marcel om de boel een beetje te bedaren.. Heren, dank voor alle ondersteuning die jullie gegeven hebben!

Binnen het STW PowerSensor project waren verschillende partners betrokken die ieder zo hun eigen bijdrage geleverd hebben. Allen wil ik danken voor de prettige samenwerking. In het bijzonder daarbij Josien en Robert. Josien, jij als postdoc met vooral veel *meten aan mensen* ervaring, hebt mij veel bijgebracht op dit vlak. Ik wil je danken voor onze prettige samenwerking wat ons, na veel tijd en energie, een mooie publicatie heeft opgeleverd. Robert, jij was de ontwikkelaar van de nieuwe krachtsensor. Ik heb met veel genoegen van je mogen leren op het gebied van sensor fabricage in [MEMS](#). Mooi dat we de, door jou ontworpen, sensor uiteindelijk ook echt in de praktijk konden brengen en dit tot een mooie publicatie heeft.

Van [BSS](#) wil ik verder Bert-Jan en Jan bedanken voor de bijdragen tijdens de begeleiding en overleggen over de interessante toepassingsgebieden van verschillende sensoren. Verder wil ik de gezellige club PhD studenten die ik heb leren kennen danken: Eva, Heidi, Peter, Robert-Jan, Dirk, Frauke, Kees, Frederiek, Fokke, Wendy, Lamia, Hossein, Thijs, Hendrik, Rick, Jan-Willem, Bart, Nick en zo zal ik er vast nog 1 vergeten. Mooi om te zien dat, ondanks onze grote verschillen in achtergronden en onderzoeksonderwerpen, er ook zo veel overeenkomsten waren in onze ervaringen en beleveningen tijdens het uitvoeren van een PhD traject. Vooral de gezamenlijke Egmond BME weekendjes, de culturele dagen in Edinburgh en het zeildagje zullen me blijven bijstaan als enorm leuke uitjes. Dat de sfeer goed was blijkt wel uit het feit dat we met enkelen jaarlijks nog afspreken om, onder bijzijn van Ralfy, nieuw levenswater *nosen en tasten*. Tijdens de promotie heb ik vele bachelor en master studen-

ten mogen begeleiden wat met eenieder van jullie altijd een leuke ervaring was. Thijs, Stijn, Jacob, Marcel, Yusi, Diana, Michelle zijn enkele namen die op welke wijze dan ook hebben bijgedragen aan dit onderzoek en waar ik jullie dankbaar voor ben. Een speciaal, doch treurig, woord naar Thomas Dijkman die zijn master niet kunnen afronden doordat hij, na een kort ziekbed, afscheid van het leven heeft moeten nemen.

Buiten de vakgroep [BSS](#) wil ik ook vele anderen danken. Allereerst had ik de eer om als enig afgevaardigde binnen het BW/BSS futsal team zitting te nemen. Super leuk om te doen maar vooral fijn om zo nu en dan de promotiefrustraties er uit te kunnen zweten, dank oud teamgenoten!

Intussen ben ik alweer bijna 3 jaar actief als docent bij hogeschool Saxion binnen de opleiding mechatronica. Geweldig om samen met een enthousiast en uiteenlopend docententeam deze jonge opleiding tot één van de paradeplaatsjes van Saxion te maken. Daarnaast geniet ik van een superleuke combinatie door samen met studenten onderzoek te doen aan relevante en maatschappelijke mechatronische vraagstukken die vanuit het bedrijfsleven worden aangeboden. Eerst bij het lectoraat Ambient Intelligence maar nu ook bij het lectoraat Mechatronica. Alle direct betrokken collega's wil ik bijzonder bedanken voor de leuke tijd die ik bij jullie heb en het feit dat mij de tijd en ruimte gegeven is om ook wat aan mijn proefschrift te kunnen doen. Al was dat met een *booming* opleiding als Mechatronica soms best lastig..

Ik wil mijn paranimfen Dirk en Anke danken dat ze mij bij willen staan tijdens de ceremonie. Dirk, we kennen elkaar vanaf het moment dat we de eerste cm bier dronken als BonomEL lid. Ondanks dat jij en Aniek naar Deventer verhuizen ga ik er vanuit dat we nog regelmatig een tochtje met de motor gaan maken of een whisky gaan doen. Anke, mijn enige zus waar ik trots op neerkijk door haar vele werkzaamheden, bezigheden en ondertussen het mooie gezinsleven samen met Koen, Krisse en Steffie.

De vele vrienden, kameraden en (schoon)familieleden ga ik allemaal niet bij naam noemen. Om toch wat specifieker te zijn wil ik de bekenden uit Bentelo, Rietmolen, Delden, Enschede, Groningen en Münster in het bijzonder danken! Ik hoop verder dat eenieder zich aangesproken voelt!

Pa en ma, dank voor grootse ondersteuning en mogelijkheden die jullie, in welke vorm dan ook, mij gegeven hebben!

Frauke, [BSS](#) heeft ons veel meer gebracht dan enkel wat kennis en kunde. Ondanks dat we nog maar relatief kort samen zijn hebben onze belevenissen mij een stuk rijker gemaakt. Ik zie een mooie toekomst tegemoet *und HDGDL!!*

*Life is and will ever remain an equation  
incapable of solution, but it contains certain known factors.*

— Nicola Tesla